INFORMATION TO USERS

This manuscript has been reproduced from the microfilm master. UMI films the text directly from the original or copy submitted. Thus, some thesis and dissertation copies are in typewriter face, while others may be from any type of computer printer.

The quality of this reproduction is dependent upon the quality of the copy submitted. Broken or indistinct print, colored or poor quality illustrations and photographs, print bleedthrough, substandard margins, and improper alignment can adversely affect reproduction.

In the unlikely event that the author did not send UMI a complete manuscript and there are missing pages, these will be noted. Also, if unauthorized copyright material had to be removed, a note will indicate the deletion.

Oversize materials (e.g., maps, drawings, charts) are reproduced by sectioning the original, beginning at the upper left-hand corner and continuing from left to right in equal sections with small overlaps.

Photographs included in the original manuscript have been reproduced xerographically in this copy. Higher quality 6" x 9" black and white photographic prints are available for any photographs or illustrations appearing in this copy for an additional charge. Contact UMI directly to order.

ProQuest Information and Learning
300 North Zeeb Road, Ann Arbor, MI 48106-1346 USA
800-521-0600

UMI®

UNIVERSITY OF OKLAHOMA

GRADUATE COLLEGE

INTERACTIONS OF ORGANIC *S*–NITROSO AND *C*–NITROSO COMPOUNDS WITH METALLOPORPHYRINS

A Dissertation

SUBMITTED TO THE GRADUATE FACULTY

in partial fulfillment of the requirements for the

degree of

Doctor of Philosophy

By

JONGHYUK LEE

Norman, Oklahoma

2002

UMI Number: 3056948

UMI Microform 3056948

ProQuest Information and Learning Company
300 North Zeeb Road
P.O. Box 1346
Ann Arbor, MI 48106-1346

INTERACTIONS OF ORGANIC *S*-NITROSO AND *C*-NITROSO COMPOUNDS WITH METALLOPORPHYRINS

A Dissertation APPROVED FOR THE
DEPARTMENT OF CHEMISTRY AND BIOCHEMISTRY

BY

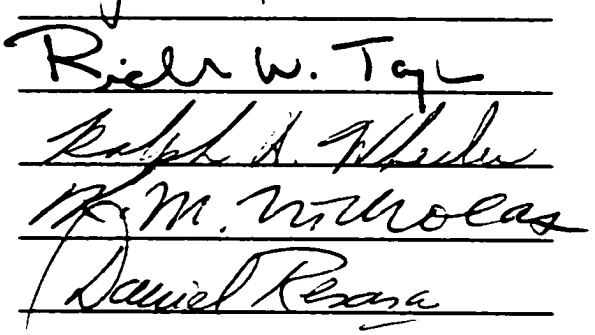

Acknowledgements

First, I would like to express my tremendous gratitude to my mentor, Dr. George B. Richter–Addo for his guidance, support, encouragement, and patience throughout my graduate studies at the University of Oklahoma. I feel very fortunate not only to have benefited from his academic guidance, but also to have enjoyed his invaluable friendship. He has led me to be a better human being as well as a good chemist over the past few years.

I would like to thank Drs. Richard Taylor, Kenneth Nicholas, Ralph Wheeler, and Daniel Resasco for serving as my advisory committee members. Their friendly advice and guidance has helped in the completion of this dissertation. I am also grateful to each of Inorganic Division Professors: Dr. Michael Ashby, Dr. Rudolf Wehmschulte, and Dr. Robert Houser. Special thanks to Drs. Masood Khan, Douglas Powell (at the University of Wisconsin, Madison), and Brendan Twamley (at the University of Idaho) for X–ray studies.

I would like to thank all my coworkers present and past in Dr. Richter–Addo's group: Dr. Geun–Bae Yi, Dr. Lin Cheng, Dr. Li Chen, Aaron Nichols, Ronnie Young, Keeshaloy Thompson, Naihui Guo, Shawn Carter, John Lilly, Myron Jones, Daniel Copeland, and Nan Xu. I have truly enjoyed working with these people. I would also like to thank other fellow Inorganic Division graduate students present and past: Dr. Danny McGuire, Dr. Susan Alguindigue, Dr. Sam Asirvatham, Dr. Kris Wise, Justin Schwane, Eric Klein, Ruibo Li, Hongfei Xi, and Hanhui Xu. I also wish to thank Dr. Jong Hwan Kwak for sharing his experience operating NMR instruments with me.

I appreciate for the financial support offered by the Department of Chemistry and Biochemistry at OU. I am also deeply grateful to the National Institutes of Health (NIH) and National Science Foundation (NSF) for the funding which made the completion of this dissertation possible.

I would like to express my deepest gratitude to my father and mother in Korea for their love and continuous support during my study abroad. I also wish to thank my brothers' families and my wife's family for their love and support. Special thanks goes to my lovely wife, Myo–Joung Sim for making it possible for me to complete this dissertation by taking care of our son while I was working. This dissertation could not have been completed without her. I also wish to dedicate this dissertation to my beautiful son, Jeffrey Lee who was born last winter. He is one of the greatest gifts which God has given to me.

Finally, I wish to praise God's name and glorify Him for blessing me. I would also like to express my sincere gratitude to the members of Norman Korean Baptist Church for their prayers.

Table of Contents

List of Tables

List of Figures

Abstract

This dissertation deals with the interactions of organic *S*–nitroso (RS–N=O) and *C*–nitroso (C–N=O) compounds with ruthenium and osmium porphyrins.

Chapter 1 of this dissertation introduces the fundamental issues involved in the chemistry and biochemistry of organic *S*– and *C*–nitroso compounds. Thus, the syntheses and properties of organic *S*– and *C*–nitroso compounds, and their reactions with heme and heme models are reviewed in Chapter 1.

Chapter 2 of this dissertation describes the syntheses of the (OEP)Os(NO)(SR) compounds via the addition of RSNO to (OEP)Os(CO) or via an alkoxide–thiolate exchange reaction. Thus, the (OEP)Os(NO)(SR) compounds (R = Me, Et, ^{i}Pr, ^{t}Bu) were prepared in 33–48% isolated yields by the formal *trans*–addition of the precursor thionitrites (RSNO) across the metal center in (OEP)Os(CO). These nitrosyl thiolate compounds were characterized by IR, ^{1}H NMR, and UV–vis spectroscopy, and by FAB mass spectrometry. Their IR spectra display bands in the 1751–1755 cm^{-1} (KBr) range, which is indicative of linear NO ligands in this class of compounds. The (OEP)Os(NO)-(SCR'$_2$CH$_2$NHC(O)Me) (R' = Me, H) compounds were also prepared either by RSNO addition to (OEP)Os(CO) (for R' = Me) or by an alkoxide–thiolate exchange reaction (for R' = H). The solid–state molecular structures of the precursor RSNO thionitrite (for R' = Me) and its disulfide were determined by single–crystal X–ray crystallography. Protonation of these (OEP)Os(NO)(SCR'$_2$CH$_2$NHC(O)Me) complexes gave the *amide*–bound [(OEP)Os(NO)(O=C(Me)NHCH$_2$CR'$_2$SH)]BF$_4$ derivatives. The latter cationic compounds were also obtained by the sequential reaction of (OEP)Os(CO) with HBF$_4$·Et$_2$O, followed by addition of the amide–thiol reagent.

Chapter 3 of this dissertation describes the syntheses of the monometallic nitrosyl thiolate–thiol complexes and their novel bimetallic μ–dithiolate derivatives by using an alkoxide–thiolate exchange method or the formal *trans*–addition of RSNO. Thus, the

monometallic nitrosyl thiolate–thiol complexes of the form (por)Ru(NO)(S$(CH_2)_n$SH) (por = TPP, n = 2; TTP, n = 3–4) were prepared in 49–58% isolated yields from the reaction of the (por)Ru(NO)(O–*i*–C_5H_{11}) alkoxide precursors with HS$(CH_2)_n$SH in CH_2Cl_2. The (OEP)Os(NO)(SCH_2CH_2SH) complex was also prepared in 70% isolated yield from the reaction of (OEP)Os(NO)(O–*i*–C_5H_{11}) with ethane–1,2–dithiol in refluxing toluene. These monometallic nitrosyl thiolate–thiol complexes were fully characterized by elemental analyses, infrared and ^{1}H NMR spectroscopy, and by FAB mass spectrometry. The symmetrical bimetallic [(por)Ru(NO)]$_2$(μ–S$(CH_2)_n$S–*S*,*S*') complexes (por$_1$ = por$_2$; i.e., TPP/TPP, TTP/TTP) were also prepared by variations of the procedures used in the preparation of their monometallic derivatives. The novel unsymmetric [(TPP)Ru(NO)](μ–SCH_2CH_2S–*S*,*S*')[Ru(NO)(OEP)] and [(OEP)Os(NO)]-(μ–SCH_2CH_2S–*S*,*S*')[Ru(NO)(TTP)] complexes were also obtained, and the experimental and simulated ^{1}H NMR spectra of the protons of the μ–dithiolate bridge indicate that all four protons (–SCH_2CH_2S–) are inequivalent.

Chapter 4 of this dissertation deals with the first isolable nitrone adducts of metalloporphyrins. Thus, the metalloporphyrin nitrone complexes (OEP)M(CO)(DMPO) (M = Ru, Os; DMPO = 5,5–dimethyl–1–pyrroline *N*–oxide) were prepared in 61–75% isolated yields from the reaction of (OEP)M(CO) with excess DMPO. These (OEP)M(CO)(DMPO) complexes were fully characterized by elemental analyses, infrared and ^{1}H NMR spectroscopy, and by ESI mass spectrometry. The molecular structures of (OEP)M(CO)(DMPO) were also determined by single–crystal X–ray crystallography and reveal a sole η^1–O binding mode of the nitrone ligand to the metal centers in (OEP)M(CO)(DMPO).

Chapter 5 of this dissertation deals with the examination of the binding of nitrosoarenes, pyridine, and 1–methylimidazole (1–MeIm) to ruthenium porphyrins. Thus, a series of the (por)Ru(ArNO)$_2$ (por = TPP, TTP; ArNO = PhNO, *o*–tolNO, N(O)-C_6H_4OMe–*p*, N(O)$C_6H_2(Me)_2$OMe–*p*) complexes were prepared in 49–75% isolated

yields from the reaction of (por)Ru(CO) with excess ArNO. The mono–nitrosoarene complexes containing the axial pyridine or 1–MeIm ligand, namely (por)Ru(PhNO)(py) (por = TPP, TTP) and (por)Ru(ArNO)(1–MeIm) (por = TPP, TTP; ArNO = PhNO, *o*–tolNO, $N(O)C_6H_4OMe$–*p*, $N(O)C_6H_2(Me)_2OMe$–*p*) were also readily prepared in 67–71% (for pyridine complexes) and 50–80% (for 1–MeIm complexes) isolated yields, respectively, from the reaction of the (por)Ru$(ArNO)_2$ with 2 equiv of pyridine or 1–MeIm. These bis– and mono–nitrosoarene complexes were characterized by infrared and ^1H NMR spectroscopy, and by FAB mass spectrometry. The assignment of the υ_{NO} of the coordinated ArNO groups in the IR spectra (KBr) was confirmed by the analyses of the IR spectra of the ^{15}N–labeled nitroso analogs. Their IR spectral data (KBr) reveal that the υ_{NO}s in these bis– and mono–nitrosoarene complexes decrease in the order (por)Ru$(ArNO)_2$ (1346–1350 cm^{-1}) > (por)Ru(PhNO)(py) (1328–1332 cm^{-1}) > (por)Ru-(ArNO)(1–MeIm) (1306–1323 cm^{-1}). Eleven of these bis– and mono–nitrosoarene complexes were also characterized by X–ray crystallography. All the nitrosoarene ligands in these bis– and mono–nitrosoarene complexes are bound to the Ru(II) centers in a η^1–N fashion. The molecular structures of the (por)Ru$(ArNO)_2$ and (por)Ru(PhNO)-(py) complexes show the perpendicular orientations of the axial ligands, whereas the ArNO and 1–MeIm ligands in (por)Ru(ArNO)(1–MeIm) are oriented parallel to each other.

Chapter 1. Introduction*

The chemistry of organic nitroso compounds (X–N=O) has received a great deal of attention largely due to the fact that it is linked to the biological actions of nitric oxide (NO). Importantly, some reports have suggested that such organic nitroso compounds are capable of interacting directly with metal center in heme–containing biomolecules such as myoglobin, hemoglobin, and cytochrome P450 to form adducts. Indeed, this possibility of a direct interaction of X–N=O with heme has led our research group to investigate, beginning in 1994, the reactions of X–N=O with synthetic metalloporphyrins.

It is well–known that the NO group or its activated forms may not only react with metal compounds to form metal nitrosyl derivatives,[1] but also react with some organic fragments to form X–N=O species. The four main types of X–N=O compounds are shown in Figure 1.1, and they are the *N*–nitroso (nitrosamine), *C*–nitroso (nitrosoalkane, nitrosoarene), *O*–nitroso (alkyl nitrite), and *S*–nitroso (alkyl/aryl thionitrite; nitrosothiol) compounds.

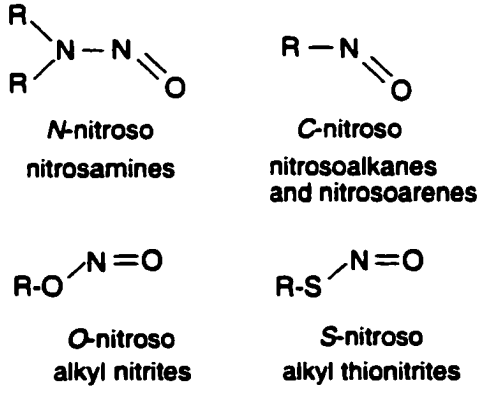

Figure 1.1. Four main types of X–N=O compounds.

---

* Reproduced in part with permission from "Interactions of Organic Nitroso Compounds with Metals." Lee, J.; Chen, L.; West, A. H.; Richter-Addo, G. B. *Chem. Rev.* **2002**, *102*, 1019-1065. Copyright 2002 American Chemical Society.

In this chapter, the syntheses and properties of organic *S*–nitroso and *C*–nitroso compounds will be briefly described. Their reactions with heme and heme models will then be discussed.

I. S–Nitroso Compounds

A. Organic Compounds

The *S*–nitroso functional group in alkyl thionitrites (RSNO, *S*–nitrosothiols) is widely recognized to be an important functional group in the biology of NO. For example, it has been proposed in some cases that metal–catalyzed release of NO from *S*–nitrosoglutathione (GSNO) may be responsible for the RSNO activation of soluble guanylyl cyclase (sGC),[2] although in other cases the activation of sGC could not be explained by a simple NO release (from RSNO) pathway.[3]

1. Synthesis

S–nitroso compounds are generally synthesized from nitrosation of the precursor thiol (RSH) by various nitrosating agents (X–NO) such as ClNO, N_2O_4, NO_2, N_2O_3, HNO_2, and RONO (eq 1.1).[4]

$$RSH + XNO \rightarrow RSNO + HX \qquad (1.1)$$

These in many ways resemble the formation of alkyl nitrites (RONO) from the corresponding alcohols, although the essentially quantitative nature of RSNO generation appears to be one major difference between *S*– and *O*–nitrosation.[4] Perhaps the most common methods in the preparation of alkyl thionitrites utilize the reaction of RSH with N_2O_4 (excess N_2O_4 gives the $RSNO_2$ product), or alkyl nitrites (RONO) in aqueous solution or in organic solvents, or acidified nitrite.[5,6] The *S*–nitrosation of thiols by alkyl nitrites in aqueous solution or in organic solvents is especially useful (eq 1.2).[7-11]

$$RONO + R'SH \rightarrow ROH + R'SNO \quad (1.2)$$

Importantly, *S*–nitrosation from alkyl nitrites might also have implications in biology. For example, Doyle and coworkers reported that the Hb(SNO) product can be obtained from the reaction of Hb with alkyl nitrites via *S*–nitrosation of hemoglobin (Hb) at the βCys93 residues.[12]

Some reports on the possibility of the direct reaction of RSH and NO are now available, however, it is likely that other nitrogen oxides are the active nitrosating species. Indeed, Sharma and coworkers have shown that NO by itself does not react with thiols at pH 7.0 except in the presence of oxygen, and that N_2O_3 is the active nitrosating species.[13]

Other less–common methods for the syntheses of RSNO include the reaction of disulfides with N_2O_4 (to give RSNO and other products), or the photolytic reaction of disulfides (RSSR; to give RS·) and NO.[4,6]

2. Spectroscopy and structure

RSNO compounds are generally red (1° or 2° alkyl thionitrites) or green (3° alkyl thionitrites), and their UV–vis spectra display bands at 330–350 nm ($\varepsilon \sim 10^3$ $M^{-1}cm^{-1}$; $n_O \rightarrow \pi^*$) and 550–600 nm ($\varepsilon \sim 20$ M^{-1} cm^{-1}; $n_N \rightarrow \pi^*$).[14]

IR spectroscopy has been a particularly useful tool to identify the *S*–nitroso group. Most RSNO compounds usually display N–O stretching frequencies in the 1480–1530 cm^{-1} range.[8,14] ^{15}N–isotope sensitive bands in the IR spectra of Ph_3CSNO, SNAP (*S*–nitroso–*N*–acetyl–penicillamine), and GSNO at 1479–1514 cm^{-1} and 650–670 cm^{-1} have also been assigned to υ_{NO} and υ_{NS}, respectively.[15]

^1H and ^{13}C NMR spectroscopies have also been used to characterize RSNO compounds. *S*–nitrosation generally shifts the α–proton resonance downfield by ~1 ppm from those of the corresponding thiols or disulfides, and the α–carbon resonance is

shifted downfield by ~7–13 ppm (stronger shift for tertiary alkyl thionitrites).[8]

Single–crystal X–ray crystallographic studies have been very useful in determining the orientations of the SNO groups in RSNO compounds. However, only a few solid–state structures of RSNO compounds are known,[15-20] and these are listed in Table 2.2 in Chapter 2. Importantly, the thionitrite functionality of *S*–nitrosocaptopril exists in a *syn* orientation,[18] whereas the structures of SNAP[15-17] and Ph_3CSNO[15] show the *anti* orientation. The structure of Ar_3CSNO compound (Ar = 3,5–bis(2,6–dimethyl-phenyl)phenyl), however, reveals both the *anti* and *syn* orientations in a 0.67:0.33 ratio.[19]

The X–ray crystal structure of Hb(SNO) has also been obtained at 1.8 Å resolution.[20] The torsion angle of O–N–S–C in this structure was 87° (i.e., neither *syn* or *anti*), however, the previously–determined related structure of SNAP was used in the modeling of the SNO groups of Hb(SNO).

3. Reactions

(1) *Thermal or photolytic decomposition.* RSNO compounds produce the disulfide and NO by thermal or photolytic decomposition.[6] The interest in the use of RSNO compounds as NO donors[21] has placed increased importance to this general reaction (eq 1.3).

$$2\,RSNO \rightarrow RSSR + 2\,NO \qquad (1.3)$$

Wang and coworkers recently reported that S–N bond homolysis requires less energy than heterolysis by ~29 kcal/mol based on their results on the thermochemistry and computational studies of various RSNO compounds.[22]

(2) *NO transfer reactions.* RSNO compounds are capable of nitrosating amines to carcinogenic nitrosamines by NO transfer.[4,6,23] Interestingly, RSNO compounds are also known to engage in *S*–transnitrosation reactions with other thiols (eq 1.4).

$$RSNO + R'SH \leftrightarrow RSH + R'SNO \quad (1.4)$$

Importantly, these *S*–transnitrosations have some biological significance. For example, *S*–transnitrosations between *S*–nitrosocysteine and glutathione (GSH) of red blood cells to form GSNO have been reported.[24]

B. Interactions with Heme and Heme Models

It has been suggested by Marletta and Stone that RSNO may be able to bind directly to the heme site of guanylyl cyclase (GC).[25] Our research group was thus interested in investigating the interactions of RSNO with metalloporphyrins of the Group 8 metals as heme models. Surprisingly, there were no reports on the reaction of RSNO with heme models prior to our group's work.

Indeed, our initial goal was to isolate adducts of RSNO with the Group 8 metalloporphyrins. However, the reaction of (OEP)Ru(CO) with 1 equiv of *S*–nitroso–*N*–acetyl–L–cysteine methyl ester generated the unexpected nitrosyl thiolate (OEP)Ru-(NO)(*S*–NACysMe) (*S*–NACysMe = *N*–acetyl–L–cysteinate methyl ester) instead of the expected RSNO–ligated complex.[26,27] This product was characterized initially by spectroscopy and then by single–crystal X–ray crystallography as shown in Figure 1.2. Thus, our group has observed that alkyl thionitrites react with metalloporphyrins of the form (por)M(CO) (M = Ru, Os) to give the unprecedented formal *trans*–addition products (por)M(NO)(SR) as shown in Figure 1.3.[26-30]

IR spectroscopic studies suggest that the *trans*–addition reactions proceed via the carbonyl thiolate complexes (por)M(CO)(SR), formed from the proposed homolysis of the S–NO bonds in the putative (por)M(CO){η^1–S(R)NO} adducts. A recent paper by Ford, Richter–Addo, and coworkers on the kinetics of the reaction of RSNO with the (OEP)Ru(CO) complex substantiates our group's initial proposal of initial *S*–binding of RSNO compound.[31]

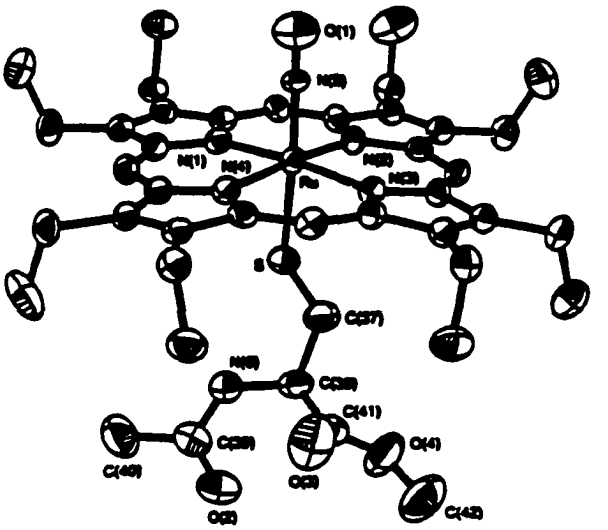

Figure 1.2. Molecular structure of (OEP)Ru(NO)(*S*-NACysMe).[26,27]

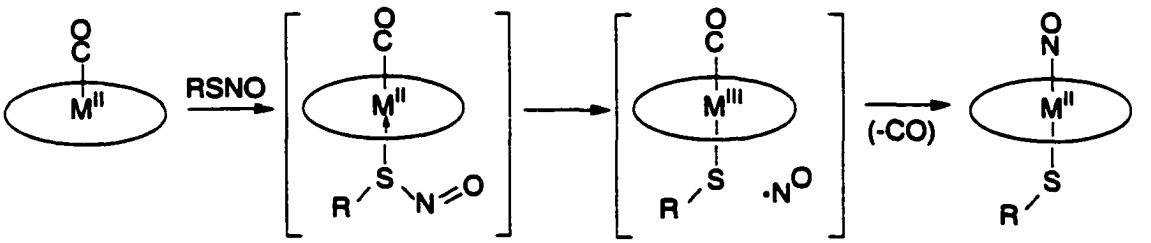

Figure 1.3. Proposed pathway for RSNO addition to Group 8 metalloporphyrins (M = Ru, Os) to generate nitrosyl thiolate products.

Unlike the case of Ru^{II} and Os^{II} porphyrins, the related reaction of RSNO (*S*–nitroso–*N*–acetyl–L–cysteine methyl ester) with a ferrous heme model, namely $(TPP)Fe(THF)_2$, resulted in the generation of the known five–coordinate (TPP)Fe(NO) compound in almost quantitative yield (Figure 1.4).[27] The possibility of a net NO transfer from RSNO to iron centers has implications in biology, and further research in this area is warranted. Interestingly, such a direct NO transfer from RSNO to non–heme iron complexes has been established recently.[32]

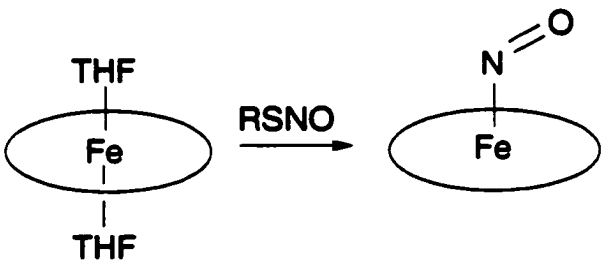

Figure 1.4. Reaction of *S*-nitroso–*N*–acetyl–L–cysteine methyl ester (RSNO) with $(TPP)Fe(THF)_2$.

II. C–Nitroso Compounds

A. Organic Compounds

The increased interest in the chemistry of organic *C*–nitroso compounds (nitrosoalkanes and nitrosoarenes) is due partly to the fact that they can directly bind to the metal centers in heme–containing biomolecules such as myoglobin, hemoglobin, cytochrome P450, and guanylyl cyclase. Importantly, it was recognized more than a century ago that nitrobenzene ($PhNO_2$) poisoning was associated with the formation of an adduct between a derivative of nitrobenzene and hemoglobin (Hb),[33,34] and a possible adduct was proposed to be a Hb–PhNO species.[35]

1. Synthesis

A variety of methods have been used for the preparation of *C*–nitroso compounds, and comprehensive reviews by Coombes and Williams have been published.[4,36] *C*–nitrosation can usually be accomplished by:

(1) *Oxidation of amines and N–substituted hydroxylamines* (e.g., by peroxy acids)

$$RNH_2 \rightarrow RNHOH \rightarrow RNO \qquad (1.5)$$

In some cases, the *N*–substituted hydroxylamine is obtained by reduction of the nitro compound (RNO_2), and then oxidation of the hydroxylamine gives the desired nitroso product.[36]

(2) *H–replacement in C–H bonds.* Nitrous acid and other nitrosating agents can react with the C–H bonds adjacent to electron–withdrawing groups (eq 1.6; X = NO_2, CN, etc.) to result in *C*–nitrosation.

$$R_2C(H)X \rightarrow R_2C(NO)X \qquad (1.6)$$

Nitrosation of ketones has been achieved in this manner. These nitrosations frequently result in the formation of oxime tautomers R'CH=NOH as the final products if the nitrosation occurs at a methylene or methyl group.

Kochi and coworkers have demonstrated the direct and selective nitrosation of arenes (polymethylbenzenes and anisoles) by the nitrosonium NO^+ cation in acetonitrile,[37] e.g.

$$C_6H_5OMe + NOBF_4 \rightarrow p\text{-}ONC_6H_4OMe + HBF_4 \qquad (1.7)$$

Aromatic nitrosations using nitrosonium ethyl sulfate have also been reported.

Furthermore, the aromatic *C*–nitroso compounds as the final products may be prepared by the reaction of alkyl nitrites with substituted phenolate ions in aqueous solution.[38]

(3) *Reaction of organometallic reagents with nitrosating agents.* The coordinated R groups in a number of organometallic compounds can be nitrosated by nitrosating agents,[39] e.g.

$$\{CH_3(CH_2)_3C{\equiv}C\}_2Hg + 2\,ClNO \rightarrow 2\,CH_3(CH_2)_3C{\equiv}CNO + HgCl_2 \qquad (1.8)$$

Similar reactions with Grignard and alkyllithium reagents have been reported.[4,36,39]

(4) *Addition of nitrosyl halides or other XNO compounds across the double bonds of alkenes.* An example of this type of reaction (by ClNO) is shown in eq 1.9.

$$R_2C{=}CR_2 + ClNO \rightarrow R_2(Cl)C\text{-}C(NO)R_2 \qquad (1.9)$$

(5) *Nitrosation of alkanes by ClNO.* The formation of RNO caused by photolysis of ClNO has been reported. Thus, it is suggested that initial generation of Cl• (and NO) by photolysis of ClNO initiates production of R• radicals which then combine with NO to give RNO. Photolysis of perfluoroalkyl iodides R_FI ($R_F = CF_3$, C_3F_7) similarly generates R_F• which can react with NO to give R_FNO.[40,41]

2. Spectroscopy and structure

C–nitroso compounds can exist either as monomers or as dimers. In addition, the dimers can be either *cis* (*Z*–dimers) or *trans* (*E*–dimers) as shown in Figure 1.5.

The spectral properties of RNO compounds depend on their structures either as monomers or *cis*– or *trans*–dimers. The monomers are generally blue (aliphatic) or green (aromatic) due to a weak $n \rightarrow \pi^*$ transition at 630–790 nm, but the dimers are colorless.[36] The *trans*–dimers of aliphatic RNO compounds have a $\pi \rightarrow \pi^*$ transition at ~276–291 nm,

and the absorption bands for the *cis*–dimers appear at 265–271 nm.

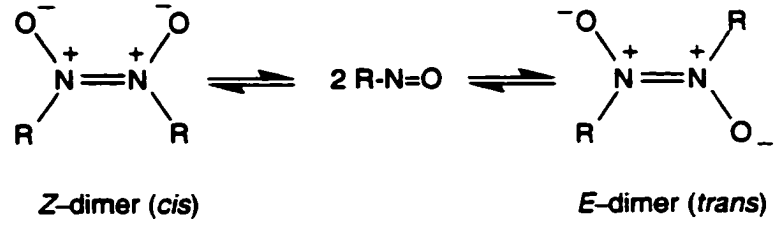

Figure 1.5. Dimerization of *C*–nitroso compounds.

Infrared spectroscopy has been very useful for the identification of *C*–nitroso compounds.[4,36,42] It is usually accepted that the NO stretching frequencies of monomeric aliphatic RNO compounds are in the 1539–1621 cm^{-1} range (e.g., CH_3NO (1564 cm^{-1}), CF_3NO (1595 cm^{-1}), and nitrosocyclohexane (1558 cm^{-1})), whereas monomeric aromatic ArNO compounds display υ_{NO} in the 1488–1513 cm^{-1} range (e.g., PhNO (1506 cm^{-1}), *p*–FC_6H_4NO (1511 cm^{-1}), and *p*–IC_6H_4NO (1488 cm^{-1})). Gowenlock and coworkers demonstrated that *cis* and *trans* isomers of dimeric RNO compounds can be distinguished by examining their characteristic bands including υ_{NO} and υ_{NN}.[43] In general, the *trans*–dimers show characteristic single strong bands due to υ_{NO} in the 1176–1290 cm^{-1} region for aliphatic RNO dimers, and in the 1253–1299 cm^{-1} region for aromatic ArNO dimers. The *cis*–dimers, on the other hand, show two bands in the 1323–1344 and 1330–1420 cm^{-1} regions for aliphatic RNO dimers, and in the1389–1397 and ~1409 cm^{-1} regions for aromatic ArNO dimers. Nitrosoalkenes $R_2C{=}C(NO)R$ show υ_{NO} bands in the 1420–1485 cm^{-1} range,[44] and the υ_{NO} for $CH_3(CH_2)_3C{\equiv}CNO$ has been reported to be at 1580 cm^{-1}.[39]

Solution variable–temperature NMR spectroscopy has also been used by Orrell and coworkers to study various substituted nitrosobenzenes.[45,46] They observed that at ambient temperature, the monomers were the major species in solution. However, lower temperatures favored the formation of the RNO dimers, with the *cis*–dimer being favored

over the *trans*–dimer.

Single–crystal X–ray crystallographic data for a number of nonaromatic and aromatic *C*–nitroso compounds are now known and listed in Tables 1.1 and 1.2. The data from microwave spectroscopy and electron diffraction for CH_3NO, CF_3NO, CH_3CH_2NO, and $CClF_2NO$ are included for comparison.

Table 1.1 lists the data for nitrosoalkanes (NO bonded through the N–atom to an sp^3 carbon atom). For the *monomeric* aliphatic RNO compounds, N–O bond lengths and C–N–O angles generally fall in the ranges of 1.1–1.22 Å range and 103–121°, respectively. The *dimeric* compounds display N–N bond lengths of 1.22–1.33 Å, which are significantly shorter than a formal N–N single bond distance of 1.42 Å,[104] and imply double–bond character to this unit. Only one X–ray crystal structure of a non–constrained *cis*–dimer of a nitrosoalkane has been determined, namely that of *cis*–$(CH_3NO)_2$. The N–N and N–O bond lengths in this compound are both 1.31(2) Å.[49] Several X–ray crystal structures of constrained *cis*–$(RNO)_2$ compounds containing a "cyclic" (R_2)–link have been reported.[63-65] The structures of these constrained compounds show N–N and N–O bond lengths of 1.29–1.32 Å and 1.25–1.27 Å, respectively. Importantly, the increased N–O bond lengths in dimeric RNO compounds relative to those of monomeric RNO compounds are consistent with a contribution of the dipolar structure (Figure 1.5). The crystal structures of the aliphatic *trans*–$(RNO)_2$ compounds reveal that N–N and N–O bond lengths fall in the ranges of 1.22–1.33 Å and 1.25–1.30 Å, respectively.

Table 1.2 lists the crystal structure data for nitrosoarenes. The N–O bond lengths in the monomeric nitrosoarene compounds generally fall in the 1.13–1.29 Å range, with the exception of a reported length of 1.34 Å for a disordered component of 9–nitrosojulolidine.[99] The related N–O bond lengths in the dimeric nitrosoarene compounds fall in the rather narrow range of 1.25–1.28 Å, although a bond length of ~1.35 Å has been reported for the *trans*–dimer of *para*–bromonitrosobenzene.[80] Both monomeric and dimeric (*trans*) structures of *para*–iodonitrosobenzene are known, and the N–O bond

Table 1.1. Structural Data for Nonaromatic *C*–Nitroso Monomers and Dimers

Compound	*mono/dimer*	N-N (Å)	C-N (Å)	N-O (Å)	C-N-O (°)	refs
CH_3NO [a]	*monomer*		1.480	1.211	113.2	[47]
CH_3NO [a]	*monomer*		1.49(3)	1.22(3)	112.6(10)	[48]
CH_3NO	*cis-dimer*	1.31(2)	1.47(3)	1.31(2)	120.0(15)	[49]
CH_3NO	*trans-dimer*	1.22	1.57	1.25	125	[50]
CF_3NO [b]	*monomer*		1.555(15)	1.171(8)	121.0(16)	[51]
CF_3NO [b]	*monomer*		1.546(8)	1.197(5)	113.2(13)	[52]
CF_3NO [a]	*monomer*		1.512(16)	1.198(4)	112.4(3)	[53]
$CClF_2NO$ [b]	*monomer*					
	syn form		1.567(5)	1.175(3)	110.8(12)	[54]
	gauche form		1.559(5)	1.179(3)	110.7(12)	

CH_3CH_2NO [a]	*monomer* *syn* form		1.567(5)	1.175(3)	110.8(12)	[55]
$O_2NCH_2CH_2NO$	*trans-dimer*	1.304(6)	1.470(4)	1.262(4)	121.38(30)	[56]
$O_2NCH_2CH(Ph)NO$	*trans-dimer*	1.301(4)	1.479(3)	1.269(3)	120.9(2)	[57]
Me_2CHCH_2NO	*trans-dimer*	1.27(2)	1.51(2)	1.30(2)	120.5	[58]
$ClMe_2CCH(Me)NO$	*trans-dimer*	1.315(4)	1.500(3)	1.270(3)	120.02(19)	[40,41]
t-BuNO	*trans-dimer*	1.309(2)	1.533(2)	1.265(2)	119.65(14)	[59]
O_2NCMe_2NO	*trans-dimer*	1.329(3)	1.506(2)	1.251(2)	121.2(1)	[60]
$(B_{10}C_{12}H_{31}O)CH_2NO$	*trans-dimer*	1.272(6)	1.485[c]	1.293(6)	121.1[c]	[61]
	*trans-dimer*	1.308(6)	1.483(5)	1.269(4)	120.7(3)	[62]

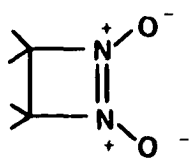		1.292(10)	1.527(7)	1.250(6)	135.4(5)	[63]
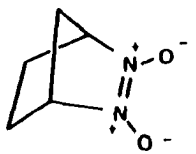		1.303(1)	1.496(2) 1.490(2)	1.256(1) 1.264(1)	128.0(1) 127.4(1)	[63]
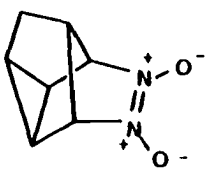		1.307(2)	1.486(2) 1.485(1)	1.259(1) 1.265(1)	128.0(1) 127.2(1)	[63]
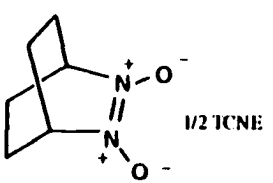		1.318[c]	1.484[c] 1.478[c]	1.267[c] 1.261[c]	124.2[c] 125.8[c]	[64]

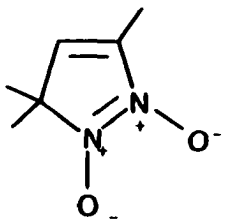		1.311(3)	1.490(3) 1.443(3)	1.265(2) 1.258(2)	126.6(2) 127.3(2)	[65]
cyclo-C_3H_5NO	*trans-dimer*	1.312(2)	1.454(3)	1.276(2)	120.75(13)	[66]
cyclo-C_4F_7NO	*monomer*		1.521(15)	1.20 [d]	111.9(22)	[67]
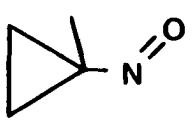	*trans-dimer*	1.321(2)	1.471(2)	1.272(2)	122.05(13)	[66]
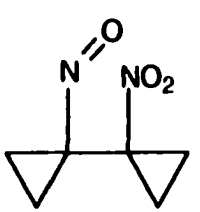	*monomer*		1.573	1.246	106.8	[68]

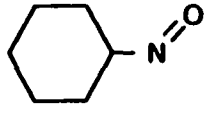	*trans-dimer*	1.319(6)	1.488(6)	1.272(6)	121.4(4)	[69]
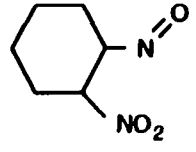	*trans-dimer*	1.302(4)	1.487(2)	1.274(3)	121.4(2)	[57]
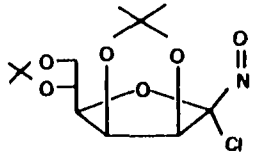	*monomer*		1.530(6)	1.171(4)	113.2	[70]
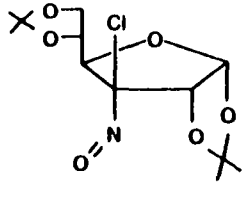	*monomer*		1.515(8)	1.153(8)	113.7(7)	[71]

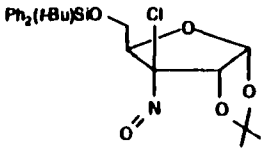	*monomer*		1.504(9)	1.178(7)	116.2(7)	[71]
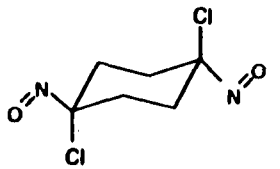	*monomer*		1.505(7)	1.139(5)	116.5(6)	[72]
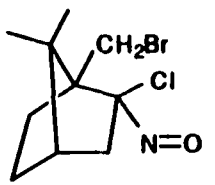	*monomer*		1.52 1.44[e]	1.16 1.21[e]	117 119[e]	[73]
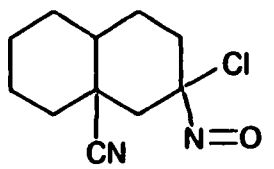	*monomer*		1.542(10)	1.121(10) 0.978(20)[f]	118.4(3)	[74]

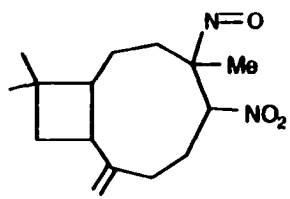	*monomer*		1.65(3)	1.10(2)	103(2)	[75]
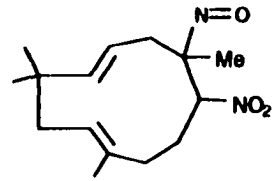	*monomer* *form 1* *form 2*		 1.51[c] 1.53[c]	 1.13[c] 1.19[c]	 119.5[c] 114.4[c]	 [76] [77]

[a] Determined by microwave spectroscopy.

[b] Determined by electron diffraction.

[c] Data obtained from the Cambridge Structural Database.

[d] This value was constrained.

[e] Data for second molecule.

[f] Data for disordered (minor) component.

Table 1.2. Structural Data for Aromatic *C*–Nitroso Monomers and Dimers

Compound	*mono/dimer*	N-N (Å)	C-N (Å)	N-O (Å)	C-N-O (°)	refs
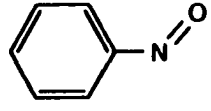	*cis-dimer*	1.321(5)	1.454(5) 1.463(5)	1.268(4) 1.261(4)	120.4(2) 120.8(3)	[78]
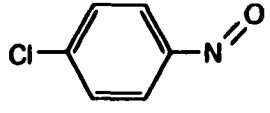	*trans-dimer*	1.318(5)	1.453(4)	1.265(3)	119.7(2)	[79]
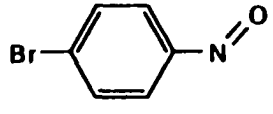	*trans-dimer*	~1.31	1.40	~1.35	~120	[80]
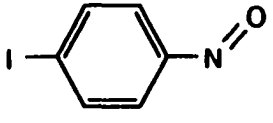	*trans-dimer*	1.316(7)	1.467(6)	1.279(5)	120.3(4)	[81]
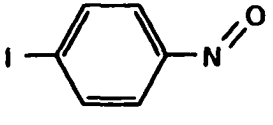	*monomer*		1.43 [a]	1.21 [a]	113.2 [a]	[72,82]

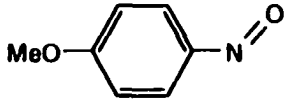	*monomer*		1.467(10)	1.228(8)	113.6(6)	[83]
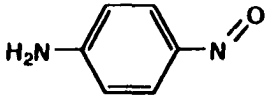 (complexed with 18C6)	*monomer*		1.460(7)	1.203(8)	108.0(5)	[84]
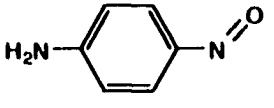 (complex with 1/2 DCH-6B)	*monomer*		1.529(9)	1.178(8)	101(1)	[84]
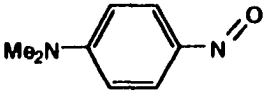	*monomer* [b]		1.390(11) [1.445(11)]	1.131(11) 1.212(11) [1.212(11) 1.292(11)]	126.2(10) 115.2(10) [116.4(10) 116.2(10)]	[85]

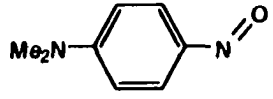 (complex with DPA)	*monomer*		1.367(2)	1.243(3)	116.1(2)	[86]
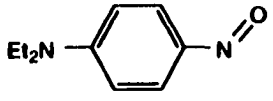	*monomer* [b]		1.438 [c] 1.458 [c]	1.253 [c] 1.215 [c]	110.9 [c] 109.9 [c]	[87]
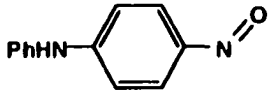	*monomer*		1.403(5)	1.256(5)	112.8(3)	[88]
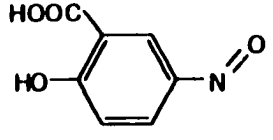	*monomer*		1.426(2)	1.234(2)	114.3(2)	[89]
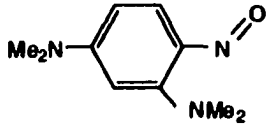	*monomer*		1.372(2)	1.276(2)	116.3(1)	[90]

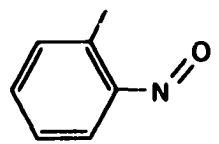	*cis-dimer*	*d*	*d*	*d*	*d*	91
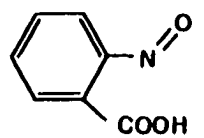	*trans-dimer*	1.308(3)	1.460(3)	1.267(3)	120.5(2)	78
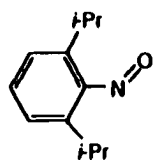	*trans-dimer*	1.323(2)	1.467(2)	1.267(2)	120.9(1)	92
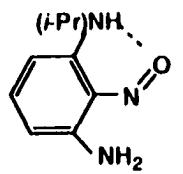	*monomer*		1.350(4) 1.352(4)	1.281(3) 1.285(3)	118.3(3) 118.2(3)	93
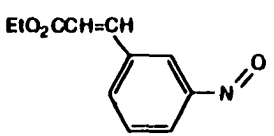	*monomer*		1.451(4)	1.229(3)	113.5(3)	94

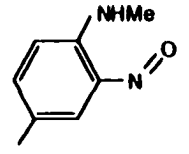	*monomer* [b]		1.371(3) 1.354(3)	1.254(2) 1.254(2)	116.8(2) 116.8(2)	[95]
	*monomer* [b]		1.429(8) [1.418(7)]	1.16(3) 1.25(3) [1.221(5)]	115.5(12) [114.8(6)]	[96]
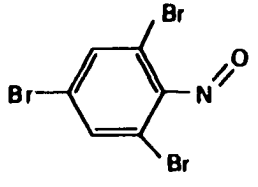	*trans-dimer*	~1.4				[97]
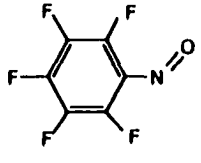	*cis-dimer*	1.324(5)	1.439(6)	1.267(5)	120.6(4) 120.8(4)	[98]

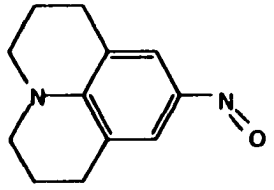	*monomer*		1.452(10)[e] 1.257(34)[f]	1.227(10)[e] 1.343(47)[f]	112.67(72)[e] 107.9(28)[f]	[99]
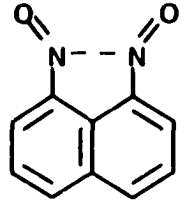		1.376(8)	1.430(8) 1.439(8)	1.274(8) 1.255(8)	128.8(4) 129.1(4)	[100]
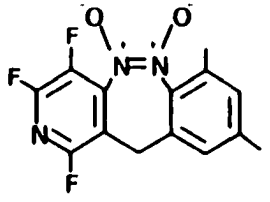		1.340(3)	1.460(3) 1.425(3)	1.252(2) 1.264(2)	120.5(2) 118.3(2)	[101]
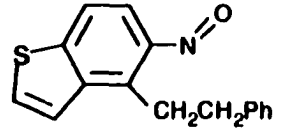	*monomer*		1.419(5)	1.213(5)	113.8(5)	[102]

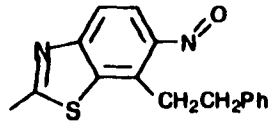	*monomer*		1.41(2)	1.23(1)	114.7(12)	[103]

[a] The data in ref 72 supersedes the data in ref 82.

[b] Two molecules in the unit cell.

[c] Data obtained from the Cambridge Structural Database.

[d] Metrical data not reported.

[e] Major component (83%).

[f] Minor component (17%).

length in the monomer is ~0.07 Å shorter than that in the dimer.[72,81,82]

B. Interactions with Heme and Heme Models

There is great interest in examining the products formed when metabolites of amines interact with heme biomolecules such as hemoglobin and cytochrome P450. The oxidation of amines to hydroxylamines or nitroso compounds, and the reduction of the *N*–oxidized derivatives are known to occur in some biological environments.[105-113] The intermediate *C*–nitroso compounds can then bind to heme biomolecules, or are involved in other reactions (such as metHb formation) in biological media.[114-116] Indeed, the study of the interactions of *C*–nitroso compounds with heme and heme models is motivated, in part, by the observation that various metabolites derived from amine oxidation or nitroaromatic reduction are involved in possible inhibition of enzymatic activity of P450 or cyclooxygenase, and that such heme–RNO species are possible products in such processes.

1. Myoglobin (Mb)

The formation of nitroso*alkane* complexes of Mb has been observed by Mansuy and coworkers.[117-119] Thus, the reaction of a number of nitroalkanes (RNO_2; R = Me, Et, *i*–Pr, pentyl, hexyl) with Mb in the presence of dithionite (pH = 7.4, phosphate buffer) resulted in the formation of new complexes absorbing at 425 nm. It is also known that nitrosoarenes react with Mb to generate the (Mb)Fe^{II}–ArNO adducts directly. Mansuy also reported that the reaction of ferrous deoxyMb with PhNO at pH 7.4 gave the adduct (Mb)Fe^{II}–PhNO with λ_{max} 427 nm.[120] Daniel Copeland in our group is currently developing this research area.

2. Hemoglobin (Hb)

The reactions of *C*–nitroso compounds with Hb are quite complex due to the fact

that four hemes are involved, and the observation that the Cys93 residue from the protein β subunit (βCys93) may also take part in such reactivity.

Nitrosoalkane complexes of hemoglobin (Hb(RNO)) have been generated by reduction of the precursor nitroalkane RNO_2 by dithionite in the presence of Hb. For example, Mansuy and coworkers reported that for $MeNO_2$ and $EtNO_2$ compounds, the reaction to generate the Hb(RNO) complexes (λ_{max} 421 nm; R = Me, Et) was completed within a 3 min period.[117,118] They proposed an *N*–binding mode of the RNO ligand based on resonance Raman spectroscopy.[117,121]

The interactions of nitrosoarenes with Hb are more complex. In general, nitrosoarenes can react with Hb at the heme iron and/or at reactive cysteine residues, as schematically shown in Figure 1.6 for nitrosobenzene.

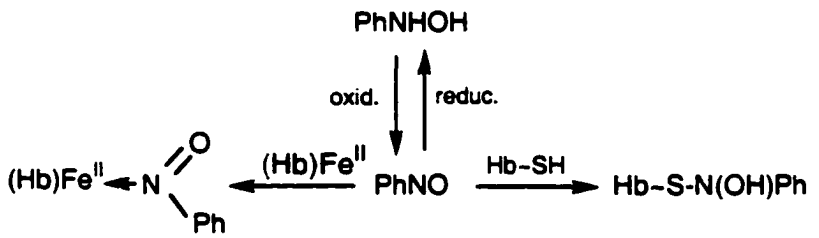

Figure 1.6. Reactions of nitrosobenzene with hemoglobin.

The reactions of the cysteine group of Hb with nitrosochloramphenicol (NOCAP; a possible metabolite chloramphenicol) have also been demonstrated by radioactive labeling (e.g., the use of ^{14}C–labeled NOCAP).[122] It was shown that the heme group of Hb was a second site for NOCAP binding, although this heme–NOCAP binding was not very efficient probably due to steric reasons.

The formation of Hb(ArNO) complexes by reactions of Hb with substituted nitrosoarenes has also been reported.[35,123-125]

3. Leghemoglobin (legHb)

The X–ray crystal structure of the ferrous (legHb)Fe^{II}–N(O)Ph adduct from *Lupinus luteus* has been obtained, and it reveals the *N*–binding mode of the PhNO ligand to the metal center (Figure 1.7).[126]

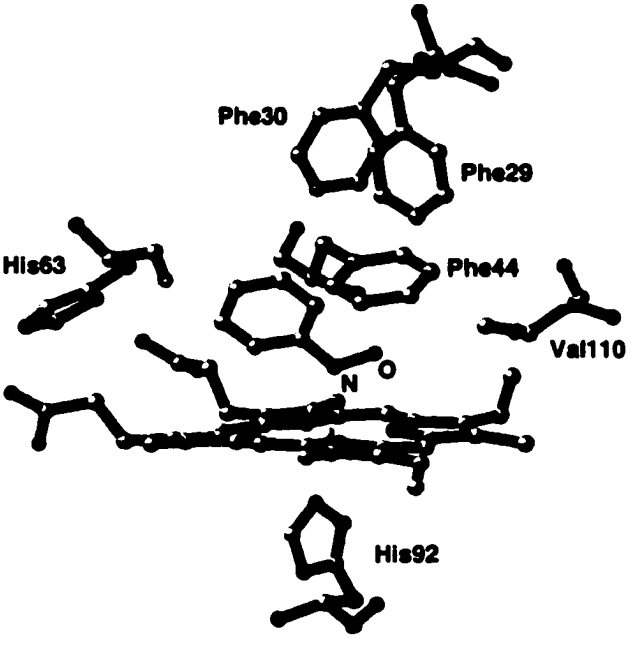

Figure 1.7. The heme site in the leghemoglobin–nitrosobenzene complex.[126] The Fe–N(O), Fe–N(His), and Fe–N(porphyrin) bonds are omitted for the sake of clarity. The X–ray coordinates were obtained from the Brookhaven Protein Data Bank.

4. Soluble Guanylyl Cyclase (sGC)

The reaction of $MeNO_2$ with ferrous sGC in the presence of dithionite (pH 7.4, 10 °C) under argon resulted in the formation of a 425 nm–absorbing complex which is attributed to a (sGC)Fe^{II}–MeNO complex.[25] This complex was not very stable in solution, and reverted to the five–coordinate ferrous sGC form within 30 min, suggesting a dissociation of the MeNO ligand (which is unstable in the free unligated

form).

5. Cytochrome P450

It has been known for quite some time that some organic *N*–containing compounds are able to form complexes absorbing at ~455 nm with cytochrome P450 during oxidative metabolism in microsomal systems, and there is the possibility that when nitroso compounds bind to heme iron, they may inhibit P450 activity.

Mansuy and coworkers studied the interaction of several 1° and 2° nitro RNO_2 compounds (R = Me, Et, *n*–pentyl, *n*–hexyl, cyclohexyl, cyclopentyl, benzyl (i.e., amphetamine)) with reduced P450, and observed the formation of 455 nm complexes. They proposed that the ligand in these complexes with λ_{max} = 455 nm was the nitroso metabolite (RNO) which was generated from reduction of the nitro compounds, or after oxidation of the amines (Figure 1.8).[118]

It was also reported by Mansuy and coworkers that arylnitroso (ArNO; Ar = Ph, *p*–chlorophenyl) complexes of NADPH–reduced liver microsomal P450 absorbing at 454 nm were generated by *(i)* direct interaction of the nitrosoarene in the absence of air (oxygen), *(ii)* reaction of the arylhydroxylamine (ArNHOH) in the presence of air (oxygen), or *(iii)* reaction of the nitroarene ($ArNO_2$) in the presence of NADPH or dithionite.[120] Cho and coworkers later examined the direct interaction of PhNO with ferric P450, and they found that the (P450)Fe^{II}–PhNO adduct was produced from the reaction of the ferric P450 with PhNO without added reductant.[127]

6. Nitric Oxide Synthase (NOS)

Nitrosomethane complexes of the oxygenase domain of NO synthase have been produced when nitromethane ($MeNO_2$) and dithionite reacted with recombinant $iNOS_{oxy}$ and $nNOS_{oxy}$ (pH 7.4, 50 mM HEPES; HEPES = 4–(2–hydroxyethyl)–1–piperazine-ethanesulfonic acid).[128] Other (NOS_{oxy})Fe^{II}–RNO complexes were also similarly

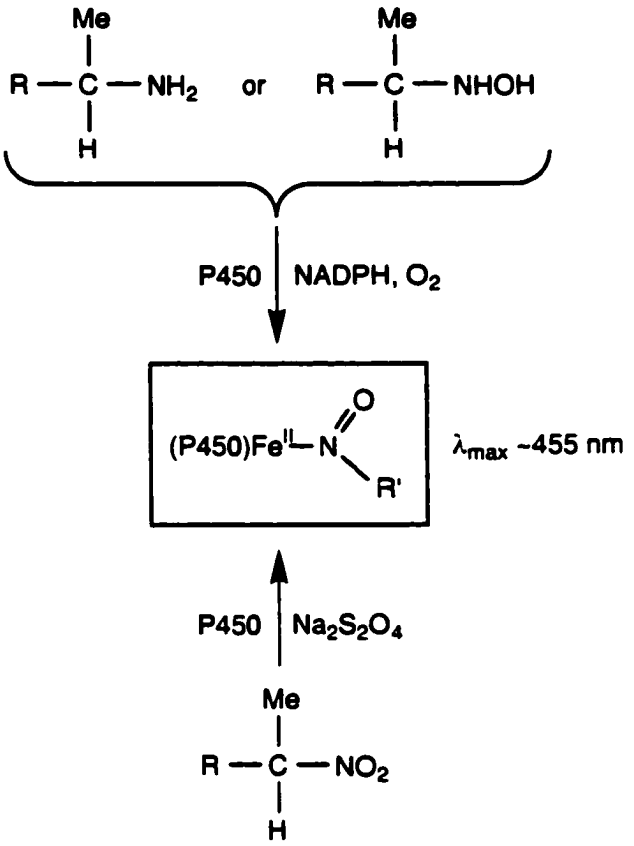

Figure 1.8. Formation of nitrosoalkane complexes of cytochrome P450 (R' = RCH(Me)–).

generated from the reaction of nitroalkanes with $iNOS_{oxy}$ or $nNOS_{oxy}$ in the presence of dithionite but in the absence of tetrahydrobiopterin.

7. Catalase

A (catalase)Fe^{II}–PhNO complex (λ_{max} 421 nm) has been proposed as a product when PhNHOH was reacted with bovine liver catalase.[129]

8. *Prostaglandin H Synthase (PGHS)*

Mansuy and Mahy observed that when *N*–hydroxyamphetamine (AmphNHOH; $PhCH_2C(Me)HNHOH$) was added to a microsomal suspension of sheep seminal vesicles under aerobic conditions in aqueous buffer (0.1M Tris–HCl, pH 8.1), a product with λ_{max} 424 nm in the difference absorption spectrum formed.[129] A similar reaction of purified reconsitituted PGHS with AmphNHOH under aerobic conditions also led to the formation of a similar product with λ_{max} 421 nm which did not form under anaerobic conditions. This 421 nm–absorbing species was proposed to be a (PGHS)Fe^{II}–AmphNO complex, since extraction with ethyl methyl ketone gave the non–protein (PPIX)Fe-(AmphNO) (PPIX = protoporphyrin(IX) dianion) species. The (PPIX)Fe(AmphNO) species was also obtained independently (eq 1.10). Incorporation of authentic ferrous (PPIX)Fe(AmphNO) into apoPGHS also generated the (PGHS)Fe^{II}(AmphNO) species .

$$\text{PGHS} \xrightarrow[\text{aerobic}]{\text{AmphNHOH}} \underset{\lambda_{max}\ 421\ nm}{\text{(PGHS)Fe}^{II}\text{-N(O)Amph}} \underset{\text{apoPGHS}}{\overset{\text{extraction}}{\rightleftharpoons}} \text{(PPIX)Fe-N(O)Amph} \qquad (1.10)$$

The analogous (PGHS)Fe^{II}–N(O)R complexes were also obtained from the reaction of other *N*–substituted hydroxylamines such as *i*–PrNHOH and PhNHOH with purified PGHS.

9. Microperoxidase

Several nitrosoalkane complexes of microperoxidase 8 with λ_{max} ~414 nm containing the Fe^{II}–RNO group (R = Me, Et, Pr, *i*–Pr, hexyl, cyclohexyl, $PhCH_2CH$-(Me)–, (*p*–ClC_6H_4)CH_2CH(Me)–) have been reported to be generated when microperoxidase 8 reacted with the hydroxylamine precursors or the nitroalkane precursors under reducing conditions.[130]

10. Heme model complexes

Metalloporphyrin complexes containing RNO ligands can generally be generated from the reactions of RNO compounds or the precursor hydroxylamines with synthetic metalloporphyrins. Such metalloporphyrin–nitrosoalkane complexes were obtained by Mansuy and coworkers for Fe from the reaction of the ferric porphyrin with the precursor hydroxylamines, and the (TPP)Fe(*i*–PrNO)(*i*–$PrNH_2$) complex was characterized by single–crystal X–ray crystallography.[131] The X–ray crystal structure of (TPP)Fe(*i*–PrNO)(*i*–$PrNH_2$) revealed the *N*–binding mode of the nitrosoalkane ligand. Our research group later demonstrated that the nature of binding of nitrosoarenes to iron porphyrins depended on a number of factors including the formal oxidation state of the iron center.[132] Thus, our group prepared the iron porphyrin nitrosoarene complexes with different oxidation states to examine the binding mode of nitrosoarenes to the metal center. Interestingly, the solid–state structure of the formally *ferrous* complex (TPP)Fe$(PhNO)_2$ revealed an *N*–binding mode of the PhNO ligands (Figure 1.9, left), whereas the corresponding structure of the *ferric* complex $[(TPP)Fe(ONAr)_2]^+$ (Ar = *p*–amino-substituted benzene) revealed an *O*–binding mode of the nitrosoarene ligands (Figure 1.9, right), presumably due to the contribution of the dipolar resonance form (Figure 1.10).

Metalloporphyrin *C*–nitroso complexes have been reported by our research group and several other groups for Mn,[133] Fe,[119,127,131,134-136] Ru,[137,138] Os,[139] and Co.[138] There are two examples (Fe and Mn) displaying the *O*–binding mode of the *C*–nitroso ligand,

Table 1.3. Selected Structural Data for *C*–Nitroso Complexes of Metalloporphyrins

Compound	C-N (Å)	N-O (Å)	C-N-O (°)	refs
N-bonded C-nitroso groups				
(TPP)Fe(*i*-PrNO)(*i*-PrNH$_2$) [a]	1.55(2) 1.54(2)	1.26(2) 1.26(2)	117(1) 115(1)	[131]
(TPP)Fe(PhNO)$_2$	1.468(4) 1.467(3)	1.237(3) 1.227(3)	112.4(2) 112.6(2)	[132]
(TPP)Fe(PhNO)(py)	1.472(4)	1.249(4)	113.2(3)	[136]
(TPP)Fe(N(O)C$_6$H$_4$NMe$_2$-*p*)(py)	1.437(8)	1.252(6)	112.3(6)	[136]
(TPP)Fe(PhNO)(1-MeIm) [a]	1.444(9) - 1.453(2)	1.254(8) - 1.267(3)	109.9(3) - 111.2(8)	[136]

(OEP)Fe(PhNO)(1-MeIm) [a]	1.448(6) 1.454(6)	1.269(5) 1.258(4)	111.7(4) 110.1(3)	[136]
$[(TPP)Co(N(O)C_6H_4NMe_2\text{-}p)_2]ClO_4$	1.35(2) 1.38(2)	1.33(2) 1.27(2)	109(2) 112(2)	[138]
$(OEP)Ru(N(O)C_6H_4NMe_2\text{-}p)_2$	1.453(7) 1.468(6)	1.248(7) 1.257(7)	115.9(5) 116.7(5)	[138]
$(TPP)Os(PhNO)_2$	1.469(5) 1.458(5)	1.249(4) 1.259(6)	112.4(3) 113.1(3)	[139]
$(TTP)Os(PhNO)_2$	1.475(14) 1.43(2)	1.298(13) 1.278(12)	109.3(11) 113.2(10)	[139]
$(TMP)Os(PhNO)_2$	1.40(2) 1.45(2)	1.31(2) 1.252(12)	110.4(12) 112.5(9)	[139]

(TTP)Os(CO)(PhNO)	1.39(3)	1.26(2)	120(2)	[139]
(OEP)Os(*o*-tolNO)$_2$	1.481(14) 1.441(14)	1.273(13) 1.219(12)	108.8(9) 116.9(10)	[139]
O-bonded C-nitroso groups				
[(TPP)Fe(ONC$_6$H$_4$NEt$_2$)$_2$]SbF$_6$	1.323(11) 1.413(13) [b]	1.157(6) 1.062(8) [b]	118.7(7) 121.8(9) [b]	[132]
[(TPP)Mn(ONC$_6$H$_4$NEt$_2$)$_2$]SbF$_6$	1.36(2) 1.356(13) [b]	1.057(10) 1.109(8) [b]	121.9(12) 122.0(9) [b]	[133]

[a] Two molecules in the unit cell.

[b] Data for the disordered component.

however, all other complexes that have been structurally characterized by X-ray crystallography display the *N*-binding mode. Single-crystal X-ray crystallographic data for *C*-nitroso complexes of metalloporphyrins are listed in Table 1.3.

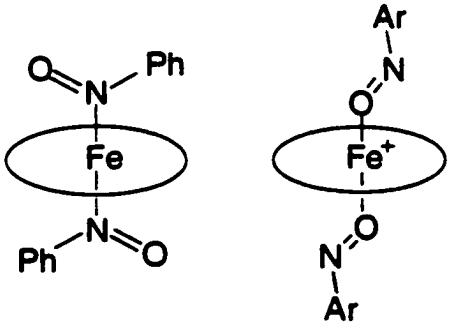

(Ar = *p*-$R_2NC_6H_4$)

Figure 1.9. Nitrosoarene binding modes in ferrous (left) and ferric (right) porphyrins.

Figure 1.10. Resonance forms of the *C*-nitroso *p*-$ONC_6H_4NR_2$.

III. Conclusion

In this chapter, I have attempted to present and discuss the fundamental issues involved in the chemistry and biochemistry of organic *S*-nitroso and *C*-nitroso compounds. With the increased attention given to the role of heme in binding and activation of biologically important nitroso compounds, further studies of the interactions of organic nitroso compounds with synthetic metalloporphyrins as heme models continue to be needed to better understand their chemical behavior in the presence of heme.

IV. References

(1) Richter-Addo, G. B.; Legzdins, P. *Metal Nitrosyls*; Oxford University Press: New York, 1992.

(2) Schrammel, A.; Pfeiffer, S.; Schmidt, K.; Koesling, D.; Mayer, B. *Mol. Pharmacol.* **1998**, *54*, 207-212.

(3) Mathews, W. R.; Kerr, S. W. *J. Pharmacol. Exp. Ther.* **1993**, *267*, 1529-1537.

(4) Williams, D. L. H. *Nitrosation*; Cambridge University Press: Cambridge, U. K., 1988.

(5) Oae, S.; Shinhama, K.; Fujimori, K.; Kim, Y. H. *Bull. Chem. Soc. Jpn.* **1980**, *53*, 775-784.

(6) Oae, S.; Shinhama, K. *Org. Prep. Proced. Int.* **1983**, *15*, 165-198.

(7) Doyle, M. P.; Terpstra, J. W.; Pickering, R. A.; LePoire, D. M. *J. Org. Chem.* **1983**, *48*, 3379-3382.

(8) Roy, B.; d'Hardemare, A. d. M.; Fontecave, M. *J. Org. Chem.* **1994**, *59*, 7019-7026.

(9) Crookes, M. J.; Williams, D. L. H. *J. Chem. Soc., Perkin Trans. 2* **1989**, 759-763.

(10) Patel, H. M. S.; Williams, D. L. H. *J. Chem. Soc., Perkin Trans. 2* **1990**, 37-42.

(11) Clancy, R.; Cederbaum, A. I.; Stoyanovsky, D. A. *J. Med. Chem.* **2001**, *44*, 2035-2038.

(12) Doyle, M. P.; Pickering, R. A.; da Conceição, J. *J. Biol. Chem.* **1984**, *259*, 80-87.

(13) Kharitonov, V. G.; Sundquist, A. R.; Sharma, V. S. *J. Biol. Chem.* **1995**, *270*, 28158-28164.

(14) Williams, D. L. H. *Acc. Chem. Res.* **1999**, *32*, 869-876.

(15) Arulsamy, N.; Bohle, D. S.; Butt, J. A.; Irvine, G. J.; Jordan, P. A.; Sagan, E. *J. Am. Chem. Soc.* **1999**, *121*, 7115-7123.

(16) Field, L.; Dilts, R. V.; Ravichandran, R.; Lenhert, P. G.; Carnahan, G. E. *J. Chem. Soc., Chem. Commun.* **1978**, 249-250.

(17) Carnahan, G. E.; Lenhert, P. G.; Ravichandran, R. *Acta Crystallogr.* **1978**, *B34*, 2645-2648.

(18) Bartberger, M. D.; Houk, K. N.; Powell, S. C.; Mannion, J. D.; Lo, K. Y.; Stamler, J. S.; Toone, E. J. *J. Am. Chem. Soc.* **2000**, *122*, 5889-5890.

(19) Goto, K.; Hino, Y.; Kawashima, T.; Kaminaga, M.; Yano, E.; Yamamoto, G.; Takagi, N.; Nagase, S. *Tetrahedron Lett.* **2000**, *41*, 8479-8483.

(20) Chan, N.-L.; Rogers, P. H.; Arnone, A. *Biochemistry* **1998**, *37*, 16459-16464.

(21) (a) Al-Sa'doni; Ferro, A. *Clinical Science* **2000**, *98*, 507-520. (b) Wang, P. G.; Xian, M.; Tang, X.; Wu, X.; Wen, Z.; Cai, T.; Janczuk, A. J. *Chem. Rev.* **2002**, *102*, 1091-1134.

(22) Lu, J.-M.; Wittbrodt, J. M.; Wang, K.; Wen, Z.; Schlegel, H. B.; Wang, P. G.; Cheng, J.-P. *J. Am. Chem. Soc.* **2001**, *123*, 2903-2904.

(23) Al-Kaabi, S. S.; Williams, D. L. H.; Bonnett, R.; Ooi, S. L. *J. Chem. Soc., Perkin Trans. 2* **1982**, 227-230.

(24) Tsikas, D.; Sandmann, J.; Rossa, S.; Gutzki, F.-M.; Frolich, J. C. *Anal. Biochem.* **1999**, *270*, 231-241.

(25) Stone, J. R.; Marletta, M. A. *Biochemistry* **1995**, *34*, 16397-16403.

(26) Yi, G.-B.; Khan, M. A.; Richter-Addo, G. B. *Chem. Commun.* **1996**, 2045-2046.

(27) Yi, G.-B.; Chen, L.; Khan, M. A.; Richter-Addo, G. B. *Inorg. Chem.* **1997**, *36*, 3876-3885.

(28) Chen, L.; Khan, M. A.; Richter-Addo, G. B. *Inorg. Chem.* **1998**, *37*, 533-540.

(29) Yi, G.-B.; Khan, M. A.; Powell, D. R.; Richter-Addo, G. B. *Inorg. Chem.* **1998**, *37*, 208-214.

(30) Richter-Addo, G. B. *Acc. Chem. Res.* **1999**, *32*, 529-536.

(31) Andreasen, L. V.; Lorkovic, I. M.; Richter-Addo, G. B.; Ford, P. C. *Nitric Oxide: Biol. Chem.* **2002**, *6*, 228-235.

(32) Butler, A. R.; Elkins-Daukes, S.; Parkin, D.; Williams, D. L. H. *Chem. Commun.* **2001**, 1732-1733.

(33) Filehne, W. *Arch. Exptl. Pathol. Pharmakol.* **1878**, *9*, 329.

(34) Loeb, R. F.; Bock, A. V.; Fitz, R. *Am. J. Med. Sci.* **1921**, *161*, 539-546. CA515:1761.

(35) Murayama, M. *J. Biol. Chem.* **1960**, *235*, 1024-1028.

(36) Coombes, R. G. *Comprehensive Org. Chem.* **1979**, *2*, 305-317.

(37) Bosch, E.; Kochi, J. K. *J. Org. Chem.* **1994**, *59*, 5573-5586.

(38) Leis, J. R.; Ríos, A.; Rodriguez-Sánchez, L. *J. Chem. Soc., Perkin Trans. 2* **1998**, 2729-2733.

(39) Robson, E.; Tedder, J. M.; Woodcock, D. J. *J. Chem. Soc. (C)* **1968**, 1324-1328.

(40) Banus, J. *J. Chem. Soc.* **1953**, 3755-3761.

(41) Banus, J. *Nature* **1953**, *171*, 173-174.

(42) Rao, C. N. R.; Bhaskar, K. R. In *The Chemistry of the Nitro and NItroso Groups. Part 1.*; Feuer, H., Ed.; Interscience: New York, 1969; pp 137-163 (Chapter 3).

(43) Gowenlock, B. G.; Spedding, H.; Trotman, J.; Whiffen, D. *J. Chem. Soc.* **1957**, *160*, 3927-3930.

(44) Gilchrist, T. L. *Chem. Soc. Rev.* **1983**, *12*, 53-73.

(45) Fletcher, D. A.; Gowenlock, B. G.; Orrell, K. G. *J. Chem. Soc., Perkin Trans. 2* **1997**, 2201-2205.

(46) Orrell, K. G.; Sik, V.; Stephenson, D. *Magn. Reson. Chem.* **1987**, *25*, 1007-1011.

(47) Turner, P. H.; Cox, A. P. *J. Chem. Soc., Faraday Trans. 2* **1976**, *74*, 533-559.

(48) Coffey, D., Jr.; Britt, C. O.; Boggs, J. E. *J. Chem. Phys.* **1968**, *49*, 591-600.

(49) Germain, P. G.; Piret, P.; Van Meerssche, M. *Acta Crystallogr.* **1963**, *16*, 109-112.

(50) Van Meerssche, M.; Germain, G. *Bull. Soc. Chim. Belg.* **1959**, *68*, 244-257.

(51) Davis, M. I.; Boggs, J. E.; Coffey, D., Jr.; Hanson, H. P. *J. Phys. Chem.* **1965**, *69*, 3727-3730.

(52) Bauer, S. H.; Andreassen, A. L. *J. Phys. Chem.* **1972**, *76*, 3099-3108.

(53) Turner, P. H.; Cox, A. P. *Chem. Phys. Lett.* **1976**, *39*, 585-587.

(54) Smart, B. A.; Brain, P. T.; Robertson, H. E.; Rankin, D. W. H. *Inorg. Chem.* **1998**, *37*, 2687-2692.

(55) Cox, A. P.; Hardy, J. A.; Randell, J.; Kroto, H. W.; Maier, M.; Milverton, D. R. *J. Chem. Soc., Faraday Trans. 2* **1994**, *90*, 2171-2182.

(56) Boer, F. P.; Turley, J. W. *J. Am. Chem. Soc.* **1969**, *91*, 1371-1375.

(57) Chiu, K. W.; Savage, P. D.; Wilkinson, G.; Williams, D. J. *Polyhedron* **1985**, *4*, 1941-1945.

(58) Dietrich, H.; Hodgkin, D. C. *J. Chem. Soc.* **1961**, *164*, 3686-3690.

(59) Gowenlock, B. G.; McCullough, K. J.; Manson, R. B. *J. Chem. Soc., Perkin Trans. 2* **1988**, 701-703.

(60) Tinant, B.; Declercq, J. P. *Bull. Soc. Chim. Belg.* **1987**, *96*, 149-163.

(61) Herzog, A.; Knobler, C. B.; Hawthorne, M. F. *Angew. Chem., Int. Ed. Engl.* **1998**, *37*, 1552-1556.

(62) Greer, M. L.; Sarker, H.; Mendicino, M. E.; Blackstock, S. C. *J. Am. Chem. Soc.* **1995**, *117*, 10460-10467.

(63) Prout, K.; Stothard, V. P.; Watkin, D. J. *Acta Crystallogr.* **1978**, *34B*, 2602-2605.

(64) Blackstock, S. C.; Poehling, K.; Greer, M. L. *J. Am. Chem. Soc.* **1995**, *117*, 6617 and 6618. Blackstock, S. C.; Poehling, K.; Greer, M. L. *J. Am. Chem. Soc.* **1997**, *119*, 1498 [Erratum].

(65) Jorgensen, P.; Koksbang, R.; Lindhardt, P. *Acta Crystallogr.* **1986**, *C42*, 1273-1274.

(66) de Boer, J. S. A. M.; Schenk, H. *J. Royal Netherlands Chem. Soc. (Rec. Trav. Chim. Pays-Bas)* **1995**, *114*, 395-397.

(67) Marsden, H. M.; Oberhammer, H.; Shreeve, J. M. *Inorg. Chem.* **1985**, *24*, 4756-4758.

(68) Kai, Y.; Knochel, P.; Kwiatkowski, S.; Dunitz, J. D.; Oth, J. F. M.; Seebach, D.; Kalinowski, H.-O. *Helv. Chim. Acta* **1982**, *65*, 137-161.

(69) Tanimura, M.; Kobori, K.; Kashigawa, M.; Kinoshita, Y. *Bull. Chem. Soc. Jpn.* **1970**, *43*, 1962-1966.

(70) Felber, H.; Kresze, G.; Prewo, R.; Vasella, A. *Helv. Chim. Acta* **1986**, *69*, 1137-1146.

(71) Hall, A.; Bailey, P. D.; Rees, D. C.; Rosair, G. M.; Wightman, R. H. *J. Chem. Soc., Perkin Trans. 1* **2000**, 329-343.

(72) Miao, F. M.; Chantry, D.; Harper, T.; Hodgkin, D. C. *Acta Cryst.* **1982**, *B38*, 3152-3155.

(73) Ferguson, G.; Fritchie, C. J.; Robertson, J. M.; Sim, G. A. *J. Chem. Soc.* **1961**, 1976-1987.

(74) Gieren, A.; Siebels, H.-J. *Angew. Chem., Int. Ed. Engl.* **1976**, *15*, 760-761.

(75) Freer, A. A.; MacAlpine, D. K.; Peacock, J. A.; Porte, A. L. *J. Chem. Soc., Perkin Trans. 2* **1985**, 971-982.

(76) MacAlpine, D. K.; Porte, A. L.; Sim, G. A. *J. Chem. Soc., Perkin Trans. 1* **1982**, 1385-1388.

(77) Khan, Z. F.; MacAlpine, D. K.; Porte, A. L.; Sim, G. A. *J. Chem. Soc., Perkin Trans. 2* **1983**, 1259-1261.

(78) Dietrich, D. A.; Paul, I. C.; Curtin, D. Y. *J. Am. Chem. Soc.* **1974**, *96*, 6372-6380.

(79) Fletcher, D. A.; Gowenlock, B. G.; Orrell, K. G.; Apperley, D. C.; Hursthouse, M. B.; Malik, K. M. A. *J. Chem. Res. (S)* **1999**, 202-203.

(80) Darwin, C.; Hodgkin, D. C. *Nature* **1950**, *166*, 827-828.

(81) Fletcher, D. A.; Gowenlock, B. G.; Orrell, K. G.; Sik, V.; Hibbs, D. E.; Hursthouse, M. B.; Malik, K. M. A. *J. Chem. Soc., Perkin Trans. 2* **1996**, 191-197.

(82) Webster, M. S. *J. Chem. Soc.* **1956**, 2841-2845.

(83) Talberg, H. J. *Acta Chem. Scand.* **1979**, *33A*, 289-296.

(84) Simonov, Y. A.; Lipkowski, J.; Suwinska, K.; Fonar, M. S.; Ganin, E. V.; Malinovskii, T. I. *Crystallogr. Reports* **1995**, *40*, 47-54.

(85) Romming, C.; Talberg, H. J. *Acta Chem. Scand.* **1973**, *27*, 2246-2248.

(86) Lewinski, K.; Nitek, W.; Milart, P. *Acta Cryst.* **1993**, *C49*, 188-190.

(87) Talberg, H. J. *Acta. Chem. Scand. A* **1977**, *31*, 743-751.

(88) Dhaneshwar, N. N.; Naik, S. N.; Tavale, S. S. *Acta Cryst.* **1991**, *C47*, 217-218.

(89) Talberg, H. J. *Acta Chem. Scand.* **1977**, *31A*, 485-491.

(90) Talberg, H. J. *Acta Chem. Scand.* **1976**, *30A*, 829-834.

(91) Azoulay, M.; Trysberg, L. *J. Appl. Cryst.* **1982**, *15*, 245-246.

(92) Gowenlock, B. G.; McCullough, K. J. *J. chem. Soc., Perkin Trans. 2* **1989**, 551-553.

(93) Samsonov, V. A.; Volodarsky, L. B.; Bagryanskaya, I. Y.; Gatilov, Y. U.; Shakirov, M. M. *Khi. Get. Soedin., SSSR* **1995**, 395-402.

(94) Talberg, H. J. *Acta Chem. Scand.* **1978**, *32A*, 401-405.

(95) Pritchard, R. G.; Heaton, G. S.; El-Nahhal, I. M. *Acta Cryst.* **1989**, *C45*, 829-831.

(96) Rowan, K. R.; Holt, E. M. *Acta Cryst.* **1995**, *C51*, 2554-2559.

(97) Fenimore, C. P. *J. Am. Chem. Soc.* **1950**, *72*, 3226-3231.

(98) Prout, C. K.; Coda, A.; Forder, R. A.; Kamenar, B. *Cryst. Struct. Commun.* **1974**, *3*, 39-42.

(99) Dunlop, R.; Hardy, A. D. U.; Mills, H. H.; Mackenzie, R. K.; MacNicol, D. D.; Williams, D. A. R. *J. Chem. Res.* **1979**, *152*, 1848-1873.

(100) Prout, C. K.; Cameron, T. S.; Dunn, R. M. A.; Hodder, O. J. R.; Viterbo, D. *Acta Crystallogr.* **1971**, *B27*, 1310-1314.

(101) Banks, R. E.; Djebli, Y.; Fields, R.; Olawore, N. O.; Pritchard, R. G.; Tsiliopoulos, E.; Mason, J. *J. Chem. Soc., Perkin Trans. 1* **1989**, 1117-1125.

(102) Prout, K.; Miao, F. M. *Acta Cryst.* **1982**, *B38*, 685-687.

(103) Prout, K.; Miao, F. M. *Acta Crystallogr.* **1982**, *B38*, 687-689.

(104) Lide, D. R., Ed. *Handbook of Chemistry and Physics*; 72 ed.; CRC Press:, 1991-1992.

(105) Fukuto, J. M.; Di Stefano, E. W.; Burstyn, J. N.; Valentine, J. S.; Cho, A. K. *Biochemistry* **1985**, *24*, 4161-4167.

(106) Kiese, M.; Schneider, C.; Waller, H. D. *Arch. Exptl. Pathol. Pharmakol.* **1957**, *231*, 158-169, and 170-175, and 176-178. *Chem. Abs.* **1957**, *151*,18039c-i.

(107) Kiese, M. *Arch. Exptl. Pathol. Pharmakol.* **1959**, *235*, 351-353, and 354-359, and 360-364. *Chem. Abs.* 53:2055*1a,h,i.*

(108) Kiese, M. *Arch. Exptl. Pathol. Pharmakol.* **1959**, *236*, 19-20. *Chem. Abs.* 53:9476b.

(109) Haan, J.; Kiese, M.; Werner, A. *Arch. Exptl. Pathol. Pharmakol.* **1959**, *235*, 365-372. *Chem. Abs.* 53:13407h.

(110) Kiese, M.; Plattig, K. H. *Arch. Exptl. Pathol. Pharmakol.* **1959**, *235*, 373-380. *Chem. Abs.* 53:13407i.

(111) Ellis, M. K.; Foster, P. M. D. *Toxicol. Lett.* **1992**, *62*, 201-208.

(112) Eyer, P.; Kampffmeyer, H.; Maister, H.; Rosch-Oehme, E. *Xenobiotica* **1980**, *10*, 499-516.

(113) Eyer, P.; Lierheimer, E. *Xenobiotica* **1980**, *10*, 517-526.

(114) O'Brien, P. J.; Wong, W. C.; Silva, J.; Khan, S. *Xenobiotica* **1990**, *20*, 945-955.

(115) Eyer, P. *Xenobiotica* **1988**, *18*, 1327-1333.

(116) Kiese, M. *Pharmacol. Rev.* **1966**, *18*, 1091-1161.

(117) Mansuy, D.; Chottard, J. C.; Chottard, G. *Eur. J. Biochem.* **1977**, *76*, 617-623.

(118) Mansuy, D.; Beaune, P.; Chottard, J. C.; Bartoli, J. F.; Gans, P. *Biochem. Pharmacol.* **1976**, *25*, 609-612.

(119) Mansuy, D.; Battioni, P.; Chottard, J. C.; Lange, M. *J. Am. Chem. Soc.* **1977**, *99*, 6441-6443.

(120) Mansuy, D.; Beaune, P.; Cresteil, T.; Bacot, C.; Chottard, J.-C.; Gans, P. *Eur. J. Biochem.* **1978**, *86*, 573-579.

(121) Chottard, G.; Mansuy, D. *Biochem. Biophys. Res. Commun.* **1977**, *77*, 1333-1338.

(122) Eyer, P.; Lierheimer, E.; Schneller, M. *Biochem. Pharmacol.* **1984**, *33*, 2299-2308.

(123) Hirota, K.; Itano, H. A. *J. Biol. Chem.* **1978**, *253*, 3477-3481.

(124) Gibson, Q. H. *Biochem. J.* **1960**, *77*, 519-526.

(125) Scheler, W. *Naturwissenschaften* **1960**, *47*, 399.

(126) Vainshtein, B. K.; Harutyunyan, E. H.; Kuranova, I. P.; Borisov, V. V.; Sosfenov, N. I.; Pavlovsky, A. G.; Grebenko, A. I.; Konareva, N. V. *Protein Data Bank* **1982**, *Structure 1LH7 and 2LH7.*

(127) Fukuto, J. M.; Brady, J. F.; Burstyn, J. N.; VanAtta, R. B.; Valentine, J. S.; Cho, A. K. *Biochemistry* **1986**, *25*, 2714-2719.

(128) Renodon, A.; Boucher, J.-L.; Wu, C.; Gachhui, R.; Sari, M.-A.; Mansuy, D.; Stuehr, D. *Biochemistry* **1998**, *37*, 6367-6374.

(129) Mahy, J. P.; Mansuy, D. *Biochemistry* **1991**, *30*, 4165-4172.

(130) Ricoux, R.; Boucher, J.-L.; Mansuy, D.; Mahy, J.-P. *Biochem. Biophys. Res. Commun.* **2000**, *278*, 217-223.

(131) Mansuy, D.; Battioni, P.; Chottard, J.-C.; Riche, C.; Chiaroni, A. *J. Am. Chem. Soc.* **1983**, *105*, 455-463.

(132) Wang, L.-S.; Chen, L.; Khan, M. A.; Richter-Addo, G. B. *Chem. Commun.* **1996**, 323-324.

(133) Fox, S. J.; Chen, L.; Khan, M. A.; Richter-Addo, G. B. *Inorg. Chem.* **1997**, *36*, 6465-6467.

(134) Mansuy, D.; Battioni, J. P.; Chottard, J. C. *J. Am. Chem. Soc.* **1978**, *100*, 4311-4312.

(135) Ozaki, H.; Kinuta, M.; Matteson, J. L.; Itano, H. A. *Biochem. Biophys. Acta* **1988**, *955*, 220-230.

(136) Godbout, N.; Sanders, L. K.; Salzmann, R.; Havlin, R. H.; Wojdelski, M.; Oldfield, E. *J. Am. Chem. Soc.* **1999**, *121*, 3829-3844.

(137) Crotti, C.; Sishta, C.; Pacheco, A.; James, B. R. *Inorg. Chim. Acta* **1988**, *141*, 13-15.

(138) Chen, L.; Fox, J. B., Jr.; Yi, G.-B.; Khan, M. A.; Richter-Addo, G. B. *J. Porph. Phthalocyanines* **2001**, *5*, 702-707.

(139) Chen, L.; Khan, M. A.; Richter-Addo, G. B.; Young, V. G., Jr.; Powell, D. R. *Inorg. Chem.* **1998**, *37*, 4689-4696.

Chapter 2. Synthesis, Characterization, and Protonation of Octaethylporphyrin Osmium Nitrosyl Complexes Containing Axial Thiolate Ligands*

Introduction

The renewed interest in the *S*–nitroso compounds (RSNO, thionitrites) stems from the fact that the chemistry of the *S*–nitroso functional group in RSNO is linked to the biology of nitric oxide, although the exact physiological relationship between RSNO and NO remains to be discerned. For example, as described in detail in Chapter 1, thiol groups (RSH) in proteins can be nitrosated,[1-4] and it has been reported that the nitrosation of the βCys93 residue of hemoglobin can occur under some conditions.[5-8] The X–ray structure of *S*–nitrosated hemoglobin has also been reported.[9]

The chemistry of RSNO compounds has been investigated by many research groups, and excellent reviews on this topic have been published.[10-16] A major breakthrough in the chemistry of RSNO compounds came when Butler, Williams, and coworkers reported that some trace metals (e.g., copper in buffered solutions) catalyze the decomposition of the *S*–nitroso functional group.[17] They have observed that when trace metal ions are removed by addition of the metal ion chelator EDTA, the RSNO decomposition was essentially halted, and the addition of excess metal ions re–established the RSNO decomposition. It has now been established that for the copper ion–catalyzed RSNO decomposition reaction, the active species is Cu^{+}, which is generated by the reduction of Cu^{2+} by thiolate anion (eqs 2.1 and 2.2).[12,18]

---

* Reproduced in part with permission from "Synthesis, Characterization, and Protonation of Octaethylporphyrin Osmium Nitrosyl Complexes Containing Axial Thiolate Ligands-X-ray Structures of an Alkyl Thionitrite (RSNO) and its (OEP)Os(NO)(SR) Addition Product." Lee, J.; Yi, G.-B.; Powell, D. R.; Khan, M. A.; Richter-Addo, G. B. *Can. J. Chem.* **2001**, *79*, 830-840.

$$Cu^{2+} + RS^- \rightarrow Cu^+ + 1/2\,RSSR \quad (2.1)$$

$$Cu^+ + RSNO \rightarrow Cu^{2+} + RS^- + NO \quad (2.2)$$

The structures of the initially–formed Cu^+–RSNO adducts (formed just prior to RSNO decomposition) are not known, and both *S*–bound and *N*–bound structures have been considered (Figure 2.1).[12] Indeed, the role of metal ions in the decomposition of biologically–active thionitrites (RSNO) continues to receive renewed attention in chemistry and biochemistry of nitric oxide.

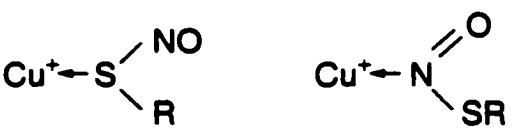

Figure 2.1. Two possible structures of the initially–formed Cu^+–RSNO adducts (formed just prior to RSNO decomposition).

Our research group has also shown that metalloporphyrin carbonyl compounds of the Group 8 metals (Ru and Os) react with RSNO to give the formal *trans*–addition products, via initial *S*–coordination of the RSNO molecule which results in NO release, followed by NO displacement of the CO ligand (Scheme 2.1).[11,19-22]

Scheme 2.1

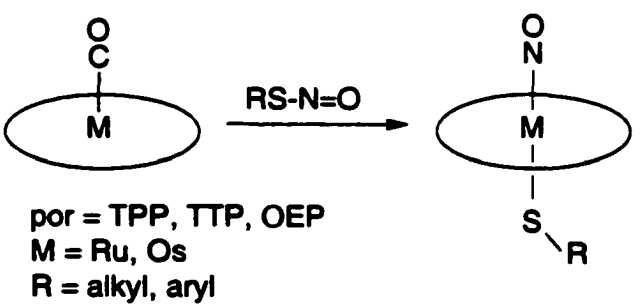

Our research group was also interested in the chemical and spectroscopic properties of the resulting six–coordinate (por)M(NO)(SR) compounds, since these are potential structural models for the NO adduct of the (por)Fe(SR) groups in cytochrome P450, chloroperoxidase, and NO synthase.[23] Furthermore, our group has been intrigued by the recent results on the reaction chemistry of the (por)M(NO)(SR) compounds. Of particular interest was our report that protonation of the ruthenium nitrosyl porphyrin complex containing an amide–thiol ligand results in an *S*–bound to *O*–bound linkage switch.[21]

In this chapter, the syntheses and characterization of an extended series of (OEP)Os(NO)(SR) compounds (R = Me, Et, ^{i}Pr, ^{t}Bu, $C(Me)_2CH_2NHC(O)Me$, CH_2CH_2-NHC(O)Me) will be discussed. Prior to this work, the *trans*–additions of RSNO to metalloporphyrins have mainly been performed for *primary* alkyl thionitrites. Only one other example of thionitrite *trans*–addition was reported for the *tertiary* alkyl thionitrite, namely $MeC(O)NHCH_2C(Me)_2SNO$.[21] Our research group was thus interested in extending the *trans*–addition reactions to *secondary* alkyl thionitrites, and also determining whether the change of "R" group in RSNO compounds makes a difference in the reactivity of RSNO (in the *trans*–addition) and in the spectroscopy of the final product. Protonation of two (OEP)Os(NO)($SCR_2CH_2NHC(O)Me$) (R = Me, H) compounds will also be described. Furthermore, the single–crystal X–ray structure of an organic thionitrite $MeC(O)NHCH_2C(Me)_2SNO$ will be reported, and will be compared with the X–ray crystal structure of its (OEP)Os(NO)(SR) addition product which was independently obtained by Dr. Geun–Bae Yi of our research group. Prior to this work, somewhat surprisingly, only four crystal structures of organic RSNO compounds had been reported, despite the recognized importance of RSNO chemistry. This chapter contains, to the best of my knowledge, the first RSNO/metal–complex pair to be characterized by X–ray crystallography. The molecular structure of the disulfide $\{MeC(O)NHCH_2C(Me)_2S–\}_2$ will also be reported.

Experimental Section

All reactions were performed under an atmosphere of prepurified nitrogen using standard Schlenk glassware and/or in an Innovative Technology Labmaster 100 Dry Box. Solutions for spectral studies were also prepared under a nitrogen atmosphere. Solvents were distilled from appropriate drying agents under nitrogen just prior to use: CH_2Cl_2 (CaH_2), hexane (CaH_2), toluene (Na).

Chemicals. (OEP)Os(CO) was prepared by literature method.[24] HBF_4 (54 wt% solution in Et_2O), $NOBF_4$, MeOH (99.8%, anhydrous), isoamyl nitrite (i–$C_5H_{11}ONO$, 97%), ^{t}BuONO (96%), methanethiol (CH_3SH, 99.5+%), ethanethiol (C_2H_5SH, 97%), 2–propanethiol ($(CH_3)_2CHSH$, 97+%), 2–methyl–2–propanethiol ($(CH_3)_3CSH$, 99%), and *N*–Acetylcysteamine (95%) were purchased from Aldrich Chemical Co. and used as received. The thionitrite $MeC(O)NHCH_2C(Me)_2SNO$ was prepared by a literature procedure.[25] Chloroform–*d* (99.8%) was obtained from Cambridge Isotope Laboratories. Elemental analyses were performed by Atlantic Microlab, Norcross, Georgia. The thionitrites (RSNO) were generated *in situ* from the reaction of ^{t}BuONO and their thiol precursors either at low temperature (R = Me) or at room temperature (R = Et, ^{i}Pr, ^{t}Bu).

Instrumentation. Infrared spectra were recorded on a Bio–Rad FT–155 FTIR spectrometer. Proton NMR spectra were obtained on Varian 400 MHz or 300 MHz spectrometers and the signals referenced to the residual signal of the solvent employed. All coupling constants are in Hz. FAB mass spectra were obtained on a VG–ZAB–E mass spectrometer. UV–vis spectra were recorded on a Hewlett–Packard model 8453 diode array instrument. Wavelengths are reported with ε values or as %–intensities for the samples whose yields were too small for accurate concentration measurements.

Preparation of (OEP)Os(NO)(SR) Compounds (R= Me, Et, ^{i}Pr, ^{t}Bu). These compounds were synthesized via a formal *trans*–addition of the RSNO across the metal center. The following reaction is representative:

To a stirred CH_2Cl_2 solution (20 mL) of (OEP)Os(CO) (0.080 g, 0.107 mmol) was added a previously prepared green mixture of 2–methyl–2–propanethiol and ^{t}BuONO (1:1.1 ratio by volume, 1:1 mol ratio, 0.16 mL in 4 mL of CH_2Cl_2, 10 min mixing time). The mixture was stirred for 30 min, during which it turned from pink red to slightly dark red. The solvent was removed in vacuo, the residue was dissolved in a CH_2Cl_2/hexane (1:3, 5 mL) mixture, and filtered through a neutral alumina column (2 x 20 cm) in air. The bright red band was collected, and the filtrate was dried in vacuo for 5 h to give (OEP)Os(NO)(S^{t}Bu)·0.9CH_2Cl_2 (0.041 g, 0.045 mmol, 42% isolated yield) as a red powder. Anal. Calcd for $C_{40}H_{53}N_5O_1S_1Os_1$·0.9$CH_2Cl_2$: C, 53.48; H, 6.01; N, 7.62; Cl, 6.95; S, 3.49. Found: C, 53.42; H, 5.95; N, 7.43; Cl, 6.75; S, 3.29. IR (CH_2Cl_2, cm^{-1}): υ_{NO} = 1758. IR (KBr, cm^{-1}): υ_{NO} = 1754 s; also 2964 m, 2932 m, 2871 m, 1468 m, 1452 m, 1382 w, 1375 w, 1316 w, 1272 m, 1154 m, 1112 w, 1056 m, 1021 m, 994 m, 963 m, 842 m, 745 m, 737 m, 718 w. ^{1}H NMR ($CDCl_3$): δ 10.29 (s, 4H, *meso*–H of OEP), 5.28 (s, CH_2Cl_2), 4.14 (m, 16H, CH_2CH$_3$ of OEP), 1.96 (t, J = 8, 24H, CH$_2$CH_3 of OEP), –2.19 (s, 9H, SC(CH_3)$_3$). Low–resolution mass spectrum (FAB): *m/z* 813 [(OEP)-Os(SC(CH$_3$)$_3$)]$^+$ (13%), 754 [(OEP)Os(NO)]$^+$ (100%), 724 [(OEP)Os]$^+$ (28%). UV–vis spectrum (λ, CH_2Cl_2): 357 (100), 446 (49), 551 (20), 585 (16) nm.

The other (OEP)Os(NO)(SR) compounds were generated similarly as red powders. The MeSNO reagent was prepared at low temperature (–78 °C) by reacting condensed methanethiol with ^{t}BuONO in CH_2Cl_2.

(OEP)Os(NO)(SMe). 48% isolated yield. IR (CH_2Cl_2, cm^{-1}): υ_{NO} = 1759. IR (KBr, cm^{-1}): υ_{NO} = 1755 s; also 2962 m, 2927 m, 2869 m, 1905 w, 1467 m, 1447 m, 1424 w, 1374 m, 1316 w, 1303 w, 1270 m, 1229 w, 1153 m, 1111 w, 1056 m, 1021 m, 994 m, 963 m, 873 w, 841 m, 802 w, 747 m, 737 m, 717 w. ^{1}H NMR ($CDCl_3$): δ 10.33 (s, 4H, *meso*–H of OEP), 4.17 (m, 16H, CH_2CH$_3$ of OEP), 2.01 (t, J = 8, 24H, CH$_2$CH_3 of OEP), –3.11 (s, 3H, SCH_3). Low–resolution mass spectrum (FAB): *m/z* 771 [(OEP)-

$Os(SCH_3)]^+$ (11%), 754 $[(OEP)Os(NO)]^+$ (100%), 724 $[(OEP)Os]^+$ (20%). UV–vis spectrum (λ (ε, $mM^{-1}\ cm^{-1}$), 1.64 x 10^{-5} M in CH_2Cl_2): 354 (53), 439 (28), 551 (12), 585 (9) nm.

(OEP)Os(NO)(SEt). 37% isolated yield. IR (CH_2Cl_2, cm^{-1}): υ_{NO} = 1758. IR (KBr, cm^{-1}): υ_{NO} = 1753 s; also 2964 m, 2929 m, 2868 m, 1640 w, 1584 w, 1466 m, 1450 m, 1373 w, 1314 w, 1272 m, 1230 w, 1153 m, 1112 w, 1057 m, 1021 m, 994 m, 964 m, 842 m, 802 w, 737 m, 718 w. ^1H NMR ($CDCl_3$): δ 10.30 (s, 4H, *meso*–H of OEP), 4.15 (m, 16H, CH_2CH_3 of OEP), 2.00 (t, J = 8, 24H, CH_2CH_3 of OEP), –1.85 (t, J = 8, 3H, SCH_2CH_3), –3.12 (q, J = 8, 2H, SCH_2CH_3). Low–resolution mass spectrum (FAB): *m/z* 815 $[(OEP)Os(NO)(SCH_2CH_3)]^+$ (6%), 754 $[(OEP)Os(NO)]^+$ (100%), 724 $[(OEP)Os]^+$ (22%). UV–vis spectrum (λ, CH_2Cl_2): 354 (100), 441 (55), 551 (22), 585 (17) nm.

(OEP)Os(NO)(S^{i}Pr). 33% isolated yield. IR (CH_2Cl_2, cm^{-1}): υ_{NO} = 1754. IR (KBr, cm^{-1}): υ_{NO} = 1751 s; also 2963 m, 2928 m, 2869 m, 1471 m, 1464 m, 1457 m,1442 w, 1374 w, 1314 w, 1271 m, 1230 w, 1154 m, 1110 w, 1056 m, 1020 m, 993 m, 963 m, 841 m, 746 m, 737 m, 718 w. ^1H NMR ($CDCl_3$): δ 10.30 (s, 4H, *meso*–H of OEP), 4.15 (q, J = 8, 16H, CH_2CH_3 of OEP), 1.98 (t, J = 8, 24H, CH_2CH_3 of OEP), –1.95 (d, J =7, 6H, $SCH(CH_3)_2$), –4.03 (m, 1H, $SCH(CH_3)_2$). Low–resolution mass spectrum (FAB): *m/z* 799 $[(OEP)Os(SCH(CH_3)_2)]^+$ (12%), 754 $[(OEP)Os(NO)]^+$ (100%), 724 $[(OEP)Os]^+$ (29%). UV–vis spectrum (λ, CH_2Cl_2): 354 (100), 441 (53), 551 (21), 585 (16) nm.

Preparation of (OEP)Os(NO)($SC(Me)_2CH_2NHC(O)Me$). To a stirred CH_2Cl_2 solution (20 mL) of (OEP)Os(CO) (0.080 g, 0.107 mmol) was added $MeC(O)NHCH_2$-$C(Me)_2SNO$ (0.019 g, 0.108 mmol). The mixture was stirred for 1 h, during which it turned from pink red to slightly dark red. The solvent was removed in vacuo, the residue was dissolved in CH_2Cl_2 (10 mL), and the solution was transferred to the top of an alumina column (2 x 20 cm). Elution with CH_2Cl_2 in air yielded a pale brown band and a

bright red band. The pale brown band was discarded, and the bright red band was collected and taken to dryness in vacuo. The resulting red product was identified as (OEP)Os(NO)(SC(Me)$_2$CH$_2$NHC(O)Me) (0.021 g, 0.023 mmol, 21% isolated yield). IR (CH_2Cl_2, cm^{-1}): υ_{NO} = 1773; υ_{CO} = 1681. IR (KBr, cm^{-1}): υ_{NO} = 1764 s; υ_{CO} = 1656 s br; also 2964 m, 2932 m, 2872 w, 1561 m, 1510 m, 1465 m, 1450 m, 1370 m, 1275 m, 1231 w, 1154 m, 1112 w, 1057 m, 1022 m, 995 m, 963 m, 845 m, 749 vs, 717 w. ^{1}H NMR ($CDCl_3$): δ 10.35 (s, 4H, *meso*–H of OEP), 4.16 (m, 16H, C*H*$_2$CH$_3$ of OEP), 1.98 (t, *J* = 8, 24H, CH$_2$C*H*$_3$ of OEP), 1.52 (br, 1H, SC(CH$_3$)$_2$CH$_2$N*H*C(O)CH$_3$), 1.23 (s, 3H, SC(CH$_3$)$_2$CH$_2$NHC(O)C*H*$_3$), –0.88 (d, *J* = 4, 2H, SC(CH$_3$)$_2$C*H*$_2$NHC(O)CH$_3$), –2.08 (s, 6H, SC(C*H*$_3$)$_2$CH$_2$NHC(O)CH$_3$). Low–resolution mass spectrum (FAB): *m/z* 870 [(OEP)Os(SC(Me)$_2$CH$_2$NHC(O)Me)]$^+$ (22%), 754 [(OEP)Os(NO)]$^+$ (100%), 724 [(OEP)Os]$^+$ (22%). UV–vis spectrum (λ, CH_2Cl_2): 357 (100), 443 (48), 552 (20), 585 (17) nm.

Prior to this study, (OEP)Os(NO)(SC(Me)$_2$CH$_2$NHC(O)Me) was also independently prepared for X–ray crystallographic study by Dr. Geun–Bae Yi of our research group.

Preparation of Disulfide {MeC(O)NHCH$_2$C(Me)$_2$S–}$_2$ (R'SSR') A MeOH solution of green thionitrite MeC(O)NHCH$_2$C(Me)$_2$SNO (0.010g, 0.057 mmol) was refluxed with vigorous stirring for 3 h under a nitrogen atmosphere, during which the color of the solution turned colorless. The solvent was dried in air, and a ^{1}H NMR spectrum of the residue in $CDCl_3$ showed the quantitative formation of the disulfide. ^{1}H NMR ($CDCl_3$) δ 5.80 (br, 2H), 3.30 (d, *J* = 6, 4H), 2.00 (s, 6H), 1.26 (s, 12H). Low–resolution mass spectrum (FAB): *m/z* 293 [R'SSR'+ H]$^+$ (76%), 146 [R'S]$^+$ (15%), 114 [R']$^+$ (100%).

This previously unreported disulfide was also prepared from the decomposition of thionitrite MeC(O)NHCH$_2$C(Me)$_2$SNO in a CH_2Cl_2/MeOH solution (1:10) by light. Suitable cryatals for X–ray crystallography were grown from a CH_2Cl_2/MeOH (1:10)

mixture of the thionitrite precursor that had been left at –10 °C under nitrogen for two weeks.

Preparation of (OEP)Os(NO)($SCH_2CH_2NHC(O)Me$). A mixture of (OEP)Os(NO)(O–*i*–C_5H_{11}) (0.050 g, 0.059 mmol)[22] and excess $HSCH_2CH_2NHC(O)Me$ (20 μL, 0.178 mmol) in xylene (20 mL) was refluxed under N_2 gas with vigorous stirring for 48 h. The solvent was removed in vacuo, and a ^1H NMR spectrum of the residue in $CDCl_3$ showed the presence of the desired thiolate product and unreacted excess thiol. The residue was dissolved in a CH_2Cl_2/hexane mixture (1:10, 55 mL), and this solution was kept at –20 °C overnight. Precipitation of the solid was enhanced by mixing of the CH_2Cl_2/hexane solution, and the supernatant solution was discarded. The remaining solid product was dried in vacuo, the residue was dissolved in a CH_2Cl_2/hexane (1:1, 5 mL) mixture, and the solution was transferred to the top of a neutral alumina column (1.5 x 15 cm). Elution with hexane in air removed unreacted thiol, and then elution with CH_2Cl_2 yielded a bright red band. This bright red band was collected and taken to dryness in vacuo. The residue was dissolved in a CH_2Cl_2/hexane (2:1, 15 mL) mixture, and slow evaporation of the solvent mixture in air gave (OEP)Os(NO)($SCH_2CH_2NHC(O)Me$) (0.034 g, 0.039 mmol, 66% isolated yield). IR (CH_2Cl_2, cm^{-1}): υ_{NO} = 1765; υ_{CO} = 1665. IR (KBr, cm^{-1}): υ_{NO} = 1756 s; υ_{CO} = 1642 m br; also 2964 m, 2930 m, 2870 m, 1465 m, 1444 m, 1372 m, 1273 m, 1230 w, 1154 m, 1111 w, 1056 m, 1020 m, 994 m, 963 m, 843 m, 745 m, 736 m, 717 w. ^1H NMR ($CDCl_3$): δ 10.34 (s, 4H, *meso*–H of OEP), 4.16 (m, 16H, CH_2CH_3 of OEP), 2.47 (br,1H, $SCH_2CH_2NHC(O)CH_3$), 2.00 (t, J = 8, 24H, CH_2CH_3 of OEP), 1.10 (s, 3H, $SCH_2CH_2NHC(O)CH_3$), 0.22 (m, 2H, $SCH_2CH_2NHC(O)CH_3$), –2.98 (m, 2H, $SCH_2CH_2NHC(O)CH_3$). Low–resolution mass spectrum (FAB): *m/z* 842 $[(OEP)Os(SCH_2CH_2NHC(O)Me)]^+$ (3%), 754 $[(OEP)Os(NO)]^+$ (100%), 724 $[(OEP)Os]^+$ (29%). UV–vis spectrum (λ (ε, mM^{-1} cm^{-1}), 1.61 x 10^{-5} M in CH_2Cl_2): 354 (60), 441 (32), 551 (13), 585 (10) nm.

Preparation of [(OEP)Os(NO)(O=C(Me)NHCH$_2$C(Me)$_2$SH)]BF$_4$. To a stirred CH_2Cl_2 solution (15 mL) of (OEP)Os(CO) (0.020 g, 0.027 mmol) was added $NOBF_4$ (0.003 g, 0.026 mmol). The color of the solution changed from pink red to slightly dark red over a 30 min period, and an IR spectrum in CH_2Cl_2 showed the replacement of the 1883 cm^{-1} assigned to the υ_{CO} of (OEP)Os(CO) with a new band at 1833 cm^{-1} assigned to the υ_{NO} of [(OEP)Os(NO)]BF_4. Solid HSC(Me)$_2$CH$_2$NHC(O)Me (0.004 g, 0.027 mmol) was then added to the reaction solution, and the mixture was stirred overnight. The solvent was removed in vacuo, and a ^{1}H NMR spectrum of the residue in $CDCl_3$ showed the presence of the desired product and a small amount of the known (OEP)Os(NO)F. The residue was dissolved in a CH_2Cl_2/hexane (1:10, 55 mL), and this solution was kept at –20 °C overnight. Precipitation of the solid was enhanced by mixing of the CH_2Cl_2/hexane solution, and the supernatant solution was discarded. The remaining solid product was washed with hexane (3 x 50 mL), and dried in vacuo. The resulting product was identified as pure [(OEP)Os(NO)(O=C(Me)NHCH$_2$C(Me)$_2$SH)]-BF_4 (0.012 g, 0.012 mmol, 46% isolated yield) by ^{1}H NMR. IR (CH_2Cl_2, cm^{-1}): υ_{NO} = 1826; υ_{CO} = 1599. IR (KBr, cm^{-1}): υ_{NO} = 1816 vs; υ_{CO} =1594 s br; also 2968 s, 2933 s, 2871 m, 1470 m, 1464 m, 1452 m, 1379 w, 1352 w, 1274 m, 1156 m, 1112 w, 1085 m, 1056 s, 1023 s, 996 m, 965 m, 849 m, 745 m, 736 w, 716 w. ^{1}H NMR ($CDCl_3$): δ 10.53 (s, 4H, *meso*–H of OEP), 5.73 (br, 1H, HSC(Me)$_2$CH$_2$N*H*C(O)CH$_3$), 4.22 (q, J = 8, 16H, C*H*$_2$CH$_3$ of OEP), 2.02 (t, J = 8, 24H, CH$_2$C*H*$_3$ of OEP), –0.14 (s, 1H, *H*SC(Me)$_2$CH$_2$NHC(O)CH$_3$), –0.56 (s, 6H, HSC(*Me*)$_2$CH$_2$NHC(O)CH$_3$), –0.71 (d, J =6, 2H, HSC(Me)$_2$C*H*$_2$NHC(O)CH$_3$), –2.98 (s, 3H, HSC(Me)$_2$CH$_2$NHC(O)C*H*$_3$). Low–resolution mass spectrum (FAB): *m/z* 901 [(OEP)Os(NO)(O=C(Me)NHCH$_2$C(Me)$_2$SH)]$^+$ (9%), 754 [(OEP)Os(NO)]$^+$ (100%), 724 [(OEP)Os]$^+$ (27%). UV–vis spectrum (λ, CH_2Cl_2): 348 (sh, 90), 362 (93), 420 (100), 538 (26), 574 (39) nm.

Preparation of [(OEP)Os(NO)(O=C(Me)NHCH$_2$CH$_2$SH)]BF$_4$. To a stirred CH_2Cl_2 solution (15 mL) of (OEP)Os(CO) (0.020 g, 0.027 mmol) was added $NOBF_4$

(0.003 g, 0.026 mmol). The color of the solution changed from pink red to slightly dark red over a 30 min period, and an IR spectrum in CH_2Cl_2 showed the replacement of the 1883 cm^{-1} assigned to the υ_{CO} of (OEP)Os(CO) with a new band at 1833 cm^{-1} assigned to the υ_{NO} of [(OEP)Os(NO)]BF_4. Liquid $HSCH_2CH_2NHC(O)Me$ (6 μL, 0.053 mmol) was then added to the reaction solution, and the mixture was stirred for 5 h. The solvent was removed in vacuo, and a ^1H NMR spectrum of the residue in $CDCl_3$ showed the presence of the desired product and unreacted excess thiol. The residue was dissolved in a CH_2Cl_2/hexane (1:10, 55 mL), and this solution was kept at –20 °C for 2 days. Precipitation of the product was enhanced by mixing of the CH_2Cl_2/hexane solution, and the supernatant solution was discarded. The precipitate was washed with hexane (5 x 50 mL), and then dissolved in CH_2Cl_2/hexane (2:1, 6 mL). Slow evaporation of the solution in a Dry Box gave [(OEP)Os(NO)(O=C(Me)NHCH$_2$CH$_2$SH)]BF_4·CH_2Cl_2 (0.010 g, 0.010 mmol, 38% isolated yield). Anal. Calcd for $C_{40}H_{53}N_6O_2S_1Os_1B_1F_4$·$CH_2Cl_2$: C, 47.17; H, 5.31; N, 8.05. Found: C, 47.24; H, 5.39; N, 8.00. IR (CH_2Cl_2, cm^{-1}): υ_{NO} = 1826; υ_{CO} = 1603. IR (KBr, cm^{-1}): υ_{NO} = 1814 s; υ_{CO} =1605 m; also 2964 m, 2932 m, 2873 m, 1574 m, 1466 m, 1450 m, 1441 m, 1378 w, 1357 w, 1315 w, 1274 m, 1230 w,1207 w, 1155 m, 1085 s, 1056 s, 1022 s, 996 s, 964 m, 849 m, 745 m, 736 m, 714 w. ^1H NMR ($CDCl_3$): δ 10.54 (s, 4H, *meso*–H of OEP), 5.74 (br, 1H, HSCH$_2$CH$_2$N*H*-C(O)CH_3), 5.28 (s, C*H*$_2$Cl$_2$), 4.23 (q, *J* = 8, 16H, C*H*$_2$CH$_3$ of OEP), 2.02 (t, *J* = 8, 24H, CH$_2$C*H*$_3$ of OEP), –0.01 (t, *J* = 9, 1H, *H*SCH$_2$CH$_2$NHC(O)CH_3), –0.41 and –0.53 (m's, 4H of HSC*H*$_2$C*H*$_2$NHC(O)CH_3), –3.04 (s, 3H, HSCH$_2$CH$_2$NHC(O)C*H*$_3$). Low–resolution mass spectrum (FAB): *m/z* 873 [(OEP)Os(NO)(O=C(Me)NHCH$_2$CH$_2$SH)]$^+$ (11%), 754 [(OEP)Os(NO)]$^+$ (100%), 724 [(OEP)Os]$^+$ (15%). UV–vis spectrum (λ, CH_2Cl_2): 346 (sh, 91), 361 (94), 421 (100), 539 (26), 575 (42) nm.

Protonation of (OEP)Os(NO)(SC(Me)$_2$CH$_2$NHC(O)Me). To a CH_2Cl_2 (10 mL) solution of (OEP)Os(NO)(SC(Me)$_2$CH$_2$NHC(O)Me) (0.010 g, 0.011 mmol) was added HBF_4·Et_2O (0.9 μL, 0.012 mmol). The reaction was monitored by IR

spectroscopy, and the reaction stopped when the IR spectrum in CH_2Cl_2 was almost identical to that of authentic [(OEP)Os(NO)(O=C(Me)NHCH$_2$C(Me)$_2$SH)]BF_4 (*ca.* 30 min). The solvent was removed in vacuo, and a ^{1}H NMR spectrum of the residue in $CDCl_3$ showed the formation of the [(OEP)Os(NO)(O=C(Me)NHCH$_2$C(Me)$_2$SH)]BF_4 in 29% yield (by ^{1}H NMR spectroscopy). The reaction mixture was stirred for a further 2 h, the solvent was removed in vacuo, and a ^{1}H NMR spectrum of the residue in $CDCl_3$ showed the presence of [(OEP)Os(NO)(O=C(Me)NHCH$_2$C(Me)$_2$SH)]BF_4, and the known (OEP)Os(NO)F in a 56:4 ratio, together with other as–yet unidentified products. Further reaction overnight yielded, by ^{1}H NMR spectroscopy, [(OEP)Os(NO)(O=C(Me)-NHCH$_2$C(Me)$_2$SH)]BF_4 and (OEP)Os(NO)F in a 67:7 ratio.

Protonation of (OEP)Os(NO)(SCH$_2$CH$_2$NHC(O)Me). To a CH_2Cl_2 (10 mL) solution of (OEP)Os(NO)(SCH$_2$CH$_2$NHC(O)Me) (0.010 g, 0.011 mmol) was added HBF_4·Et_2O (0.9 μL, 0.012 mmol). The mixture was stirred overnight. The solvent was removed in vacuo, and a ^{1}H NMR spectrum of the residue in $CDCl_3$ showed the formation of a mixture of [(OEP)Os(NO)(O=C(Me)NHCH$_2$CH$_2$SH)]BF_4 and the known (OEP)Os(NO)F in a 78:15 ratio based on integrations of the *meso*–H's of their OEP ligands.

Results and Discussion

Synthesis of Nitrosyl Thiolate Complexes. The reaction of the alkyl thionitrites (RSNO; R = Me, Et, ^{i}Pr, ^{t}Bu) with the (OEP)Os(CO) compound produces the (OEP)Os(NO)(SR) complexes via a formal *trans*–addition reaction in 33–48% isolated yields (Scheme 2.2). Thus, (OEP)Os(CO) reacts with the MeSNO reagent in CH_2Cl_2 at room temperature to generate the (OEP)Os(NO)(SMe) complex. The MeSNO compound was generated *in situ* from the bubbling of gaseous MeSH through a stirred CH_2Cl_2 solution of ^{t}BuONO at –78 °C (dry ice bath). The formation of MeSNO was confirmed by the color change of the solution mixture to red, consistent with the fact that the

primary or *secondary* alkyl thionitrites are generally red, whereas the *tertiary* alkyl thionitrites are green as mentioned in Chapter 1. The other (OEP)Os(NO)(SR) (R = Et, ^{i}Pr, ^{t}Bu) complexes were also generated similarly. The RSNO reagents (R = Et, ^{i}Pr, ^{t}Bu) were generated *in situ* from the reaction of liquid RSH compounds with ^{t}BuONO in CH_2Cl_2 at room temperature. EtSNO (*primary* alkyl thionitrite) and ^{i}PrSNO (*secondary* alkyl thionitrite) are red, and ^{t}BuSNO (*tertiary* alkyl thionitrite) is green.

Scheme 2.2

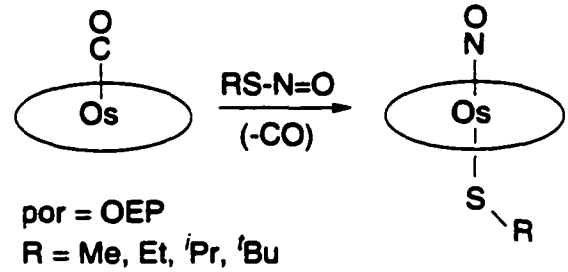

These red nitrosyl thiolate products are moderately air–stable in solution, and can be stored in air in the solid state for at least 1 month without noticeable decomposition. They are freely soluble in CH_2Cl_2 but only slightly soluble in hexane. According to the Enemark–Feltham notation,[26-28] these (OEP)Os(NO)(SR) nitrosyl thiolates products have the $\{OsNO\}^6$ formulation, and are expected to have linear Os–NO linkages. Their spectroscopic properties are consistent with their formulation as such. For example, their IR spectra in CH_2Cl_2 reveal strong bands in the1754–1759 cm^{-1}, which is indicative of linear NO ligands for this class of compounds.[23] This range is similar to that observed for related (OEP)Os(NO)(OR) alkoxide compounds,[22,29] but is higher than that observed for the organometallic (OEP)Os(NO)R compounds (1703–1748 cm^{-1}; R = alkyl, aryl).[30]

Our research group previously showed that the organometallic nitrosyl complexes of osmium porphyrins are generated from the sequential reaction of (OEP)Os(CO) with

$NOPF_6$ followed by reaction with RMgX (X = Cl, Br) (Scheme 2.3), and that the nitrosyl stretching frequencies in the (OEP)Os(NO)R (R = Me, Et, ^{i}Pr, ^{t}Bu) compounds in CH_2Cl_2 decrease in the order (OEP)Os(NO)Me (1720 cm^{-1}) > (OEP)Os(NO)Et (1710 cm^{-1}) > (OEP)Os(NO)(^{i}Pr) (1703 cm^{-1}) ≈ (OEP)Os(NO)(^{t}Bu) (1703 cm^{-1}). This order is consistent with increased electron donation of the R groups.[30]

Scheme 2.3

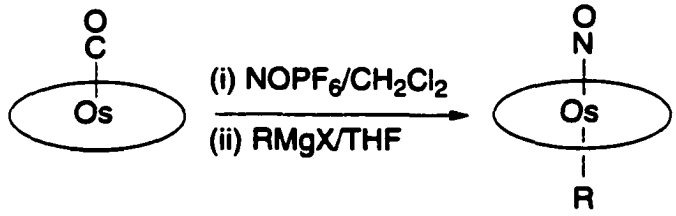

por = OEP
R = Me, Et, ^{i}Pr, ^{t}Bu, *p*-C_6H_4F
X = Cl, Br

Interestingly, however, the IR spectra of the alkyl *thiolate* (OEP)Os(NO)(SR) compounds in CH_2Cl_2 show that the υ_{NO}s fall in a very narrow range: (OEP)Os(NO)(SMe) (1759 cm^{-1}) ≈ (OEP)Os(NO)(SEt) (1758 cm^{-1}) ≈ (OEP)Os(NO)(S^{t}Bu) (1758 cm^{-1}) > (OEP)Os-(NO)(S^{i}Pr) (1754 cm^{-1}). These IR spectrospcopic data indicate that unlike the organometallic (OEP)Os(NO)R compounds, the presence of the sulfur atom in these (OEP)Os(NO)(SR) compounds may mask the direct interaction of the alkyl groups with the metal center, causing a less dramatic variation in Os→NO back–donation of electron density.

The ^{1}H NMR spectra of the (OEP)Os(NO)(SR) compounds in $CDCl_3$ show that the δ_{meso} peaks of the OEP macrocycle decrease slightly from the (OEP)Os(NO)(SMe) (10.33 ppm) to the (OEP)Os(NO)(S^{t}Bu) (10.29 ppm), consistent with a slight *cis*–influence of the axial thiolate ligands. For comparison, the δ_{meso} peaks in the related

(OEP)Os(NO)(OR) *alkoxide* compounds are at 10.44 ppm (R = Me) or 10.32 ppm (R = Et, ^{i}Pr, hexyl, cyclohexyl).[29] Similar *cis*–effects of axial ligands in (OEP)Os–containing compounds have previously been examined by Buchler.[31] The upfield–shift of all the peaks for the coordinated thiolate ligands in the ^{1}H NMR spectra of these (OEP)Os(NO)-(SR) compounds in $CDCl_3$ relative to those of the free thiols is consistent with the expected influence of the porphyrin ring current. For example, the α–CH resonances for the coordinated thiolate ligands appear upfield at ca. –3.12 ppm (for the SCH_3 and SCH_2CH_3 compounds) and at –4.03 ppm for the $SCH(CH_3)_3$ derivative. The presence of the two methyl substituents in the isopropyl group is expected to place the α–CH proton in closer proximity to the porphyrin ring current. The β–CH protons also appear upfield at –1.85 ppm (for SCH_2CH_3), –1.95 ppm (for $SCH(CH_3)_2$), and –2.19 ppm (for $SC(CH_3)_3$). The UV–vis spectra of these (OEP)Os(NO)(SR) compounds are similar to that of the previously reported nitrosyl thiolate compound (OEP)Os(NO)(S–*i*–C_5H_{11}).[22]

In general, the mass spectra (FAB) of the (OEP)Os(NO)(SR) compounds show ion fragments assigned to loss of the NO ligands or loss of the thiols. In the case of (OEP)Os(NO)(SEt), however, the mass spectrum also shows the parent ion at *m/z* 815.

Amide–Containing Thiolate Complexes. Organic thionitrites containing other heteroatoms such as *S*–nitroso–*N*–acetyl–penicillamine, *S*–nitrosoglutathione, and *S*–nitrosocysteine are biologically relevant.[10,12] Indeed, our research group has been interested in determining the preferred binding or reaction modes of such thionitrites with Group 8 metalloporphyrins and heme. Prior to this work, our group showed that the reaction of (OEP)Ru(CO) with the *amide*–containing 1–(acetylamino)–2–methyl-propane–2–thionitrite (containing a *tertiary* carbon next to sulfur) produces the nitrosyl thiolate complex in 91% isolated yield.[21] Interestingly, protonation to this *amide*–containing thiolate complex leads to a net rearrangement of the binding mode of the resulting thiol ligand to give the cationic $[(OEP)Ru(NO)(O{=}C(Me)NHCH_2C(Me)_2SH)]$-$BF_4$ involving the *amide*–bound form of the thiol ligand. Our research group was thus

interested in extending this protonation chemistry to the related *amide*–containing thiolate ligated osmium complexes.

In this work, the reaction of 1 equiv of solid 1–(acetylamino)–2–methylpropane–2–thionitrite with the (OEP)Os(CO) compound in CH_2Cl_2 at room temperature results in the formation of the red (OEP)Os(NO)(SC(Me)$_2$CH$_2$NHC(O)Me) in 21% isolated yield via the formal *trans*–addition reaction (Scheme 2.4). Indeed, IR spectroscopic monitoring of this reaction in CH_2Cl_2 showed the replacement of the 1883 cm^{-1} band due to the υ_{CO} of (OEP)Os(CO) with two new bands at 1773 and 1681 cm^{-1} assigned to the υ_{NO} and υ_{CO} of (OEP)Os(NO)(SC(Me)$_2$CH$_2$NHC(O)Me), respectively.

Scheme 2.4

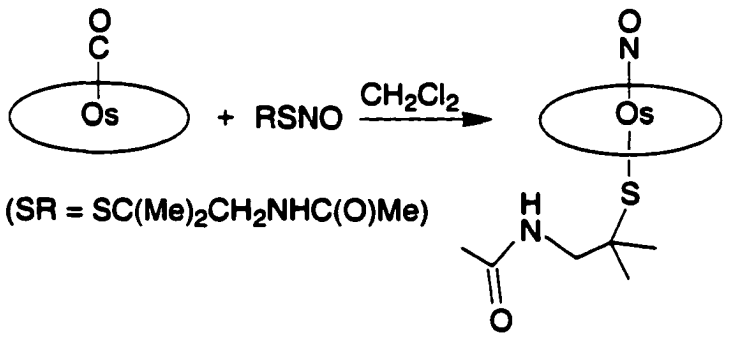

This red product is moderately air–stable in solution and can be stored in air in the solid state for at least one week without noticeable decomposition. It is readily soluble in CH_2Cl_2 but slightly soluble in hexane. Its IR spectrum shows bands at 1764 and 1656 cm^{-1} (KBr) assigned to υ_{NO} and υ_{CO}, respectively. The υ_{NO} band is slightly higher than those of the other (OEP)Os(NO)(SR) compounds (1751–1755 cm^{-1}) described earlier in this chapter, however, it also is within the range seen for linear NO ligands in (por)Os(NO)–containing complexes.[23] The υ_{CO} of the amide group of the thiolate ligand is close to that of the precursor thionitrite (1655 cm^{-1}). The ^{1}H NMR spectrum of (OEP)Os(NO)(SC(Me)$_2$CH$_2$NHC(O)Me) in $CDCl_3$ shows that the chemical

shifts of all the peaks due to the coordinated thiolate ligand are almost identical to those of the ruthenium analog (OEP)Ru(NO)(SC(Me)$_2$CH$_2$NHC(O)Me).[21] The UV–vis spectrum of this complex is also similar to those of the other (OEP)Os(NO)(SR) complexes. The mass spectrum (FAB) of this compound shows ion fragments at *m/z* 870 (loss of the NO ligand) or at *m/z* 754 (loss of the thiol).

Dr. Geun–Bae Yi of our research group was able to independently obtain single crystals of the (OEP)Os(NO)(SC(Me)$_2$CH$_2$NHC(O)Me) product suitable for X–ray crystallography.[32] The molecular structure of (OEP)Os(NO)(SC(Me)$_2$CH$_2$NHC(O)Me) is shown in Figure 2.2.

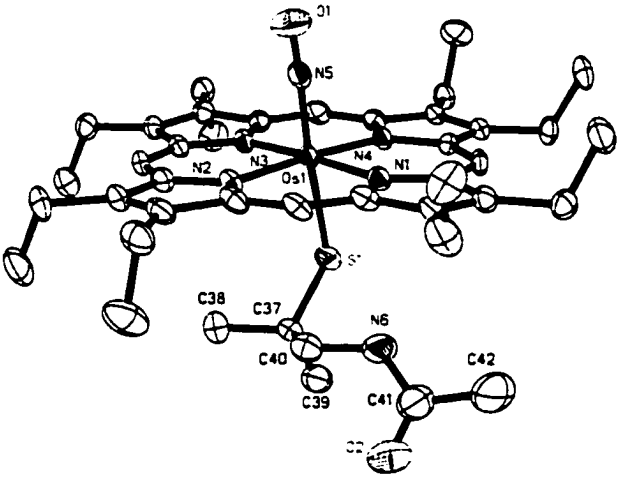

Figure 2.2. Molecular structure of (OEP)Os(NO)(SC(Me)$_2$CH$_2$NHC(O)Me).[32]

The Os–N(O) and N–O bond lengths are 1.781(5) and 1.126(6) Å, respectively, and the Os–N–O bond is essentially linear with a bond angle of 176.8(5)°.

As mentioned in the introduction section, organic thionitrites continue to receive renewed attention due partly to their biological roles. Although many research groups have so far tried to obtain the crystal structures of these RSNO compounds, the number of the structurally characterized RSNO compounds has been extremely limited largely

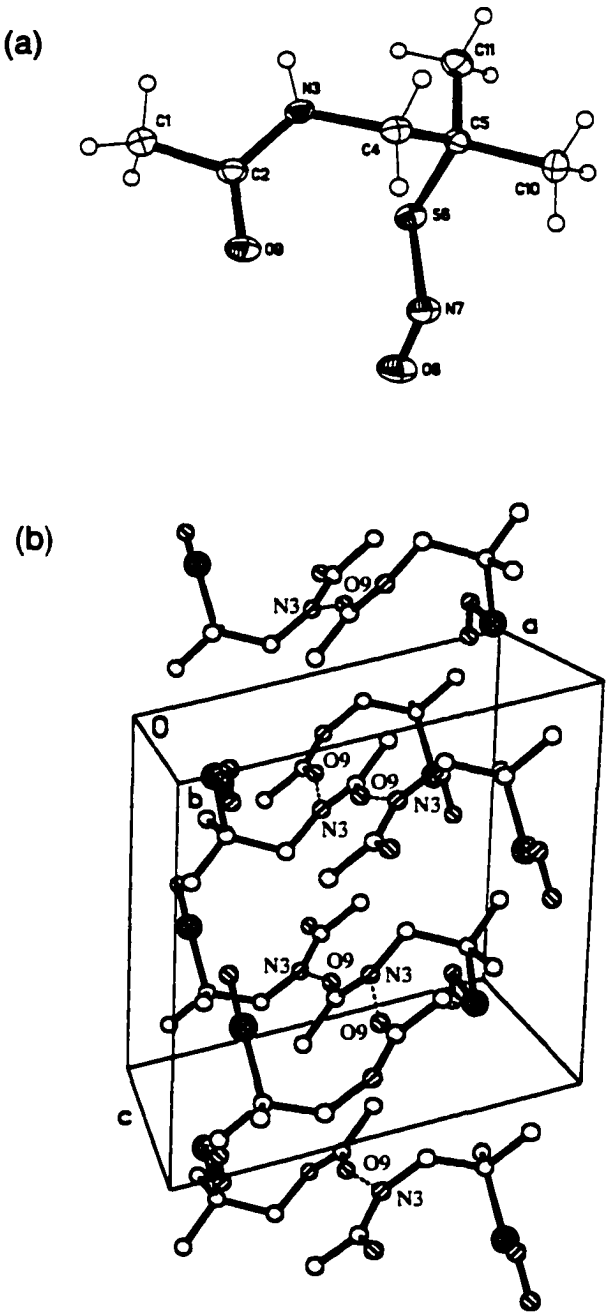

Figure 2.3. (a) Molecular structure of $MeC(O)NHCH_2C(Me)_2SNO$. (b) View of the unit cell. Dashed line represents *intermolecular* hydrogen–bonding.

Table 2.1. Bond lengths (Å) and angles (°) for $MeC(O)NHCH_2C(Me)_2SNO$

Bond Lengths (Å)			
C(1)-C(2)	1.508(2)	C(5)-C(11)	1.533(2)
C(2)-O(9)	1.232(2)	C(5)-S(6)	1.8290(17)
C(2)-N(3)	1.343(2)	S(6)-N(7)	1.7545(17)
N(3)-C(4)	1.451(2)	N(7)-O(8)	1.206(2)
C(4)-C(5)	1.532(2)	N(3)···O(9')[a]	2.902(2)
C(5)-C(10)	1.532(2)		

Bond Angles (°)			
O(9)-C(2)-N(3)	122.37(16)	C(10)-C(5)-C(11)	110.67(14)
O(9)-C(2)-C(1)	121.80(16)	C(4)-C(5)-S(6)	110.80(10)
N(3)-C(2)-C(1)	115.83(15)	C(10)-C(5)-S(6)	111.04(12)
C(2)-N(3)-C(4)	122.25(14)	C(11)-C(5)-S(6)	103.71(13)
N(3)-C(4)-C(5)	114.25(13)	N(7)-S(6)-C(5)	99.44(8)
C(4)-C(5)-C(10)	109.19(15)	O(8)-N(7)-S(6)	114.90(16)
C(4)-C(5)-C(11)	111.37(14)		

[a] This represents an interaction between adjacent molecules, and is the distance between the amide nitrogen and the carbonyl group of a different molecule (see Figure 2.3b).

due to their instability (i.e., most of RSNO compounds readily decompose to the corresponding disulfide RSSR). Our research group has also been interested in determining the structures of biologically important RSNO compounds over the last few years.

Fortunately, the solid–state X–ray crystal structure of organic $MeC(O)NHCH_2$-$C(Me)_2SNO$ thionitrite was obtained in this work. The molecular structure of $MeC(O)$-$NHCH_2C(Me)_2SNO$ is shown in Figure 2.3, and bond lengths and angles are listed in Table 2.1. Surprisingly, only four other RSNO solid–state structures have been reported in the literature prior to this work, namely those of *S*–nitroso–*N*–acetyl–penicillamine,[33-35] Ph_3CSNO,[35] *S*–nitrosocaptopril,[36] and Ar_3CSNO (Ar = 3,5–bis(2,6–dimethylphenyl)-phenyl)[37] (Figure 2.4).

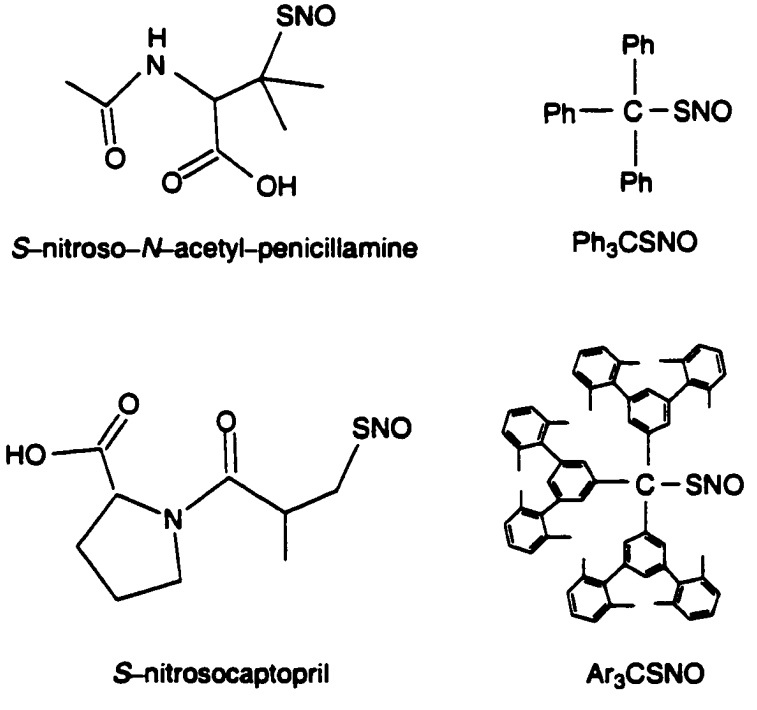

S–nitroso–*N*–acetyl–penicillamine

Ph_3CSNO

S–nitrosocaptopril

Ar_3CSNO

Figure 2.4. The structurally characterized RSNO compounds.

Table 2.2. Metric Parameters for Structurally Characterized Alkyl Thionitrites

Compound		N-O (Å)	S-N (Å)	C-S (Å)	S-N-O (°)	C-S-N (°)	ϕ^a	refs
$MeC(O)NHCH_2C(Me)_2SNO$		1.206(2)	1.754(2)	1.829(2)	114.9(2)	99.44(8)	178.51	this work
S-nitroso-*N*-acetyl-penicillamine[b]		1.199(2)	1.763(2)	1.833(1)	113.99(11)	100.80(7)	176.3	[33, 34]
S-nitroso-*N*-acetyl-penicillamine[c]		1.206(3)	1.762(3)	1.842	114.9(2)	96.56(8)	179.7	[35]
Ph_3CSNO		1.177(6)	1.792(5)	1.867(3)	114.0(4)	102.1(2)	175.7	[35]
S-nitrosocaptopril		1.206	1.766	1.800	117.7	103.7	0.68	[36]
Ar_3CSNO[d]	*(anti)*	1.205 (6)	1.781(5)	1.841(4)	111.4(6)	104.2(3)	179.6	[37]
	(syn)	1.189(12)			123.6(7)		7.3	[37]

[a] Defined as the O-N-S-C torsion angle. [b] Crystallized from methanol/water. [c] Crystallized from acetonitrile.
[d] Ar = 3,5-bis(2,6-dimethylphenyl)phenyl, with *anti:syn* ratio of 0.67:0.33.

Their selected structural parameters are shown in Table 2.2, as are those for MeC(O)-$NHCH_2C(Me)_2SNO$. The thionitrite functionality of $MeC(O)NHCH_2C(Me)_2SNO$ (Figure 2.3) exists in an *anti* orientation, similar to that seen in *S*–nitroso–*N*–acetyl–penicillamine and Ph_3CSNO. The N(7)–S(6)–C(5)–C(4) torsion angle is 66.65(12)°, whereas that of S(6)–C(5)–C(4)–N(3) is 54.10(17)°. Examination of the metrical parameters of $MeC(O)NHCH_2C(Me)_2SNO$ and those of its Os derivative (Figure 2.2) reveals an expanded bond angle around the sulfur atom in the Os compound (121.8(2)°) relative to that in the free thionitrite (99.44(8)°). Furthermore, the amide C=O bond length of 1.232(2) Å in the free thionitrite is slightly longer than that in the Os derivative (1.196(9) Å), however, this may be a result of the moderate *inter*molecular C=O···HN hydrogen–bonding[38] observed in the crystal structure of the thionitrite (see Figure 2.3b).

In addition, the molecular structure of disulfide $\{MeC(O)NHCH_2C(Me)_2S–\}_2$ was obtained (Figure 2.5), and this compound was generated from the decomposition of thionitrite $MeC(O)NHCH_2C(Me)_2SNO$ under laboratory lightning. Bond lengths and angles are listed in Table 2.3. X–ray crystallographic study reveals that the molecule has a crystallographically imposed center of symmetry. The bond angle of 105.82(8)° around the sulfur atom is larger than that of the free thionitrite (99.44(8)°), but smaller than that of $(OEP)Os(NO)(SC(Me)_2CH_2NHC(O)Me)$ (121.8(2)°). The amide C=O bond length of 1.233(3) Å is almost identical to that of the free thionitrite (1.232(2) Å), indicating that the environment around the amide C=O is similar to that observed for the free thionitrite (i.e., the presence of *inter*molecular C=O···HN hydrogen–bonding) (see Figure 2.5b). Although many disulfides had been characterized by X–ray crystallography, to the best of my knowledge, only one example of the structurally characterized RSNO/RSSR pair, namely Ph_3CSNO[35] and $(Ph_3CS–)_2$,[39] was known prior to this work.

The $(OEP)Os(NO)(SCH_2CH_2NHC(O)Me)$ compounds (containing a *primary* carbon atom next to sulfur) was also prepared from an *alkoxide–thiolate* exchange reaction. Thus, the reaction of the *amide*–containing *N*–acetylcysteamine thiol with

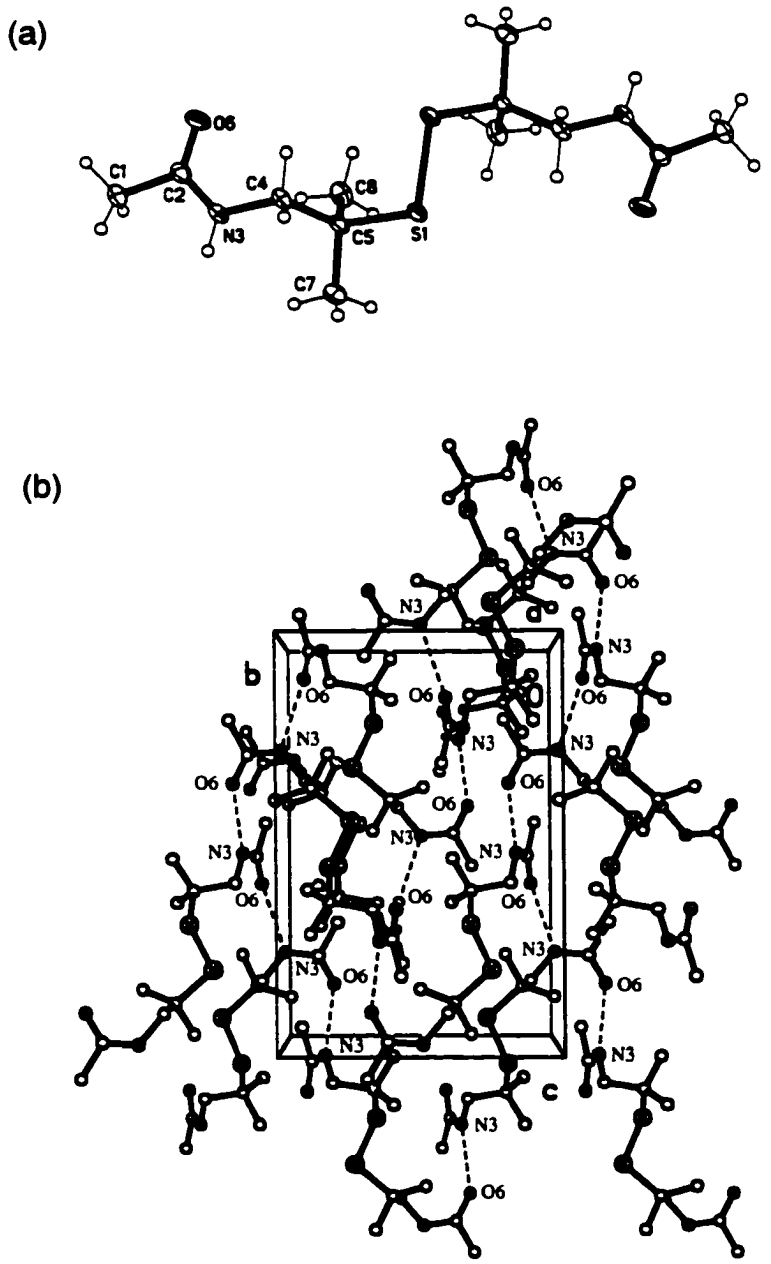

Figure 2.5. (a) Molecular structure of $\{MeC(O)NHCH_2C(Me)_2S-\}_2$. (b) View of the unit cell. Dashed line represents *intermolecular* hydrogen-bonding.

Table 2.3. Bond lengths (Å) and angles (°) for $\{MeC(O)NHCH_2C(Me)_2S-\}_2$

Bond Lengths (Å)			
S(1)-C(5)	1.855(2)	N(3)-C(4)	1.457(3)
S(1)-S(1)#1	2.0441(11)	C(4)-C(5)	1.535(3)
C(1)-C(2)	1.508(3)	C(5)-C(8)	1.516(3)
C(2)-O(6)	1.233(3)	C(5)-C(7)	1.526(3)
C(2)-N(3)	1.332(3)	N(3)···O(6')[a]	2.814(3)
Bond Angles (°)			
C(5)-S(1)-S(1)#1	105.82(8)	C(8)-C(5)-C(7)	111.8(2)
O(6)-C(2)-N(3)	123.0(2)	C(8)-C(5)-C(4)	111.8(2)
O(6)-C(2)-C(1)	121.0(2)	C(7)-C(5)-C(4)	110.70(19)
N(3)-C(2)-C(1)	116.0(2)	C(8)-C(5)-S(1)	113.03(15)
C(2)-N(3)-C(4)	124.76(19)	C(7)-C(5)-S(1)	103.13(16)
N(3)-C(4)-C(5)	114.07(18)	C(4)-C(5)-S(1)	105.94(14)

Symmetry transformations used to generate equivalent atoms: #1 -y+1, -x+1, -z+1/2

[a] This represents an interaction between adjacent molecules, and is the distance between the amide nitrogen and the carbonyl group of a different molecule (see Figure 2.5b).

(OEP)Os(NO)(O–*i*–C_5H_{11}) in refluxing xylene generates the desired (OEP)Os(NO)-($SCH_2CH_2NHC(O)Me$) product in 66% isolated yield (Scheme 2.5).

Scheme 2.5

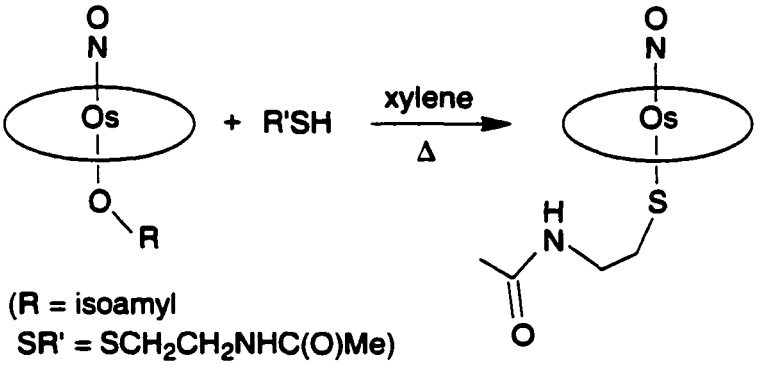

Relatively high temperatures (e.g., refluxing xylene) and long reaction times (ca. 48 h) are required for this reaction to proceed to completion. For example, the (OEP)Os-(NO)($SCH_2CH_2NHC(O)Me$) compound was not formed by the use of refluxing toluene. Furthermore, the ^1H NMR spectrum of the crude product mixture in $CDCl_3$ (after 48 h reaction in refluxing xylene) only showed the presence of the desired thiolate complex and unreacted organic thiol, implying a quantitative conversion to the product.

This red (OEP)Os(NO)($SCH_2CH_2NHC(O)Me$) product is moderately air–stable in solution and is stable in the solid state. It is readily soluble in CH_2Cl_2 and slightly soluble in hexane. Its IR spectrum as a KBr pellet shows bands at 1756 and 1642 cm^{-1} assigned to υ_{NO} and υ_{CO}, respectively. The υ_{NO} and υ_{CO} bands are slightly shifted by 8 cm^{-1} and 14 cm^{-1} , respectively, to lower wavenumbers relative to those of the (OEP)Os-(NO)($SC(Me)_2CH_2NHC(O)Me$) product of Scheme 2.4. The ^1H NMR spectrum of (OEP)Os(NO)($SCH_2CH_2NHC(O)Me$) in $CDCl_3$ is also similar to that of the product of Scheme 2.4, with the notable exception of the presence of the peak at –2.98 ppm due to the –SCH_2CH_2– protons. All the peaks in the ^1H NMR spectrum due to the coordinated

thiolate ligand are shifted upfield relative to those of the free thiol. For example, the peaks for the OsSCH_2– protons appear at –2.98 ppm, which is shifted by 5.63 ppm upfield from that of the free thiol ligand (at 2.65 ppm). The mass spectrum (FAB) of this compound shows ion fragments at *m/z* 842 (loss of the NO ligand), or at *m/z* 754 (loss of the thiol).

Protonation Reactions. Protonation of the *amide*–containing (OEP)Os(NO)(S-C(R)$_2$CH$_2$NHC(O)Me) complexes (R = Me, H) with 1 equiv of HBF$_4$·Et$_2$O in CH$_2$Cl$_2$ results in the formation of the cationic complexes containing the *amide*–bound form of the thiol ligands shown in Scheme 2.6.

Scheme 2.6

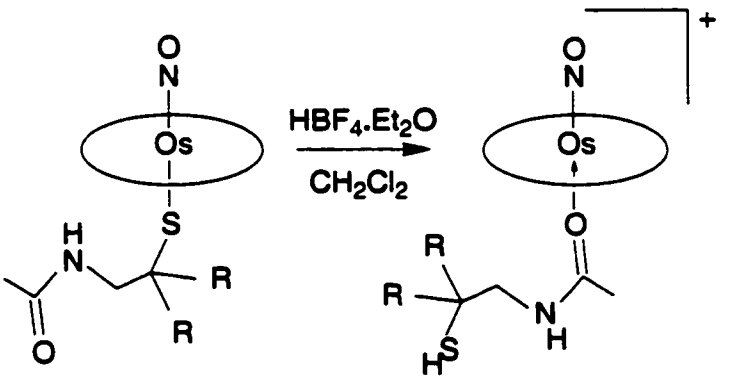

(R = Me, H)

For the case where R = Me, the *amide*–bound [(OEP)Os(NO)(O=C(Me)NHCH$_2$-C(Me)$_2$SH)]BF$_4$ product is obtained in 67% yield (by ^{1}H NMR spectroscopy). IR (in CH$_2$Cl$_2$) and ^{1}H NMR (in CDCl$_3$) spectroscopic monitoring of this reaction reveals the simultaneous formation of the known (OEP)Os(NO)F compound in 7 % yield (by ^{1}H NMR spectroscopy) which may presumably be from fluoride abstraction from the tetrafluoroborate anion in [(OEP)Os(NO)]BF$_4$. This *amide*–bound cationic [(OEP)-

Os(NO)(O=C(Me)NHCH$_2$C(Me)$_2$SH)]BF$_4$ product was also obtained in 46% isolated yield from the sequential reaction of (OEP)Os(CO) with NOBF$_4$ (to produce [(OEP)Os-(NO)]BF$_4$), followed by addition of the organic thiol. Similar by–products to those formed in the protonation reaction (Scheme 2.6) are also observed in this reaction. This cationic product is moderately air–stable in solution, showing signs of decomposition to the known (OEP)Os(NO)F complex in solution over a one week period, however, it is air–stable in the solid state. Its IR spectrum shows bands at 1816 and 1594 cm^{-1} (KBr) assigned to υ_{NO} and υ_{CO}, respectively. The υ_{NO} is 52 cm^{-1} higher than that of the neutral *thiolate*–bound precursor, consistent with less Os→NO back–donation in this cationic complex. Furthermore, the shift in υ_{CO} of the coordinated amide–thiol ligand from 1656 cm^{-1} in the neutral osmium thiolate precursor to 1594 cm^{-1} in the cationic derivative indicates a lowering of the C=O bond order in the cationic product complex, consistent with *O*–binding of the amide functional group. This lowering of the C=O bond order in the coordinated amide–thiol ligand is best explained by a contribution of the dipolar resonance structure (Figure 2.6, right). Thus, the dipolar resonance contribution might stabilize the amide η^1–O binding to osmium center.

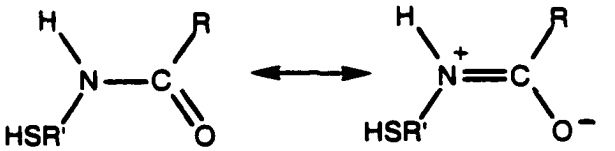

Figure 2.6. Resonance forms of the amide–thiol ligand.

A similar IR spectral change has been observed in the related protonation reaction of (OEP)Ru(NO)(SC(Me)$_2$CH$_2$NHC(O)Me), for which our group was able to obtain X–ray crystal structures of both the *thiolate*–bound starting complex and the *amide*–bound product.[21] The ^{1}H NMR spectrum of this cationic [(OEP)Os(NO)(O=C(Me)NHCH$_2$-

$C(Me)_2SH)]BF_4$ product (in $CDCl_3$) reveals that all the ligand peaks (except for the $C(CH_3)$=O peak) are shifted downfield from those of the coordinated thiolate in the neutral thiolate precursor. The $C(CH_3)$=O peak (at –2.98 ppm) is shifted by 4.21 ppm upfield from that of the thiolate precursor, reflecting the closer proximity of $C(CH_3)$=O to the porphyrin ring current due to the coordination of the amide C=O to osmium center in the cationic product. This ^{1}H NMR spectroscopic feature is consistent with the *amide*–bound form of the thiol ligand in the cationic product. The mass spectrum (FAB) of this compound shows ion fragments at *m/z* 901 (loss of BF_4), or *m/z* 754 (loss of BF_4 and amide–thiol).

When R = H in Scheme 2.6, the $[(OEP)Os(NO)(O=C(Me)NHCH_2CH_2SH)]BF_4$ derivative was obtained in 78% yield (by ^{1}H NMR spectroscopy). The known fluoride (OEP)Os(NO)F compound was also observed as the major by–product (in 15% yield by ^{1}H NMR spectroscopy) in this reaction. The elementally–pure *amide*–bound cationic $[(OEP)Os(NO)(O=C(Me)NHCH_2CH_2SH)]BF_4$ product was also obtained in 38% isolated yield from the reaction of *in situ* generated $[(OEP)Os(NO)]BF_4$ with the organic thiol. This cationic compound is air–stable in the solid–state. The υ_{NO} of the cationic product (as a KBr pellet) is 58 cm^{-1} higher than that of the neutral precursor. As was the case where R = Me, the shift in υ_{CO} of the coordinated ligand from 1642 cm^{-1} in the neutral thiolate precursor to 1605 cm^{-1} in the cationic derivative also indicates a lowering of the C=O bond order in this *amide*–bound form of the thiol ligand in the cationic product complex. The ^{1}H NMR spectrum of this cationic product in $CDCl_3$ shows that the SCH_2– and the amide N*H* peaks are shifted downfield from those of the coordinated thiolate in the precursor neutral complex, consistent with a placement of these groups further from the metal center. Furthermore, the upfield–shift of the amide $C(CH_3)$=O protons indicates an *amide*–binding to the metal center. The mass spectrum (FAB) of this compound shows ion fragments at *m/z* 873 (loss of BF_4), or *m/z* 754 (loss of BF_4 and amide–thiol).

Conclusion

In summary, a new series of stable nitrosyl thiolate (OEP)Os(NO)(SR) complexes (R = Me, Et, ^{i}Pr, ^{t}Bu) have been prepared from the formal *trans*–addition of the precursor thionitrites (RSNO) across the metal center in (OEP)Os(CO). These osmium nitrosyl thiolates have been characterized by infrared and ^{1}H NMR spectroscopy, and by mass spectrometry. For the (OEP)Os(NO)(SR) (R = Me, Et, ^{i}Pr, ^{t}Bu) compounds, the change of "R" group in the RSNO compounds does not show a significant difference in the reactivity of RSNO in the *trans*–addition reaction. This work also demonstrates that thionitrite *trans*–addition can occur for a *secondary* alkyl thionitrite. Their IR spectra reveal that unlike the related organometallic (OEP)Os(NO)R (R = Me, Et, ^{i}Pr, ^{t}Bu) compounds, the presence of the sulfur atom in the (OEP)Os(NO)(SR) compounds results in masking the direct interaction of the alkyl groups with metal center. Two such (OEP)Os(NO)(SR) complexes with *amide*–containing thiolate ligands have also been generated via the formal *trans*–addition or alkoxide–thiolate exchange reaction. The addition of a proton to these complexes shows an interesting chemistry. Thus, protonation of the *amide*–containing thiolate complexes with tetrafluoroboric acid results in the formation of the *amide*–bound cationic derivatives via a net rearrangement of the protonated amide–thiol ligands. This implies a contribution of the dipolar resonance structure of the amide–thiol ligand and the low affinity of thiols (RSH) for the cationic Os–NO center. Importantly, a related pair of RSNO and RSSR compounds were also characterized by single–crystal X–ray crystallography. With the increased interest in thermal and photolytic decomposition of RSNO to RSSR and NO largely due to the importance of RSNO compounds as NO donors, the structural information on RSNO/RSSR pair compounds could potentially provide chemical insight on the nature of this reaction.

References

(1) Stamler, J. S.; Simon, D. I.; Osborne, J. A.; Mullins, M. E.; Jaraki, O.; Michel, T.; Singel, D. J.; Loscalzo, J. *Proc. Natl. Acad. Sci. U.S.A.* **1992**, *89*, 444-448.

(2) Mirza, U. A.; Chait, B. T.; Lander, H. M. *J. Biol. Chem.* **1995**, *270*, 17185-17188.

(3) Park, J.-W. *Biochem. Biophys. Res. Commun.* **1988**, *152*, 916-920.

(4) Stamler, J. S. *Cell* **1994**, *78*, 931-936.

(5) Doyle, M. P.; Pickering, R. A.; da Conceição, J. *J. Biol. Chem.* **1984**, *259*, 80-87.

(6) Gow, A. J.; Stamler, J. S. *Nature* **1998**, *391*, 169-173.

(7) McMahon, T. J.; Stamler, J. S. *Methods Enzymol.* **1999**, *301*, 99-114, and references therein.

(8) Patel, R. P.; Hogg, N.; Spencer, N. Y.; Kalyanaraman, B.; Matalon, S.; Darley-Usmar, V. M. *J. Biol. Chem.* **1999**, *274*, 15487-15492.

(9) Chan, N.-L.; Rogers, P. H.; Arnone, A. *Biochemistry* **1998**, *37*, 16459-16464.

(10) Butler, A. R.; Rhodes, P. *Anal. Biochem.* **1997**, *249*, 1-9.

(11) Richter-Addo, G. B. *Acc. Chem. Res.* **1999**, *32*, 529-536.

(12) Williams, D. L. H. *Acc. Chem. Res.* **1999**, *32*, 869-876.

(13) Williams, D. L. H. *Nitrosation*; Cambridge University Press: Cambridge, U. K., 1988.

(14) Butler, A. R.; Flitney, F. W.; Williams, D. L. H. *TIPS* **1995**, *16*, 18-22.

(15) Oae, S.; Shinhama, K. *Org. Prep. Proced. Int.* **1983**, *15*, 165-198.

(16) Upchurch, G. R., Jr.; Welch, G. N.; Loscalzo, J. *Adv. Pharmacol.* **1995**, *34*, 343-349.

(17) McAninly, J.; Williams, D. L. H.; Askew, S. C.; Butler, A. R.; Russell, C. *J. Chem. Soc., Chem. Commun.* **1993**, 1758-1759.

(18) Dicks, A. P.; Swift, H. R.; Williams, D. L. H.; Butler, A. R.; Al-Sa'doni, H. H.; Cox, B. G. *J. Chem. Soc., Perkin Trans. 2* **1996**, 481-487.

(19) Yi, G.-B.; Khan, M. A.; Richter-Addo, G. B. *Chem. Commun.* **1996**, 2045-2046.

(20) Yi, G.-B.; Chen, L.; Khan, M. A.; Richter-Addo, G. B. *Inorg. Chem.* **1997**, *36*, 3876-3885.

(21) Yi, G.-B.; Khan, M. A.; Powell, D. R.; Richter-Addo, G. B. *Inorg. Chem.* **1998**, *37*, 208-214.

(22) Chen, L.; Khan, M. A.; Richter-Addo, G. B. *Inorg. Chem.* **1998**, *37*, 533-540.

(23) Cheng, L.; Richter-Addo, G. B. In *The Porphyrin Handbook*; Guilard, R., Smith, K., Kadish, K. M., Eds.; Academic Press: New York, 2000; Vol. 4 (Biochemistry and Binding: Activation of Small Molecules), pp 219-291.

(24) Che, C.-M.; Poon, C.-K.; Chung, W.-C.; Gray, H. B. *Inorg. Chem.* **1985**, *24*, 1277-1278.

(25) Roy, B.; d'Hardemare, A. d. M.; Fontecave, M. *J. Org. Chem.* **1994**, *59*, 7019-7026.

(26) Enemark, J. H.; Feltham, R. D. *Coord. Chem. Rev.* **1974**, *13*, 339-406.

(27) Feltham, R. D.; Enemark, J. H. *Top. Stereochem.* **1981**, *12*, 155-215.

(28) Westcott, B. L.; Enemark, J. H. In *Inorganic Electronic Structure and Spectroscopy*; Lever, A. B. P., Solomon, E. I., Eds.; Wiley and Sons: New York, 1999; Vol. 2 (Applications and Case Studies), p Chapter 7.

(29) Cheng, L.; Powell, D. R.; Khan, M. A.; Richter-Addo, G. B. *Inorg. Chem.* **2001**, *40*, 125-133.

(30) Cheng, L.; Chen, L.; Chung, H.-S.; Khan, M. A.; Richter-Addo, G. B.; Young, V. G., Jr. *Organometallics* **1998**, *17*, 3853-3864.

(31) Buchler, J. W.; Kokisch, W.; Smith, P. D. *Struct. Bonding* **1978**, *34*, 79-134.

(32) Lee, J.; Yi, G.-B.; Powell, D. R.; Khan, M. A.; Richter-Addo, G. B. *Can. J. Chem.* **2001**, *79*, 830-840.

(33) Field, L.; Dilts, R. V.; Ravichandran, R.; Lenhert, P. G.; Carnahan, G. E. *J. Chem. Soc., Chem. Commun.* **1978**, 249-250.

(34) Carnahan, G. E.; Lenhert, P. G.; Ravichandran, R. *Acta Crystallogr.* **1978**, *B34*, 2645-2648.

(35) Arulsamy, N.; Bohle, D. S.; Butt, J. A.; Irvine, G. J.; Jordan, P. A.; Sagan, E. *J. Am. Chem. Soc.* **1999**, *121*, 7115-7123.

(36) Bartberger, M. D.; Houk, K. N.; Powell, S. C.; Mannion, J. D.; Lo, K. Y.; Stamler, J. S.; Toone, E. J. *J. Am. Chem. Soc.* **2000**, *122*, 5889-5890.

(37) Goto, K.; Hino, Y.; Kawashima, T.; Kaminaga, M.; Yano, E.; Yamamoto, G.; Takagi, N.; Nagase, S. *Tetrahedron Lett.* **2000**, *41*, 8479-8483.

(38) Jeffrey, G. A. *An Introduction to Hydrogen Bonding*; Oxford University Press: New York, 1997.

(39) Ostrowski, M.; Jeske, J.; Jones, P. G.; du Mont, W.-W. *Chem. Ber.* **1993**, *126*, 1355-1359.

Chapter 3. Synthesis and Characterization of Thiolate–Thiol Complexes of Ruthenium and Osmium Nitrosyl Porphyrins and Their Symmetrical and Unsymmetrical Dithiolate–Bridged Bimetallic Derivatives*

Introduction

As mentioned in Chapter 2, the increased interest in the syntheses of compounds of the form (por)M(NO)(SR) (M = transition metal; por = porphyrinato dianion) is largely due to the fact that they are potential structural models for the NO adducts of cytochrome P450, chloroperoxidase, and NO synthase.[1] Our research group has reported the convenient syntheses of such (por)M(NO)(SR) compounds of Ru and Os by the unusual formal *trans*–additions of alkyl thionitrites (RSNO) to the metalloporphyrin carbonyl and non–carbonyl precursors.[2-6] Our group also prepared the nitrosyl thiolate complexes of ruthenium porphyrins from the reaction of $[(OEP)Ru(NO)(H_2O)]BF_4$ with thiolate anions (Scheme 3.1).[7]

Scheme 3.1

$$[(OEP)Ru(NO)(H_2O)]^+ + SR^- \longrightarrow (OEP)Ru(NO)(SR)$$

$$(SR = SCH_2CF_3,\ SC_6F_4H)$$

Furthermore, Bohle and coworkers showed that the (TTP)Ru(NO)(OMe) alkoxide compound can be effectively used for the syntheses of metalloporphyrin nitrosyl thiolate

---

* Reproduced in part with permission from "Synthesis and Characterization of Thiolate-Thiol Complexes of Ruthenium Nitrosyl Porphyrins and Their Symmetrical and Unsymmetrical Dithiolate-Bridged Bimetallic Derivatives." Lee, J.; Yi, G.-B.; Khan, M. A.; Richter-Addo, G. B. *Inorg. Chem.* **1999**, *38*, 4578-4584. Copyright 1999 American Chemical Society, and "Synthesis, Characterization, and Protonation of Octaethylporphyrin Osmium Nitrosyl Complexes Containing Axial Thiolate Ligands-X-ray Structures of an Alkyl Thionitrite (RSNO) and its (OEP)Os(NO)(SR) Addition Product." Lee, J.; Yi, G.-B.; Powell, D. R.; Khan, M. A.; Richter-Addo, G. B. *Can. J. Chem.* **2001**, *79*, 830-840. Copyright 2001 National Research Council of Canada.

compounds.[8,9] Thus, the precursor (TTP)Ru(NO)(OMe) compound reacts with thiols (RSH ; R = H, *p*–tolyl) to generate the (TTP)Ru(NO)(SR) compounds via an alkoxide–thiolate exchange reaction (Scheme 3.2).

Scheme 3.2

$$(TTP)Ru(NO)(OMe) + RSH \longrightarrow (TTP)Ru(NO)(SR)$$
$$(R = H, p\text{-tolyl})$$

Our research group has also examined spectroscopic and structural relationships between the (por)M(NO)(SR) complexes and their alkoxide (por)M(NO)(OR) analogues (M = Ru, Os).[2-4] In investigating these (por)M(NO)(SR) complexes, our group was interested in examining the potential synthetic utility of (por)M(NO)(S$(CH_2)_n$SH) complexes that contain a thiolate functionality (bound to the central metal) and a free thiol group. In particular, our group was interested in preparing the hitherto unreported μ–dithiolate complexes of the form [(por)M(NO)]$_2$(μ–S$(CH_2)_n$S–*S*,*S*'), since these bimetallic porphyrin complexes containing μ–dithiolate ligands might be an interesting new class of compounds in terms of both synthetic and coordination chemistry. Although related bimetallic porphyrin complexes containing bridging sulfido, alkyl, oxo, and related ligands are known, somewhat surprisingly, there were no reports on μ–dithiolate metalloporphyrins prior to this work. Furthermore, to the best of my knowledge, only two examples of the (por)M(NO)–containing dimers were reported prior to this work. Thus, Scheidt and coworkers recently reported the molecular structure of {[(OEP)Fe(NO)]$_2$-(μ-Prz)}$(ClO_4)_2$ (Prz = pyrazine) containing bridging pyrazine ligand.[10] Our group also obtained the nitrosyl μ–oxo dimer complex [(OEP)Os(NO)]$_2$(μ–O) as a by–product from the sequential reaction of (OEP)Os(CO) with $NOPF_6$ followed by Grignard reagents (Scheme 3.3), and this nitrosyl μ–oxo dimer was characterized by X–ray crystallography.[11] Interestingly, it was observed that unlike other metalloporphyrin

μ–oxo dimers, the μ–O ligand in [(OEP)Os(NO)]$_2$(μ–O) is fairly unreactive towards acid attack. Our group suggested that this might be due to the presence of two axial π–acid NO ligands which withdraw electron density from the μ–oxo bridge.[1]

Scheme 3.3

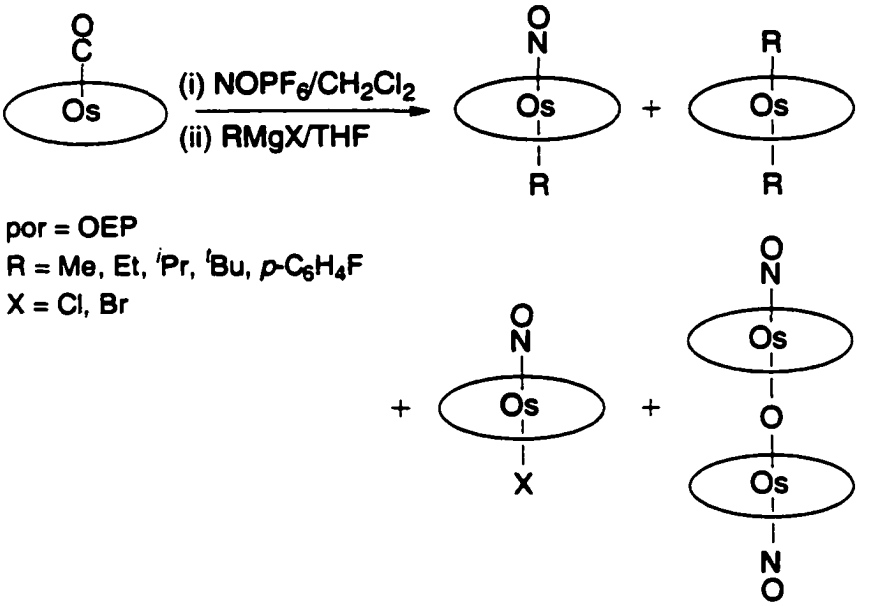

The ethane–1,2–dithiolate (edt) ligand is known to exhibit diverse coordination chemistry.[12-15] In general, the ethane–1,2–dithiolate ligand may bind to metals in one of five ways (Figure 3.1), and all these binding modes have been characterized by single–crystal X-ray crystallography. Excellent work on the syntheses of type **E** complexes containing "*straight–chain*" bridging ethane–1,2–dithiolate (edt) ligand, in which our group was particularly interested, has been accomplished by Holm and coworkers. For example, they reported the synthesis of the anionic complex {[Fe_4S_4(L·S_3)]$_2$(μ–edt–*S,S'*)}$^{4-}$ (L·S_3 = 1,3,5–tris[(4,6–dimethyl–3–mercaptophenyl)thio]–2,4,6–tris(*p*–tolylthio)benzene(3–)) from the reaction of single–cubane cluster [Fe_4S_4(L·S_3)Cl]$^{2-}$ with 0.5 equiv of $Na_2(SCH_2CH_2S)$ (Scheme 3.4), and this compound was characterized by X–ray crystallography.[16]

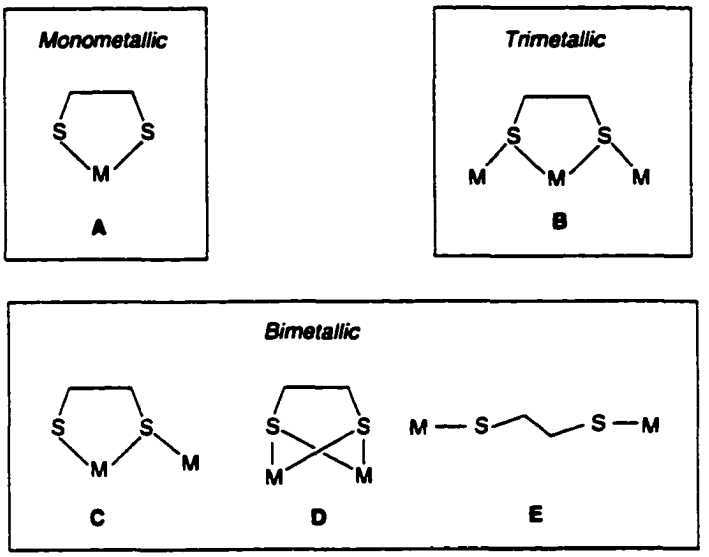

Figure 3.1. Binding modes in metal–edt (edt = ethane–1,2–dithiolate) complexes established by single–crystal X–ray crystallography.

Scheme 3.4

$$2[Fe_4S_4(L^{\bullet}S_3)Cl]^{2-} + Na_2[SCH_2CH_2S] \longrightarrow \{[Fe_4S_4(L^{\bullet}S_3)]_2(\mu\text{-edt-}S,S')\}^{4-} + 2NaCl$$

Although numerous transition metal complexes containing chelating ethane–1,2–dithiolate and related ligands have been reported, surprisingly only a small handful of transition metal complexes containing "*straight–chain*" bridging M(μ–S(CH$_2$)$_n$S–*S,S'*)M' units have been synthesized. Examples of the latter binding modes with transition metals and other elements include those of Au,[17] Mo,[18] Zr,[19] Fe,[16] Ti,[20] Sn,[21] and Sb.[22]

In this chapter, the syntheses of monometallic nitrosyl thiolate–thiol complexes of the form (por)M(NO)(S(CH$_2$)$_n$SH) (M = Ru, Os) will be discussed. The successful syntheses of bimetallic ruthenium and osmium complexes containing μ–dithiolate ligands (edt = ethane–1,2–dithiolate; pdt = propane–1,3–dithiolate; btd = butane–1,4–dithiolate), which use variations of an alkoxide–thiolate exchange method (described in Scheme 3.2)

and formal *trans*–additions of alkyl thionitrites (RSNO), will also be described. Importantly, their spectroscopic properties will be discussed in detail. Indeed, our research group was interested in examining how the presence of two porphyrins and the change of the chain length of the bridging dithiolate ligand affect the spectroscopic properties of bimetallic μ–dithiolate compounds. In particular, our group was interested in the synthesis of unsymmetrical bimetallic μ–dithiolate complex, since the presence of two distinctly different porphyrins or metalloporphyrins in an unsymmetrical bimetallic μ–dithiolate complex is expected to make a big difference in the spectroscopy from the related symmetrical bimetallic μ–ditholate complex. To the best of my knowledge, these are the first bimetallic porphyrin complexes containing μ–dithiolate ligands to be prepared for any metal.

Experimental Section

All reactions were performed under an atmosphere of prepurified nitrogen using standard Schlenk glassware and/or in an Innovative Technology Labmaster 100 Dry Box. Solutions for spectral studies were also prepared under a nitrogen atmosphere. Solvents were distilled from appropriate drying agents under nitrogen just prior to use: CH_2Cl_2 (CaH_2), hexane (Na/benzophenone/tetraglyme or CaH_2), toluene (Na).

Chemicals. Compounds (por)Ru(CO) (por = TTP, TPP),[23] and (OEP)Os(CO)[24] were prepared by published procedures. Isoamyl nitrite (97%), (OEP)Ru(CO), ^{t}BuONO (96%), ethane–1,2–dithiol (edtH_2, $HSCH_2CH_2SH$, 90+%), propane–1,3–dithiol (pdtH_2, $HSCH_2CH_2CH_2SH$, 99%), and butane–1,4–dithiol (bdtH_2, $HSCH_2CH_2CH_2CH_2SH$, 97%) were purchased from Aldrich Chemical Co. and used as received. Chloroform–*d* (99.8%, Cambridge Isotope Laboratories) was vacuum distilled from CaH_2 under nitrogen prior to use. Elemental analyses were performed by Atlantic Microlab, Norcross, Georgia.

Instrumentation. Infrared spectra were recorded on a Bio–Rad FT–155 FTIR spectrometer. Proton NMR spectra were obtained on Varian 400 MHz or 300 MHz

spectrometers and the signals referenced to the residual signal of the solvent employed. All coupling constants are in Hz. FAB mass spectra were obtained on a VG–ZAB–E mass spectrometer.

Preparation of (TPP)Ru(NO)(SCH_2CH_2SH). To a stirred CH_2Cl_2 solution (20 mL) of (TPP)Ru(NO)(O–*i*–C_5H_{11})[25] (0.150 g, 0.180 mmol) was added ethane–1,2–dithiol (50 μL, 0.54 mmol). The color of the reaction solution changed from purple to green over a 10 min period. The solvent was removed in vacuo, and the residue was dissolved in CH_2Cl_2 (10 mL) and filtered through a silica column (160–200 mesh, 2.5 x 30 cm). A green band was collected, and the solvent removed in vacuo to give (TPP)Ru(NO)(SCH_2-CH_2SH) (0.085 g, 0.102 mmol, 57%) as a green powder. Anal. Calcd for $C_{46}H_{33}ON_5S_2$-Ru_1: C, 66.01; H, 3.97; N, 8.37; S, 7.66. Found: C, 65.87; H, 4.06; N, 8.27; S, 7.77. IR (CH_2Cl_2, cm^{-1}): υ_{NO} = 1803. IR (KBr, cm^{-1}): υ_{NO} = 1792 s; also 3052 w, 3025 w, 1595 m, 1527 w, 1487 w, 1447 w, 1348 m, 1305 w, 1262 w, 1206 w, 1176 m, 1072 m, 1014 s, 796 m, 752 s, 704 s, 527 w. ^1H NMR ($CDCl_3$): δ 8.94 (s, 8H, *pyrrole*–H of TPP), 8.25 (m, 8H of TPP), 7.76 (m, 12H of TPP), –0.09 (t, *J* = 8, 1H, SCH_2CH_2SH), –0.78 (apparent q(dt), *J* = 8/ 8, 2H, SCH_2CH_2SH), –2.30 (t, *J* = 8, 2H, SCH_2CH_2SH). Low–resolution mass spectrum (FAB): *m/z* 744 $[(TPP)Ru(NO)]^+$ (100%), 714 $[(TPP)Ru]^+$ (58%).

Preparation of (OEP)Os(NO)(SCH_2CH_2SH). A mixture of (OEP)Os(NO)(O–*i*–C_5H_{11})[2] (0.100 g, 0.119 mmol) and excess $HSCH_2CH_2SH$ (0.1 mL, 1.073 mmol) in toluene (20 mL) was refluxed under N_2 gas with vigorous stirring for 48 h. The color change of the solution was not observed. The solvent was removed in vacuo, and a ^1H NMR spectrum of the residue in $CDCl_3$ showed the presence of the desired thiolate–thiol product and some unreacted thiol. The residue was dissolved in a CH_2Cl_2/hexane (2:1, 10 mL), and the solution was transferred to the top of a silica gel column (2 x 20 cm). Elution with a CH_2Cl_2/hexane (2:1) mixture in air yielded a pale red band and a bright red band. After a pale red band was discarded, a bright red band was collected by

eluting with CH_2Cl_2. The filtrate was dried in vacuo, the residue was dissolved in a CH_2Cl_2/hexane (10 mL, 3:1), and slow evaporation of the solvent mixture in air gave (OEP)Os(NO)(SCH_2CH_2SH)·0.85CH_2Cl_2 (0.076 g, 0.083 mmol, 70% isolated yield). Anal. Calcd for $C_{38}H_{49}N_5O_1S_2Os_1$·0.85$CH_2Cl_2$: C, 50.81; H, 5.56; N, 7.63; Cl, 6.56; S, 6.98. Found: C, 50.67; H, 5.46; N, 7.46; Cl, 6.88; S, 7.32. IR (CH_2Cl_2, cm^{-1}): υ_{NO} = 1764. IR (KBr, cm^{-1}): υ_{NO} = 1756 s; also 2964 m, 2932 m, 2870 m, 1690 w, 1467 m, 1451 m, 1373 m, 1316 w, 1272 m, 1230 w, 1154 m, 1111 w, 1057 m, 1021 m, 994 m, 964 m, 842 m, 746 m, 737 m, 716 w. ^1H NMR ($CDCl_3$): δ 10.35 (s, 4H, *meso*–H of OEP), 5.28 (s, CH_2Cl_2), 4.18 (m, 16H, CH_2CH_3 of OEP), 2.02 (t, J = 8, 24H, CH_2CH_3 of OEP), –0.30 (t, J = 8, 1H, SCH_2CH_2SH), –1.17 (m, 2H, SCH_2CH_2SH), –2.76 (m, 2H, SCH_2CH_2SH). Low–resolution mass spectrum (FAB): *m/z* 817 [(OEP)Os(SCH_2CH_2SH)]$^+$ (5%), 754 [(OEP)Os(NO)]$^+$ (100%), 724 [(OEP)Os]$^+$ (24%).

Preparation of [(TPP)Ru(NO)]$_2$(μ–edt–*S,S'*). To a CH_2Cl_2 (20 mL) solution of (TPP)Ru(NO)(O–*i*–C_5H_{11})[25] (0.075 g, 0.090 mmol) was added ethane–1,2–dithiol (9 μL, 0.1 mmol). The reaction mixture was stirred for 1 h, during which time the color changed from dark purple to green. More (TPP)Ru(NO)(O–*i*–C_5H_{11}) (0.075 g, 0.090 mmol) was added, and the reaction mixture was stirred for a further 3 h. The solvent was removed in vacuo, and a ^1H NMR spectrum of the residue in $CDCl_3$ showed the presence of the desired bimetallic product and (TPP)Ru(NO)(SCH_2CH_2SH) in a 1:2 mole ratio, together with some unreacted (TPP)Ru(NO)(O–*i*–C_5H_{11}). The reaction mixture was stirred overnight. The solvent was removed in vacuo, and the residue was dissolved in a CH_2Cl_2/hexane (2:1) mixture and chromatographed through a silica column (2.5 x 30 cm). The first green band was collected, and the solvent removed in vacuo to give [(TPP)Ru(NO)]$_2$(μ–edt–*S,S'*) (0.032 g, 0.020 mmol, 22% (based on Ru)) as a green powder. Anal. Calcd for $C_{90}H_{60}O_2N_{10}S_2Ru_2$: C, 68.42; H, 3.83; N, 8.87; S, 4.06. Found: C, 68.27; H, 4.01; N, 8.61; S, 4.21. IR (CH_2Cl_2, cm^{-1}): υ_{NO} = 1802. IR (KBr, cm^{-1}): υ_{NO}

= 1779 s; also 3052 vw, 3024 vw, 1596 m, 1528 w, 1486 m, 1440 m, 1349 m, 1306 m, 1260 w, 1208 w, 1175 m, 1071 s, 1014 s, 795 s, 751 s, 702 s, 666 w, 527 w. ^{1}H NMR ($CDCl_3$): δ 8.52 (s, 16H, *pyrrole*–H of TPP), 8.00 (d, J = 7, 8H of TPP), 7.68 (m, 20H of TPP), 7.44 (m, 12H of TPP), –5.73 (s, 4H, SCH_2CH_2S). Low–resolution mass spectrum (FAB): *m/z* 745 $[(TPP)Ru(NO) + H]^+$ (100%), 714 $[(TPP)Ru]^+$ (35%).

Leaving the reaction mixture to stir overnight (*ca.* 12 h total reaction time) resulted in an altered mole ratio (determined by ^{1}H NMR spectroscopy) of the desired bimetallic product, (TPP)Ru(NO)(SCH_2CH_2SH), and unreacted (TPP)Ru(NO)(O–*i*–C_5H_{11}) of 3:2:2, however, decomposition products began to form as well. In our experience, a 4–6 h reaction time maximized the formation of the desired bimetallic product in 34–40% isolated yields (based on Ru).

Preparation of [(TTP)Ru(NO)]$_2$(μ–edt–*S,S'*). To a CH_2Cl_2 (20 mL) solution of (TTP)Ru(NO)(O–*i*–C_5H_{11})[3,4] (0.075 g, 0.084 mmol) was added ethane–1,2–dithiol (8 μL, 0.09 mmol). The reaction mixture was stirred for 1 h, during which time the color changed from dark purple to green. More (TTP)Ru(NO)(O–*i*–C_5H_{11}) (0.075 g, 0.084 mmol) was added, and the reaction mixture stirred for a further 3 h. The solvent was removed in vacuo, and a ^{1}H NMR spectrum of the residue in $CDCl_3$ showed the presence of the desired bimetallic product, (TTP)Ru(NO)(SCH_2CH_2SH),[25] and unreacted alkoxide in a 1:2:2 mole ratio. The reaction mixture was stirred overnight. The solvent was removed in vacuo, and the residue was dissolved in a CH_2Cl_2/hexane (2:1, 15 mL) mixture and was chromatographed through a silica column (2.5 x 30 cm). The first green band was collected, and the solvent removed in vacuo to give [(TTP)Ru(NO)]$_2$(μ–edt–*S,S'*) (0.045 g, 0.026 mmol, 31% (based on Ru)) as a green powder. Anal. Calcd for $C_{98}H_{76}O_2N_{10}S_2Ru_2{\cdot}CH_2Cl_2$: C, 66.91; H, 4.42; N, 7.88; S, 3.61. Found: C, 66.85; H, 4.45; N, 7.97; S, 3.65. IR (CH_2Cl_2, cm^{-1}): υ_{NO} = 1788. IR (KBr, cm^{-1}): υ_{NO} = 1770 s; also 3022 w, 2918 w, 2865 w, 1527 m, 1511 m, 1494 m, 1446 m, 1349 m, 1304 m, 1268 w, 1212 m, 1182 m, 1108 w, 1073 m, 1014 s, 846 w, 797 vs, 712 s, 522 s, 450 w. ^{1}H

NMR ($CDCl_3$): δ 8.53 (s, 16H, *pyrrole*–H of TTP), 7.88 (d, J = 9, 8H, *o*–H of TTP), 7.46 (d, J = 7, 8H, *o'*-H of TTP), 7.26 (m, 16H, *m*–H of TTP), 5.28 (s, CH_2Cl_2), 2.68 (s, 24H, CH_3 of TTP), –5.73 (s, 4H, SCH_2CH_2S). Low–resolution mass spectrum (FAB): *m/z* 1690 $[[(TTP)Ru(NO)]_2(\mu\text{–}SCH_2CH_2S)]^+$ (0.2%), 800 $[(TTP)Ru(NO)]^+$ (100%), 770 $[(TTP)Ru]^+$ (41%).

As was the case of the TPP analog, leaving the reaction mixture to stir overnight (*ca.* 12 h total reaction time) resulted in an altered mole ratio of the desired bimetallic product, (TTP)Ru(NO)(SCH_2CH_2SH), and unreacted (TTP)Ru(NO)(O–*i*–C_5H_{11}) of *ca.* 3:2:2, however, decomposition products began to form as well (decreasing the yield of the bimetallic product). In our experience, a 4–6 h reaction time maximized the formation of the desired bimetallic product in 36–45% isolated yields (based on Ru).

Preparation of [(TPP)Ru(NO)](μ–edt–*S,S'*)[Ru(NO)(OEP)]. To a CH_2Cl_2 (20 mL) solution of (TPP)Ru(NO)(SCH_2CH_2SH) (0.050 g, 0.060 mmol) was added ^{t}BuONO (50 μL, 0.40 mmol) for 10 min. To this solution was added (OEP)Ru(CO) (0.050 g, 0.075 mmol) and the solution was stirred for a further 10 min, during which time the color changed from green to brown–purple. The solvent was removed in vacuo, and the residue was dissolved in CH_2Cl_2/hexane (1:1, 15 mL) and filtered through a basic alumina column (2.5 x 30 cm). After removal of solvent, a 20:5:1 mixture of [(TPP)Ru-(NO)](μ–edt–*S,S'*)[Ru(NO)(OEP)], $[(TPP)Ru(NO)]_2$(μ–edt–*S,S'*), and $[(OEP)Ru(NO)]_2$-(μ–edt–*S,S'*)[25] was obtained (0.022 g, *ca.* 24% combined yield). This solid mixture of the three bimetallic compounds was dissolved in CH_2Cl_2/hexane (1:1, 10 mL), and the solution was chromatographed through a second basic alumina column (2.5 x 40 cm). A red band eluted first, overlapping with a second brown band. This second brown band was collected, which consisted only of [(TPP)Ru(NO)](μ–edt–*S,S'*)[Ru(NO)(OEP)] and $[(TPP)Ru(NO)]_2$(μ–edt–*S,S'*). After redissolving the mixture (obtained from the second band) in CH_2Cl_2/hexane (1:2, 10 mL), the solution was chromatographed through a basic alumina column (2.5 x 40 cm). The first portion of a red–brown band was collected to

give a small amount of [(OEP)Ru(NO)]$_2$(μ–edt–*S,S'*) and some [(TPP)Ru(NO)](μ–edt–*S,S'*)[Ru(NO)(OEP)]. The second (major) portion of this brown band was also collected to give spectroscopically pure [(TPP)Ru(NO)](μ–edt–*S,S'*)[Ru(NO)(OEP)]·0.3CH_2Cl_2 (0.005 g, 0.003 mmol, 5% yield (based on Ru)). Anal. Calcd for $C_{82}H_{76}O_2N_{10}S_2Ru_2$·0.3$CH_2Cl_2$: C, 64.80; H, 5.06; N, 9.18. Found: C, 64.99; H, 5.69; N, 8.77. IR (CH_2Cl_2, cm^{-1}): υ_{NO} = 1786. IR (KBr, cm^{-1}): υ_{NO} = 1770 s; also 2964 m, 2930 w, 2868 w, 1594 w, 1521 w, 1490 w, 1468 w, 1455 w, 1372 w, 1307 w, 1271 w, 1176 w, 1150 w, 1066 w, 1016 s, 996 m, 994 w, 908 w, 838 w, 796 w, 750 m, 733 m, 703 m. ^{1}H NMR ($CDCl_3$): δ 9.74 (s, 4H, *meso*–H of OEP), δ 8.46 (s, 8H, *pyrrole*–H of TPP), 7.96 (d, 4H, *J* = 8, Ph of TPP), 7.74 (m, 8H, Ph of TPP), 7.62 (m, 8H, Ph of TPP), 5.28 (s, CH_2Cl_2), 3.82 (m, 16H, C$H_2$$CH_3$ of OEP), 1.68 (t, 24H, CH_2CH_3 of OEP), –5.87 (app m (see text), 2H, SC$H_2$$CH_2$S), –5.97 (app m (see text), 2H, SCH_2CH_2S).

Attempted Preparation of [(OEP)Os(NO)](μ–edt–*S,S'*)[Ru(NO)(TTP)]. To a CH_2Cl_2 (20 mL) solution of (OEP)Os(NO)(SCH_2CH_2SH)·0.85CH_2Cl_2 (0.020 g, 0.022 mmol) was added ^{t}BuONO (5 μL, 0.04 mmol), and the reaction mixture was stirred for 10 min. To this solution was added (TTP)Ru(CO) (0.018 g, 0.022 mmol), and the solution was stirred for a further 10 min, during which time its color turned from dark red to brown–purple. The solvent was removed in vacuo, and a ^{1}H NMR spectrum of the residue in $CDCl_3$ showed the formation of a mixture of the desired mixed bimetallic [(OEP)Os(NO)](μ–edt–*S,S'*)[Ru(NO)(TTP)] and [(OEP)Os(NO)]$_2$(μ–edt–*S,S'*) (a singlet at –6.27 ppm) in a 70:1 ratio (by ^{1}H NMR spectroscopy), together with several unidentified products in total 29% yield. Attempts to obtain spectroscopically pure [(OEP)Os(NO)](μ–edt–*S,S'*)[Ru(NO)(TTP)] were unsuccessful, since it is unstable in solution and there is little difference of solubility between this air–sensitive product and by–products. ^{1}H NMR ($CDCl_3$) δ 9.81 (s, 4H, *meso*–H of OEP), 8.51 (s, 8H, *pyrrole*–H of TTP), 7.87 (br d, *J* = 7, 4H of TTP), 7.46 (m, 12H of TTP), 3.85 (m, 16H, C$H_2$$CH_3$ of OEP), 2.73 (s, 12H, CH_3 of TTP), 1.71 (t, *J* = 8, 24H, CH_2CH_3 of OEP), –5.92 (app m

(see text), 2H, SCH_2CH_2S), –6.01 (app m (see text), 2H, SCH_2CH_2S).

Preparation of (TTP)Ru(NO)($SCH_2CH_2CH_2SH$). To a stirred CH_2Cl_2 solution (20 mL) of (TTP)Ru(NO)(O–*i*–C_5H_{11})[3,4] (0.100 g, 0.113 mmol) was added propane–1,3–dithiol (50 μL, 0.49 mmol). The color of the reaction solution changed from dark purple to green over a 1 h period. The solvent was removed in vacuo, and the crude product was dissolved in CH_2Cl_2/hexane (1/1) and filtered through a silica column (2.5 x 30 cm). A green band was collected. Solvent removal from the resulting green solution gave (TTP)Ru(NO)($SCH_2CH_2CH_2SH$)·0.4pdtH_2·0.3CH_2Cl_2·0.4hexane (0.056 g, 0.055 mmol, 49%) as a green powder. Anal. Calcd for $C_{51}H_{43}ON_5S_2Ru_1$·0.4pdtH_2·0.3CH_2Cl_2·0.4 hexane: C, 65.26; H, 5.23; N, 6.93; S, 8.89 ; Cl, 2.11. Found: C, 66.52; H, 4.90; N, 7.24; S, 9.24; Cl, 2.46. IR(CH_2Cl_2, cm^{-1}): υ_{NO} = 1799. IR (KBr, cm^{-1}): υ_{NO} = 1779 s; also 3019 w, 2919 m, 2863 w, 1526 w, 1511 w, 1493 w, 1436 w, 1349 m, 1304 m, 1259 w, 1212 m, 1181 m, 1108 w, 1072 m, 1014 s, 846 w, 797 s, 714 m, 523 m. ^1H NMR ($CDCl_3$): δ 8.93 (s, 8H, *pyrrole*–H of TTP), 8.12 (d, *J* = 8, 8H of TTP), 7.55 (d, *J* = 8, 8H of TTP), 5.28 (s, 0.6H, CH_2Cl_2), 2.70 (s, 12H, CH_3 of TTP), 2.63 (pdtH_2), 1.88 (pdtH_2), 1.31 (pdtH_2), 1.27 (br, hexane), 0.88 (t, hexane), 0.54 (apparent q(dt), *J* = 7/8, 2H, $SCH_2CH_2CH_2SH$), –0.09 (t, *J* = 8, 1H, $SCH_2CH_2CH_2SH$), –1.07 (apparent quintet, *J* = 7, 2H, $SCH_2CH_2CH_2SH$), –2.55 (t, *J* = 7, 2H, $SCH_2CH_2CH_2SH$). Low–resolution mass spectrum (FAB): *m/z* 800 $[(TTP)Ru(NO)]^+$ (100%), 770 $[(TTP)Ru]^+$ (97%).

Preparation of $[(TTP)Ru(NO)]_2$(μ–pdt–*S,S'*). To a CH_2Cl_2 (20 mL) solution of (TTP)Ru(NO)(O–*i*–C_5H_{11})[3,4] (0.50 g, 0.056 mmol) was added propane–1,3–dithiol (6 μL, 0.06 mmol) and the mixture stirred for 1 hr, during which time the color changed from dark purple to green. To this solution was added more (TTP)Ru(NO)(O–*i*–C_5H_{11}) (0.500 g, 0.056 mmol) and the solution was stirred for 3 h, during which time the color changed from green to red–green. The solvent was removed in vacuo, and a ^1H NMR spectrum of the residue in $CDCl_3$ showed the presence of the desired but unstable bimetallic product and unreacted (TTP)Ru(NO)(O–*i*–C_5H_{11}) in a 4:1 mole ratio, together with an as–yet

unidentified decomposition product (*ca.* 30%). The residue was dissolved in CH_2Cl_2/hexane (2/1) and chromatographed through a silica column (2.5 x 20 cm). The first green band was collected, and [(TTP)Ru(NO)]$_2$(μ–pdt–*S,S'*)·0.2CH_2Cl_2 (0.015 g, 0.009 mmol, 16% (based on Ru)) was isolated as a green powder by solvent removal. Anal. Calcd for $C_{99}H_{78}O_2N_{10}S_2Ru_2$·0.2$CH_2Cl_2$: C, 69.15; H, 4.59; N, 8.13. Found: C, 69.26; H, 4.82; N, 7.73. IR(CH_2Cl_2, cm^{-1}): υ_{NO} = 1790. IR (KBr, cm^{-1}): υ_{NO} = 1772 s; also 3021 w, 2922 w, 1560 vw, 1526 w, 1510 m, 1495 m, 1445 m, 1350 m, 1305 w, 1213 w, 1182 m, 1108 w, 1073 m, 1015 s, 797 s, 714 m, 523 s. ^{1}H NMR ($CDCl_3$): δ 8.63 (s, 16H, *pyrrole*–H of TTP), 7.93 (d, *J* = 8, 8H of TTP), 7.53 (d, *J* = 8, 8H of TTP), 7.47 (d, *J* = 8, 8H of TTP), 7.28 (d, *J* = 8, 8H of TTP) , 5.28 (s, 0.4H, C*H*$_2Cl_2$), 2.68 (s, 24H, C*H*$_3$ of TTP), –4.18 (t, 4H, *J* = 8, SC*H*$_2$CH$_2$C*H*$_2$S), –4.64 (app m, 2H, SCH$_2$C*H*$_2$CH$_2$S). Low–resolution mass spectrum (FAB): *m/z* 800 [(TTP)Ru(NO)]$^+$ (100 %), 770 [(TTP)Ru]$^+$ (84%).

Preparation of (TTP)Ru(NO)(SCH$_2$CH$_2$CH$_2$CH$_2$SH). To a stirred CH_2Cl_2 solution (20 mL) of (TTP)Ru(NO)(O–*i*–C_5H_{11})[3,4] (0.150 g, 0.169 mmol) was added butane–1,4–dithiol (50 μL, 0.41 mmol). The color of the reaction solution changed from dark purple to green over a 1 h period. The solvent was removed in vacuo, and the residue dissolved in CH_2Cl_2/hexane (2/1) solvent and filtered through a silica column (2.5 x 30 cm). A green band was collected. The solvent was removed from this green band, and (TTP)Ru(NO)(SCH$_2$CH$_2$CH$_2$CH$_2$SH)·0.2bdtH_2 (0.093 g, 0.098 mmol, 58%) was isolated as a green powder. Anal. Calcd for $C_{52}H_{45}ON_5S_2Ru_1$·0.2bdtH_2: C, 67.06; H, 5.01; N, 7.41; S, 8.14. Found: C, 67.21; H, 5.47; N, 7.17; S, 8.10. IR (CH_2Cl_2, cm^{-1}): υ_{NO} = 1794. IR (KBr, cm^{-1}): υ_{NO} = 1770 m; also 3024 w, 2921 m, 2851w, 1566 m, 1554 m, 1529 w, 1513 w, 1444 w, 1384 w, 1349 m, 1303 w, 1265 w, 1211 w, 1181 m, 1107 w, 1072 m, 1014 s, 797 vs, 714 s, 523 m. ^{1}H NMR ($CDCl_3$): δ 8.92 (s, 8H, *pyrrole*–H of TTP), 8.10 (d, *J* = 8, 8H of TTP), 7.55 (d, *J* = 8, 8H of TTP), 2.70 (s, 12H, C*H*$_3$ of TTP), 2.50 (bdtH_2), 1.70 (bdtH_2), 1.33 (bdtH_2), 1.27 (m, 2H, SCH$_2$CH$_2$CH$_2$C*H*$_2$SH), 0.62 (t, *J*

= 8, 1H, $SCH_2CH_2CH_2CH_2SH$), –0.26 (m, 2H, $SCH_2CH_2CH_2CH_2SH$), –1.35 (m, 2H, $SCH_2CH_2CH_2CH_2SH$), –2.65 (t, J = 8, 2H, $SCH_2CH_2CH_2CH_2SH$). Low–resolution mass spectrum (FAB): *m/z* 800 $[(TTP)Ru(NO)]^+$ (100%), 770 $[(TTP)Ru]^+$ (61%).

Attempted Preparation of [(TTP)Ru(NO)]$_2$(μ–bdt–*S,S'*). To a CH_2Cl_2 (30 mL) solution of (TTP)Ru(NO)(O–*i*–C_5H_{11})[3,4] (0.100 g, 0.113 mmol) was added butane–1,4–dithiol (14 μL, 0.12 mmol) and the mixture stirred for 1 hr, during which time the color changed from dark purple to green. To this solution was added more (TTP)Ru(NO)-(O–*i*–C_5H_{11}) (0.100 g, 0.113 mmol) and the solution was stirred for an additional 3 h, during which time the color changed from green to red–green. Chromatography of the resulting product(s) through a silica column gave a 5:1 mole ratio (by ^1H NMR spectroscopy) of [(TTP)Ru(NO)]$_2$(μ–bdt–*S,S'*) and (TTP)Ru(NO)($SCH_2CH_2CH_2CH_2$-SH), and a small amount (*ca.* 10%) of a third product which appears to arise from the decomposition of the bimetallic product. Attempts to obtain spectroscopically pure [(TTP)Ru(NO)]$_2$(μ–bdt–*S,S'*) was unsuccessful, since it is very unstable in solution and decomposes to this as–yet unidentified product. ^1H NMR ($CDCl_3$) of [(TTP)Ru(NO)]$_2$-(μ–bdt–*S,S'*): δ 8.68 (s, 16H, *pyrrole*–H of TTP), 7.96 (d, J = 8, 8H of TTP), 7.67 (d, J = 8, 8H of TTP), 7.47 (d, J = 8, 8H of TTP), 7.29 (d, J = 8, 8H of TTP), 2.66 (s, 24H, CH_3 of TTP), –3.11 (br, 4H, $SCH_2CH_2CH_2CH_2S$), –3.71 (br, 4H, $SCH_2CH_2CH_2$-CH_2S).

Results and Discussion

Monometallic Thiolate–Thiol Complexes. The monometallic (TPP)Ru(NO)(S-CH_2CH_2SH) thiolate–thiol complex was prepared by an alkoxide–thiolate exchange reaction. Thus, the reaction of the (TPP)Ru(NO)(O–*i*–C_5H_{11}) alkoxide complex with excess ethane–1,2–dithiol in CH_2Cl_2 at room temperature generates the monometallic thiolate–thiol derivative in 57% isolated yield as shown in Scheme 3.5. The related tetratolylporphyrin complex, namely (TTP)Ru(NO)(SCH_2CH_2SH) was prepared

similarly by Dr. Geun-Bae Yi of our research group.[25]

Scheme 3.5

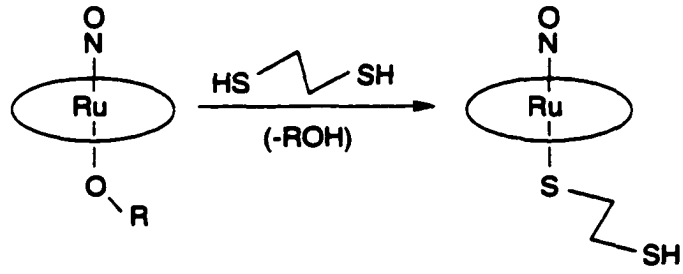

por = TPP (57%)
R = i-C_5H_{11}

The monometallic product of Scheme 3.5 is a moderately air-stable green solid, showing no signs of decomposition in the solid state in air after 1 week. However, it is air-sensitive in solution. This monometallic thiolate-thiol complex is soluble in CH_2Cl_2 and benzene, but is insoluble in hexane. Its IR spectrum (CH_2Cl_2) shows a band at 1803 cm^{-1} due to υ_{NO}. This is within the range observed for linear NO ligands in (por)Ru-(NO)-containing complexes.[1] Its ^1H NMR spectrum shows, in addition to the porphyrin macrocycle signals, peaks at -2.30 ppm (t, SCH_2CH_2SH), -0.78 ppm (dt, SCH_2CH_2-SH), and -0.09 ppm (t, SCH_2CH_2SH) assigned to the coordinated thiolate-thiol ligand. These chemical shifts are very similar to those of (TTP)Ru(NO)(SCH_2CH_2SH), but are shifted slightly downfield by ca. 0.2-0.5 ppm from those of (OEP)Ru(NO)(SCH_2CH_2-SH)[25] which was synthesized by Dr. Geun-Bae Yi (see below). This indicates that the ring current effects of OEP macrocycle on the thiolate-thiol ligand are greater than those of TPP or TTP macrocycle. The greatest shift occurs for the $RuSCH_2$-hydrogens. Thus, the chemical shifts of the α-methylene protons of the thiolate-thiol groups (i.e., $Ru-SCH_2CH_2SH$) are similar in the TPP (-2.30 ppm) and TTP (-2.31 ppm) cases, but

Table 3.1. α–Methylene ^{1}H NMR Shifts ($CDCl_3$) for Group 8 Nitrosyl Porphyrin Alkanethiolates

Compound	δ, ppm	refs
Monometallic		
(OEP)Ru(NO)(SCH_2CF_3)	–2.87	[7]
(OEP)Ru(NO)(SCH_2CH{NHC(O)Me}C(O)OMe)	–2.61, –3.16	[4]
(OEP)Os(NO)(SCH_2CH_3)	–3.12	[6]
(TTP)Os(NO)(SCH_2CH_2CHMe$_2$)	–2.73	[4]
(OEP)Os(NO)(SCH_2CH_2CHMe$_2$)	–3.26	[2]
(OEP)Os(NO)(SCH_2CH_2NHC(O)Me)	–2.98	[6]
(OEP)Ru(NO)(SCH_2CH_2SH)	–2.78	[25]
(TPP)Ru(NO)(SCH_2CH_2SH)	–2.30	this work
(TTP)Ru(NO)(SCH_2CH_2SH)	–2.31	[25]
(TTP)Ru(NO)(SCH_2CH_2CH_2SH)	–2.55	this work
(TTP)Ru(NO)(SCH_2CH_2CH_2CH_2SH)	–2.65	this work
(OEP)Os(NO)(SCH_2CH_2SH)	–2.76	this work
Bimetallic		
[(TPP)Ru(NO)]$_2$(μ–SCH_2CH_2S–*S*,*S*')	–5.73	this work
[(TTP)Ru(NO)]$_2$(μ–SCH_2CH_2S–*S*,*S*')	–5.73	this work
[(OEP)Ru(NO)]$_2$(μ–SCH_2CH_2S–*S*,*S*')	–6.20	[25]
[(TTP)Ru(NO)]$_2$(μ–SCH_2CH_2CH_2S–*S*,*S*')	–4.18	this work
[(TTP)Ru(NO)]$_2$(μ–SCH_2(CH_2)$_2$CH_2S–*S*,*S*')	–3.71	this work

are shifted upfield in the OEP case (–2.78 ppm). However, these chemical shifts of the α–methylene protons of the thiolate–thiol group are in the same region as those of other alkanethiolate complexes of ruthenium nitrosyl porphyrins (see Table 3.1). The mass spectrum (FAB) of (TPP)Ru(NO)(SCH_2CH_2SH) shows an ion fragment assigned to loss of the thiolate–thiol ligand.

At the time, Dr. Geun–Bae Yi was also able to independently synthesize (OEP)Ru(NO)(SCH_2CH_2SH) from the reaction of (OEP)Ru(CO) with the $HSCH_2CH_2$–SNO (generated *in situ* from the reaction of ethane–1,2–dithiol and ^{t}BuONO).[25] Thus, (OEP)Ru(CO) reacts with a red mixture of ethane–1,2–dithiol and ^{t}BuONO in CH_2Cl_2 at room temperature to generate the desired monometallic thiolate–thiol complex via a formal *trans*–addition of RSNO as shown in Scheme 3.6.

Scheme 3.6

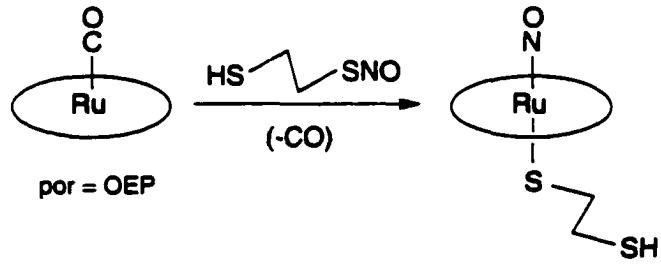

Interestingly, Dr. Yi found that unlike the TPP and TTP cases, the alkoxide–thiolate exchange method described in Scheme 3.5 was not effective in preparing the (OEP)Ru–(NO)(SCH_2CH_2SH) complex. Indeed, the reaction of (OEP)Ru(NO)(O–*i*–C_5H_{11}) with ethane–1,2–dithiol in CH_2Cl_2 at room temperature did not produce the (OEP)Ru(NO)–(SCH_2CH_2SH) complex. Our research group was thus interested in determining whether the related (OEP)Os–containing derivatives can be obtained from the alkoxide–thiolate exchange method. As in the case of (OEP)Ru(NO)(SCH_2CH_2SH), the (OEP)Os(NO)–

(SCH_2CH_2SH) complex was not generated from the reaction of (OEP)Os(NO)(O–*i*–C_5H_{11}) with ethane–1,2–dithiol in CH_2Cl_2 at room temperature. However, when vigorous reaction conditions were employed, the (OEP)Os(NO)(SCH_2CH_2SH) complex was successfully produced via the alkoxide–thiolate exchange. Thus, the (OEP)Os(NO)-(O–*i*–C_5H_{11}) alkoxide complex reacts with excess ethane–1,2–dithiol in toluene under refluxing conditions for 48 h to generate the monometallic thiolate–thiol derivative in 70% isolated yield as shown in Scheme 3.7.

Scheme 3.7

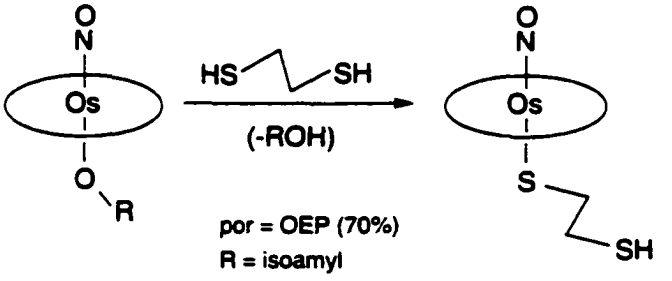

It was observed that the alkoxide–thiolate exchange method is more efficient in preparing this (OEP)Os(NO)(SCH_2CH_2SH) complex in high yield compared with the formal *trans*–addition reaction. Thus, the ^1H NMR spectrum (in $CDCl_3$) of the crude product mixture (after 48 h reaction in refluxing toluene) reveals a quantitative conversion of (OEP)Os(NO)(O–*i*–C_5H_{11}) to (OEP)Os(NO)(SCH_2CH_2SH). Unlike the ruthenium analog (OEP)Ru(NO)(SCH_2CH_2SH), this red (OEP)Os(NO)(SCH_2CH_2SH) complex is moderately air–stable in solution, showing no signs of decomposition for at least 8 h. It can also be stored in air in the solid state for at least one week without noticeable decomposition. This osmium nitrosyl thiolate–thiol complex is freely soluble in CH_2Cl_2 but only slightly soluble in hexane.

The IR spectrum of (OEP)Os(NO)(SCH_2CH_2SH) (as a KBr pellet) shows a band at 1756 cm^{-1} assigned to υ_{NO}. Its ^1H NMR spectrum shows, in addition to the characteristic OEP signals, signals at –2.76 ppm (SCH_2CH_2SH), –1.17 ppm (SCH_2CH_2-SH), and –0.30 ppm (SCH_2CH_2SH) due to the coordinated thiolate–thiol ligand. These chemical shifts of the thiolate–thiol ligand in the (OEP)Os(NO)(SCH_2CH_2SH) complex are very similar to those in the ruthenium analog. Although the mass spectrum (FAB) does not show the parent ion, it shows ion fragments at *m/z* 817 (loss of the NO ligand) or at *m/z* 754 (loss of the thiolate–thiol ligand).

The analogous 3–carbon and 4–carbon ruthenium thiolate–thiol complexes, namely (TTP)Ru(NO)($SCH_2CH_2CH_2SH$) and (TTP)Ru(NO)($SCH_2CH_2CH_2CH_2SH$) were also prepared as green powders in 49% and 58% isolated yields, respectively, by the alkoxide–thiolate exchange method similar to that described in Scheme 3.5. Their IR spectra (as KBr pellets) show bands at 1779 cm^{-1} (for the 3–carbon derivative) and at 1770 cm^{-1} (for the 4–carbon derivative), respectively, assigned to υ_{NO}. The α–methylene proton chemical shifts for the three monometallic TTP complexes including (TTP)Ru-(NO)(SCH_2CH_2SH) are slightly upfield shifted in the order edtH (–2.31) > pdtH (–2.55 ppm) > bdtH (–2.65 ppm) (see Table 3.1).

Bimetallic μ–Dithiolate Complexes. In collaboration with Dr. Geun–Bae Yi, I synthesized the symmetrical bimetallic [(por)Ru(NO)]$_2$(μ–edt–*S,S'*) (por = TPP, TTP) μ–dithiolate derivatives, and the reaction proceeded in two steps as judged by ^1H NMR spectroscopy. For example, the reaction of the (TPP)Ru(NO)(O–*i*–C_5H_{11}) alkoxide complex with 1 equiv of ethane–1,2–dithiol produces the monometallic thiolate–thiol derivative, and then the addition of 1 equiv of (TPP)Ru(NO)(O–*i*–C_5H_{11}) to the reaction mixture results in the generation of the desired bimetallic μ–dithiolate derivative (Scheme 3.8). At the time, Dr. Geun–Bae Yi also independently synthesized the related octaethylporphyrin complex [(OEP)Ru(NO)]$_2$(μ–edt–*S,S'*) by a variation of the formal *trans*–addition reaction similar to the procedures used for the preparation of the

unsymmetrical bimetallic complexes (see Schemes 3.9 and 3.10 shown below).[25]

Scheme 3.8

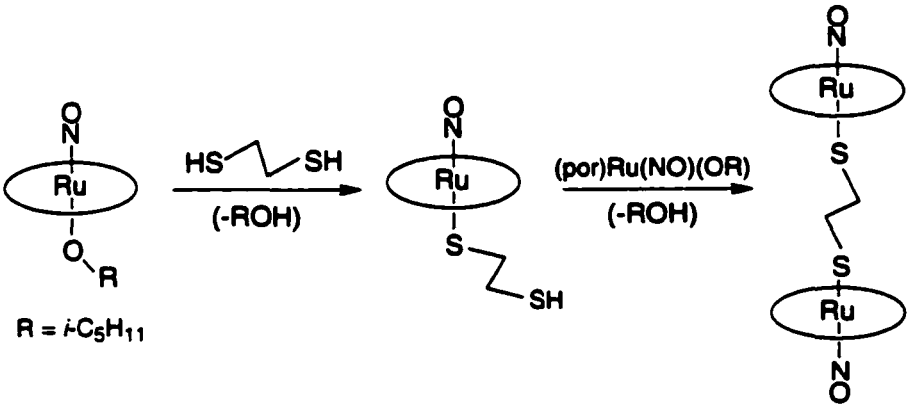

In general, the final TPP/TPP and TTP/TTP bimetallic products are isolated in low yields, due partly to the fact that the second step of the reaction is slow, and the bimetallic products are thermally sensitive and decompose in solution as the reaction progresses. Thus, it has been found that a 4–6 h reaction time generally results in fair yields of the desired TPP/TPP and TTP/TTP bimetallic products. These bimetallic complexes are very air–sensitive both in the solid state and in solution. Hence, the chromatographic purification of the bimetallic complexes was performed under N_2, and the silica column was dried in vacuo over 3 h prior to the purification of the products. They are soluble in CH_2Cl_2 and benzene, but are insoluble in hexane.

Their IR spectra (CH_2Cl_2) show that the υ_{NO} values (1802 cm^{-1} for TPP complex and 1788 cm^{-1} for TTP complex) are similar to those of their monometallic precursors. As expected, the most noticeable change between these bimetallic derivatives and their monometallic precursors lies in their ^1H NMR spectra. Their ^1H NMR spectra show the

single peak at –5.73 ppm due to the μ–edt dithiolate protons in both the symmetric TPP/TPP and TTP/TTP bimetallic derivatives, indicating that all four protons (–SCH_2-CH_2S–) are equivalent. Importantly, this value is shifted further upfield by ~3.4 ppm from the corresponding α–methylene signals in the monometallic precursors, reflecting the contributions of the ring currents effects from both porphyrins to the resonances of the bridging dithiolate protons. Furthermore, this value is shifted slightly downfield by 0.47 ppm from the analogous [(OEP)Ru(NO)]$_2$(μ–edt–*S,S'*) derivative (δ –6.20 ppm), which is almost identical to the 0.47–0.48 ppm downfield shift observed for the methylene protons in the monometallic (por)Ru(NO)(SCH_2CH_2SH) complexes when the TPP (δ –2.30 ppm) and TTP (δ –2.31 ppm) derivatives are compared with the OEP analogue (δ –2.78 ppm) (see Table 3.1). This is also consistent with the greater ring current effects of the OEP macrocycle relative to those of the tetraarylporphyrin macrocycles.

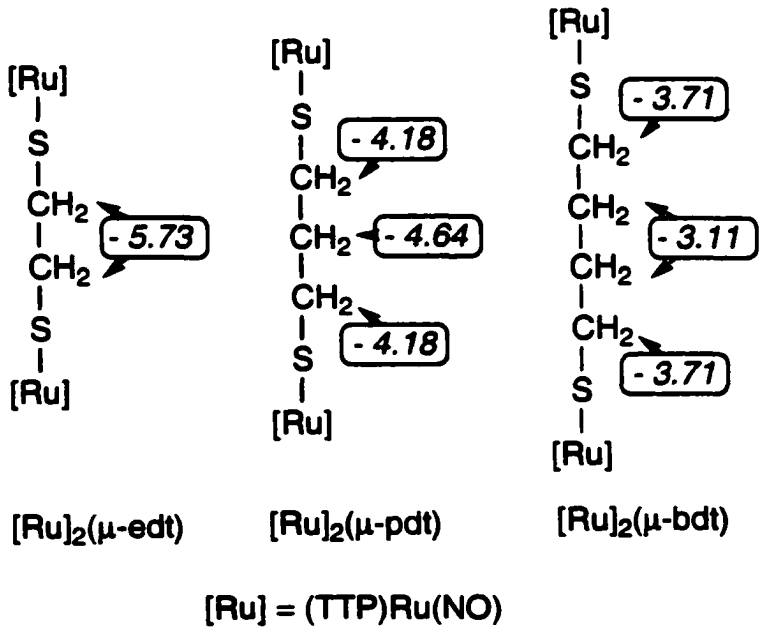

Figure 3.2. Proton chemical shifts of [(TTP)Ru(NO)]$_2$(μ–dithiolate) complexes (in $CDCl_3$).

The 3–carbon and 4–carbon bridged dithiolate derivatives of TTP have also been prepared similarly. Interestingly, as the chain length of the bridging dithiolate ligand increases, the chemical shifts of the α–methylene protons approach more closely those of the monometallic complexes (i.e., less upfield shifted; Figure 3.2 and Table 3.1), indicative of the increased distance between these protons and the second (more distant) porphyrin. Furthermore, the signals for the central $-CH_2-$ protons are less upfield–shifted in the order μ–edt (–5.73 ppm) < μ–pdt (–4.64 ppm) < μ–bdt (–3.11 ppm) as seen in Figure 3.2, indicative of less contributions of the ring current effects from the two porphyrin units to the resonances of the central $-CH_2-$ protons due to increased distances between these protons and the porphyrin rings.

The unsymmetrical mixed TPP/OEP bimetallic complex was also successfully synthesized. However, this TPP/OEP mixed bimetallic complex could not be prepared by the alkoxide–thiolate exchange reaction of Scheme 3.8. Rather, a variation of the formal *trans*–addition reaction of RSNO to (OEP)Ru(CO) was employed to attain this synthetic objective. Thus, the reaction of (TPP)Ru(NO)(SCH_2CH_2SH) with ^{t}BuONO followed by addition of (OEP)Ru(CO) to the reaction solution generates the unsymmetrical TPP/OEP bimetallic complex in very low isolated yields (*ca.* 5%) (Scheme 3.9). The putative (TPP)Ru(NO)(SCH_2CH_2SNO) complex could not be isolated because it is very air–sensitive and thermally unstable. However, its formation was inferred from its subsequent reaction with (OEP)Ru(CO) to give the desired bimetallic TPP/OEP product of Scheme 3.9, namely [(TPP)Ru(NO)](μ–edt–*S,S'*)[Ru(NO)(OEP)]. Interestingly, the symmetrical bimetallic complexes, namely [(OEP)Ru(NO)]$_2$(μ–edt–*S,S'*) and [(TPP)-Ru(NO)]$_2$(μ–edt–*S,S'*) were also formed as by–products through an as–yet unknown mechanism. It has also been observed that the reaction of (TPP)Ru(NO)(SCH_2CH_2SNO) with (OEP)Ru(CO) is more efficient in the formation of the desired bimetallic derivative than the reaction of (OEP)Ru(NO)(SCH_2CH_2SNO) with (TPP)Ru(CO). Indeed, the ^{1}H NMR spectrum of the latter reaction mixture revealed the formation of the [(TPP)Ru-

$(NO)]_2(\mu$–edt–*S,S'*) compound as a major product. This is consistent with our research group's earlier observations that RSNO additions to (OEP)Ru(CO) were cleaner than the analogous additions to (TPP)Ru(CO).[3,4,26]

Scheme 3.9

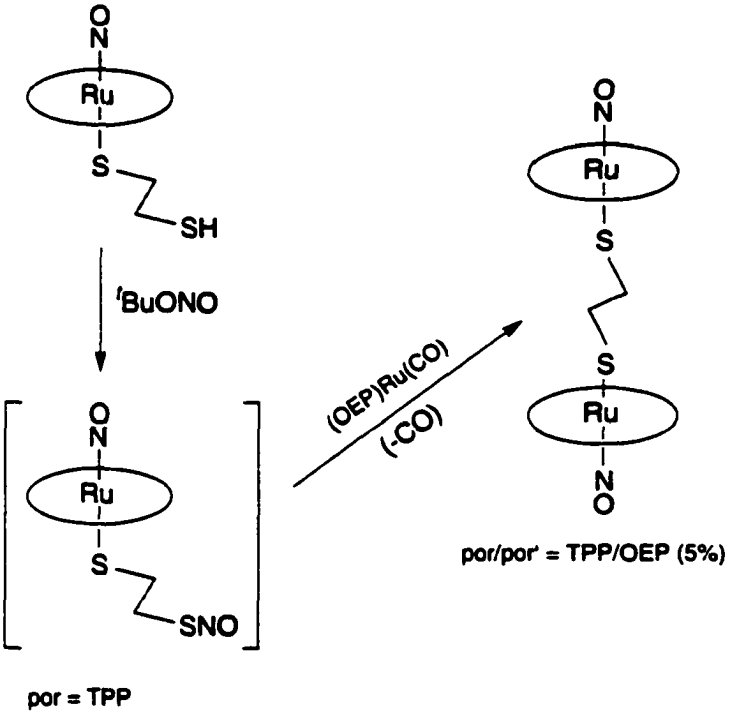

A representative 300 MHz ^{1}H NMR spectrum of the crude product mixture of the TPP/OEP mixed bimetallic preparation, showing only the region containing the resonances of the bridging thiolate protons, is shown in Figure 3.3c. The single peak at –5.73 ppm is due to $[(TPP)Ru(NO)]_2(\mu$–edt–*S,S'*) (Figure 3.3a), whereas the single peak at –6.20 ppm is due to $[(OEP)Ru(NO)]_2(\mu$–edt–*S,S'*) (Figure 3.3b). The plethora of peaks in the center region is assigned to the bridging methylene protons of the unsymmetrical [(TPP)Ru(NO)](μ–edt–*S,S'*)[Ru(NO)(OEP)] complex, and these protons display an AA'BB' coupling pattern.[27] The position of the peaks (in ^{1}H NMR spectrum)

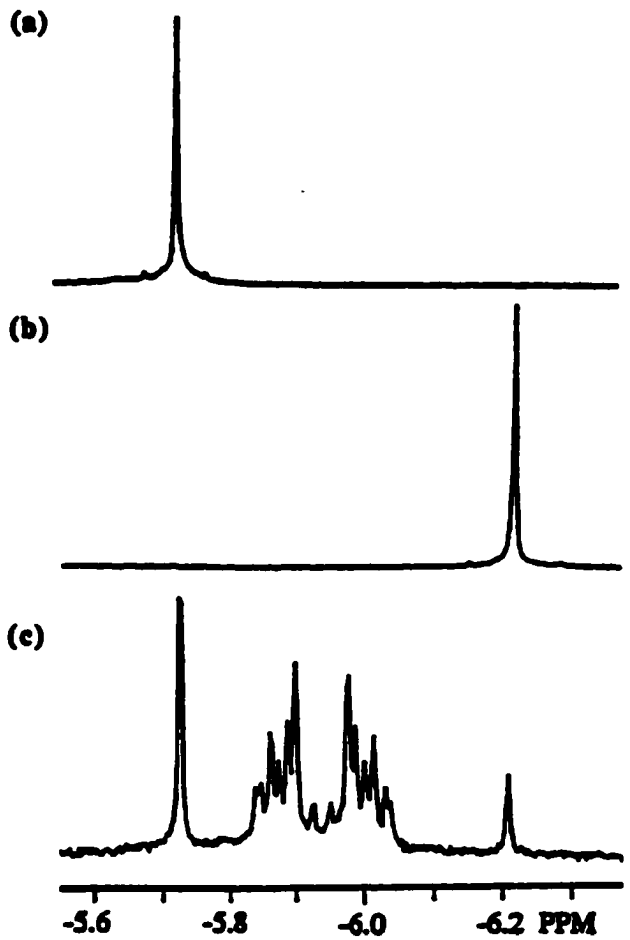

Figure 3.3. Upfield region of the 300 MHz ^{1}H NMR spectra of (a) [(TPP)Ru(NO)]$_2$(μ–edt–*S*,*S*'), (b) [(OEP)Ru(NO)]$_2$(μ–edt–*S*,*S*'), and (c) the product mixture obtained during the preparation of [(TPP)Ru(NO)](μ–edt–*S*,*S*')[Ru(NO)(OEP)].

for the bridging methylene protons of the TPP/OEP mixed bimetallic complex is reasonable, since the extent of the ring current effects of the TPP/OEP macrocycles in [(TPP)Ru(NO)](μ–edt–*S*,*S*')[Ru(NO)(OEP)] is expected to be greater than that of two TPP macrocycles in [(TPP)Ru(NO)]$_2$(μ–edt–*S*,*S*') but be smaller than that of two OEP macrocycles in [(OEP)Ru(NO)]$_2$(μ–edt–*S*,*S*').

The 400 MHz ^{1}H NMR spectrum for these methylene protons is shown in Figure 3.4a. The computer simulation of this pattern is shown in Figure 3.4b, and gives $J_{AB'}$ = $J_{A'B}$ = 11.2 Hz, $J_{AA'}$ = $J_{BB'}$ = –12.2 Hz, J_{AB} = 5 Hz, $J_{A'B'}$ = 3.7 Hz, and $\Delta\upsilon_{AB}$ = 51 Hz. Needless to say, it is the presence of two distinctly different porphyrins in this novel TPP/OEP derivative that causes the inequivalence of the μ–edt protons.

A similar methodology (to that described in Scheme 3.9) was also employed to prepare the heterobimetallic [(OEP)Os(NO)](μ–edt–*S*,*S*')[Ru(NO)(TTP)] derivative. Thus, the reaction of (OEP)Os(NO)(SCH$_2$CH$_2$SH) with ^{t}BuONO generates the putative (OEP)Os(NO)(SCH$_2$CH$_2$SNO) compound, which can then be reacted with (TTP)Ru-(CO) to give the heterobimetallic [(OEP)Os(NO)](μ–edt–*S*,*S*')[Ru(NO)(TTP)] derivative (Scheme 3.10) in 70% yield by ^{1}H NMR spectroscopy.

Scheme 3.10

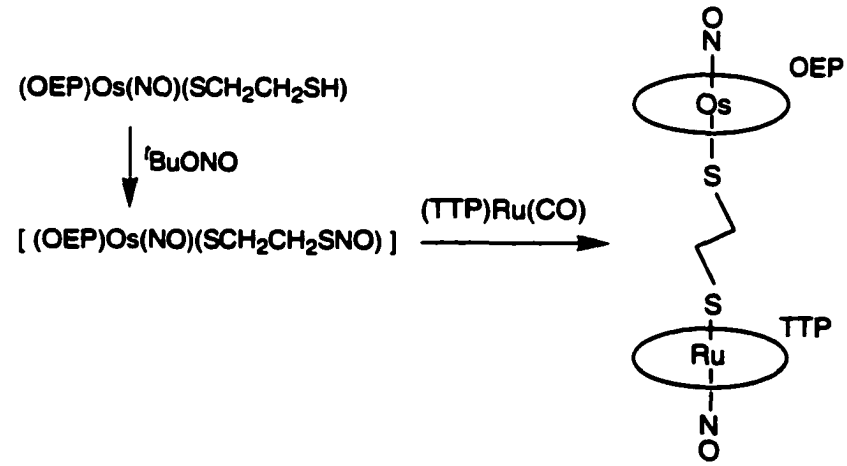

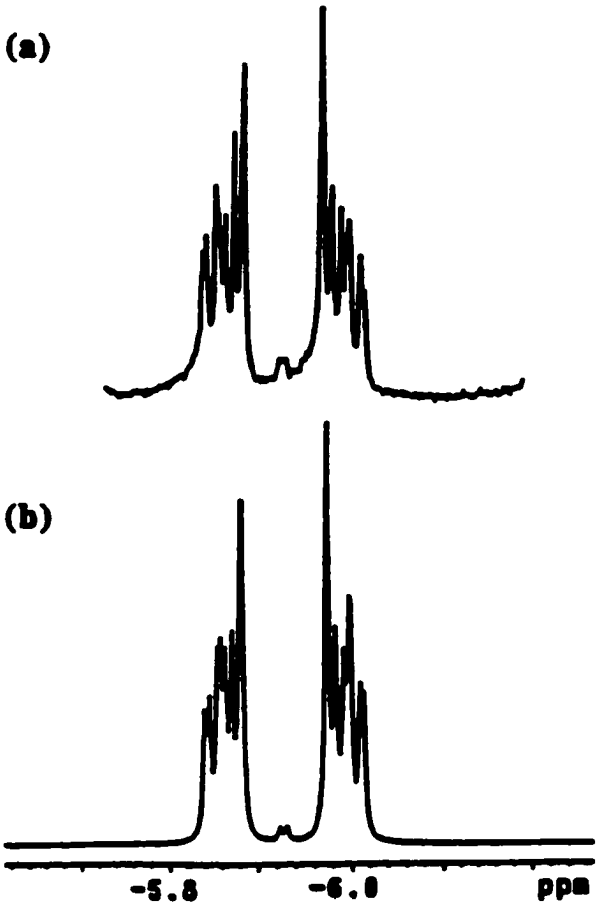

Figure 3.4. Upfield region of the 400 MHz ^{1}H NMR spectrum of [(TPP)Ru(NO)](μ–edt–*S,S'*)[Ru(NO)(OEP)]: (a) experimental spectrum (sample in $CDCl_3$), and (b) computer simulation.

Although a spectroscopically pure sample of this air–sensitive compound was not obtained (the major by–product was [(OEP)Os(NO)]$_2$(μ–edt–*S,S'*)), the ^{1}H NMR spectrum of the product mixture (of Scheme 3.10) shows, in addition to the signals for two porphyrin macrocycles (TTP and OEP), an AA'BB' coupling pattern[27] consisting of two clusters of peaks centered at *ca.* –5.92 ppm and –6.01 ppm (Figure 3.5) assigned to the μ–SCH_2CH_2S– protons; spectral simulation gave $J_{AB'} = J_{A'B}$ = 13.4 Hz, $J_{AA'} = J_{BB'}$ = –12.6 Hz, J_{AB} = 6 Hz, $J_{A'B'}$ = 3.6 Hz, and $\Delta\upsilon_{AB}$= 43 Hz. Due to the presence of two distinctly different metalloporphyrin moieties in this bimetallic derivative, it is not surprising that the AA'BB' coupling pattern observed is almost identical to that of the related unsymmetrical [(TPP)Ru(NO)](μ–edt–*S,S'*)[Ru(NO)(OEP)] compound of Figure 3.4.

As in the case of [(TPP)Ru(NO)](μ–edt–*S,S'*)[Ru(NO)(OEP)], there are several notes of interest regarding the synthesis of [(OEP)Os(NO)](μ–edt–*S,S'*)[Ru(NO)(TTP)]. The (OEP)Os/(TTP)Ru bimetallic complex was not formed via the expected alkoxide–thiolate exchange reaction. For example, the reaction of the (OEP)Os(NO)(SCH_2CH_2-SH) complex with (TTP)Ru(NO)(O–*i*–C_5H_{11}) did not produce the bimetallic derivative. In addition, the reaction of (OEP)Os(NO)(SCH_2CH_2SNO) with (TTP)Ru(CO) is more efficient in the formation of the desired bimetallic derivative than the reaction of (TTP)Ru(NO)(SCH_2CH_2SNO) with (OEP)Os(CO). Indeed, the latter reaction showed the formation of the [(TTP)Ru(NO)]$_2$(μ–edt–*S,S'*) (δ_{SCH_2} –5.73 ppm) compound as the major product (by ^{1}H NMR spectroscopy). In any event, the successful reaction of (OEP)Os(NO)(SCH_2CH_2SNO) with (TTP)Ru(CO) is consistent with our research group's earlier observations that RSNO additions to (por)Ru(CO) were faster and cleaner than the analogous additions to (por)Os(CO).[4]

Conclusion

Monometallic thiolate–thiol complexes of ruthenium and osmium nitrosyl

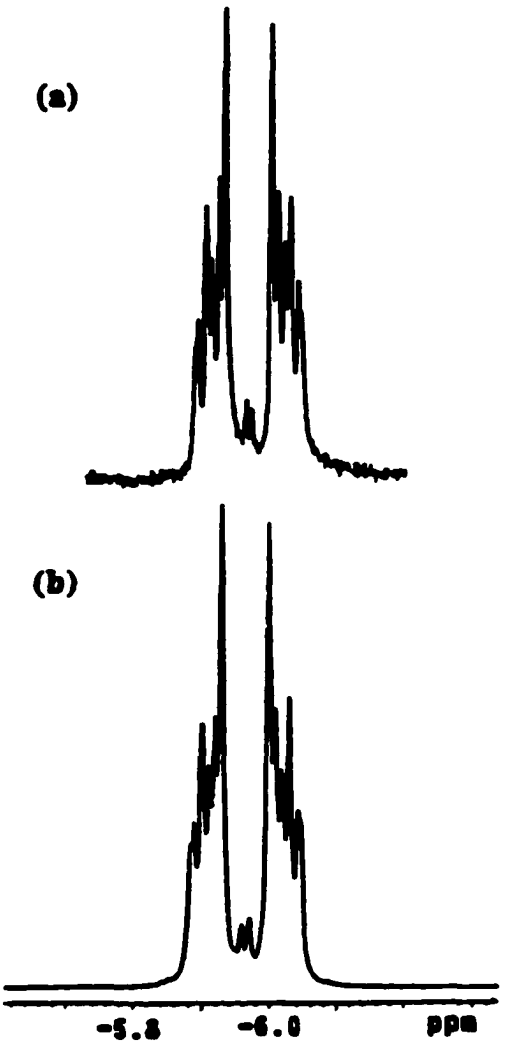

Figure 3.5. Upfield region of the 400 MHz ^{1}H NMR spectrum of [(OEP)Os(NO)](μ-edt-*S*,*S*')[Ru(NO)(TTP)]: (a) experimental spectrum (sample in $CDCl_3$), and (b) computer simulation.

porphyrins have been prepared, and their novel symmetrical bimetallic μ–dithiolate derivatives have also been prepared. These monometallic and bimetallic complexes have been fully characterized by elemental analyses, infrared and ^{1}H NMR spectroscopy, and by mass spectrometry. To the best of my knowledge, these bimetallic μ–dithiolate complexes are the first examples reported for any metalloporphyrin. Interestingly, the ^{1}H NMR spectra of the symmetric TPP/TPP and TTP/TTP bimetallic μ–edt dithiolate complexes of ruthenium porphyrins show the *single* peak for the μ–edt dithiolate ligands, reflecting the equivalence of the μ–edt protons. Furthermore, the chemical shift of this single peak is shifted further upfield from the corresponding α–methylene signals in the monometallic precursors, indicative of the increased ring current effects due to the presence of two porphyrins. The ^{1}H NMR spectra of the 3–carbon and 4–carbon bridged dithiolate derivatives of TTP also reveal that as the chain length of μ–dithiolate ligand increases, the chemical shifts of the α–methylene protons become similar to those of the monometallic thiolate–thiol complexes, implying the decreased ring current effects due to the increased distance between these protons and the second (more distant) porphyrin. Importantly, two novel unsymmetrical bimetallic complexes, namely [(TPP)Ru(NO)](μ–edt–*S,S'*)[Ru(NO)(OEP)] and [(OEP)Os(NO)](μ–edt–*S,S'*)[Ru(NO)-(TTP)] have also been obtained, and the experimental and simulated ^{1}H NMR spectra of the protons of the μ–dithiolate bridge indicate that all four protons (–SC*H*$_2$-C*H*$_2$S–) are inequivalent. These symmetrical and unsymmetrical nitrosyl bimetallic complexes might be an interesting new class of compounds for further study. For example, I observed that the reaction of symmetrical bimetallic [(OEP)Ru(NO)]$_2$(μ–edt–*S,S'*) complex with ca. 3 equiv of $HBF_4 \cdot Et_2O$ gives the previously reported [(OEP)Ru-(NO)(H_2O)]BF_4[7,28] and free $HSCH_2CH_2SH$ (by ^{1}H NMR spectroscopy). Hence, determining which sulfur atom is more reactive towards electrophilic attack between (por)Os(NO)(*S*CH_2–) and (por)Ru(NO)(*S*CH_2–) moieties in [(por)Os(NO)](μ–edt–*S,S'*)[Ru(NO)(por)] could be an interesting topic due to the importance of the

trans–effects from the nitrosyl ligand to the axial ligand in the six–coordinate nitrosyl metalloporphyrins. Furthermore, the [(por)Co(NO)](μ–edt–*S,S'*)[Ru(NO)(por)] complexes which may presumably contain both *bent* NO (in (por)Co(NO) fragment) and *linear* NO (in (por)Ru(NO) fragment) could also be synthesized for the study of the relative *trans*–effects between *bent* and *linear* nitrosyl ligands in the same compound.

References

(1) Cheng, L.; Richter-Addo, G. B. *Binding and Activation of Nitric Oxide by Metalloporphyrins and Heme* In The Porphyrin Handbook; Kadish, K. M.; Smith, K. M.; Guilard, G., Eds.; Academic Press: New York, 2000; Vol. 4 (Biochemistry and Binding: Activation of Small Molecules), pp 219-291.

(2) Chen, L.; Khan, M. A.; Richter-Addo, G. B. *Inorg. Chem.* **1998**, *37*, 533-540.

(3) Yi, G.-B.; Khan, M. A.; Richter-Addo, G. B. *Chem. Commun.* **1996**, 2045-2046.

(4) Yi, G.-B.; Chen, L.; Khan, M. A.; Richter-Addo, G. B. *Inorg. Chem.* **1997**, *36*, 3876-3885.

(5) Yi, G.-B.; Khan, M. A.; Powell, D. R.; Richter-Addo, G. B. *Inorg. Chem.* **1998**, *37*, 208-214.

(6) Lee, J.; Yi, G.-B.; Powell, D. R.; Khan, M. A.; Richter-Addo, G. B. *Can. J. Chem.* **2001**, *79*, 830-840.

(7) Yi, G.-B.; Khan, M. A.; Richter-Addo, G. B. *Inorg. Chem.* **1996**, *35*, 3453-3454.

(8) Bohle, D. S.; Hung, C.-H.; Smith, B. D. *Inorg. Chem.* **1998**, *37*, 5798-5806.

(9) Bohle, D. S.; Goodson, P. A.; Smith, B. D. *Polyhedron* **1996**, *15*, 3147-3150.

(10) Ellison, M. K.; Scheidt, W. R. *J. Am. Chem. Soc.* **1999**, *121*, 5210-5219.

(11) Cheng, L.; Chen, L.; Chung, H.-S.; Khan, M. A.; Richter-Addo, G. B.; Young, V. G., Jr. *Organometallics* **1998**, *17*, 3853-3864.

(12) Rao, C. P.; Dorfman, J. R.; Holm, R. H. *Inorg. Chem.* **1986**, *25*, 428-439.

(13) Mukherjee, R. N.; Rao, C. P.; Holm, R. H. *Inorg. Chem.* **1986**, *25*, 2979.

(14) Hsieh, T.-C.; Nicholson, T.; Zubieta, J. *Inorg. Chem.* **1988**, *27*, 241-250.

(15) Forniés-Cámer, J.; Masdeu-Bultó, A. M.; Claver, C.; Cardin, C. J. *Inorg. Chem.* **1998**, *37*, 2626-2632.

(16) Stack, T. D. P.; Carney, M. J.; Holm, R. H. *J. Am. Chem. Soc.* **1989**, *111*, 1670-1676.

(17) Narayanaswamy, R.; Young, M. A.; Parkhurst, E.; Ouellette, M.; Kerr, M. E.; Ho, D. M.; Elder, R. C.; Bruce, A. E.; Bruce, M. R. M. *Inorg. Chem.* **1993**, *32*, 2506-2517.

(18) Danzer, W.; Fehlhammer, W. P.; Liu, A. T.; Thiel, G.; Beck, W. *Chem. Ber.* **1982**, *115*, 1682-1693.

(19) Stephan, D. W. *Organometallics* **1991**, *10*, 2037-2045.

(20) Nadasdi, T. T.; Stephan, D. W. *Organometallics* **1992**, *11*, 116-122.

(21) Holmes, R. R.; Shafieezad, S.; Holmes, J. M.; Day, R. O. *Inorg. Chem.* **1988**, *27*, 1232-1237.

(22) Hoffmann, H. M.; Dräger, M. *Z. Naturforsch.* **1986**, *41B*, 1455-1460.

(23) Rillema, D. P.; Nagle, J. K.; Barringer, L. F., Jr.; Meyer, T. J. *J. Am. Chem. Soc.* **1981**, *103*, 56-62.

(24) Che, C.-M.; Poon, C.-K.; Chung, W.-C.; Gray, H. B. *Inorg. Chem.* **1985**, *24*, 1277-1278.

(25) Lee, J.; Yi, G.-B.; Khan, M. A.; Richter-Addo, G. B. *Inorg. Chem.* **1999**, *38*, 4578-4584.

(26) Richter-Addo, G. B. *Acc. Chem. Res.* **1999**, *32*, 529-536.

(27) Bovey, F. A.; Jelinski, L.; Mirau, P. A. *Nuclear Magnetic Resonance Spectroscopy*; Academic Press: San Diego, 1988; pp 183-192 and 592-601.

(28) Chen, L.; Yi, G.-B.; Wang, L.-S.; Dharmawardana, U. R.; Dart, A. C.; Khan, M. A.; Richter-Addo, G. B. *Inorg. Chem.* **1998**, *37*, 4677-4688.

Chapter 4. Nitrones are Suitable Ligands for Heme Models: Synthesis and Molecular Structures of the First Metalloporphyrin Nitrone Complexes (OEP)M(CO)(DMPO) (M = Ru, Os; DMPO = 5,5-dimethyl-1-pyrroline *N*-oxide)*

Introduction

Nitrones belong to the general class of RN(O)=X compounds (X is a carbon-linked group) (Figure 4.1),[1] and contain the *C*-nitroso functional group. They can be readily synthesized by a variety of methods including *(i)* condensation of carbonyl compounds ($R_2C=O$) with hydroxylamines,[2-4] *(ii)* catalytic oxidation of secondary amines or hydroxylamines by metal-peroxo complexes,[5-7] and *(iii)* oxidation of *N,N*-disubstituted hydroxylamines by HgO, Ag_2O, ferricyanide, and other oxidants.[2,8]

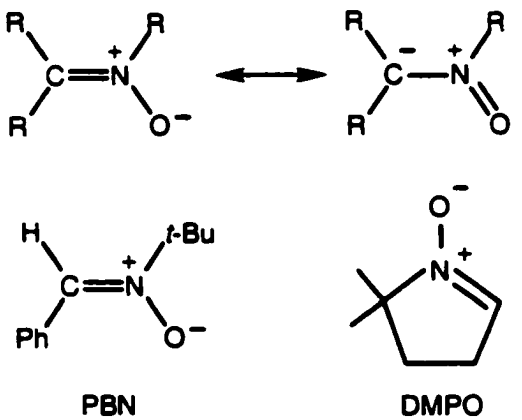

Figure 4.1. Resonance forms of the nitrone functional group, and two examples of nitrones.

---

* "Nitrones are Suitable Ligands for Heme Models: X-ray Crystal Structure of the First Metalloporphyrin Nitrone Complex." Lee, J.; Twamley, B.; Richter-Addo, G. B. *Chem. Commun.* **2002**, 380-381. Reproduced in part by permission of The Royal Society of Chemistry.

Nitrones are frequently used as spin traps.[9] In addition, they are useful precursors in organic synthesis. For example, nitrones can react with olefins to generate the 5–membered isoxazolidines via the [3+2] cycloaddition reaction (Scheme 4.1).[2,10]

Scheme 4.1

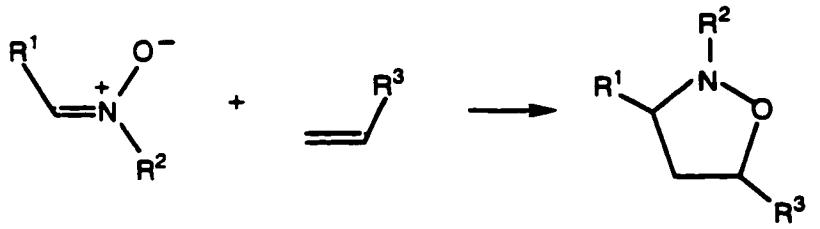

Interestingly, nitrones are now known to be produced during the oxidation of some amines by cytochrome P450. Excellent work by Lindeke and coworkers has shown that the *in vitro* metabolism of norbenzphetamine ($PhCH_2CH(Me)NHCH_2Ph$) by cytochrome P450 gives the hydroxylamine and the nitrone metabolites.[11] Guengerich and coworkers also showed that cytochrome P450 catalyzes the oxidation of cycloalkylamines to nitrones.[12] Importantly, however, it has also been proposed that some nitrones are capable of serving as ligands for cytochrome P450[13] and hemoglobin.[14] PBN (α–phenyl–*tert*–butylnitrone; Figure 4.1) has also been shown to decompose photolytically to NO, which was trapped by heme and non–heme proteins to give metal–NO products.[15] Despite the obvious importance in heme–dependent biochemistry and relevance to amine oxidation chemistry, no nitrone complexes of synthetic heme models had been reported prior to this work.

Indeed, only a few metal complexes containing nitrones as ligands were known prior to this work. To the best of my knowledge, the known metal–nitrone complexes were prepared from one of six synthetic methods, and only the first method appears general for the preparation of metal–nitrone complexes: *(i)* simple adduct formation of nitrones with metal complexes,[8,10,16,17] *(ii)* decomposition of metal nitroxide complexes,[18]

(iii) addition of ^{t}BuN=O to a cationic Re carbyne complex,[19] *(iv)* addition of ^{t}BuN=O to a Pt–coordinated ethylene,[20] *(v)* insertion of ArN=O into the Fe=CHAr bond,[21] and *(vi)* reactions of oximes with Pt–allene complexes.[22] Furthermore, only a handful of metal complexes of nitrones have been characterized by X–ray crystallography. There are three main ways in which the nitrone ligands bind to metals in the structurally characterized metal–nitrone complexes (Figure 4.2).

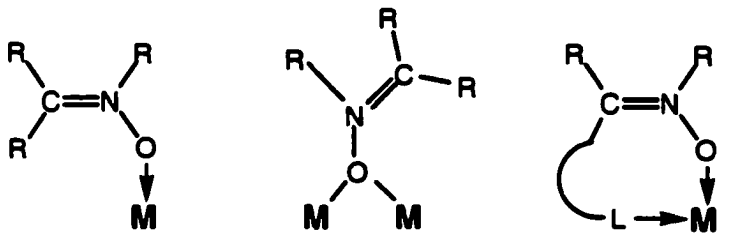

Figure 4.2. Binding modes in metal–nitrone complexes established by single–crystal X–ray crystallography.

Scheme 4.2

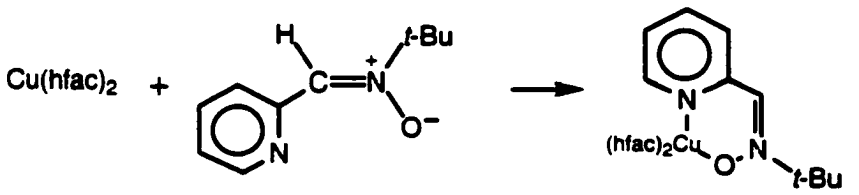

Examples of type **A** complexes in which the nitrone O–atom serves as an η^1 donor include those of Ti,[10] Fe,[8,21] Co,[18] and Ge.[16] Type **B** complexes containing μ,η^1–O bridging nitrone ligands are known for Mn,[8,23] Co,[8] and Ni.[8] The η^2–O,L metallocycles (type **C**) are also generated when *N–tert*–butyl–α–(2–pyridyl)nitrone is reacted with some metal hexafluoroacetylacetonate (hfac) complexes,[8] and the example of Cu is

shown in Scheme 4.2. Related other metallocycles in which the metal–O–N=C group occurs (metal = Re, Pt) have also been reported.[19,20,22]

In this chapter, the successful syntheses and characterization of the first thermally stable metalloporphyrin nitrone complexes will be described. The single–crystal X–ray structures of these compounds will also be reported. Our research group was interested in determining how nitrones bind to the metal centers in synthetic metalloporphyrins, and how the coordinated nitrone ligands function in metalloporphyrin nitrone complexes. Hence, the spectroscopic and crystallographic results on these metalloporphyrin nitrone complexes will be discussed in detail in this chapter. To the best of my knowledge, these are first examples of nitrone complexes reported for any synthetic metalloporphyrin.

Experimental Section

All reactions were performed under an atmosphere of prepurified nitrogen using standard Schlenk glassware and/or in an Innovative Technology Labmaster 100 Dry Box. Solutions for spectral studies were also prepared under a nitrogen atmosphere. Solvents were distilled from appropriate drying agents under nitrogen just prior to use: CH_2Cl_2 (CaH_2), hexane (CaH_2), heptane (CaH_2), and toluene (Na).

Chemicals. (OEP)Os(CO) was prepared by the literature method.[24] (OEP)Ru-(CO) and 5,5–dimethyl–1–pyrroline *N*–oxide (DMPO, 97%) were purchased from Aldrich Chemical Co. and used as received. Chloroform–*d* (99.8%) was obtained from Cambridge Isotope Laboratories. Elemental analyses were performed by Atlantic Microlab, Norcross, Georgia.

Instrumentation. Infrared spectra were recorded on a Bio–Rad FT–155 FTIR spectrometer. Proton NMR spectra were obtained on Varian 400 MHz or 300 MHz spectrometers and the signals referenced to the residual signal of the solvent employed. All coupling constants are in Hz. Electrospray mass spectrometry was performed using a

Micromass Q–TOF instrument.

Preparation of (OEP)Ru(CO)(DMPO). Excess DMPO (0.1 g, ca. 0.9 mmol) was added to a toluene (10 mL) solution of (OEP)Ru(CO) (0.030 g, 0.045 mmol) under a nitrogen atmosphere, and the solution was heated to reflux for 15 min, during which it turned from red to slightly dark red. The solvent was removed in vacuo, and the residue was redissolved in CH_2Cl_2/hexane (1:1, 10 mL). Slow evaporation of the solution under a nitrogen atmosphere resulted in the generation of red crystals which were washed with hexane (10 mL) and dried in vacuo to give the product (OEP)Ru(CO)(DMPO) $\cdot 0.19CH_2Cl_2 \cdot 0.5H_2O$ (0.027 g, 0.034 mmol, 75% isolated yield). Anal. Calcd for $C_{43}H_{55}N_5O_2Ru_1 \cdot 0.19CH_2Cl_2 \cdot 0.5H_2O$: C, 64.83; H, 7.10; N, 8.75; Cl, 1.68. Found: C, 64.61; H, 6.97; N, 8.77; Cl, 1.45. IR (KBr, cm^{-1}): υ_{CO} = 1914 s; also 2961 m, 2930 w, 2869 w, 1593 w, 1538 vw, 1466 m, 1453 m, 1371 w, 1316 vw, 1304 vw, 1272 m, 1230 m, 1215 vw, 1198 vw, 1148 m, 1111 w, 1056 m, 1019 m, 991 w, 960 m, 840 m, 746 w, 712 vw, 666 vw, 583 vw. ^{1}H NMR ($CDCl_3$): δ 9.82 (s, 4H, *meso*–H of OEP), 5.28 (s, CH_2Cl_2), 3.98 (m, 16H, CH_2CH_3 of OEP), 1.88 (t, J = 8, 24H, CH_2CH_3 of OEP). The peaks for DMPO were very weak at room temperature. ^{1}H NMR ($CDCl_3$, –40 °C): δ 9.81 (s, 4H, *meso*–H of OEP), 5.27 (s, CH_2Cl_2), 3.97 (m, 16H, CH_2CH_3 of OEP), 1.84 (t, J = 8, 24H, CH_2CH_3 of OEP), 0.65 (br t, 2H of DMPO), 0.18 (m, overlapping 1H and 2H of DMPO), –1.67 (s, 6H, CH_3 of DMPO). High–resolution mass spectrum (ESI) for [(OEP)Ru(CO)(DMPO) + H]$^+$ ($C_{43}H_{56}N_5O_2Ru_1$): *m/z* 776.3563. Calculated 776.3477.

A suitable crystal for structure determination was grown by slow evaporation of toluene/heptane (1:1) solution of the compound at room temperature under inert atmosphere.

Preparation of (OEP)Os(CO)(DMPO). Excess DMPO (0.1 g, ca. 0.9 mmol) was added to a toluene (10 mL) solution of (OEP)Os(CO) (0.030 g, 0.040 mmol) under a nitrogen atmosphere, and the solution was heated to reflux for 15 min, during which it turned from pink red to dark red. The solvent was removed in vacuo, and the residue was

redissolved in CH_2Cl_2/hexane (1:2, 9 mL). Slow evaporation of the solution under a nitrogen atmosphere resulted in the generation of dark red crystals which were washed with hexane (10 mL) and dried in vacuo to give the product (OEP)Os(CO)(DMPO) $\cdot 0.5CH_2Cl_2$ (0.022 g, 0.024 mmol, 61% isolated yield). Anal. Calcd for $C_{43}H_{55}N_5O_2Os_1 \cdot 0.5CH_2Cl_2$: C, 57.63; H, 6.23; N, 7.72. Found: C, 57.66; H, 6.23; N, 7.59. IR (KBr, cm^{-1}): υ_{CO} = 1883 s ; also 2961 m, 2931 w, 2868 w, 1598 w, 1466 m, 1452 m, 1371 m, 1316 vw, 1304 vw, 1273 m, 1232 m, 1191 w, 1149 m, 1111 w, 1056 m, 1019 m, 992 w, 961 m, 842 m, 742 w, 716 w. ^1H NMR ($CDCl_3$): δ 9.66 (s, 4H, *meso*–H of OEP), 5.27 (s, CH_2Cl_2), 3.95 (m, 16H, CH_2CH_3 of OEP), 1.87 (t, J = 8, 24H, CH_2CH_3 of OEP), 0.68 (br t, 2H of DMPO), 0.30 (br s, 1H of DMPO), 0.22 (t, J = 7, 2H of DMPO), –1.60 (br s, 6H, CH_3 of DMPO). High–resolution mass spectrum (ESI) for $[(OEP)Os(CO)(DMPO)]^+$ ($C_{43}H_{55}N_5O_2Os_1$): *m/z* 865.3893. Calculated 865.3971.

A suitable crystal for structure determination was grown by slow evaporation of CH_2Cl_2/hexane (1:2) solution of the compound at room temperature under inert atmosphere.

Results and Discussion

The reaction of (OEP)Ru(CO) with excess DMPO in refluxing toluene for 15 min produced the (OEP)Ru(CO)(DMPO) complex in 75% isolated yield (Scheme 4.3).

Scheme 4.3

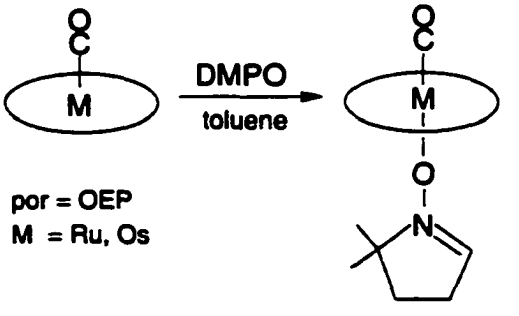

The osmium derivative (OEP)Os(CO)(DMPO) was also prepared similarly in 61% isolated yield.

The IR spectrum of (OEP)Ru(CO)(DMPO) (as a KBr pellet) reveals a υ_{CO} of 1914 cm^{-1}, which is 16 cm^{-1} lower in energy than the υ_{CO} of the starting (OEP)Ru(CO) at 1930 cm^{-1} (Figure 4.3). The lowering of the υ_{CO} is *opposite* to that seen for (OEP)-Ru(CO)(N(O)$C_6H_4NMe_2$-*p*)[25] which contains an *N*–bound nitrosoarene ligand that behaves as a net π–acid in this complex, but is similar to that seen for (OEP)Ru(CO)-($ONNEt_2$) (υ_{CO} 1910 cm^{-1})[26] which contains an *O*–bound axial nitrosamine ligand. This IR spectroscopic feature indicates that like the nitrosamine Et_2NNO ligand in (OEP)Ru(CO)($ONNEt_2$), the coordinated DMPO ligand in (OEP)Ru(CO)(DMPO) acts as an electron donor towards the (OEP)Ru(CO) fragment, which makes more electron density available for Ru^{II}–CO back–donation, thus causing the lowering of the υ_{CO}. The υ_{CO} band of (OEP)Os(CO)(DMPO) (1883 cm^{-1}) is also shifted by 11 cm^{-1} to lower wavenumbers relative to that of the starting (OEP)Os(CO) complex (1894 cm^{-1}) (Figure 4.4), and is identical to that of the nitrosamine complex (OEP)Os(CO)($ONNEt_2$).[26]

The ^1H NMR spectrum of (OEP)Ru(CO)(DMPO) in $CDCl_3$ shows that at room temperature, the coordinated nitrone DMPO peaks are not clearly observed. However, the nitrone DMPO peaks can be observed at low temperature (–40 °C) (Figure 4.5). Unlike the ruthenium derivative, the ^1H NMR spectrum (in $CDCl_3$) of (OEP)Os(CO)(DMPO) displays peaks due to the coordinated DMPO at room temperature. Interestingly, these ^1H NMR features are *opposite* to those seen for the (OEP)M(CO)($ONNEt_2$) complexes (M = Ru, Os).[26]

In order to unambiguously determine the mode of linkage of the nitrone ligand toward the metal center in (OEP)Ru(CO)(DMPO), suitable crystals for a single–crystal X–ray crystallographic analysis were grown. The molecular structure of (OEP)Ru-(CO)(DMPO) is shown in Figure 4.6. Bond lengths and angles are listed in Tables 4.1 and 4.2, respectively.

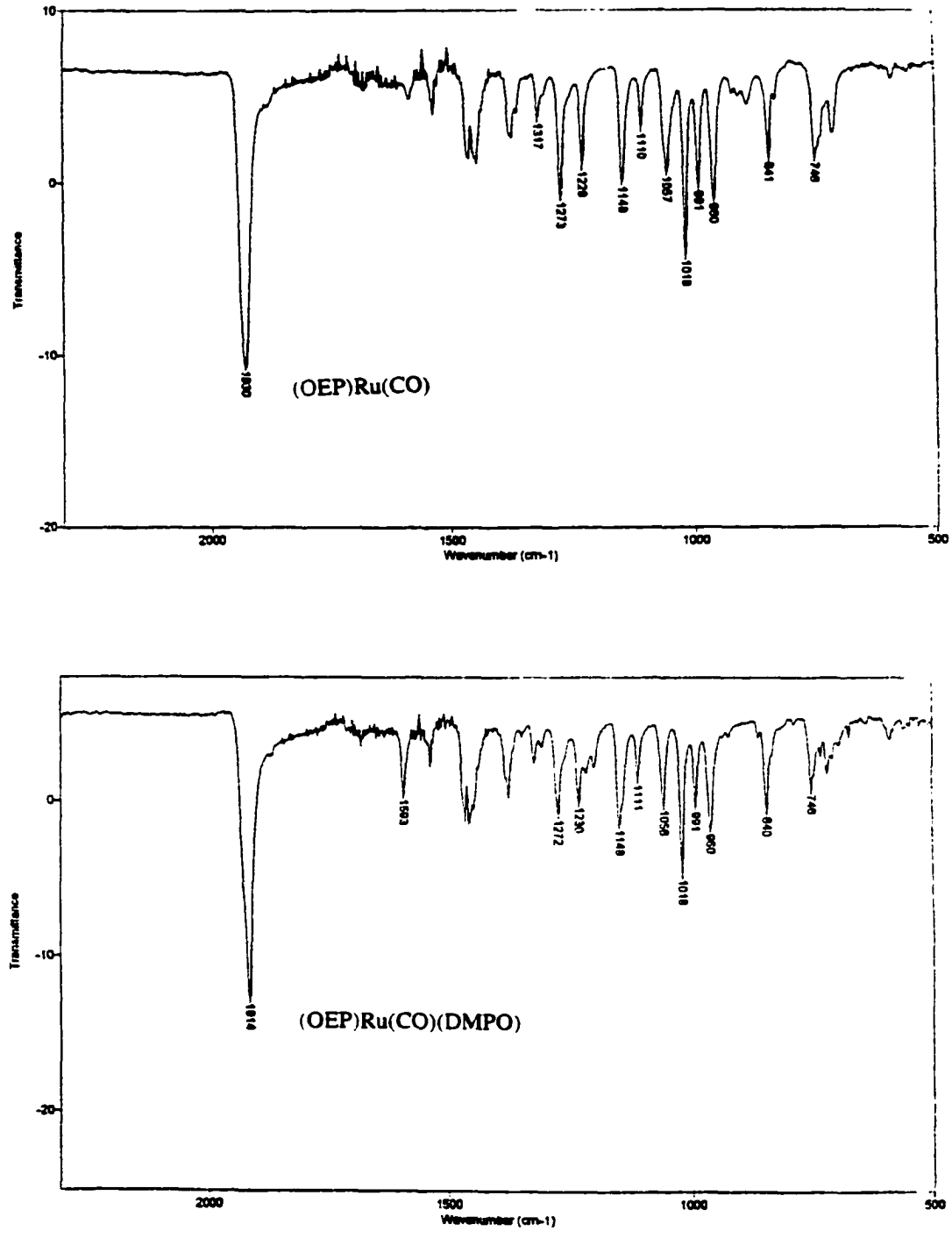

Figure 4.3. IR spectra (KBr) of (OEP)Ru(CO) (top) and (OEP)Ru(CO)(DMPO) (bottom).

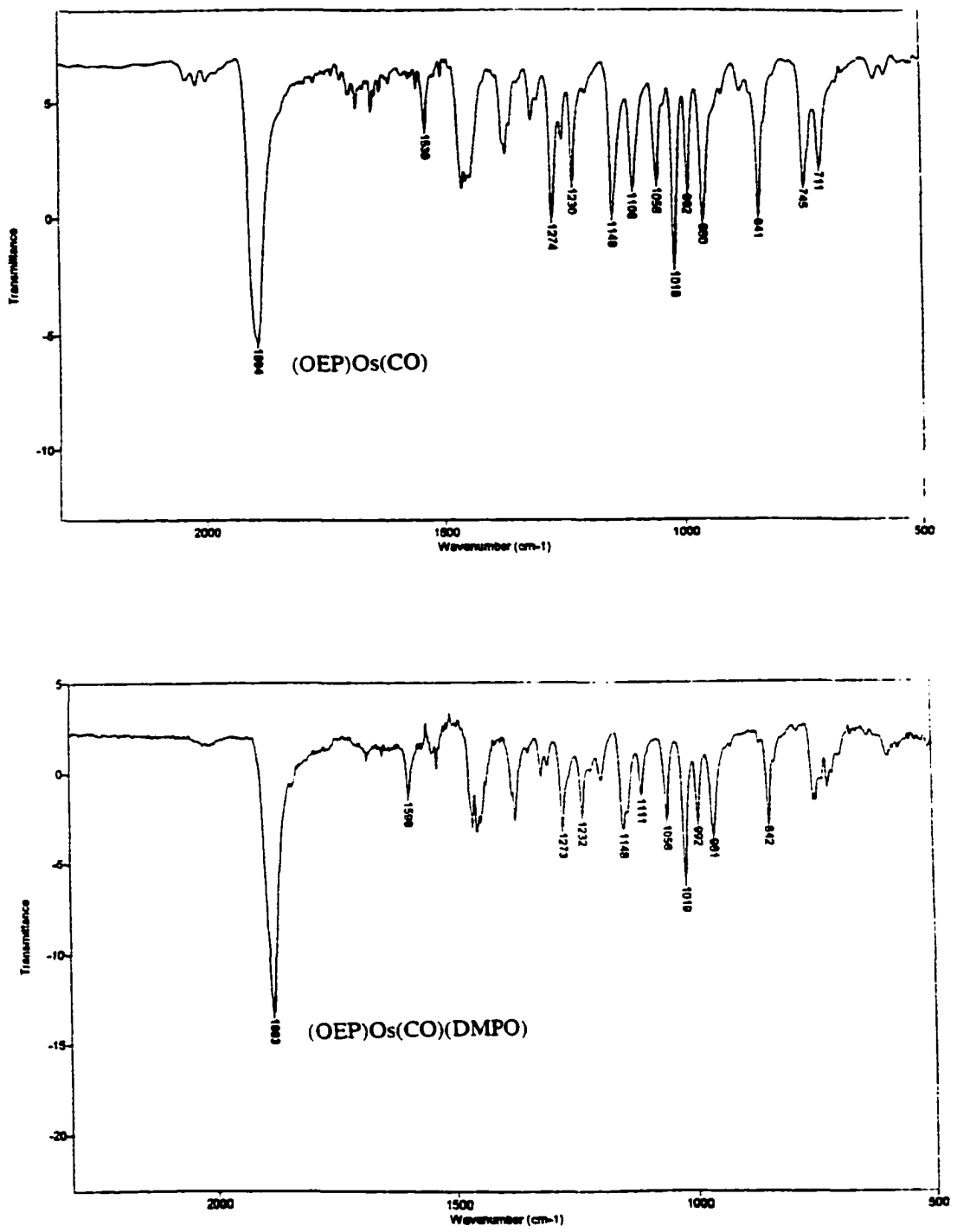

Figure 4.4. IR spectra (KBr) of (OEP)Os(CO) (top) and (OEP)Os(CO)(DMPO) (bottom).

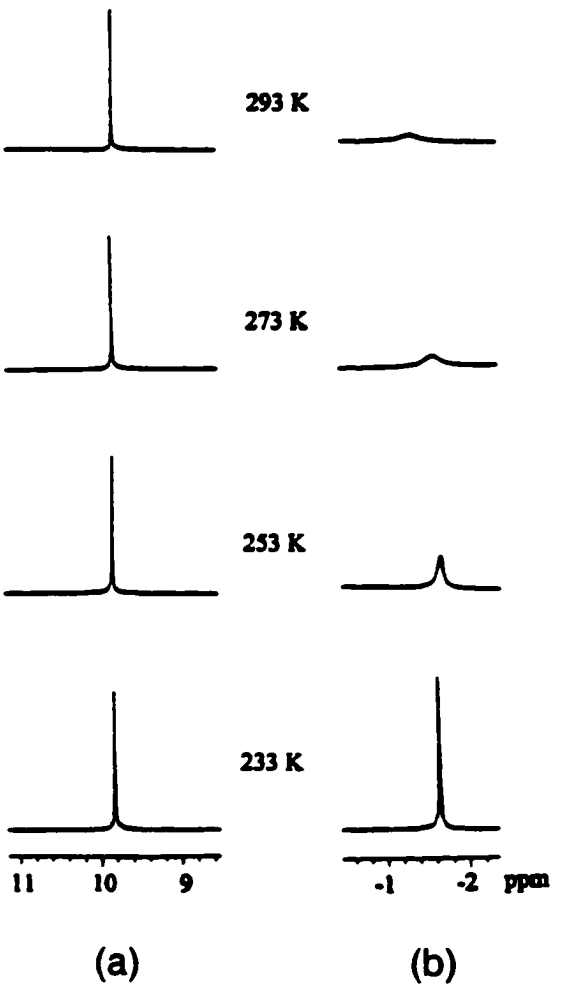

Figure 4.5. Comparison of the change with temperature of the 300 MHz ^{1}H NMR spectra of (OEP)Ru(CO)(DMPO) (in $CDCl_3$). (a) The peak for *meso* protons of the OEP macrocycle. (b) The peak for two CH_3 protons of the *coordinated* DMPO.

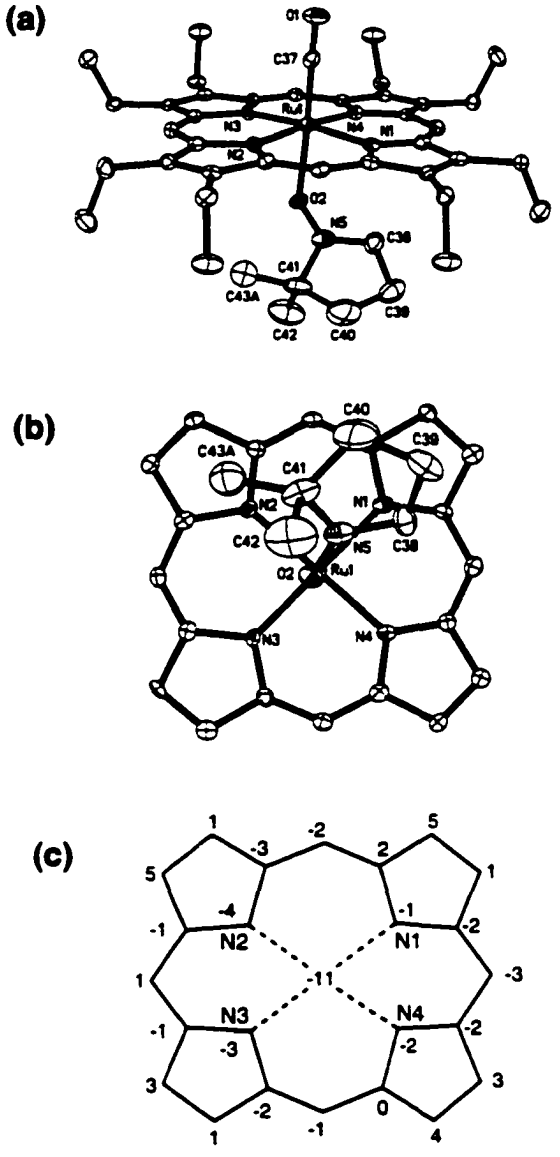

Figure 4.6. (a) Molecular structure of (OEP)Ru(CO)(DMPO). (b) View of the orientation of the nitrone ligand relative to the porphyrin skeleton. (c) Perpendicular atom displacements (in units of 0.01 Å) of the porphyrin core from the 24–atom mean porphyrin plane.

Table 4.1. Bond lengths (Å) for (OEP)Ru(CO)(DMPO)

Ru(1)-C(37)	1.816(6)	C(5)-C(25)	1.498(8)
Ru(1)-N(3)	2.051(9)	C(6)-C(7)	1.396(8)
Ru(1)-N(4)	2.055(5)	C(7)-C(8)	1.376(10)
Ru(1)-N(2)	2.058(4)	C(8)-C(9)	1.450(14)
Ru(1)-N(1)	2.069(10)	C(9)-C(10)	1.380(12)
Ru(1)-O(2)	2.214(4)	C(9)-C(27)	1.498(14)
N(1)-C(18)	1.345(13)	C(10)-C(11)	1.443(8)
N(1)-C(1)	1.388(10)	C(10)-C(29)	1.493(7)
N(2)-C(3)	1.366(7)	C(11)-C(12)	1.380(8)
N(2)-C(6)	1.380(7)	C(12)-C(13)	1.386(8)
N(3)-C(11)	1.363(9)	C(13)-C(14)	1.465(7)
N(3)-C(8)	1.394(12)	C(14)-C(15)	1.369(8)
N(4)-C(13)	1.367(7)	C(14)-C(31)	1.494(7)
N(4)-C(16)	1.368(7)	C(15)-C(16)	1.460(7)
N(5)-O(2)	1.299(6)	C(15)-C(33)	1.499(8)
N(5)-C(38)	1.312(9)	C(16)-C(17)	1.385(7)
N(5)-C(41)	1.486(9)	C(17)-C(18)	1.411(9)
O(1)-C(37)	1.167(7)	C(18)-C(19)	1.453(16)
C(1)-C(2)	1.398(8)	C(19)-C(20)	1.359(13)
C(1)-C(20)	1.446(8)	C(19)-C(35)	1.506(16)
C(2)-C(3)	1.386(8)	C(20)-C(21)	1.515(7)
C(3)-C(4)	1.451(7)	C(21)-C(22)	1.534(8)
C(4)-C(5)	1.355(8)	C(23)-C(24)	1.536(8)
C(4)-C(23)	1.506(7)	C(25)-C(26)	1.503(9)
C(5)-C(6)	1.462(7)	C(27)-C(28)	1.500(9)

C(29)-C(30)	1.547(8)	C(39)-C(40)	1.463(14)
C(31)-C(32)	1.524(8)	C(40)-C(41)	1.539(13)
C(33)-C(34)	1.511(8)	C(41)-C(42)	1.490(11)
C(35)-C(36)	1.518(9)	C(41)-C(43B)	1.527(15)
C(38)-C(39)	1.458(10)	C(41)-C(43A)	1.536(13)

Table 4.2. Bond angles (°) for (OEP)Ru(CO)(DMPO)

C(37)-Ru(1)-N(3)	94.2(3)	N(2)-Ru(1)-O(2)	87.29(16)
C(37)-Ru(1)-N(4)	91.4(2)	N(1)-Ru(1)-O(2)	92.4(2)
N(3)-Ru(1)-N(4)	89.9(2)	C(18)-N(1)-C(1)	107.2(8)
C(37)-Ru(1)-N(2)	93.1(2)	C(18)-N(1)-Ru(1)	127.3(6)
N(3)-Ru(1)-N(2)	90.4(2)	C(1)-N(1)-Ru(1)	125.4(6)
N(4)-Ru(1)-N(2)	175.48(18)	C(3)-N(2)-C(6)	107.0(4)
C(37)-Ru(1)-N(1)	90.9(3)	C(3)-N(2)-Ru(1)	126.8(4)
N(3)-Ru(1)-N(1)	174.8(3)	C(6)-N(2)-Ru(1)	126.2(3)
N(4)-Ru(1)-N(1)	89.2(3)	C(11)-N(3)-C(8)	107.2(7)
N(2)-Ru(1)-N(1)	90.2(3)	C(11)-N(3)-Ru(1)	126.7(5)
C(37)-Ru(1)-O(2)	176.7(2)	C(8)-N(3)-Ru(1)	126.1(6)
N(3)-Ru(1)-O(2)	82.5(2)	C(13)-N(4)-C(16)	107.4(4)
N(4)-Ru(1)-O(2)	88.26(16)	C(13)-N(4)-Ru(1)	125.9(4)
C(16)-N(4)-Ru(1)	126.7(3)	C(38)-N(5)-C(41)	111.6(6)
O(2)-N(5)-C(38)	125.3(5)	N(5)-O(2)-Ru(1)	122.2(3)
O(2)-N(5)-C(41)	123.0(6)	N(1)-C(1)-C(2)	124.8(6)

N(1)-C(1)-C(20)	108.6(6)	N(3)-C(11)-C(10)	110.1(6)
C(2)-C(1)-C(20)	126.5(5)	C(12)-C(11)-C(10)	125.5(5)
C(3)-C(2)-C(1)	128.0(5)	C(11)-C(12)-C(13)	127.9(5)
N(2)-C(3)-C(2)	124.8(5)	N(4)-C(13)-C(12)	125.1(5)
N(2)-C(3)-C(4)	109.9(5)	N(4)-C(13)-C(14)	109.6(5)
C(2)-C(3)-C(4)	125.3(5)	C(12)-C(13)-C(14)	125.4(5)
C(5)-C(4)-C(3)	107.1(5)	C(15)-C(14)-C(13)	106.6(4)
C(5)-C(4)-C(23)	128.2(5)	C(15)-C(14)-C(31)	129.1(5)
C(3)-C(4)-C(23)	124.6(5)	C(13)-C(14)-C(31)	124.3(5)
C(4)-C(5)-C(6)	106.9(5)	C(14)-C(15)-C(16)	106.6(5)
C(4)-C(5)-C(25)	128.3(5)	C(14)-C(15)-C(33)	127.4(5)
C(6)-C(5)-C(25)	124.8(5)	C(16)-C(15)-C(33)	126.0(5)
N(2)-C(6)-C(7)	124.3(5)	N(4)-C(16)-C(17)	125.0(5)
N(2)-C(6)-C(5)	109.0(5)	N(4)-C(16)-C(15)	109.8(4)
C(7)-C(6)-C(5)	126.6(5)	C(17)-C(16)-C(15)	125.2(5)
C(8)-C(7)-C(6)	128.5(6)	C(16)-C(17)-C(18)	127.3(6)
C(7)-C(8)-N(3)	124.5(8)	N(1)-C(18)-C(17)	124.3(7)
C(7)-C(8)-C(9)	126.6(8)	C(19)-C(35)-C(36)	114.3(6)
N(3)-C(8)-C(9)	109.0(8)	O(1)-C(37)-Ru(1)	178.5(6)
C(10)-C(9)-C(8)	106.7(9)	N(5)-C(38)-C(39)	112.3(7)
C(10)-C(9)-C(27)	128.7(8)	C(38)-C(39)-C(40)	102.5(7)
C(8)-C(9)-C(27)	124.5(9)	C(39)-C(40)-C(41)	107.1(7)
C(9)-C(10)-C(11)	107.1(6)	N(5)-C(41)-C(42)	107.2(7)
C(9)-C(10)-C(29)	127.1(7)	N(5)-C(41)-C(43B)	114.3(9)
C(11)-C(10)-C(29)	125.9(5)	C(42)-C(41)-C(43B)	130.3(11)
N(3)-C(11)-C(12)	124.5(6)	N(5)-C(41)-C(43A)	108.7(10)

C(42)-C(41)-C(43A)	107.7(10)	C(19)-C(20)-C(1)	107.5(7)
C(43B)-C(41)-C(43A)	33.6(9)	C(19)-C(20)-C(21)	129.3(8)
N(5)-C(41)-C(40)	99.1(7)	C(1)-C(20)-C(21)	123.3(5)
C(42)-C(41)-C(40)	110.8(8)	C(20)-C(21)-C(22)	112.2(5)
C(43B)-C(41)-C(40)	88.8(12)	C(4)-C(23)-C(24)	111.3(5)
C(43A)-C(41)-C(40)	122.1(9)	C(5)-C(25)-C(26)	113.1(6)
N(1)-C(18)-C(19)	110.4(8)	C(9)-C(27)-C(28)	114.3(6)
C(17)-C(18)-C(19)	125.4(8)	C(10)-C(29)-C(30)	113.0(5)
C(20)-C(19)-C(18)	106.3(10)	C(14)-C(31)-C(32)	113.8(4)
C(20)-C(19)-C(35)	127.6(10)	C(15)-C(33)-C(34)	114.4(5)
C(18)-C(19)-C(35)	126.1(9)		

The Ru–C(O) and C–O bond lengths are 1.816(6) and 1.167(7) Å, respectively, and the Ru–C–O bond angle is 178.5(6)°. These data are similar to those determined for other structurally characterized (OEP)Ru(CO)–containing complexes (Table 4.3).[26-32] The Ru–N(por) bond lengths lie in the range 2.051(9)–2.069(10) Å, and the Ru atom is displaced by 0.11 Å from the 24–atom mean porphyrin plane toward the π–acid CO ligand. The porphyrin macrocycle exhibits a *dome* distortion. The most chemically interesting feature of the structure of (OEP)Ru(CO)(DMPO) is that the nitrone ligand is bound to the Ru^{II} center in a η^1–O fashion. The axial Ru–O(nitrone) distance is 2.214(4) Å and lies within the 2.123(9)–2.348(3) Å range observed for other non–nitrosyl Ru^{II} porphyrins with *O*–donor ligands.[26-29,33-40] The nitrone O–N and N=C bond lengths are 1.299(6) Å and 1.312(9) Å, respectively, and the Ru–O–N bond angle is 122.2(3)°. To the best of my knowledge, the crystal structure of DMPO has not been reported. However, the metrical parameters of the DMPO moiety in (OEP)Ru(CO)(DMPO) are suggestive of a dominant contribution of the $R_2C=N^+(R)–O^-$ resonance form (Figure 4.1, top left) for this ligand. For example, the nitrone N–C(38) bond length of 1.312(9) Å is significantly shorter than the nitrone N–C(41) bond length of 1.486(9) Å, implying double–bond character to this N–C(38) unit.

The molecular structure of (OEP)Os(CO)(DMPO) was also obtained (Figure 4.7). Bond lengths and angles are listed in Tables 4.4 and 4.5. Unlike the X–ray crystal structure of (OEP)Ru(CO)(DMPO), the overall data quality for the molecular structure of (OEP)Os(CO)(DMPO) was limited due to the poor quality crystals resulting from the presence of minor twin component. Furthermore, the axial nitrone group is highly disordered and is indicated by its high thermal motion.

The Os–C(O) and C–O bond lengths are 1.836(19) and 1.24(3) Å, respectively, and the Os–C–O bond angle is 175.1(18)°. Prior to this work, to the best of my knowledge, only seven other solid–state structures of the (por)Os(CO)–containing complexes were reported,[26,30,41-44] and their selected structural parameters are shown in

Table 4.3. Selected Structural Data for (OEP)Ru(CO)–Containing Complexes

Compound	Ru-C(O) (Å)	C-O (Å)	Ru-C-O (°)	refs
(OEP)Ru(CO)(H_2O)	1.785(4)	1.150(4)	178.5(3)	[27]
(OEP)Ru(CO)(Et_2NNO)	1.788(9)	1.181(10)	177.0(7)	[26,28]
(OEP)Ru(CO)(TEMPO) [a]	1.798(5)	1.150(5)	178.6	[29]
(OEP)Ru(CO)(1-MeIm)	1.829(5)	1.156(5)	177.3(4)	[30]
(OEP)Ru(CO)(η^1-por*) [b]	1.801(6)	1.165(7)	179.7(6)	[31]
(OEP)Ru(CO)·C_{60}	1.798 [c]	1.144 [c]	179.7 [c]	[32]
(OEP)Ru(CO)(DMPO)	1.816(6)	1.167(7)	178.5(6)	this work

[a] TEMPO = 2,2,6,6-tetramethylpiperidine-1-oxyl.

[b] por* = 5-pyridyl-10,15,20-triphenylporphyrinato dianion.

[c] Data obtained from the Cambridge Structural Database.

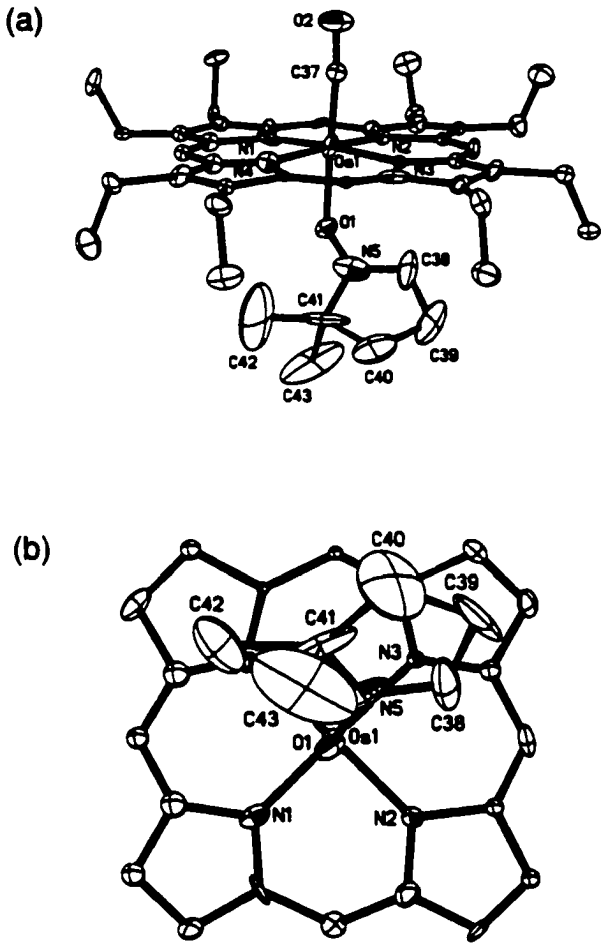

Figure 4.7. (a) Molecular structure of (OEP)Os(CO)(DMPO). (b) View of the orientation of the nitrone ligand relative to the porphyrin skeleton.

Table 4.4. Bond lengths (Å) for (OEP)Os(CO)(DMPO)

Os(1)-C(37)	1.836(19)	C(10)-C(11)	1.44(2)
Os(1)-N(1)	1.993(17)	C(21)-C(22)	1.54(3)
Os(1)-N(2)	2.026(13)	C(23)-C(24)	1.57(2)
Os(1)-N(3)	2.077(11)	C(25)-C(26)	1.45(3)
Os(1)-N(4)	2.103(18)	C(27)-C(28)	1.45(3)
Os(1)-O(1)	2.141(14)	C(37)-O(2)	1.24(3)
N(1)-C(4)	1.35(3)	N(3)-C(11)	1.333(18)
N(1)-C(1)	1.44(2)	N(3)-C(14)	1.37(2)
N(2)-C(6)	1.41(2)	N(4)-C(19)	1.26(3)
N(2)-C(9)	1.455(19)	N(4)-C(16)	1.34(2)
C(1)-C(20)	1.38(2)	C(11)-C(12)	1.41(2)
C(1)-C(2)	1.47(3)	C(12)-C(13)	1.32(3)
C(2)-C(3)	1.43(2)	C(12)-C(29)	1.53(2)
C(2)-C(21)	1.46(2)	C(13)-C(14)	1.50(3)
C(3)-C(4)	1.41(2)	C(13)-C(31)	1.52(2)
C(3)-C(23)	1.50(2)	C(14)-C(15)	1.29(2)
C(4)-C(5)	1.44(2)	C(15)-C(16)	1.419(15)
C(5)-C(6)	1.43(2)	C(16)-C(17)	1.446(18)
C(6)-C(7)	1.42(2)	C(17)-C(18)	1.40(3)
C(7)-C(8)	1.31(2)	C(17)-C(33)	1.46(3)
C(7)-C(25)	1.51(2)	C(18)-C(19)	1.48(3)
C(8)-C(9)	1.45(2)	C(18)-C(35)	1.50(3)
C(8)-C(27)	1.54(2)	C(19)-C(20)	1.36(3)
C(9)-C(10)	1.35(3)	C(29)-C(30)	1.57(3)

C(31)-C(32)	1.53(3)	C(40)-C(41)	1.508(17)
C(33)-C(34)	1.54(3)	C(41)-N(5)	1.457(15)
C(35)-C(36)	1.56(3)	C(41)-C(42)	1.541(14)
C(38)-N(5)	1.340(16)	C(41)-C(43)	1.54(2)
C(38)-C(39)	1.502(17)	O(1)-N(5)	1.30(2)
C(39)-C(40)	1.509(18)		

Table 4.5. Bond angles (°) for (OEP)Os(CO)(DMPO)

C(37)-Os(1)-N(1)	96.1(7)	C(4)-N(1)-C(1)	102.1(15)
C(37)-Os(1)-N(2)	90.0(7)	C(4)-N(1)-Os(1)	132.9(12)
N(1)-Os(1)-N(2)	87.8(6)	C(1)-N(1)-Os(1)	125.0(12)
C(37)-Os(1)-N(3)	88.8(6)	C(6)-N(2)-C(9)	101.6(12)
N(1)-Os(1)-N(3)	174.8(5)	C(6)-N(2)-Os(1)	131.4(11)
N(2)-Os(1)-N(3)	90.3(4)	C(9)-N(2)-Os(1)	127.0(10)
C(37)-Os(1)-N(4)	93.9(6)	C(20)-C(1)-N(1)	126.1(16)
N(1)-Os(1)-N(4)	90.4(5)	C(20)-C(1)-C(2)	123.1(15)
N(2)-Os(1)-N(4)	175.8(5)	N(1)-C(1)-C(2)	110.8(16)
N(3)-Os(1)-N(4)	91.2(6)	C(3)-C(2)-C(21)	126.4(16)
C(37)-Os(1)-O(1)	175.9(7)	C(3)-C(2)-C(1)	105.5(15)
N(1)-Os(1)-O(1)	82.8(4)	C(21)-C(2)-C(1)	128.0(16)
N(2)-Os(1)-O(1)	86.1(4)	C(4)-C(3)-C(2)	104.3(15)
N(3)-Os(1)-O(1)	92.2(5)	C(4)-C(3)-C(23)	126.5(16)
N(4)-Os(1)-O(1)	90.0(6)	C(2)-C(3)-C(23)	129.2(15)

N(1)-C(4)-C(3)	117.3(16)	C(19)-N(4)-Os(1)	122.5(16)
N(1)-C(4)-C(5)	119.9(15)	C(16)-N(4)-Os(1)	121.3(12)
C(3)-C(4)-C(5)	122.9(17)	N(3)-C(11)-C(12)	108.9(13)
C(6)-C(5)-C(4)	129.8(16)	N(3)-C(11)-C(10)	124.8(12)
N(2)-C(6)-C(5)	117.7(15)	C(12)-C(11)-C(10)	126.2(13)
N(2)-C(6)-C(7)	113.2(16)	C(13)-C(12)-C(11)	107.9(15)
C(5)-C(6)-C(7)	128.5(17)	C(13)-C(12)-C(29)	126.9(17)
C(8)-C(7)-C(6)	106.7(16)	C(11)-C(12)-C(29)	124.5(15)
C(8)-C(7)-C(25)	130.8(16)	C(12)-C(13)-C(14)	108.1(15)
C(6)-C(7)-C(25)	122.4(17)	C(12)-C(13)-C(31)	128.7(16)
C(7)-C(8)-C(9)	110.3(13)	C(14)-C(13)-C(31)	123.1(15)
C(7)-C(8)-C(27)	129.6(16)	C(15)-C(14)-N(3)	131.2(19)
C(9)-C(8)-C(27)	120.0(14)	C(15)-C(14)-C(13)	125.3(16)
C(10)-C(9)-N(2)	122.1(14)	N(3)-C(14)-C(13)	103.5(15)
C(10)-C(9)-C(8)	129.9(14)	C(14)-C(15)-C(16)	124.3(13)
N(2)-C(9)-C(8)	107.9(12)	N(4)-C(16)-C(15)	129.7(12)
C(9)-C(10)-C(11)	129.1(14)	N(4)-C(16)-C(17)	105.9(12)
C(2)-C(21)-C(22)	113.6(15)	C(15)-C(16)-C(17)	124.4(11)
C(3)-C(23)-C(24)	109.5(16)	C(18)-C(17)-C(16)	105.4(14)
C(26)-C(25)-C(7)	113.9(16)	C(18)-C(17)-C(33)	128.7(16)
C(28)-C(27)-C(8)	113.6(17)	C(16)-C(17)-C(33)	125.9(15)
O(2)-C(37)-Os(1)	175.1(18)	C(17)-C(18)-C(19)	106.6(16)
C(11)-N(3)-C(14)	111.2(14)	C(17)-C(18)-C(35)	123.4(18)
C(11)-N(3)-Os(1)	126.6(10)	C(19)-C(18)-C(35)	130(2)
C(14)-N(3)-Os(1)	122.2(12)	N(4)-C(19)-C(20)	134(2)
C(19)-N(4)-C(16)	116.0(17)	N(4)-C(19)-C(18)	105.7(19)

C(20)-C(19)-C(18)	120.1(18)	N(5)-C(41)-C(42)	116(2)
C(19)-C(20)-C(1)	121.9(14)	C(40)-C(41)-C(42)	136(2)
C(12)-C(29)-C(30)	115.3(15)	N(5)-C(41)-C(43)	118.7(17)
C(13)-C(31)-C(32)	111.3(17)	C(40)-C(41)-C(43)	98(2)
C(17)-C(33)-C(34)	112.2(18)	C(42)-C(41)-C(43)	85(3)
C(18)-C(35)-C(36)	113.6(18)	N(5)-O(1)-Os(1)	123.2(12)
N(5)-C(38)-C(39)	111.6(16)	O(1)-N(5)-C(38)	119.8(14)
C(38)-C(39)-C(40)	100.0(15)	O(1)-N(5)-C(41)	125.8(14)
C(41)-C(40)-C(39)	111.4(17)	C(38)-N(5)-C(41)	114.1(15)
N(5)-C(41)-C(40)	100.0(14)		

Table 4.6. Selected Structural Data for (por)Os(CO)–Containing Complexes

Compound	Os-N(por) (Å)	Os-C(O) (Å)	C-O (Å)	Os-C-O (°)	refs
$(OEPMe_2)Os(CO)(py)$	2.067 av.	1.828(5)	1.151(7)	178.9(14)	[41]
$(TTP)Os(CO)(Et_2NNO)$	2.055 av.	1.818(11)	1.140(12)	177.9(10)	[26]
(TTP)Os(CO)(PhNO)	2.077 av.	1.93(2)	1.144(5)	175(4)	[42]
(TPP)Os(CO)(py)	2.062 av.	1.817(9)	1.190(9)	178.3(7)	[43]
(TPP)Os(CO)(1-MeIm)	2.052 av.	1.846(9)	1.150(10)	176.8(9)	[43]
(OEP)Os(CO)(1-MeIm)	2.060 av.	1.817(13)	1.171(13)	177.0(9)	[30]
(dpp)Os(CO)(py) [a]	2.050 av. [b]	1.840 [b]	1.184 [b]	162.9 [b]	[44]
(OEP)Os(CO)(DMPO)	2.050 av.	1.836(19)	1.24(3)	175.1(18)	this work

[a] dpp = 2,3,5,7,8,10,12,13,15,17,18,20-dodecaphenylporphyrinato dianion.

[b] Data obtained from the Cambridge Structural Database.

Table 4.6. The average Os–N(por) bond length is 2.050 Å, which is within the 2.050–2.077 Å range observed for other structurally characterized (por)Os(CO)–containing complexes.

Although the nature of disorder of the axial nitrone group precludes a meaningful comparison of bond lengths and angles of the nitrone DMPO ligand in the Os compound with the related (OEP)Ru(CO)(DMPO) complex, the structure of (OEP)Os(CO)(DMPO) clearly indicates that the nitrone ligand is bound to the Os^{II} center in a η^1–O fashion. The axial Os–O(nitrone) and nitrone O–N bond lengths are 2.141(14) and 1.30(2) Å, respectively. The nitrone N=C and N–C distances are 1.340(16) and 1.457(15) Å, respectively. These values are also consistent with a dominant contribution of the $R_2C{=}N^+(R){-}O^-$ resonance form. The Os–O–N bond angle is 123.2(12)°.

Attempts to extend to other nitrones have not yet been successful. Nevertheless, this work has formed the basis for future work in our lab on the metalloporphyrin–induced reaction chemistry of nitrones.

Conclusion

In summary, the first metalloporphyrin nitrone complexes (OEP)M(CO)(DMPO) (M = Ru, Os) have been prepared and fully characterized by elemental analyses, infrared and ^1H NMR spectroscopy, and by mass spectrometry. Importantly, a comparison of the IR spectra of these compounds with those of (OEP)M(CO)($ONNEt_2$) (M = Ru, Os) reveals that the nitrone DMPO and the nitrosamine Et_2NNO ligands have a similar ligand basicity in these compounds. The molecular structures of these complexes have also been determined by single–crystal X–ray crystallography. The spectroscopic and crystallographic results on these metalloporphyrin nitrone complexes show for the first time that nitrones are suitable ligands for the metal centers in heme models, and that the $R_2C{=}N^+(R){-}O^-$ resonance contribution stabilizes the η^1–O binding to the metal center. Prior to this work, no structural information was available on how nitrones could interact

with the metal centers in hemes. Hence, the study of the binding of nitrones to the metal centers in synthetic metalloporphyrins could provide chemical insight on the nature of the interactions of nitrones with hemes.

References

(1) Breuer, E. In *The Chemistry of Amino, Nitroso and Nitro Compounds and Their Derivatives. Supplement F: Part 1*; Patai, S., Ed.; John Wiley and Sons: New York, 1982; Chapter 13.

(2) Confalone, P. N.; Huie, E. M. *Org. React.* **1988**, *36*, 1-173.

(3) Robl, J. A.; Hwu, J. R. *J. Org. Chem.* **1985**, *50*, 5913-5916.

(4) Hwu, J. R.; Robl, J. A.; Wang, N.; Anderson, D. A.; Ku, J.; Chen, E. *J. Chem. Soc., Perkin Trans. 1* **1989**, 1823-1831.

(5) Murray, R. W.; Iyanar, K.; Chen, J.; Wearing, J. T. *J. Org. Chem.* **1996**, *61*, 8099-8102.

(6) Ballistreri, F. P.; Barbuzzi, E. G. M.; Tomaselli, G. A.; Toscano, R. M. *J. Org. Chem.* **1996**, *61*, 6381-6387.

(7) Cholvad, V.; Stasko, A.; Tkac, A.; Buchanenko, A. L.; Malik, L. *Collect. Czech. Chem. Commun.* **1981**, *46*, 823-832.

(8) Villamena, F. A.; Dickman, M. H.; Crist, D. R. *Inorg. Chem.* **1998**, *37*, 1446-1453.

(9) Rehorek, D. *Chem. Soc. Rev.* **1991**, *20*, 341-353.

(10) Ellis, W. W.; Gavrilova, A.; Liable-Sands, L.; Rheingold, A. L.; Bosnich, B. *Organometallics* **1999**, *18*, 332-338.

(11) Hirata, M.; Lindeke, B.; Orrenius, S. *Biochem. Pharmacol.* **1979**, *28*, 479-484.

(12) Bondon, A.; Macdonald, T. L.; Harris, T. M.; Guengerich, F. P. *J. Biol. Chem.* **1989**, *264*, 1988-1997.

(13) Albano, E.; Cheeseman, K. H.; Tomasi, A.; Carini, R.; Dianzani, M. U.; Slater, T. F. *Biochem. Pharmacol.* **1986**, *35*, 3955-3960.

(14) Kiese, M.; Plattig, K. H. *Arch. Exptl. Pathol. Pharmakol.* **1958**, *233*, 484-494. *Chem. Abs.* **452**:13104i.

(15) Chamulitrat, W.; Jordan, S. J.; Mason, R. P.; Saito, K.; Cutler, R. G. *J. Biol. Chem.* **1993**, *268*, 11520-11527.

(16) Castel, A.; Riviere, P.; Satge, J.; Ahbala, M. *J. Organomet. Chem.* **1987**, *328*, 123-132.

(17) Kluiber, R. W.; Horrocks, W. D. W., Jr. *Inorg. Chim. Acta* **1970**, *4*, 183-186.

(18) Burdukov, A. B.; Ovcharenko, V. I.; Sagdeev, R. Z.; Pervukhina, N. V.; Ikorskii, V. N.; Kirilyuk, I. A.; Grigor'ev, I. A. *Polyhedron* **1996**, *15*, 4211-4219.

(19) Handwerker, B. M.; Garrett, K. E.; Nagle, K. L.; Geoffroy, G. L.; Rheingold, A. L. *Organometallics* **1990**, *9*, 1562-1575.

(20) Mansuy, D.; Dreme, M.; Chottard, J.-C.; Girault, J.-P.; Guilhem, J. *J. Am. Chem. Soc.* **1980**, *102*, 844-845.

(21) Peng, W.-J.; Gamble, A. S.; Templeton, J. L.; Brookhart, M. *Inorg. Chem.* **1990**, *29*, 463-467.

(22) Hutton, A. T.; McEwan, D. M.; Shaw, B. L.; Wilkinson, S. W. *J. Chem. Soc., Dalton Trans.* **1983**, 2011-2013.

(23) Carducci, M. D.; Doedens, R. J. *Inorg, Chem.* **1989**, *28*, 2492-2494.

(24) Che, C.-M.; Poon, C.-K.; Chung, W.-C.; Gray, H. B. *Inorg. Chem.* **1985**, *24*, 1277-1278.

(25) Chen, L.; Fox, J. B., Jr.; Yi, G.-B.; Khan, M. A.; Richter-Addo, G. B. *J. Porph. Phthalocyanines* **2001**, *5*, 702-707.

(26) Chen, L.; Yi, G.-B.; Wang, L.-S.; Dharmawardana, U. R.; Dart, A. C.; Khan, M. A.; Richter-Addo, G. B. *Inorg. Chem.* **1998**, *37*, 4677-4688.

(27) Kadish, K. M.; Hu, Y.; Mu, X. H. *J. Heterocycl. Chem.* **1991**, *28*, 1821-1824.

(28) Yi, G.-B.; Khan, M. A.; Richter-Addo, G. B. *Inorg. Chem.* **1996**, *35*, 3453-3454.

(29) Seyler, J. W.; Fanwick, P. E.; Leidner, C. R. *Inorg. Chem.* **1992**, *31*, 3699-3700.

(30) Salzmann, R.; McMahon, M. T.; Godbout, N.; Sanders, L. K.; Wojdelski, M.; Oldfield, E. *J. Am. Chem. Soc.* **1999**, *121*, 3818-3828.

(31) Funatsu, K.; Kimura, A.; Imamura, T.; Ichimura, A.; Sasaki, Y. *Inorg. Chem.* **1997**, *36*, 1625-1635.

(32) Ishii, T.; Aizawa, N.; Yamashita, M.; Matsuzaka, H.; Kodama, T.; Kikuchi, K.; Ikemoto, I.; Iwasa, Y. *J. Chem. Soc., Dalton Trans.* **2000**, 4407-4412.

(33) Bonnet, J. J.; Eaton, S. S.; Eaton, G. R.; Holm, R. H.; Ibers, J. A. *J. Am. Chem. Soc.* **1973**, *95*, 2141-2149.

(34) Lo, W.-C.; Che, C.-M.; Cheng, K.-F.; Mak, T. C. W. *Chem. Commun.* **1997**, 1205-1206.

(35) Groves, J. T.; Han, Y.; Van_engen, D. *J. Chem. Soc., Chem. Commun.* **1990**, 436-437.

(36) Birnbaum, E. R.; Schaefer, W. P.; Labinger, J. A.; Bercaw, J. E.; Gray, H. B. *Inorg. Chem.* **1995**, *34*, 1751-1755.

(37) Le Maux, P.; Bahri, H.; Simonneaux, G.; Toupet, L. *Inorg. Chem.* **1995**, *34*, 4691-4697.

(38) Slebodnick, C.; Kim, K.; Ibers, J. A. *Inorg. Chem.* **1993**, *32*, 5338-5342.

(39) Camenzind, M. J.; James, B. R.; Dolphin, D.; Sparapany, J. W.; Ibers, J. A. *Inorg. Chem.* **1988**, *27*, 3054-3057.

(40) Galardon, E.; Le Maux, P.; Toupet, L.; Simonneaux, G. *Organometallics* **1998**, *17*, 565-569.

(41) Buchler, J. W.; Lay, K. L.; Smith, P. D.; Scheidt, W. R.; Rupprecht, G. A.; Kenny, J. E. *J. Organomet. Chem.* **1976**, *110*, 109-120.

(42) Chen, L.; Khan, M. A.; Richter-Addo, G. B.; Young, V. G., Jr.; Powell, D. R. *Inorg. Chem.* **1998**, *37*, 4689-4696.

(43) Salzmann, R.; Ziegler, C. J.; Godbout, N.; McMahon, M. T.; Suslick, K. S.; Oldfield, E. *J. Am. Chem. Soc.* **1998**, *120*, 11323-11334.

(44) Liu, C.-J.; Yu, W.-Y.; Peng, S.-M.; Mak, T. C. W.; Che, C.-M. *J. Chem. Soc., Dalton Trans.* **1998**, 1805-1812.

Chapter 5. Synthesis, Characterization, and Solid–State Molecular Structures of Bis– and Mono–Nitrosoarene Complexes of Ruthenium Porphyrins*

Introduction

The binding of nitrosobenzene and related *C*–nitroso compounds (RNO; R = alkyl, aryl) to the metal centers in heme biomolecules is a naturally–occurring phenomenon, and evidence for RNO binding to the heme site has been established for myoglobin,[1] hemoglobin,[2] cytochrome P450,[3] and guanylyl cyclase,[4] and other heme biomolecules. For example, various amine–containing drugs can be metabolized by cytochrome P450 to result in RNO formation and binding to the heme, and the tight binding of the RNO group can inhibit the enzymatic activity. Furthermore, the formation of the PhNO adduct of hemoglobin has been known to be associated with $PhNO_2$ poisoning.[5]

As described in detail in Chapter 1, the formation of various nitrosoalkane and nitrosoarene adducts of hemes has been observed from *(i)* the reaction of nitro compounds with heme–containing biomolecules under reducing conditions and *(ii)* the direct interaction of nitroso compounds with the metal centers in heme. The X–ray crystal structure of the PhNO adduct of leghemoglobin, namely (legHb)Fe^{II}–N(O)Ph, was obtained.[6] Recently, Daniel Copeland of our research group was also able to observe that when the ferric cytochrome P450 is reacted with primary and secondary aliphatic nitro compounds (RNO_2; R = Me, Et, propyl, *i*–Pr) in the presence of dithionite, the P450–nitrosoalkane complexes are generated. He has also extended this to myoglobin.

There are nine main ways in which a *C*–nitroso compound may bind to metals.

---

* Reproduced in part with permission from "Synthesis and Solid-State Molecular Structures of Bis- and Mono-Nitrosobenzene Complexes of Ruthenium Porphyrins." Lee, J.; Twamley, B.; Richter-Addo, G. B. *Can. J. Chem.* **2002**, In press. Copyright 2002 National Research Council of Canada.

All these binding modes have been confirmed by single–crystal X–ray crystallography, and they are shown in Figure 5.1. The mode in which the *C*–nitroso compound binds depends on a number of factors including the type, nature, and number of metal center(s) and the type of "R" group in the RNO compounds (we have reviewed this area in ref. 7).

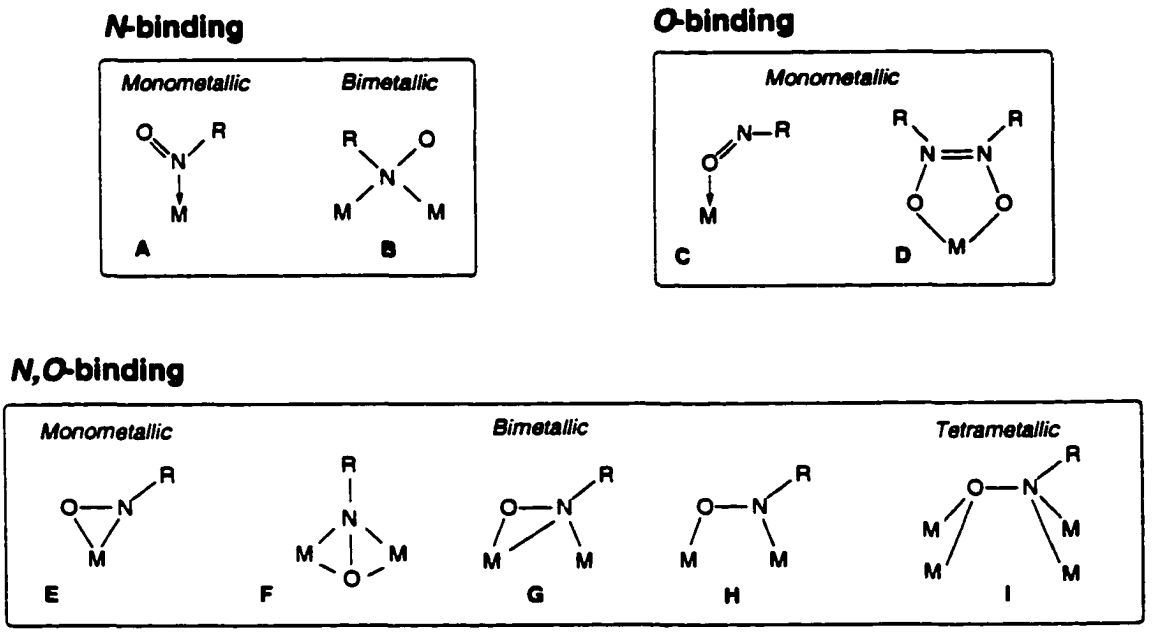

Figure 5.1. Binding modes in metal–RNO complexes established by single–crystal X–ray crystallography.

Although fifteen structurally characterized *C*–nitroso complexes of metalloporphyrins are known for Fe,[8-10] Mn,[11] Ru,[12] Os,[13] and Co[12] (see Table 1.3 in Chapter 1), structural information on the binding of *C*–nitroso compounds to metals (shown in Figure 5.1) has so far been mostly obtained as a result of work with non–porphyrin compounds.[7] Furthermore, very little information is currently available on the nature of the interaction between *C*–nitroso compounds and the metal centers in heme. Hence, further structural studies on synthetic *C*–nitroso complexes of metalloporphyrins are needed to better understand the nature of the binding of *C*–nitroso compounds to heme centers.

Our research group has indeed been interested, over the last few years, in determining the binding modes of nitrosoarene (ArNO) to the Group 8 metalloporphyrins as synthetic heme models. For example, our research group showed that nitrosobenzene (PhNO) binds to ferrous d^6 porphyrin in an *N*–binding mode, whereas *p*–diethylamino-substituted nitrosobenzene (*p*–$ONC_6H_4NEt_2$) binds to ferric d^5 porphyrin in an *O*–binding mode.[9] Our group was particularly interested in RNO binding to Ru(II) porphyrins, since the latter species can serve as good models for low–spin d^6 systems similar to low–spin ferrous heme.

In this chapter, the syntheses and characterization of various bis– and mono–nitrosoarene complexes of ruthenium porphyrins will be discussed. The first examples of metalloporphyrin nitrosoanisole complexes will also be introduced. Our research group recently showed that the *p*–aminosubstituted nitrosobenzenes could also bind to d^6 metal centers in metalloporphyrins via the *N*-bining mode,[12] although they are bound to the d^5 metalloporphyrins in a η^1–O fashion, presumably due to the contribution of the dipolar resonance form. Our research group was thus interested in determining whether this reaction chemistry and *O*–binding mode could be extended to nitrosoanisole compounds in which the dipolar resonance forms are also possible (Figure 5.2).

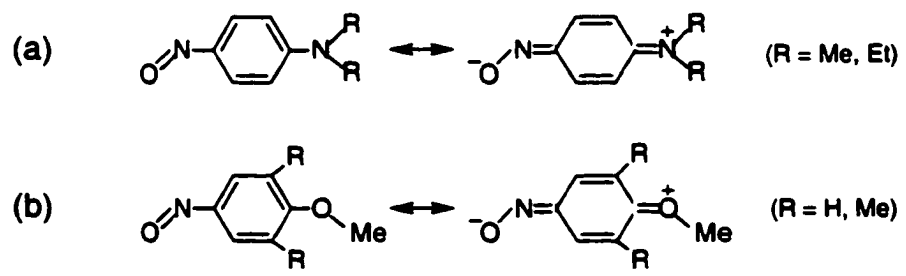

Figure 5.2. Two examples of the *C*–nitroso compounds in which the dipolar resonance forms are possible. (a) *p*–aminosubstituted nitroso-benzenes and (b) nitrosoanisoles.

The single–crystal X–ray structures of these bis– and mono–nitrosoarene compounds will also be reported. Although the crystal structures of the mono–nitrosoarene complexes of the form (por)M(ArNO)L were known for Fe,[10] no structural information was available on the mono–nitrosoarene complexes of ruthenium porphyrins prior to this work. Furthermore, only one crystal structure of a bis–nitrosoarene complex of ruthenium porphyrin has been reported.[12] Importantly, the effect of the axial pyridine or 1–MeIm ligand on the orientation of the *trans* ArNO ligand will also be discussed. Finally, the IR and ^{1}H NMR spectral data for these bis– and mono–nitrosoarene compounds will also be analyzed as a function of porphyrin macrocycle, axial ligand, and nature of substituent in ArNO.

Experimental Section

All reactions were performed under an atmosphere of prepurified nitrogen using standard Schlenk glassware and/or in an Innovative Technology Labmaster 100 Dry Box. Solutions for spectral studies were also prepared under a nitrogen atmosphere. Solvents were distilled from appropriate drying agents under nitrogen just prior to use: CH_2Cl_2 (CaH_2), hexane (CaH_2), toluene (Na).

Chemicals. (TPP)Ru(CO) and (TTP)Ru(CO) were prepared by published procedures.[14] PhNO (97%), *o*–tolNO (97%), anhydrous pyridine (99.8%), and 1–methylimidazole (1–MeIm, 99+%) were purchased from Aldrich Chemical Co. and used as received. 4–Nitrosoanisole (*p*–ONC_6H_4OMe) and 2,6–dimethyl–4–nitrosoanisole (*p*–$ONC_6H_2(Me)_2OMe$) were prepared by literature methods.[15] $^{15}NOBF_4$ was synthesized by a published procedure[16] using $Na^{15}NO_2$ (99% isotopic purity, Isotec). Chloroform–*d* (99.8%) was obtained from Cambridge Isotope Laboratories.

Instrumentation. Infrared spectra were recorded on a Bio–Rad FT–155 FTIR spectrometer. Proton NMR spectra were obtained on Varian 400 MHz spectrometer and the signals referenced to the residual signal of the solvent employed. All coupling

constants are in Hz. FAB mass spectra were obtained on a VG–ZAB–E mass spectrometer. UV–vis spectra were recorded on a Hewlett–Packard model 8453 diode array instrument. Wavelengths are reported with ε values or as %–intensities for the samples whose yields were too small for accurate concentration measurements.

Synthesis of *p*–O^{15}NC$_6$H$_4$OMe. This ^{15}N–labeled 4–nitrosoanisole was synthesized by the direct nitrosation of anisole with ^{15}NOBF$_4$ in acetonitrile (i.e., the same procedure for the preparation of *p*–O^{14}NC$_6$H$_4$OMe).[15] The ^{1}H NMR spectrum of *p*–O^{15}NC$_6$H$_4$OMe was identical to that of *p*–O^{14}NC$_6$H$_4$OMe. IR (KBr, cm^{-1}): 1600 s, 1583 m, 1504 s, 1463 w, 1444 m, 1406 s, 1331 w, 1296 w, 1268 vs, 1190 m, 1112 vs, 1024 s, 840 vs, 756 m.

Preparation of (por)Ru(ArNO)$_2$ compounds (por = TPP, TTP; ArNO = PhNO, *o*–tolNO, N(O)C$_6$H$_4$OMe–*p*, N(O)C$_6$H$_2$(Me)$_2$OMe–*p*). These compounds were prepared from the reaction of (por)Ru(CO) with the corresponding excess nitrosoarene compounds. The following reaction is representative:

(TPP)Ru(CO) (0.100 g, 0.135 mmol) and excess PhNO (0.040 g, 0.362 mmol) were dissolved in CH_2Cl_2 (20 mL). The reaction mixture was stirred at room temperature for 30 min, during which time it turned from red to brown. The solvent was removed in vacuo. The residue was redissolved in CH_2Cl_2 (10 mL), and the product solution was transferred to the top of a neutral alumina column (2 x 20 cm) and eluted with CH_2Cl_2 in air. The brown product was collected and dried in vacuo. The residue was dissolved in CH_2Cl_2 (10 mL). Slow evaporation of the solvent in air gave crystalline (TPP)Ru-(PhNO)$_2$ (0.086 g, 0.093 mmol, 69% isolated yield). IR (KBr, cm^{-1}): υ_{NO} = 1348 s (overlapping with porphyrin band); also 3055 vw, 3024 vw, 1597 m, 1587 vw, 1529 w, 1487 w, 1454 w, 1441 w, 1306 m, 1208 w, 1177 w, 1157 vw, 1072 m, 1010 vs, 859 m, 833 w, 794 m, 754 s, 737 vw, 714 w, 702 s, 665 w, 528 vw. ^{1}H NMR ($CDCl_3$): δ 8.54 (s, 8H, *pyrrole*–H of TPP), 8.12 (m, 8H, *o*–H of TPP), 7.71 (m, 12H, *m/p*–H of TPP), 6.46 (br t, 2H, *p*–H of PhNO), 5.99 (br t, 4H, *m*–H of PhNO), 2.41 (br d, J = 6.8, 4H, *o*–H of

PhNO). Low–resolution mass spectrum (FAB): *m/z* 851 [(TPP)Ru(NO)(PhNO)]$^+$ (26%), 821 [(TPP)Ru(PhNO)]$^+$ (19%), 714 [(TPP)Ru]$^+$ (100%). UV–vis spectrum (λ (ε, mM^{-1} cm^{-1}), 5.18 x 10^{-6} M in CH_2Cl_2): 307 (37), 411 (184), 525 (17) nm. A suitable crystal for structure determination was grown by recrystallization of the compound from a CH_2Cl_2/hexane (1:10) mixture left for 1 week at –20 °C.

The other (por)Ru(ArNO)$_2$ compounds were generated similarly, except for two nitrosoanisole compounds. Two nitrosoanisole complexes (TTP)Ru(N(O)C_6H_4OMe–*p*)$_2$ and (TTP)Ru(N(O)C_6H_2(Me)$_2$OMe–*p*)$_2$ were synthesized in refluxing toluene (30 min reaction time).

(TPP)Ru(*o*–tolNO)$_2$. 54% isolated yield. IR (KBr, cm^{-1}): υ_{NO} = 1350 s (overlapping with porphyrin band); also 3055 vw, 3022 vw, 2956 vw, 2924 vw, 1597 m, 1529 w, 1482 w, 1440 w, 1307 m, 1278 w, 1207 w, 1176 w, 1157 w, 1071 m, 1010 vs, 879 m, 859 m, 794 m, 753 s, 715 m, 702 s, 663 w, 528 vw. ^{1}H NMR ($CDCl_3$): δ 8.56 (s, 8H, *pyrrole*–H of TPP), 8.05 (m, 8H, *o*–H of TPP), 7.70 (m, 12H, *m/p*–H of TPP), 6.28 (br, 2H, *p*–H of *o*–tolNO), 5.77 (br, 4H, *m*–H of *o*–tolNO), 1.52 (br, 2H, *o*–H of *o*–tolNO), –1.23 (br, 6H, CH_3 of *o*–tolNO). Low–resolution mass spectrum (FAB): *m/z* 835 [(TPP)Ru(*o*–tolNO)]$^+$ (45%), 714 [(TPP)Ru]$^+$ (100%). A suitable crystal for structure determination was grown by slow evaporation of CH_2Cl_2/hexane (1:1) solution of the compound at room temperature under inert atmosphere.

(TTP)Ru(PhNO)$_2$. 75% isolated yield. IR (KBr, cm^{-1}): υ_{NO} = 1346 s (overlapping with porphyrin band); also 3022 vw, 2921 vw, 1586 vw, 1529 w, 1454 w, 1305 m, 1212 w, 1181 m, 1108 w, 1072 m, 1010 vs, 858 m, 798 s, 766 m, 716 m, 691 m, 669 w, 643 vw, 524 m. ^{1}H NMR ($CDCl_3$): δ 8.54 (s, 8H, *pyrrole*–H of TTP), 7.99 (d, *J* = 8, 8H, *o*–H of TTP), 7.50 (d, *J* = 8, 8H, *m*–H of TTP), 6.43 (br, 2H, *p*–H of PhNO), 5.95 (br, 4H, *m*–H of PhNO), 2.67 (s,12H, CH_3 of TTP), 2.38 (br, 4H, *o*–H of PhNO). Low–resolution mass spectrum (FAB): *m/z* 907 [(TTP)Ru(NO)(PhNO)]$^+$ (32%), 877 [(TTP)-Ru(PhNO)]$^+$ (15%), 770 [(TTP)Ru]$^+$ (100%). UV–vis spectrum (λ, CH_2Cl_2): 310 (18),

413 (100), 525 (9) nm.

(TTP)Ru(*o*–tolNO)$_2$. 71% isolated yield. IR (KBr, cm^{-1}): υ_{NO} = 1350 s (overlapping with porphyrin band); also 3022 vw, 2956 vw, 2921 vw, 1529 w, 1512 vw, 1480 vw, 1455 vw, 1306 m, 1278 vw, 1263 vw, 1212 w, 1181 m, 1115 w, 1107 w, 1071 m, 1011 vs, 880 m, 859 m, 798 s, 752 m, 719 m, 661 vw, 642 w, 525 m. ^{1}H NMR ($CDCl_3$): δ 8.57 (s, 8H, *pyrrole*–H of TTP), 7.93 (d, J = 8, 8H, *o*–H of TTP), 7.49 (d, J = 8, 8H, *m*–H of TTP), 6.25 (br, 2H, *p*–H of *o*–tolNO), 5.73 (br, 4H, *m*–H of *o*–tolNO), 2.68 (s,12H, CH_3 of TTP), 1.53 (br, 2H, *o*–H of *o*–tolNO), –1.26 (br, 6H, CH_3 of *o*–tolNO). Low–resolution mass spectrum (FAB): *m/z* 891 [(TTP)Ru(*o*–tolNO)]$^+$ (24%), 770 [(TTP)Ru]$^+$ (100%). A suitable crystal for structure determination was grown by recrystallization of the compound from a CH_2Cl_2/hexane (1:2) mixture left for 3 weeks at –20 °C.

(TTP)Ru(N(O)C$_6$H$_4$OMe–*p*)$_2$. 49% isolated yield. IR (KBr, cm^{-1}): υ_{NO} = 1348 s (overlapping with porphyrin band); also 3020 vw, 2922 vw, 2836 vw, 1595 s, 1584 s, 1528 w, 1497 m, 1461 w, 1439 w, 1425 w, 1329 m, 1304 m, 1257 vs, 1212 w, 1180 m, 1134 s, 1109 m, 1070 m, 1031 m, 1009 vs, 866 m, 833 m, 797 s, 777 w, 716 m, 671 vw, 645 vw, 613 m, 525 m. ^{1}H NMR ($CDCl_3$): δ 8.52 (s, 8H, *pyrrole*–H of TTP), 8.01 (d, J = 8, 8H, *o*–H of TTP), 7.50 (d, J = 8, 8H, *m*–H of TTP), 5.43 (br, 4H, *m*–H of N(O)-C$_6$*H*$_4$OMe–*p*), 3.35 (br s, 6H, C*H*$_3$O of N(O)C$_6$H$_4$O*Me*–*p*), 2.67 (s,12H, CH_3 of TTP), 2.56 (br, 4H, *o*–H of N(O)C$_6$*H*$_4$OMe–*p*). Low–resolution mass spectrum (FAB): *m/z* 907 [(TTP)Ru(N(O)C$_6$H$_4$OMe–*p*)]$^+$ (61%), 770 [(TTP)Ru]$^+$ (100%).

(TTP)Ru(^{15}N(O)C$_6$H$_4$OMe–*p*)$_2$. IR (KBr, cm^{-1}): υ_{NO} = 1318 s.

(TTP)Ru(N(O)C$_6$H$_2$(Me)$_2$OMe–*p*)$_2$. 52% isolated yield. IR (KBr, cm^{-1}): υ_{NO} = 1346 s (overlapping with porphyrin band); also 3022 vw, 2962 w, 2922 w, 2863 vw, 1587 w, 1549 vw, 1528 w, 1474 w, 1447 w, 1413 w, 1304 m, 1263 m, 1222 m, 1180 m, 1105 s, 1070 m, 1009 vs, 967 w, 873 vw, 798 vs, 753 vw, 715 m, 694 w, 526 m. ^{1}H NMR ($CDCl_3$): δ 8.56 (s, 8H, *pyrrole*–H of TTP), 7.99 (d, J = 8, 8H, *o*–H of TTP), 7.50

(d, J = 8, 8H, *m*–H of TTP), 3.21 (br s, 6H, CH_3O of N(O)C_6H_2(Me)$_2$O*Me–p*), 2.67 (s,12H, CH_3 of TTP), 2.09 (br s, 4H, *o*–H of N(O)C_6H_2(Me)$_2$OMe–*p*), 1.45 (br s, 12H, CH_3 of N(O)C_6H_2(*Me*)$_2$OMe–*p*). Low–resolution mass spectrum (FAB): *m/z* 935 [(TTP)Ru(N(O)C_6H_2(Me)$_2$OMe–*p*)]$^+$ (31%), 770 [(TTP)Ru]$^+$ (100%). A suitable crystal for structure determination was grown by recrystallization of the compound from a CH_2Cl_2/hexane solution (1:10) left for 3 days at –20 °C.

Preparation of (por)Ru(PhNO)(py) compounds (por = TPP, TTP). These compounds were prepared from the reaction of the precursor (por)Ru(PhNO)$_2$ with 2 equiv of pyridine. The following reaction is representative:

To a CH_2Cl_2 (10 mL) solution of (TPP)Ru(PhNO)$_2$ (0.020 g, 0.021 mmol) was added 2 equiv of pyridine. This mixture was stirred at room temperature for 30 min, during which time it turned from brown to red–purple. The solvent was removed in vacuo. A ^{1}H NMR spectrum of the residue in $CDCl_3$ showed the quantitative formation of (TPP)Ru(PhNO)(py), together with the presence of some unreacted pyridine. Spectroscopically pure (TPP)Ru(PhNO)(py) was obtained in 71% yield by recrystallization of the residue from a CH_2Cl_2/hexane solution (1:3) at –20 °C. IR (KBr, cm^{-1}): υ_{NO} = 1328 s; also 3075 vw, 3052 w, 3023 w, 1598 m, 1529 w, 1485 w, 1442 m, 1346 m sh, 1308 m sh, 1217 w, 1177 w, 1155 w, 1071 m, 1008 vs, 888 vw, 833 vw, 793 m, 753 s, 714 w, 700 s, 664 w, 527 w. ^{1}H NMR ($CDCl_3$): δ 8.42 (s, 8H, *pyrrole*–H of TPP), 8.05 (m, 8H, *o*–H of TPP), 7.65 (m, 12H, *m/p*–H of TPP), 6.40 (tt, J = 7.2/0.8, 1H, *p*–H of PhNO), 6.09 (tt, J = 7.6/1.6, 1H, *p*–H of pyridine), 5.96 (m, 2H, *m*–H of PhNO), 5.24 (m, 2H, *m*–H of pyridine), 2.55 (m, 2H, *o*–H of PhNO), 1.76 (m, 2H, *o*–H of pyridine). Low–resolution mass spectrum (FAB): *m/z* 900 [(TPP)Ru(PhNO)(py)]$^+$ (7%), 851 [(TPP)Ru(NO)(PhNO)]$^+$ (*proposed*; 24%), 821 [(TPP)Ru(PhNO)]$^+$ (40%), 793 [(TPP)Ru(py)]$^+$ (9%), 714 [(TPP)Ru]$^+$ (100%). UV–vis spectrum (λ (ε, mM^{-1} cm^{-1}), 3.30 x 10^{-6} M in CH_2Cl_2): 308 (34), 411 (230), 533 (18) nm. Suitable crystals for X–ray crystallography were grown from a CH_2Cl_2/hexane solution (1:3) left for 1 week at

–20 °C.

The (TTP)Ru(PhNO)(py) compound was generated similarly.

(TTP)Ru(PhNO)(py). 67% isolated yield. IR (KBr, cm^{-1}): υ_{NO} = 1332 s; also 3077 vw, 3023 vw, 2955 vw, 2920 vw, 1602 w, 1528 m, 1510 w, 1487 w, 1445 m, 1400 vw, 1347 m, 1306 m, 1262 w, 1212 w, 1181 m, 1153 w, 1108 m, 1069 m, 1037 vw, 1007 vs, 886 w, 847 vw, 800 s, 764 w, 754 w, 715 m, 691 m, 665 vw, 644 vw, 523 m. ^1H NMR ($CDCl_3$): δ 8.42 (s, 8H, *pyrrole*–H of TTP), 7.94 (dd, *J* = 7.6/1.6, 4H, *o*–H of TTP), 7.90 (dd, *J* = 7.6/1.6, 4H, *o'*–H of TTP), 7.48 (br d, *J* = 7.6, 4H, *m*–H of TTP), 7.43 (br d, *J* = 7.6, 4H, *m'*–H of TTP), 6.36 (tt, *J* = 7.2/0.8, 1H, *p*–H of PhNO), 6.07 (tt, *J* = 7.6/1.6, 1H, *p*–H of pyridine), 5.93 (m, 2H, *m*–H of PhNO), 5.22 (m, 2H, *m*–H of pyridine), 2.65 (s,12H, CH_3 of TTP), 2.52 (m, 2H, *o*–H of PhNO), 1.74 (m, 2H, *o*–H of pyridine). Low–resolution mass spectrum (FAB): *m/z* 907 $[(TTP)Ru(NO)(PhNO)]^+$ (*proposed*; 46%), 770 $[(TTP)Ru]^+$ (100%). UV–vis spectrum (λ, CH_2Cl_2): 310 (10), 413 (100), 533 (5) nm. Suitable crystals for X–ray crystallography were grown from a CH_2Cl_2/hexane solution (1:5) left for 2 weeks at –20 °C.

Preparation of (por)Ru(ArNO)(1–MeIm) compounds (por = TPP, TTP; ArNO = PhNO, *o*–tolNO, $N(O)C_6H_4OMe$–*p*, $N(O)C_6H_2(Me)_2OMe$–*p*). These compounds were prepared from the reaction of the precursor $(por)Ru(ArNO)_2$ with 2 equiv of 1–MeIm. The following reaction is representative:

To a CH_2Cl_2 (10 mL) solution of $(TPP)Ru(PhNO)_2$ (0.020 g, 0.021 mmol) was added 2 equiv of 1–MeIm. This mixture was stirred at room temperature for 30 min, during which time it turned from brown to red–purple. The solvent was removed in vacuo. A ^1H NMR spectrum of the residue in $CDCl_3$ showed the quantitative formation of (TPP)Ru(PhNO)(1–MeIm), together with the presence of some unreacted 1–MeIm. Spectroscopically pure (TPP)Ru(PhNO)(1–MeIm) was obtained in 80% yield by recrystallization of the residue from a CH_2Cl_2/hexane solution (1:3) at –20 °C. IR (KBr, cm^{-1}): υ_{NO} = 1322 s; also 3127 vw, 3052 w, 3022 w, 1596 m, 1529 m, 1482 w, 1440 m,

1348 m, 1303 m sh, 1237 w, 1207 w, 1177 w, 1157 w, 1109 w, 1072 m, 1008 vs, 949 vw, 924 vw, 888 vw, 833 vw, 815 vw, 793 m, 752 s, 701 s, 665 w, 615 w, 527 w. ^{1}H NMR ($CDCl_3$): δ 8.37 (s, 8H, *pyrrole*–H of TPP), 8.05 (m, 8H, *o*–H of TPP), 7.64 (m, 12H, *m/p*–H of TPP), 6.39 (tt, J = 7.2/1.2, 1H, *p*–H of PhNO), 5.96 (m, 2H, *m*–H of PhNO), 4.74 (dd (apparent t), J = 1.2/1.2, 1H of 1–MeIm), 2.64 (m, 2H, *o*–H of PhNO), 2.18 (s, 3H, CH_3 of 1–MeIm), 1.58 (br dd (apparent br t), 1H of 1–MeIm), 1.22 (dd (apparent t), J = 1.2/1.2, 1H of 1–MeIm). Low–resolution mass spectrum (FAB): *m/z* 903 [(TPP)-Ru(PhNO)(1–MeIm)]$^+$ (18%), 822 [(TPP)Ru(PhNO) + H]$^+$ (19%), 796 [(TPP)Ru(1–MeIm)]$^+$ (51%), 714 [(TPP)Ru]$^+$ (100%). UV–vis spectrum (λ (ε, mM^{-1} cm^{-1}), 3.19 x 10^{-6} M in CH_2Cl_2): 307 (42), 413 (257), 533 (24) nm. Suitable crystals for X–ray crystallography were grown from a CH_2Cl_2/hexane solution (1:3) left for 2 weeks at –20 °C.

The other (por)Ru(ArNO)(1–MeIm) compounds were generated similarly.

(TPP)Ru(*o*–tolNO)(1–MeIm). 50% isolated yield. IR (KBr, cm^{-1}): υ_{NO} = 1320 s, 1311 s; also 3127 vw, 3054 w, 3022 w, 2954 w, 2920 w, 1597 m, 1530 m, 1488 w, 1440 m, 1348 m, 1334 m, 1236 w, 1206 w, 1175 w, 1156 vw, 1108 w, 1090 w, 1070 m, 1007 vs, 948 w, 906 w, 834 vw, 818 vw, 793 m, 754 s, 714 w, 702 m, 665 w, 615 w, 529 w. ^{1}H NMR ($CDCl_3$): δ 8.37 (s, 8H, *pyrrole*–H of TPP), 8.01 (m, 8H, *o*–H of TPP), 7.63 (m, 12H, *m/p*–H of TPP), 6.26 (ddd (apparent td), J = 7.6/7.6/1.2, 1H, *p*–H of *o*–tolNO), 5.81 (br d, J = 7.6, 1H, *m*–H of *o*–tolNO), 5.74 (br dd (apparent br t), J = 7.6/7.6, 1H, *m'*–H of *o*–tolNO), 4.71 (dd (apparent t), J = 1.2/1.2, 1H of 1–MeIm), 2.17 (s, 3H, CH_3 of 1–MeIm), 2.08 (dd, J = 7.6/1.2, 1H, *o*–H of *o*–tolNO), 1.50 (br dd (apparent br t), 1H of 1–MeIm), 1.14 (dd (apparent t), J = 1.2/1.2, 1H of 1–MeIm), –0.99 (s, 3H, CH_3 of *o*–tolNO). Low–resolution mass spectrum (FAB): *m/z* 917 [(TPP)Ru(*o*–tolNO)(1–MeIm)]$^+$ (17%), 835 [(TPP)Ru(*o*–tolNO)]$^+$ (20%), 796 [(TPP)Ru(1–MeIm)]$^+$ (39%), 714 [(TPP)Ru]$^+$ (100%). Suitable crystals for X–ray crystallography were grown from a toluene/hexane solution (5:1) left for 1 week at –20 °C.

(TTP)Ru(PhNO)(1–MeIm). 57% isolated yield. IR (KBr, cm^{-1}): υ_{NO} = 1321 s; also 3127 vw, 3020 w, 2953 vw, 2921 w, 2869 vw, 1530 m, 1506 w, 1449 w, 1348 m, 1287 w, 1237 w, 1212 w, 1181 m, 1108 m, 1092 w, 1071 m, 1007 vs, 947 vw, 886 w, 847 vw, 798 s, 764 w, 716 m, 694 m, 667 vw, 644 vw, 524 m. ^{1}H NMR ($CDCl_3$): δ 8.38 (s, 8H, *pyrrole*–H of TTP), 7.95 (dd, *J* = 7.6/1.6, 4H, *o*–H of TTP), 7.89 (dd, *J* = 7.6/1.6, 4H, *o'*–H of TTP), 7.47 (br d, *J* = 7.6, 4H, *m*–H of TTP), 7.42 (br d, *J* = 7.6, 4H, *m'*–H of TTP), 6.36 (br t, *J* = 8, 1H, *p*–H of PhNO), 5.93 (br t, *J* = 8, 2H, *m*–H of PhNO), 4.71 (br dd (apparent br t), 1H of 1–MeIm), 2.65 (s,12H, C*H*$_3$ of TTP), 2.62 (br d, *J* = 8, 2H, *o*–H of PhNO), 2.16 (s, 3H, C*H*$_3$ of 1–MeIm), 1.56 (br, 1H of 1–MeIm), 1.20 (br dd (apparent br t), 1H of 1–MeIm). Low–resolution mass spectrum (FAB): *m/z* 959 [(TTP)Ru(PhNO)(1–MeIm)]$^+$ (23%), 877 [(TTP)Ru(PhNO)]$^+$ (20%), 852 [(TTP)Ru(1–MeIm)]$^+$ (48%), 770 [(TTP)Ru]$^+$ (100%). UV–vis spectrum (λ, CH_2Cl_2): 310 (8), 414 (100), 533 (4) nm. Suitable crystals for X–ray crystallography were grown from a CH_2Cl_2/hexane solution (1:5) left overnight at –20 °C.

(TTP)Ru(*o*–tolNO)(1–MeIm). 58% isolated yield. IR (KBr, cm^{-1}): υ_{NO} = 1311 s ; also 3127 vw, 3021 w, 2954 vw, 2921 w, 2867 vw, 1529 m, 1514 w, 1479 w, 1442 w, 1347 m, 1284 w sh, 1237 w, 1211 w, 1181 w, 1108 m, 1072 m, 1008 vs, 947 vw, 906 w, 797 s, 755 w, 718 m, 672 vw, 658 w, 616 vw, 524 m. ^{1}H NMR ($CDCl_3$): δ 8.38 (s, 8H, *pyrrole*–H of TTP), 7.90 (dd (overlapping with *o'*–H of TTP), 4H, *o*–H of TTP), 7.87 (dd (overlapping with *o*–H of TTP), 4H, *o'*–H of TTP), 7.45 (br d, *J* = 7.6, 4H, *m*–H of TTP), 7.41 (br d, *J* = 7.6, 4H, *m'*–H of TTP), 6.23 (br ddd (apparent br td), *J* = 7.6/7.6/1.2, 1H, *p*–H of *o*–tolNO), 5.78 (br d, *J* = 7.6, 1H, *m*–H of *o*–tolNO), 5.71 (br dd (apparent br t), *J* = 7.6/7.6, 1H, *m'*–H of *o*–tolNO), 4.68 (dd (apparent t), *J* = 1.6/1.6, 1H of 1–MeIm), 2.64 (s,12H, C*H*$_3$ of TTP), 2.14 (s, 3H, C*H*$_3$ of 1–MeIm), 2.05 (br dd, *J* = 7.6/1.2, 1H, *o*–H of *o*–tolNO), 1.47 (br dd (apparent br t), 1H of 1–MeIm), 1.11 (dd (apparent t), *J* = 1.6/1.6, 1H of 1–MeIm), –1.01 (s, 3H, C*H*$_3$ of *o*–tolNO). Low–resolution mass spectrum (FAB): *m/z* 973 [(TTP)Ru(*o*–tolNO)(1–MeIm)]$^+$ (10%), 891 [(TTP)Ru(*o*–tolNO)]$^+$ (26%), 852

[(TTP)Ru(1–MeIm)]$^+$ (45%), 770 [(TTP)Ru]$^+$ (100%). Suitable crystals for X–ray crystallography were grown from a CH_2Cl_2/hexane solution (1:3) left for 1 week at –20 °C.

(TTP)Ru(N(O)C$_6$H$_4$OMe–*p*)(1–MeIm). 70% isolated yield. IR (KBr, cm^{-1}): υ_{NO} = 1323 s, 1306 s; also 3127 vw, 3021 w, 2921 w, 1599 w, 1563 w, 1528 m, 1510 w, 1497 m,1460 w, 1441 w, 1348 m, 1246 s, 1212 w, 1182 m, 1156 w, 1108 m, 1072 m, 1034 w, 1008 vs, 947 vw, 903 w, 831 w, 797 s, 717 m, 671 w, 616 w, 524 w. ^{1}H NMR ($CDCl_3$): δ 8.37 (s, 8H, *pyrrole*–H of TTP), 7.96 (dd, *J* = 7.6/2.0, 4H, *o*–H of TTP), 7.90 (dd, *J* = 7.6/2.0, 4H, *o'*–H of TTP), 7.47 (br d, *J* = 7.6, 4H, *m*–H of TTP), 7.42 (br d, *J* = 7.6, 4H, *m'*–H of TTP), 5.44 (m, 1H, *m*–H of N(O)C$_6$*H*$_4$OMe–*p*), 4.70 (dd (apparent t), *J* = 1.2/1.2, 1H of 1–MeIm), 3.40 (s, 3H, C*H*$_3$O of N(O)C$_6$H$_4$O*Me*–*p*), 2.67 (d (overlapping with C*H*$_3$ of TTP), 2H, *o*–H of N(O)C$_6$*H*$_4$OMe–*p*), 2.64 (s,12H, C*H*$_3$ of TTP), 2.15 (s, 3H, C*H*$_3$ of 1–MeIm), 1.56 (br, 1H of 1–MeIm), 1.20 (dd (apparent t), *J* = 1.2/1.2, 1H of 1–MeIm). Low–resolution mass spectrum (FAB): *m/z* 989 [(TTP)Ru(N(O)C$_6$H$_4$OMe–*p*)(1–MeIm)]$^+$ (11%), 907 [(TTP)Ru(N(O)C$_6$H$_4$OMe–*p*)]$^+$ (19%), 852 [(TTP)Ru(1–MeIm)]$^+$ (35%), 770 [(TTP)Ru]$^+$ (100%).

(TTP)Ru(^{15}N(O)C$_6$H$_4$OMe–*p*)(1–MeIm). IR (KBr, cm^{-1}): υ_{NO} = 1296 s, 1275 s.

(TTP)Ru(N(O)C$_6$H$_2$(Me)$_2$OMe–*p*)(1–MeIm). 78% isolated yield. IR (KBr, cm^{-1}): υ_{NO} = 1321 s, 1309 s; also 3124 vw, 3019 vw, 2951 vw, 2920 w, 1530 m, 1469 w, 1453 w, 1347 m, 1286 w, 1214 m, 1181 m, 1127 w, 1109 m, 1091 w, 1072 m, 1007 vs, 947 vw, 885 vw, 848 vw, 799 s, 717 m, 615 vw, 524 m. ^{1}H NMR ($CDCl_3$): δ 8.38 (s, 8H, *pyrrole*–H of TTP), 7.95 (dd, *J* = 7.6/2.0, 4H, *o*–H of TTP), 7.90 (dd, *J* = 7.6/2.0, 4H, *o'*–H of TTP), 7.47 (br d, *J* = 7.6, 4H, *m*–H of TTP), 7.42 (br d, *J* = 7.6, 4H, *m'*–H of TTP), 4.71 (dd (apparent t), *J* = 1.2/1.2, 1H of 1–MeIm), 3.27 (s, 3H, C*H*$_3$O of N(O)-C$_6$H$_2$(Me)$_2$O*Me*–*p*), 2.65 (s,12H, C*H*$_3$ of TTP), 2.22 (s, 2H, *o*–H of N(O)C$_6$*H*$_2$(Me)$_2$-OMe–*p*), 2.16 (s, 3H, C*H*$_3$ of 1–MeIm), 1.59 (br, 1H of 1–MeIm), 1.45 (s, 6H, C*H*$_3$ of N(O)C$_6$H$_2$(*Me*)$_2$OMe–*p*), 1.23 (dd (apparent t), *J* = 1.2/1.2, 1H of 1–MeIm). Low–

resolution mass spectrum (FAB): *m/z* 1017 [(TTP)Ru(N(O)$C_6H_2(Me)_2$OMe-*p*)(1-MeIm)]$^+$ (14%), 935 [(TTP)Ru(N(O)$C_6H_2(Me)_2$OMe-*p*)]$^+$ (17%), 852 [(TTP)Ru(1-MeIm)]$^+$ (37%), 770 [(TTP)Ru]$^+$ (100%). Suitable crystals for X-ray crystallography were grown by slow evaporation of CH_2Cl_2/hexane (1:1) solution of the compound at room temperature under inert atmosphere.

Results and Discussion

Synthesis of Bis- and Mono-Nitrosoarene Complexes. James and coworkers previously reported the synthesis of (OEP)Ru(PhNO)$_2$ from the reaction of (OEP)Ru-(CO) with excess PhNO in CH_2Cl_2.[17] Using similar methodology, our research group recently synthesized and reported the related compound (OEP)Ru(N(O)$C_6H_4NMe_2$-*p*)$_2$.[12]

In this work, this synthetic methodology was also employed to prepare the bis-nitrosoarene complexes of *tetraaryl*porphyrin complexes of Ru. Thus, the reaction of excess ArNO (ArNO = PhNO, *o*-tolNO, N(O)C_6H_4OMe-*p*, N(O)$C_6H_2(Me)_2$OMe-*p*) with the (por)Ru(CO) compounds (por = TPP, TTP) in CH_2Cl_2 or refluxing toluene generates the bis-nitrosoarene complexes (por)Ru(ArNO)$_2$ in 49-75% isolated yields (Scheme 5.1).

Scheme 5.1

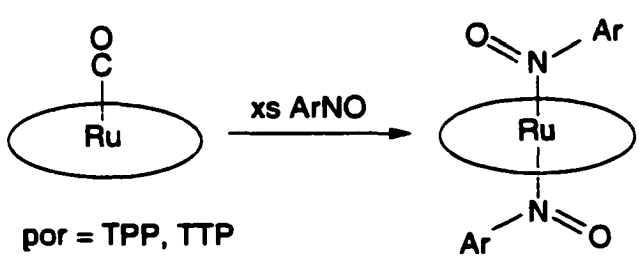

These brown bis-nitrosoarene complexes are moderately air-stable in solution and can be stored in air in the solid state for several months without noticeable

decomposition. They are soluble in CH_2Cl_2 and toluene, but are insoluble in hexane.

In our group's previous work with the analogous osmium compounds, we showed that when the (por)Os(CO) compounds (por = TTP, TMP, OEP) are reacted with 1 equiv of PhNO in CH_2Cl_2 at room temperature, the formation of the (por)Os(CO)(PhNO) intermediates is observable by IR spectroscopy.[13] In the case of (TPP)Ru(CO), however, the (TPP)Ru(CO)(PhNO) intermediate was not observed under the same conditions, suggestive of the fast conversion of (TPP)Ru(CO) to (TPP)Ru(PhNO)$_2$. James and coworkers also reported a similar result from the reaction of (OEP)Ru(CO) with 1 equiv of PhNO.[17] Thus, they observed that the reaction of (OEP)Ru(CO) with 1 equiv of PhNO at 20 °C results in a simple conversion of a half of (OEP)Ru(CO) to (OEP)Ru(PhNO)$_2$. This implies that PhNO additions to (por)Ru(CO) to give the bis–nitrosobenzene derivatives are faster than the analogous additions to (por)Os(CO). The reaction of *o*–tolNO with (por)Ru(CO) also showed the fast conversion of the carbonyl compounds to (por)Ru(*o*–tolNO)$_2$. However, when (TTP)Ru(CO) was reacted with 4–nitrosoanisole in CH_2Cl_2 at room temperature, the formation of the (TTP)Ru(CO)(N(O)C_6H_4OMe–*p*) intermediate was observed by IR monitoring, indicative of the slow substitution of CO by the second 4–nitrosoanisole. Thus, the IR spectrum of the reaction mixture in CH_2Cl_2 shows a new band at 1967 cm^{-1} assigned to the υ_{CO}, which is 31 cm^{-1} higher in energy than that of the starting (TTP)Ru(CO) at 1936 cm^{-1} in CH_2Cl_2. Indeed, this feature of an increased υ_{CO} indicates that 4–nitrosoanisole acts as a π–acid ligand toward the (TTP)Ru(CO) fragment, resulting in decreased back–bonding of electron density into the π^* orbitals of CO and raising υ_{CO}. Our research group recently also reported that when (OEP)Ru(CO) is reacted with *p*–$ONC_6H_4NMe_2$ in CH_2Cl_2 at room temperature, IR monitoring reveals the formation of the intermediate (OEP)Ru(CO)(N(O)$C_6H_4NMe_2$–*p*), and that its υ_{CO} at 1932 cm^{-1} is shifted by 11 cm^{-1} to higher wavenumbers relative to the υ_{CO} of the starting (OEP)Ru(CO) at 1921 cm^{-1}.[12] Unlike in the cases of PhNO and *o*–tolNO, this slow substitution of CO by ArNO observed in the reaction of (por)Ru(CO)

with *p*–$ONC_6H_4NMe_2$ or nitrosoanisoles might be expected to be due to the presence of the dipolar resonance form in these free nitrosoarene compounds (see Figure 5.2). Due to the slow reaction of (TTP)Ru(CO) with nitrosoanisole compounds in CH_2Cl_2 at room temperature, two bis–nitrosoanisole complexes, namely (TTP)Ru($N(O)C_6H_4OMe$–*p*)$_2$ and (TTP)Ru($N(O)C_6H_2(Me)_2OMe$–*p*)$_2$ were synthesized under more vigorous conditions (i.e., refluxing toluene).

Many heme–containing biomolecules contain histidine as the axial proximal ligand. Thus, our research group was interested in synthesizing the axially–unsymmetrical (por)Ru(ArNO)L (L = pyridine or 1–MeIm) complexes to examine their spectroscopic properties and to determine the effect of the axial pyridine or 1–MeIm ligand on the binding of ArNO in the (por)Ru(ArNO)L complexes.

The mono–nitrosoarene complexes containing the axial pyridine or 1–MeIm ligand, namely (por)Ru(PhNO)(py) (por = TPP, TTP) and (por)Ru(ArNO)(1–MeIm) (por = TPP, TTP; ArNO = PhNO, *o*–tolNO, $N(O)C_6H_4OMe$–*p*, $N(O)C_6H_2(Me)_2OMe$–*p*), are readily prepared via substitution reactions. Thus, the reaction of (por)Ru(PhNO)$_2$ with ~2 equiv of pyridine or 1–MeIm produces the corresponding mono–nitrosoarene complexes in 67–71% (for pyridine complexes) and 50–80% (for 1–MeIm complexes) isolated yields, respectively, as shown in Scheme 5.2. The ^1H NMR spectra of the crude product mixtures in $CDCl_3$ (after 30 min reaction time in CH_2Cl_2 at room temperature followed by solvent removal *in vacuo* and redissolving the product in $CDCl_3$) showed the presence of the desired mono–nitrosoarene complexes and unreacted organic pyridine or 1–MeIm as the only H–containing species. Despite the use of an excess of pyridine or 1–MeIm in these reactions, the formation of the mono–nitrosoarene complexes as the only Ru–containing products indicates that only one ArNO ligand in the (por)Ru(ArNO)$_2$ complexes is susceptible to substitution reaction under these reaction conditions. A similar observation has been made by James and coworkers who reported that (OEP)Ru(PhNO)$_2$ reacts with 2 equiv of pyridine at room temperature to generate the

Scheme 5.2

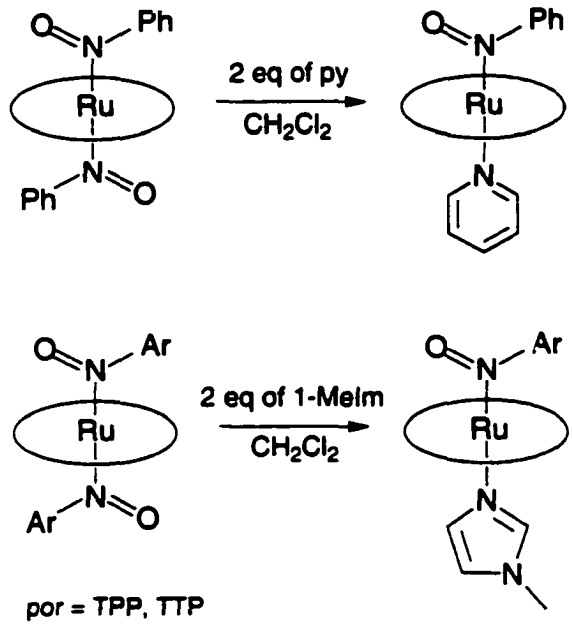

mono–substituted product (OEP)Ru(PhNO)(py) within 10 min.[17] Interestingly, Dr. Li Chen of our research group noted in her dissertation that when (OEP)Os(PhNO)$_2$ was reacted with pyridine at room temperature, no substitution of PhNO by pyridine was observed for several hours. Thus, I performed the reaction of (OEP)Os(PhNO)$_2$ with 1–MeIm at room temperature to examine substitution of PhNO by 1–MeIm. When (OEP)Os(PhNO)$_2$ was reacted with 2 equiv of 1–MeIm in CH_2Cl_2 at room temperature for 1h, the ^{1}H NMR spectrum of the reaction mixture in $CDCl_3$ showed the presence of a 1:4 mixture of (OEP)Os(PhNO)(1–MeIm) and (OEP)Os(PhNO)$_2$. However, the reaction in refluxing toluene resulted in the quantitative conversion of (OEP)Os(PhNO)$_2$ to (OEP)Os(PhNO)(1–MeIm) within 1h.[18]

These red–purple mono–nitrosoarene complexes of Ru are moderately air–stable, showing no signs of decomposition in air after 1 month in the solid state and at least 8h in solution. As with their bis–nitrosoarene precursors, they are soluble in CH_2Cl_2

and toluene, but are insoluble in hexane.

Spectroscopic Characterization. The IR spectra of the new (por)Ru(ArNO)$_2$ complexes (as KBr pellets) show new bands in the 1346–1350 cm^{-1} range assigned to the υ_{NO} of the coordinated ArNO groups. Employing *p*–O^{15}NC$_6$H$_4$OMe (i.e., nitroso ^{15}N–labeled) in the reaction to produce (TTP)Ru(N(O)C$_6$H$_4$OMe–*p*)$_2$ results in the υ_{NO} band at 1348 cm^{-1} (overlapping with a porphyrin band) being shifted to lower wavenumber (1318 cm^{-1}; $\Delta\upsilon_{NO}$ = –30 cm^{-1}), consistent with the assignment of this band to υ_{NO} (see Figure 5.3). The marked drop in υ_{NO} from free PhNO at 1506 cm^{-1} to (TPP)Ru(PhNO)$_2$ at 1348 cm^{-1} is consistent with the view that the π^* orbitals of the PhNO ligands withdraw electron density from the "(TPP)Ru" fragment in the (TPP)Ru(PhNO)$_2$ complex. Further evidence of the ArNO ligands behaving as π–acids in these complexes comes from the X–ray crystal structures of (por)Ru(ArNO)$_2$ (see later).

The IR spectra of the mono–nitrosoarene complexes (as KBr pellets) also show one or two new band(s) in the 1328–1332 cm^{-1} range (for pyridine complexes) and the 1306–1323 cm^{-1} range (for 1–MeIm complexes), respectively, assigned to υ_{NO}. Interestingly, the IR spectra (KBr) of three (por)Ru(ArNO)(1–MeIm) complexes, namely (TPP)Ru(*o*–tolNO)(1–MeIm), (TTP)Ru(N(O)C$_6$H$_4$OMe–*p*)(1–MeIm), and (TTP)Ru-(N(O)C$_6$H$_2$(Me)$_2$OMe–*p*)(1–MeIm), show split υ_{NO} bands with comparable intensity. For example, the IR spectrum of (TPP)Ru(N(O)C$_6$H$_4$OMe–*p*)(1–MeIm) shows two strong bands at 1323 cm^{-1} and 1306 cm^{-1}. These two bands are both assigned as υ_{NO}, and this assignment for (TTP)Ru(N(O)C$_6$H$_4$OMe–*p*)(1–MeIm) was confirmed by the analysis of the IR spectrum of the *p*–O^{15}NC$_6$H$_4$OMe analogue ($\upsilon_{^{15}NO}$ = 1296 and 1275 cm^{-1}, $\Delta\upsilon_{NO}$ = –27 and –31 cm^{-1}; see Figure 5.4). The presence of two bands may presumably be due to the existence of the different conformations of (por)Ru(ArNO)(1–MeIm) in the solid state (see Figure 5.5).[19] Indeed, the fact that the presence of two bands is observed only for the mono–nitrosoarene complexes containing the unsymmetrical

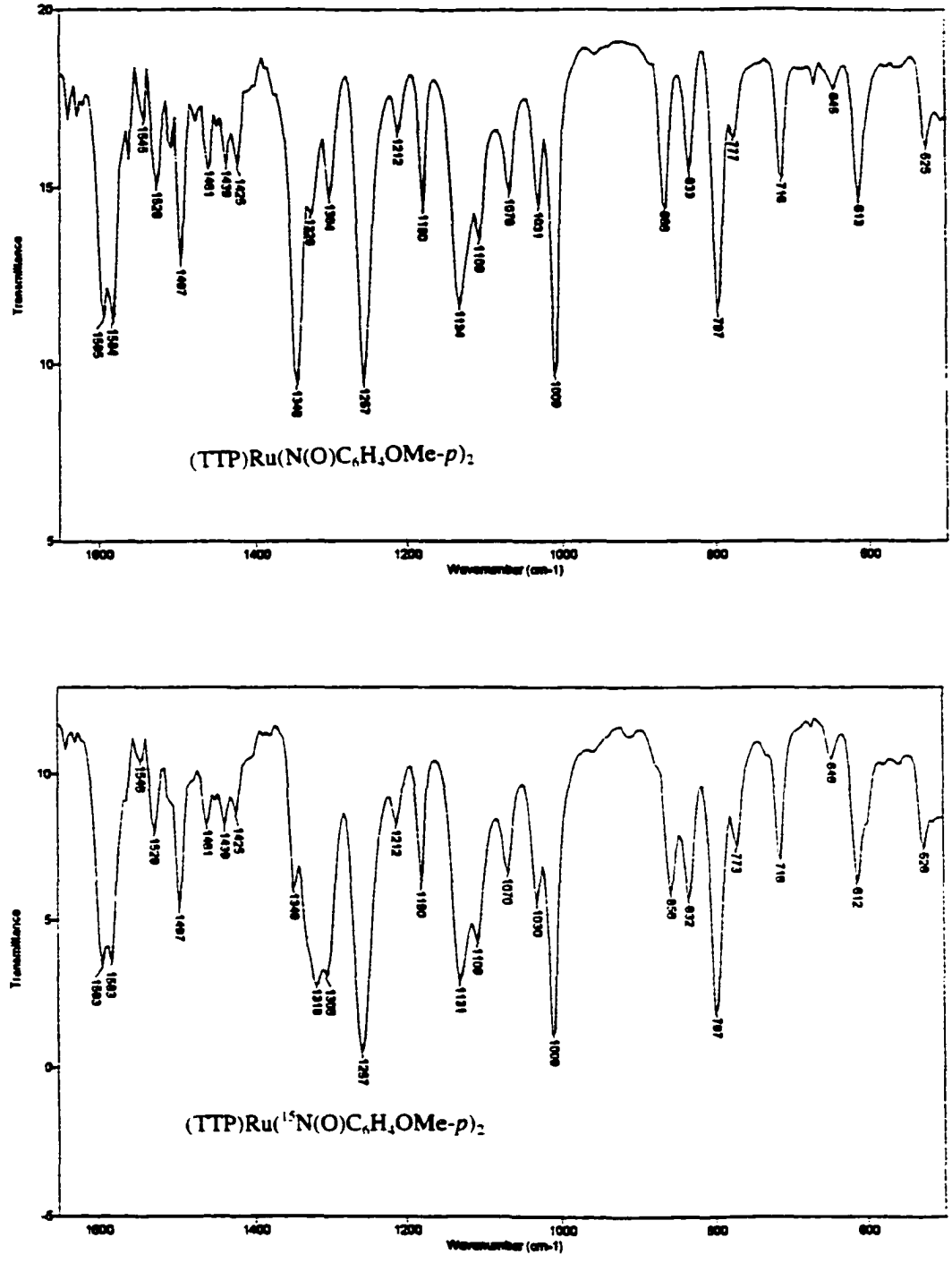

Figure 5.3. IR spectra of (TTP)Ru(N(O)C_6H_4OMe–*p*)$_2$ (top) (the υ_{NO} band at 1348 cm^{-1} overlaps with a porphyrin band) and (TTP)Ru(^{15}N(O)-C_6H_4OMe–*p*)$_2$ (bottom).

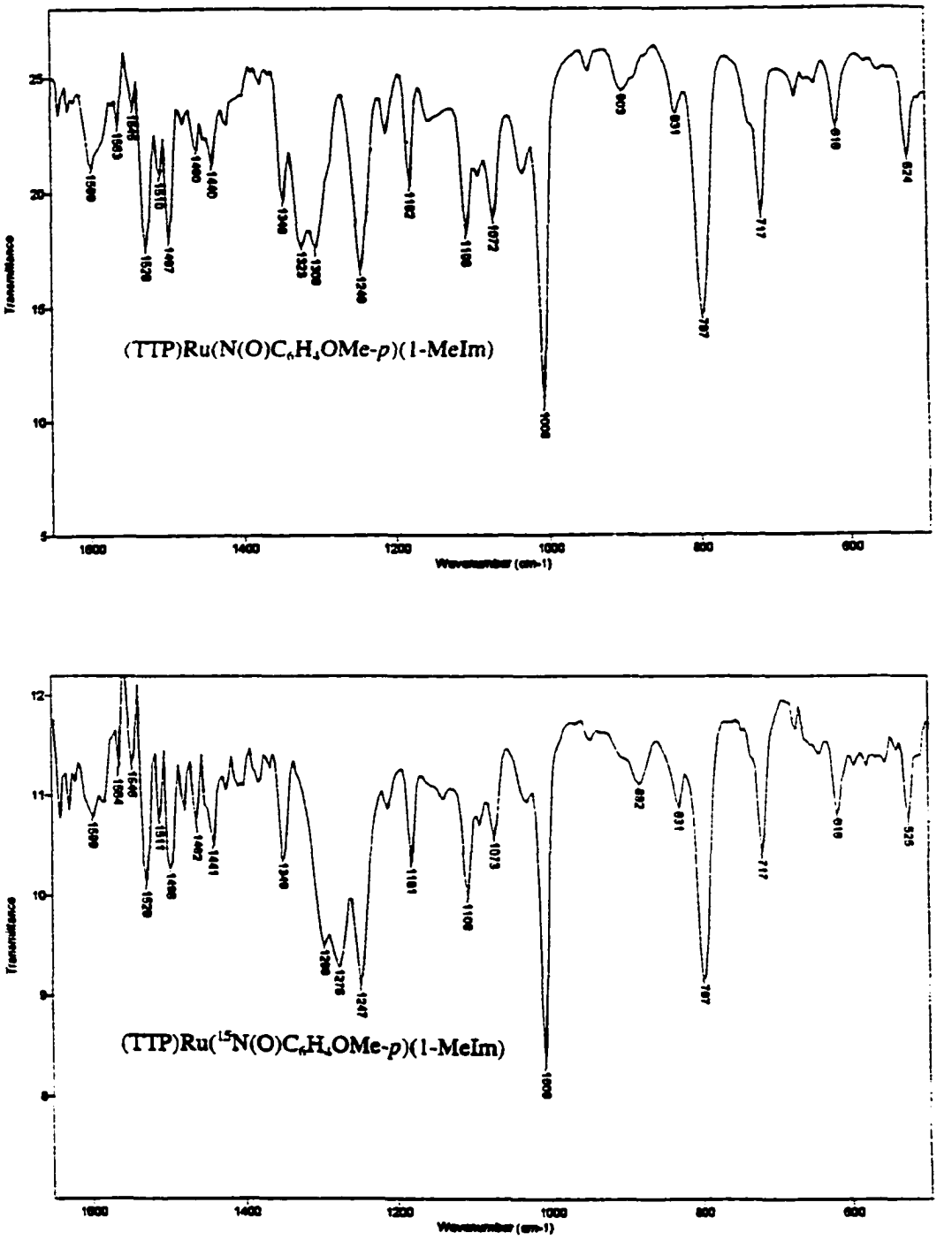

Figure 5.4. IR spectra of (TTP)Ru(N(O)C_6H_4OMe–*p*)(1–MeIm) (top) and (TTP)Ru(^{15}N(O)C_6H_4OMe–*p*)(1–MeIm) (bottom).

1–MeIm ligand supports this assumption. The solid–state crystal structures of the (por)Ru(ArNO)(1–MeIm) complexes also show that both conformations are indeed possible (see Figure 5.19).

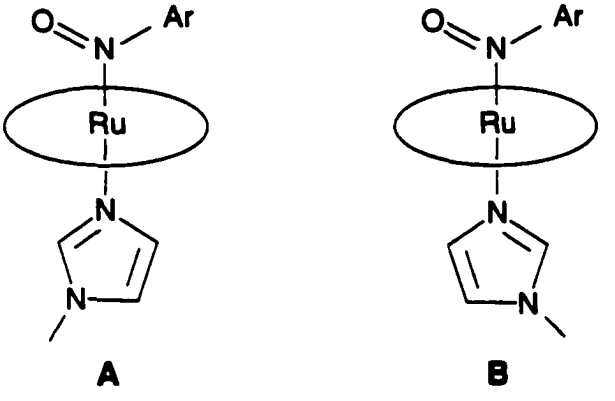

Figure 5.5. Possible two conformations of (por)Ru(ArNO)(1–MeIm) in the solid state.

Comparison of the IR spectra of the bis–nitrosoarene complexes with those of the mono–nitrosoarene complexes reveals that the υ_{NO}s of the mono–nitrosoarene complexes are shifted by ~20 cm^{-1} to lower wavenumbers relative to the bis–nitrosoarene precursors. This shifting of υ_{NO} to lower wavenumbers is consistent with the replacement of one of the π–acid ArNO ligands (in the bis–nitrosoarene precursor) with the more basic pyridine or 1–MeIm ligand, which results in more Ru→N(O)Ar back–donation in the mono–nitrosoarene complexes. Furthermore, the NO stretching frequencies of (por)Ru(PhNO)(py) are slightly higher than those of (por)Ru(ArNO)(1–MeIm), reflecting the stronger electron–donating ability of the 1–MeIm ligand to the (por)Ru moiety relative to the pyridine ligand in the mono–nitrosoarene complexes.

The ^1H NMR spectra of the (por)Ru$(ArNO)_2$ complexes in $CDCl_3$ show, as expected, peaks for both the porphyrin macrocycle and the ArNO ligands in these

diamagnetic and formally d^6 Ru(II) complexes. Furthermore, the ^{1}H NMR spectra of the *p*–substituted tetraphenylporphyrin complexes, namely the (TTP)Ru(ArNO)$_2$ compounds, show only one set of *o*– and *m*–H peaks of the *meso*–aryl substituents on the porphyrin rings, suggesting axial symmetry in these complexes or fast rotation of the porphyrin aryl substituents on the NMR time scale. The ^{1}H NMR spectra (in $CDCl_3$) of the mono–nitrosoarene complexes also reveal, in addition to porphyrin signals, peaks due to both the coordinated ArNO and pyridine or 1–MeIm ligands. The chemical shifts of the $\delta_{pyrrole}$ protons of these bis– and mono–nitrosoarene complexes in the ^{1}H NMR spectra (in $CDCl_3$) decrease slightly in the order (por)Ru(ArNO)$_2$ (8.52–8.57 ppm) > (por)Ru-(PhNO)(py) (8.42 ppm) > (por)Ru(ArNO)(1–MeIm) (8.37–8.38 ppm), indicative of a slight increase in electron–density of the porphyrin macrocycles in the mono–nitrosoarene complexes relative to the bis–nitrosoarene complexes.[20] This ^{1}H NMR feature is consistent with the IR spectroscopic results. Importantly, the ^{1}H NMR spectra of the *p*–substituted tetraphenyl complexes, namely the (TTP)Ru(ArNO)(1–MeIm) compounds, reveal that the *ortho*–protons of the *meso*–aryl substituents on the porphyrin rings are not equivalent, and the *meta*–protons are also non–equivalent, suggesting slow rotation of the porphyrin aryl substituents. This is a common feature for *p*–substituted tetraphenyl porphyrin complexes of the form (por)M(X)(Y) containing different ligands on each face of the porphyrin plane.[21,22]

The UV–vis spectra of (TPP)Ru(PhNO)$_2$, (TPP)Ru(PhNO)(py), and (TPP)Ru-(PhNO)(1–MeIm) in CH_2Cl_2 all show three bands including a strong soret band at 411–413 nm and a β–band at 525–533 nm. Buchler and coworkers previously showed that the wavelength of the β–band in the (TPP)Ru–containing complexes may be used as a measure of the relative Ru→TPP back–bonding ability.[20] Thus, they proposed that the increased Ru→TPP back–donation will result in a hypsochromic shift of the β–band. Interestingly, however, our UV–vis spectroscopic results are *opposite* to the proposal by Buchler and coworkers. Thus, although the IR and ^{1}H NMR spectra show the increased

electron–density of the porphyrin macrocycles in the mono–nitrosoarene complexes relative to the bis–nitrosoarene complexes, the UV–vis spectra reveal that the β–band of (TPP)Ru(PhNO)(py) (533 nm) is bathochromically shifted relative to the β–band of (TPP)Ru(PhNO)$_2$ (525 nm). Furthermore, the β–band of (TPP)Ru(PhNO)(1–MeIm) is identical to that of (TPP)Ru(PhNO)(py). The UV–vis spectra of the related TTP analogs also show a similar trend.

In general, the mass spectra (FAB) of the (por)Ru(ArNO)$_2$ compounds show ion fragments assigned to loss of one ArNO ligand or loss of two ArNO ligands. In the cases of the mono–nitrosoarene complexes, the mass spectra show the parent ion and ion fragments assigned to loss of ArNO ligand, loss of the pyridine or 1–MeIm ligand, and loss of two axial ligands.

X–ray Crystallographic Characterization. Single–crystal X–ray structures of eleven bis– and mono–nitrosoarene complexes were obtained, in order to ascertain the effects of *(i)* the porphyrin and *(ii)* the axial ligand in the structures of these species.

1. Bis–nitrosoarene complexes. The molecular structures of four bis–nitrosoarene compounds are shown in Figures 5.6–5.9. Selected bond lengths and bond angles are also listed in Tables 5.1–5.8 (see Appendix placed at the end of this dissertation). The (TPP)Ru(*o*–tolNO)$_2$ complex exhibits disorder (Figure 5.9). Important structural parameters for the three crystallographically ordered compounds are summarized in Figure 5.10.

As can been seen in Figures 5.6–5.9, the nitrosoarene ligands are attached to the formally Ru(II) centers via an η^1–N bonding mode. The Ru–N(por) distances for the three bis–nitrosoarene crystallographically ordered complexes fall in the range of 2.041(3)–2.060(2) Å (see Figure 5.10), and these are similar to those seen for other structurally characterized (por)Ru^{II}–containing complexes.[12,23-48] The sum of angles around the nitroso nitrogen all are ~360°, indicative of the planarity around the nitroso N–atoms. The axial Ru–N(ArNO) and O–N(Ar) bond lengths fall in the ranges of

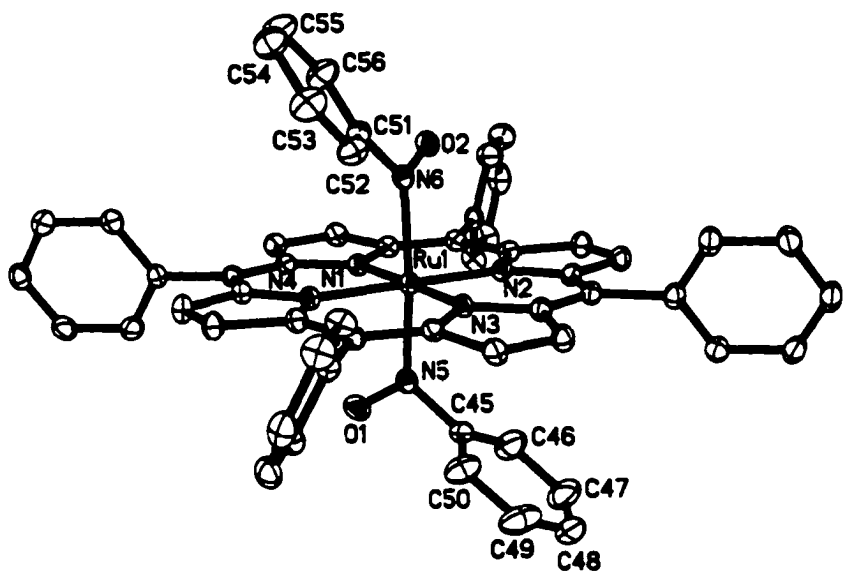

Figure 5.6. Molecular structure of (TPP)Ru(PhNO)$_2$.

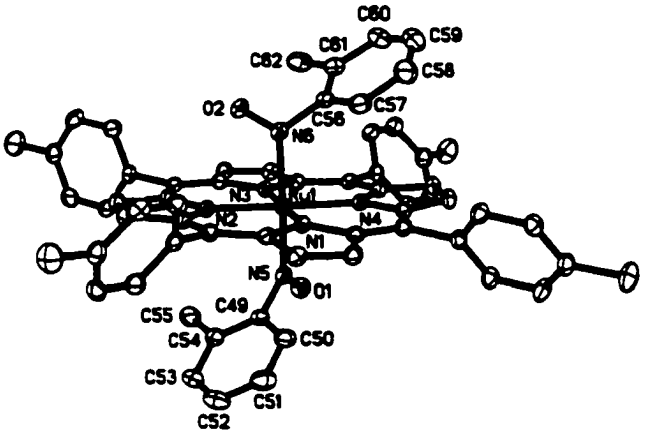

Figure 5.7. Molecular structure of (TTP)Ru(*o*-tolNO)$_2$.

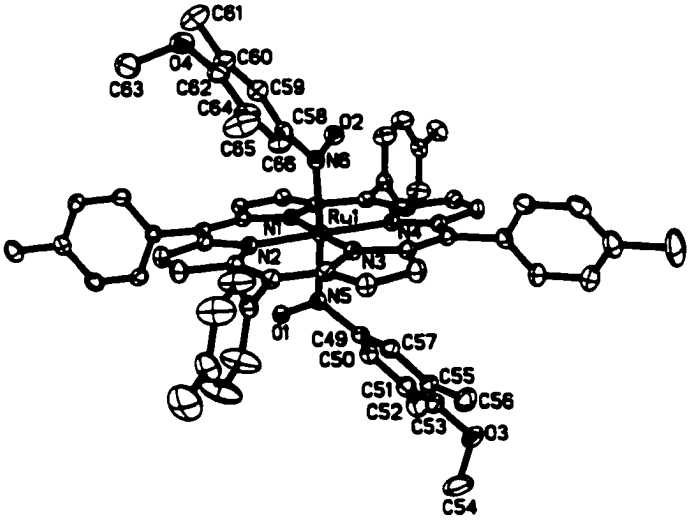

Figure 5.8. Molecular structure of (TTP)Ru(N(O)C$_6$H$_2$(Me)$_2$OMe-*p*)$_2$.

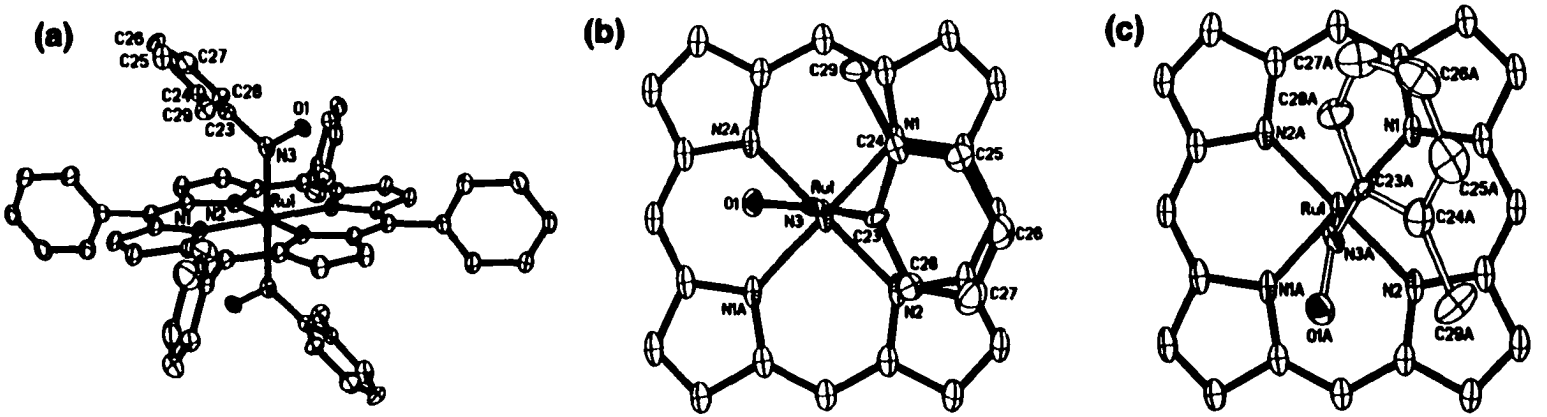

Figure 5.9. Molecular structure of (TPP)Ru(*o*-tolNO)$_2$. (a) View showing only one set of the disordered *o*-tolNO groups. (b) View along the N3–Ru1 bond, showing the orientation of the axial *o*-tolNO group with respect to the porphyrin skeleton. (c) View along the N3A–Ru1 bond of the second disordered *o*-tolNO position.

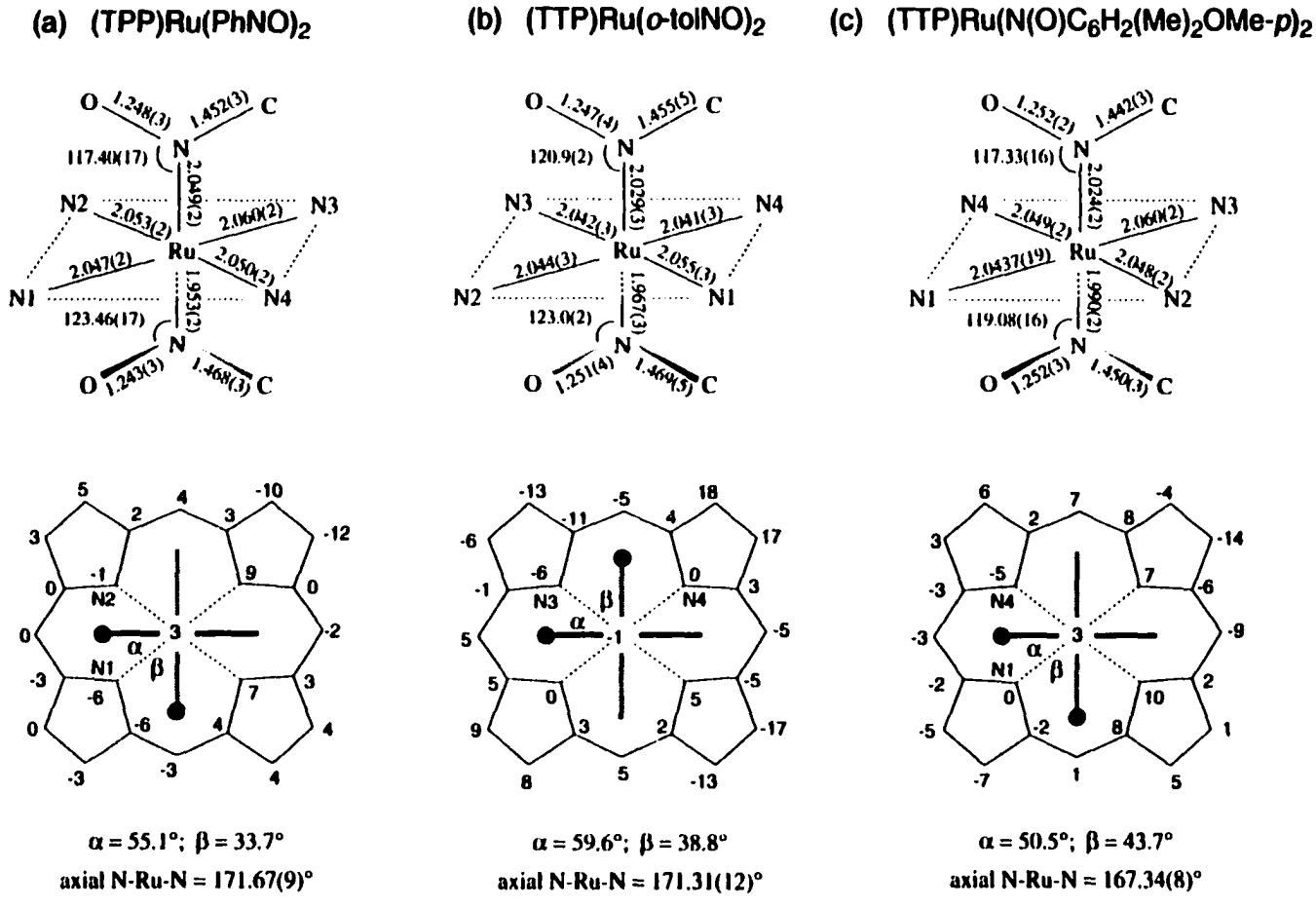

Figure 5.10. Structural data for (por)Ru(ArNO)$_2$ (por = TPP, TTP). Selected bond lengths and angles are shown at the top. Perpendicular atom displacements from the 24-atom porphyrin plane (in 0.01 Å units) are shown at the bottom. Also shown are the nitrosoarene orientations: α and β are torsion angles involving O-N-Ru-N(por). The solid dot represents the nitroso oxygen atom, the solid line represents the O-N-C unit of the ArNO ligand situated above the porphyrin plane, and the dashed line represents the equivalent group situated below the porphyrin plane.

1.953(2)–2.049(2) Å and 1.243(3)–1.252(3) Å, respectively. The axial N–Ru–N bond angles in these bis–nitrosoarene complexes lie in the 167.34(8)–171.67(9)° range (bottom of Figure 5.10), and this range deviates only slightly from strict linearity.

Perpendicular atom displacements of the atoms in the porphyrin skeleton from the 24–atom mean porphyrin plane are shown in the bottom of Figure 5.10. The porphyrin macrocycles of three bis–nitrosoarene complexes all exhibit a *saddle* distortion, and the Ru atoms residue in the plane of the porphyrin (calculated displacements from the 24–atom mean porphyrin plane of only 0.01–0.03 Å). The axial ligand orientations in three bis–nitrosoarene complexes are also shown in Figure 5.10. The ArNO ligands in (por)Ru(ArNO)$_2$ are oriented perpendicular to each other, and their C–NO groups essentially bisect porphyrin nitrogens.

The molecular structure of the bis–nitrosoarene complex (TPP)Ru(*o*–tolNO)$_2$ is shown in Figure 5.9. The molecule lies on the crystallographic center of symmetry, and the axial nitrosoarene ligand is disordered over two positions. The Ru–N(por) distances of 2.042(2) Å are within the range observed for the other bis–nitrosoarene complexes discussed in this chapter. The Ru–N(ArNO) and N–O distances are 1.994(4) and 1.221(5) Å, respectively. For the second disordered component, the corresponding values are 2.040(3) and 1.285(5) Å, respectively.

2. Mono–nitrosoarene complexes. The molecular structures of (por)Ru(PhNO)-(py) (por = TPP, TTP) are shown in Figures 5.11 and 5.12. Selected bond lengths and bond angles are also listed in Tables 5.9–5.12 (see Appendix placed at the end of this dissertation). Important structural parameters for these mono–nitrosobenzene complexes containing the pyridine ligand are summarized in Figure 5.13.

The nitrosobenzene ligands are bound to the Ru(II) center in an η^1–N fashion. The Ru–N(por) distances for two (por)Ru(PhNO)(py) complexes fall in the range of 2.034(3)–2.055(3) Å (see Figure 5.13). The sum of angles around the nitroso nitrogen are ~360°. The axial Ru–N(PhNO) and O–N(Ph) bond lengths in the (por)Ru(PhNO)(py)

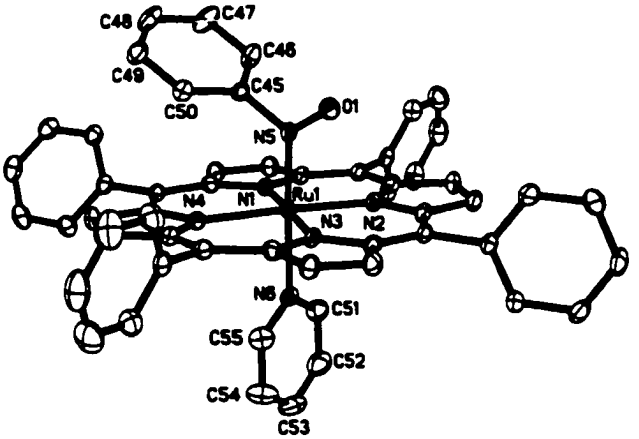

Figure 5.11. Molecular structure of (TPP)Ru(PhNO)py.

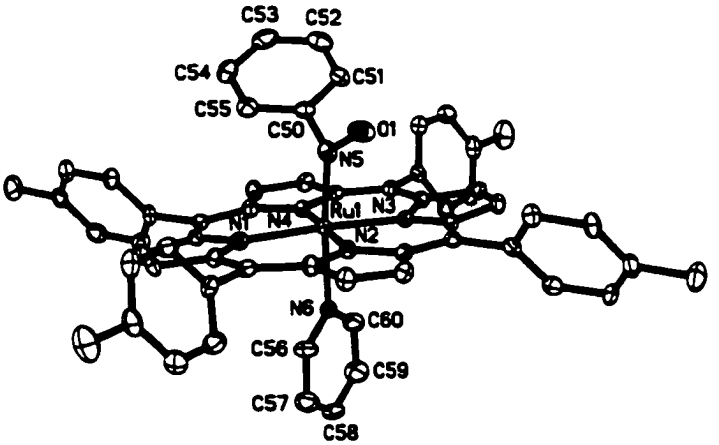

Figure 5.12. Molecular structure of (TTP)Ru(PhNO)py.

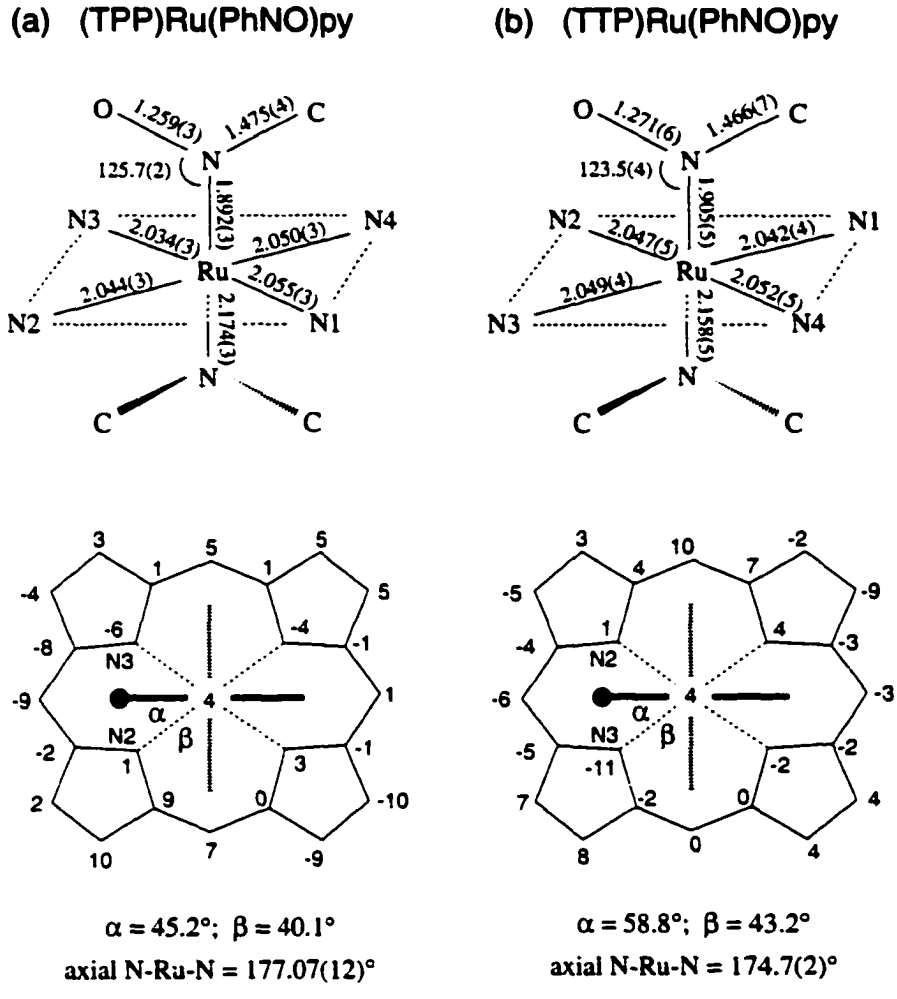

Figure 5.13. Structural data for (por)Ru(PhNO)py (por = TPP, TTP). Selected bond lengths and angles are shown at the top. Perpendicular atom displacements from the 24–atom porphyrin plane (in 0.01 Å units) are shown at the bottom. Also shown are the orientations between PhNO and pyridine at the bottom: α and β are torsion angles involving O–N–Ru–N(por) (for PhNO) and C–N–Ru–N(por) (for pyridine), respectively. The solid dot represents the nitroso oxygen atom, the solid line represents the O–N–C unit of the PhNO ligand situated above the porphyrin plane, and dashed line represents C–N–C unit of the pyridine ligand situated below the porphyrin plane.

complexes fall in the ranges of 1.892(3)–1.905(5) Å and 1.259(3)–1.271(6) Å, respectively. The axial N–Ru–N bond angles are 177.07(12) (for TPP complex) and 174.7(2)° (for TTP complex). These N–Ru–N bond angles are closer to 180° than those seen for the bis–nitrosoarene complexes.

Perpendicular atom displacements of the atoms in the porphyrin skeleton from the 24–atom mean porphyrin plane are shown in the bottom of Figure 5.13, and unlike (por)Ru(ArNO)$_2$, the porphyrin macrocycles of (TPP)Ru(PhNO)(py) and (TTP)-Ru(PhNO)(py) exhibit a *ruffled* distortion. The Ru atoms are both displaced by 0.04 Å from the 24–atom mean porphyrin plane toward the nitrosobenzene ligands. The axial ligand orientations in (por)Ru(PhNO)(py) are also shown in Figure 5.13. The axial ligand orientations observed for (por)Ru(PhNO)(py) are very similar to those observed for (por)Ru(ArNO)$_2$. Thus, the PhNO and pyridine ligands in (por)Ru(PhNO)(py) are oriented perpendicular to each other.

The molecular structures of five mono–nitrosoarene compounds containing the axial 1–MeIm ligand were also obtained and shown in Figures 5.14–5.18. Selected bond lengths and bond angles are listed in Tables 5.13–5.22 (see Appendix placed at the end of this dissertation). Two of these mono–nitrosoarene complexes, namely (TTP)Ru-(PhNO)(1–MeIm) and (TTP)Ru(*o*–tolNO)(1–MeIm) exhibit disorders (Figures 5.17 and 5.18). Important structural parameters for the three (por)Ru(ArNO)(1–MeIm) crystallographically ordered complexes are summarized in Figure 5.19.

As with the (por)Ru(ArNO)$_2$ and (por)Ru(PhNO)(py) complexes, the nitrosoarene ligands in these 1–MeIm–containing nitrosoarene complexes all are bound to the Ru(II) centers via an η^1–N bonding mode. The Ru–N(por) distances for the three (por)Ru-(ArNO)(1–MeIm) crystallographically ordered complexes range from 2.039(4) Å to 2.062(5) Å (see Figure 5.19). The sum of angles around the nitroso nitrogen all are very close to 360°. The axial Ru–N(ArNO) and O–N(Ar) bond lengths in three (por)Ru-(ArNO)(1–MeIm) complexes fall in the ranges of 1.884(6)–1.919(5) Å and

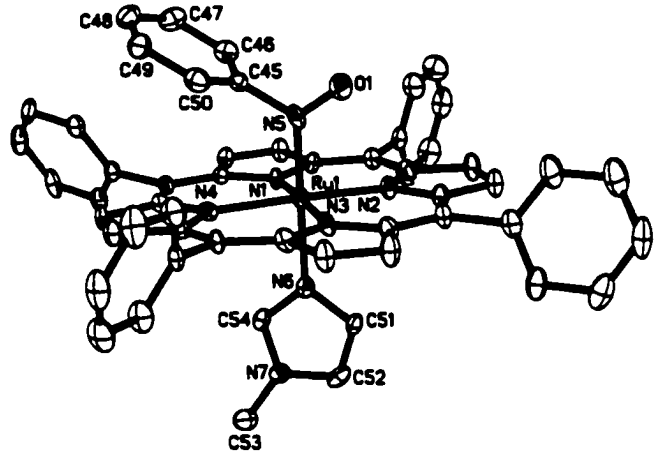

Figure 5.14. Molecular structure of (TPP)Ru(PhNO)(1–MeIm).

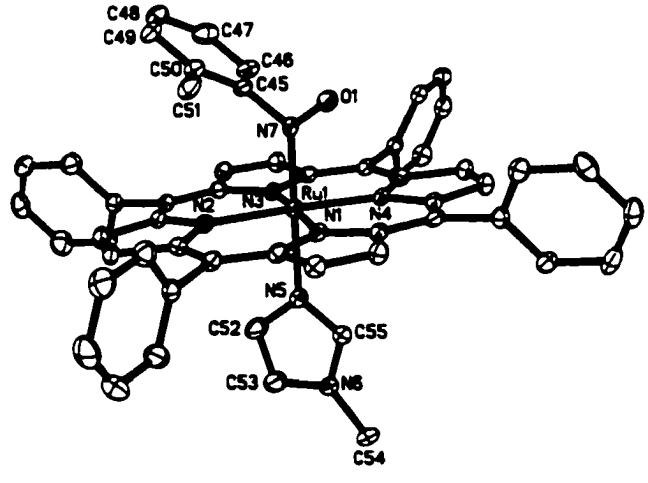

Figure 5.15. Molecular structure of (TPP)Ru(*o*–tolNO)(1–MeIm).

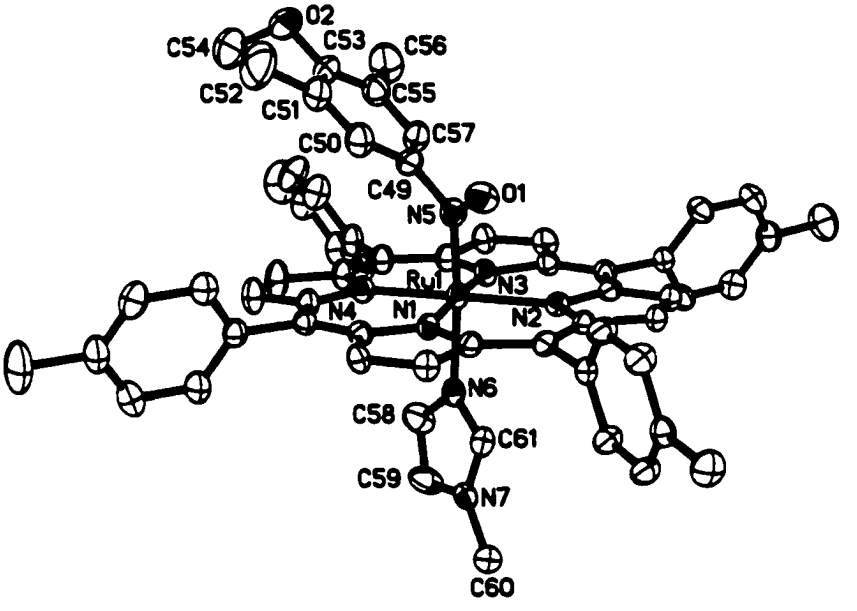

Figure 5.16. Molecular structure of (TTP)Ru(N(O)$C_6H_2(Me)_2$OMe–*p*)(1–MeIm).

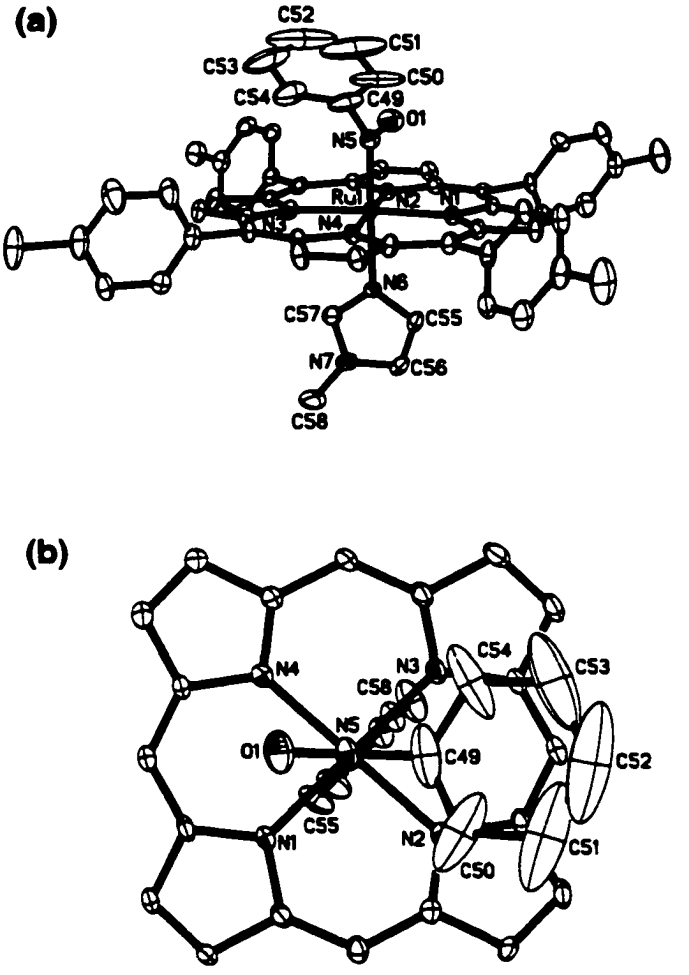

Figure 5.17. (a) Molecular structure of (TTP)Ru(PhNO)(1–MeIm). The carbon atoms (C49–C54) of the phenyl group of the PhNO ligand are disordered and display high thermal parameters. (b) Top view of the porphyrin core, showing the relative orientation between the PhNO and 1–MeIm ligands.

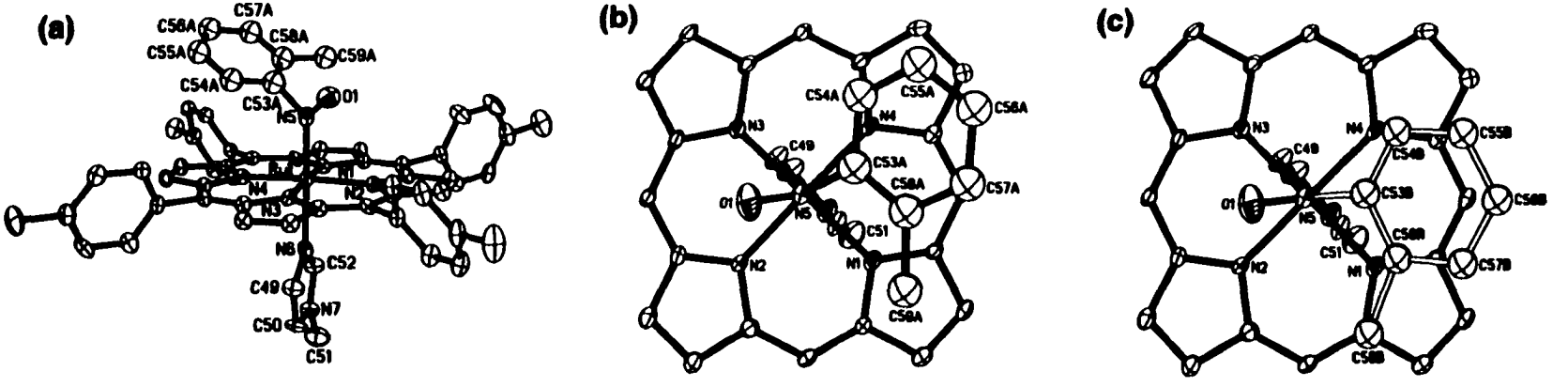

Figure 5.18. Molecular structure of (TTP)Ru(*o*-tolNO)(1-MeIm). (a) View showing only one of the two disordered positions of the nitrosoarene *o*-tolyl ring. (b) Top view of the porphyrin core, showing the relative orentation between the *o*-tolNO and 1-MeIm ligands. (c) Top view of the porphyrin core, showing the relative orientation between the second disordered *o*-tolNO and 1-MeIm ligands.

(a) (TPP)Ru(PhNO)(1-MeIm) (b) (TPP)Ru(*o*-tolNO)(1-MeIm) (c) (TTP)Ru(N(O)$C_6H_2(Me)_2OMe$-*p*)(1-MeIm)

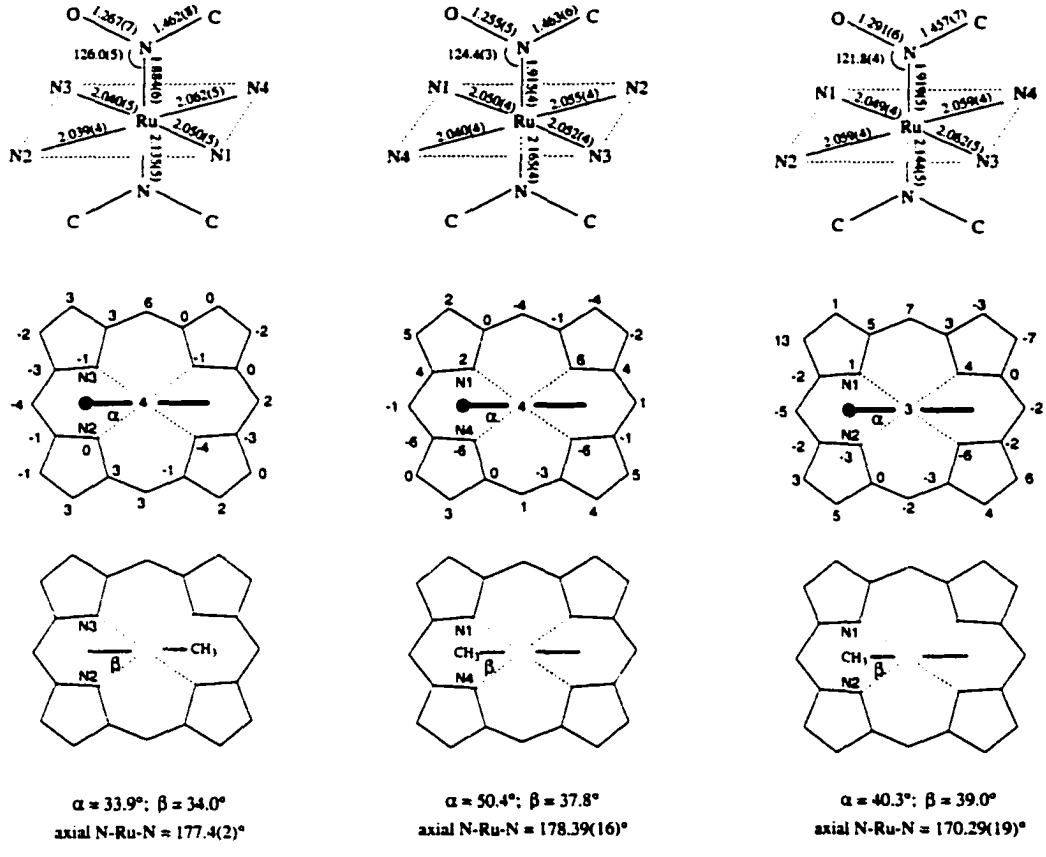

Figure 5.19. Structural data for (por)Ru(ArNO)(1–MeIm) (por = TPP, TTP). Selected bond lengths and angles are shown at the top. Perpendicular atom displacements from the 24–atom porphyrin plane (in 0.01 Å units) are shown at the middle. Also shown are the orientations between ArNO and 1–MeIm at the middle and the bottom: α and β are torsion angles involving O–N–Ru–N(por) (for ArNO) and C–N–Ru–N(por) (for 1–MeIm), respectively. The solid dot represents the nitroso oxygen atom, the solid line represents the O–N–C unit of the ArNO ligand situated above the porphyrin plane, and dashed line represents C–N–C unit of the 1–MeIm ligand situated below the porphyrin plane.

1.255(5)–1.291(6) Å, respectively. Two (por)Ru(ArNO)(1–MeIm) complexes, namely (TPP)Ru(PhNO)(1–MeIm) (177.4(2)°) and (TPP)Ru(*o*–tolNO)(1–MeIm) (178.39(16)°) show the linearity of the axial N–Ru–N bond, whereas the molecular structure of (TTP)Ru(N(O)$C_6H_2(Me)_2$OMe–*p*)(1–MeIm) reveals the axial N–Ru–N bond angle of 170.29(19)°.

Perpendicular atom displacements of the atoms in the porphyrin skeleton from the 24–atom mean porphyrin plane are shown in the middle of Figure 5.19. As with the pyridine–containing nitrosoarene complexes, the porphyrin macrocycle of (TPP)Ru-(PhNO)(1–MeIm) exhibits a *ruffled* distortion. The (TPP)Ru(*o*–tolNO)(1–MeIm) and (TTP)Ru(N(O)$C_6H_2(Me)_2$OMe–*p*)(1–MeIm) complexes are also distorted from the porphyrin plane, however, their distortions are not clearly determined as one of the four main types of distortions (i.e., *saddle, ruffle, dome, wave*) which are generally found in porphyrins and metalloporphyrins. The displacements of the Ru atoms from the 24–atom mean porphyrin plane are very similar to those observed for the (por)Ru(PhNO)(py) complexes. The axial ligand orientations in three (por)Ru(ArNO)(1–MeIm) complexes are also shown in Figure 5.19. Interestingly, and unlike in the cases of (por)Ru$(ArNO)_2$ and (por)Ru(PhNO)(py), the ArNO and 1–MeIm ligands in three (por)Ru(ArNO)(1–MeIm) complexes are oriented parallel to each other, and their C–NO (for ArNO) and C–N–C (for 1–MeIm) groups essentially bisect porphyrin nitrogens.

The molecular structures of two (por)Ru(ArNO)(1–MeIm) complexes containing the disordered arene rings of the nitrosoarene ligands, namely (TTP)Ru(PhNO)(1–MeIm) and (TTP)Ru(*o*–tolNO)(1–MeIm), were also obtained and are shown in Figures 5.17 and 5.18. In the case of (TTP)Ru(PhNO)(1–MeIm), the disordered phenyl ring is indicated by its high thermal motion. The Ru–N(por) distances of these two mono–nitrosoarene complexes are in the 2.030(5) Å to 2.058(5) Å range. Their Ru–N(ArNO) and N–O distances are 1.884(5) Å and 1.251(6) Å for (TTP)Ru(PhNO)(1–MeIm), and 1.871(7) Å and 1.285(8) Å for (TTP)Ru(*o*–tolNO)(1–MeIm), respectively. These values are similar

to those seen for the other mono–nitrosoarene complexes described in this chapter.

*3. **Discussion.*** There are several notes of interest regarding the molecular structures of the eight bis– and mono–nitrosoarene crystallographically ordered complexes (Figures 5.10, 5.13, and 5.19). For example, the axial Ru–N(ArNO) bond lengths (1.953(2)–2.049(2) Å) in the bis–nitrosoarene complexes are slightly longer than the related axial Ru–N(ArNO) distances of 1.892(3)–1.905(5) Å (for pyridine complexes) and 1.884(6)–1.919(5) Å (for 1–MeIm complexes) seen in the mono–nitrosoarene complexes, and this observation is suggestive of *decreased* Ru–N(O)Ar back–bonding in (por)Ru(ArNO)$_2$ relative to those in (por)Ru(PhNO)(py) and (por)Ru(ArNO)(1–MeIm). This view is consistent with the IR and ^{1}H NMR spectroscopic results discussed in the previous section. Although the IR and ^{1}H NMR spectra reveal the evidence that the 1–MeIm ligand in the mono–nitrosoarene complexes shows a slightly stronger electron–donating ability than the pyridine ligand, there are no significant differences of the axial Ru–N(ArNO) distances within the mono–nitrosoarene complexes containing the pyridine or 1–MeIm ligand in the solid state. The O–N(Ar) bond lengths are not significantly different within these bis– and mono–nitrosoarene complexes.

The axial N–Ru–N bond angles seen for these bis– and mono–nitrosoarene complexes are also somewhat intriguing, since the largest deviations from the strict linearity are observed for the very bulky (2,6–dimethyl–4–nitrosoanisole)–containing complexes (i.e., (TTP)Ru(N(O)C$_6$H$_2$(Me)$_2$OMe–*p*)$_2$ (167.34(8)°) and (TTP)Ru(N(O)-C$_6$H$_2$(Me)$_2$OMe–*p*)(1–MeIm) (170.29(19)°). Thus, this implies that the deviations from the linearity could be (at least partly) determined by sterics. Furthermore, the porphyrin ring distortions observed for these bis– and mono–nitrosoarene complexes of ruthenium porphyrins provide an interesting comparison with those observed by Oldfield and coworkers for the related (TPP)Fe(ArNO)–containing complexes. Prior to this work, Oldfield and coworkers examined the structural data for sixteen Group 8 (Fe, Ru, Os) metalloporphyrin complexes, and concluded that the porphyrin ring distortion is closely

related to the porphyrin ring substituent and the axial ligand.[10,38,49] They proposed that the porphyrin ring distortions due to the differences of the axial ligands occur when the porphyrin complex contains only one bulky ("*distorting*") ligand such as PhNO, NODMA, and 1–MeIm which interacts with a bulky ring substituent such as phenyl. In addition, they suggested that the presence of the bulky two axial ligands causes a net overall zero distortion. Indeed, they observed that the porphyrin macrocycles of the pyridine–containing nitrosoarene complexes, namely (TPP)Fe(PhNO)(py) and (TPP)Fe(N(O)$C_6H_4NMe_2$–*p*)(py), are much more distorted from ideal planarity relative to the 1–MeIm–containing nitrosoarene complexes (i.e., (TPP)Fe(PhNO)(1–MeIm) and (OEP)Fe(PhNO)(1–MeIm)).[10] In the cases of (por)Ru(ArNO)–containing complexes, however, the largest porphyrin ring distortion is seen for (TTP)Ru(*o*–tolNO)$_2$. Furthermore, the extent of the porphyrin ring distortion seen for (TTP)Ru(N(O)C_6H_2-$(Me)_2$OMe–*p*)$_2$ containing two very bulky 2,6–dimethyl–4–nitrosoanisole ligands is slightly greater than that seen for (TTP)Ru(PhNO)(py) containing only one bulky axial PhNO ligand. Indeed, our results observed for the (por)Ru(ArNO)–containing complexes suggest that for the (por)Ru(ArNO)–containing complexes, the sterics are not closely related to the porphyrin ring distortion (although it has an effect on the axial N–Ru–N linearity).

The most chemically interesting features of the structures of these (por)Ru-(ArNO)–containing complexes are the axial ligand orientations. Indeed, the examination of the axial ligand orientations in heme model complexes is of importance, due partly to the fact that the axial ligand orientations are affected by the electronic structure of the metal center (e.g., low–spin Fe(II), low–spin Fe(III)), and the properties of the axial ligands in heme model complexes (e.g., π–donor, π–acceptor) could be predicted from the axial ligand orientations. For example, our research group previously reported the single–crystal X–ray structure of the (TPP)Fe(PhNO)$_2$ complex containing two axial π–acidic PhNO ligands, and proposed that the presence of two axial π–acid ligands

results in the perpendicular orientation of the axial ligands, and that this maximizes the π–back bonding from the HOMOs of the low–spin (TPP)Fe(II) fragment (namely the filled d_{xz} and d_{yz} orbitals) into the empty π* orbitals of the axial PhNO ligands.[9] Our group has observed similar perpendicular axial ArNO ligand orientations in (por)Os-$(ArNO)_2$ complexes.[13] Scheidt and coworkers also reported that the molecular structure of the low–spin ferrous $[(T_{piv}PP)Fe(NO_2)(NO)]^-$ complex containing two axial π–acid ligands shows the perpendicular orientation of the axial ligands.[50] Furthermore, they observed that the molecular structures of two low–spin ferric complexes, namely $[(T_{piv}PP)Fe(NO_2)(py)]$ and $[(T_{piv}PP)Fe(NO_2)(HIm)]$ (HIm = imidazole), show the perpendicular orientations of the axial ligands, and proposed on the basis of these results that both pyridine and imidazole ligands would behave as π–donors in these low–spin Fe(III) complexes containing an axial π–acidic nitrite ligand.[51] Thus, they suggested that the perpendicular orientations of the axial ligands in these ferric complexes are capable of maximizing π–acceptor interaction between the π–acidic nitrite and the filled d_π orbital of Fe(III), and π–donor interaction between the pyridine (or imidazole) ligand and the half–filled d_π orbital of Fe(III). Indeed, and as expected, the ArNO ligands in (por)Ru-$(ArNO)_2$ are oriented perpendicular to each other, indicating that the ArNO ligands act as π–acids in these complexes.

The axial ligand orientations observed for the solid–state structures of the (por)Ru(PhNO)(py) and (por)Ru(ArNO)(1–MeIm) complexes provide an interesting comparison with those seen for (por)Ru$(ArNO)_2$. As with the bis–nitrosoarene complexes, *the PhNO and pyridine ligands in (por)Ru(PhNO)(py) are oriented perpendicular to each other.* Interestingly, however, *the ArNO and 1–MeIm ligands in (por)Ru(ArNO)(1–MeIm) are nearly parallel to each other.* These axial ligand orientations observed for (por)Ru(PhNO)(py) and (por)Ru(ArNO)(1–MeIm) suggest that the pyridine ligand could behave as a π–acid, whereas the 1–MeIm ligand could act as a π–donor in these mono–nitrosoarene complexes of ruthenium porphyrins. Indeed, the

parallel orientations seen for (por)Ru(ArNO)(1–MeIm) might be expected to maximize the π–back bonding from one of two filled d_π orbitals of Ru(II) into the empty π* orbital of ArNO ligand.

Conclusion

In summary, a series of the (por)Ru(ArNO)$_2$ complexes have been prepared, and one ArNO ligand in these bis–nitrosoarene complexes is readily substituted by pyridine or 1–MeIm to give the corresponding (por)Ru(ArNO)L compounds (L = pyridine or 1–MeIm). These nitrosoarene complexes have been characterized by infrared and ^{1}H NMR spectroscopy, and by mass spectrometry. The assignment of the υ_{NO} of the coordinated ArNO groups in the IR spectra (as KBr pellets) was confirmed by the analyses of the IR sepctra of the ^{15}N–labeled analogs. The IR spectral data (KBr) reveal that the υ_{NO}s in these bis– and mono–nitrosoarene complexes decrease in the order (por)Ru(ArNO)$_2$ > (por)Ru(PhNO)(py) > (por)Ru(ArNO)(1–MeIm). The ^{1}H NMR spectral data (in $CDCl_3$) also show that the $\delta_{pyrrole}$ protons of these bis– and mono–nitrosoarene complexes decrease slightly in the order (por)Ru(ArNO)$_2$ > (por)Ru(PhNO)(py) > (por)Ru(ArNO)-(1–MeIm). These IR and ^{1}H NMR spectroscopic results indicate that the coordination of pyridine or 1–MeIm increases the electron–density of the porphyrin macrocycles in the mono–nitrosoarene complexes. Eleven of these bis– and mono–nitrosoarene complexes have also been characterized by X–ray crystallography. All the molecular structures reveal the *N*–binding of ArNO ligands to the formally Ru(II) porphyrins independent of ArNO and porphyrin macrocycles. Importantly, the axial ligand orientations observed in the mono–nitrosoarene complexes containing the axial pyridine or 1–MeIm ligand suggest that the pyridine ligand could behave as a π–acid, whereas the 1–MeIm ligand could act as a π–donor in these mono–nitrosoarene complexes. This is somewhat intriguing, largely due to the fact that a number of metalloporphyrin complexes containing the axial pyridine ligand, in addition to the imidazole complexes,

have been synthesized as the model of heme containing the axial histidine, although an imidazole is more suitable as the model of a histidine. Hence, the observation that the pyridine and 1–MeIm ligands exhibit the different properties in the mono–nitrosoarene complexes indicates that caution is needed in choosing the pyridine complex as the model of the adduct of the organic *C*–nitroso compounds with heme containing the axial histidine.

References

(1) Mansuy, D.; Chottard, J. C.; Chottard, G. *Eur. J. Biochem.* **1977**, *76*, 617-623.

(2) Gibson, Q. H. *Biochem. J.* **1960**, *77*, 519-526.

(3) Fukuto, J. M.; Brady, J. F.; Burstyn, J. N.; VanAtta, R. B.; Valentine, J. S.; Cho, A. K. *Biochemistry* **1986**, *25*, 2714-2719.

(4) Stone, J. R.; Marletta, M. A. *Biochemistry* **1995**, *34*, 16397-16403.

(5) Murayama, M. *J. Biol. Chem.* **1960**, *235*, 1024-1028.

(6) Vainshtein, B. K.; Harutyunyan, E. H.; Kuranova, I. P.; Borisov, V. V.; Sosfenov, N. I.; Pavlovsky, A. G.; Grebenko, A. I.; Konareva, N. V. *Protein Data Bank* **1982**, *Structure 1LH7 and 2LH7*.

(7) Lee, J.; Chen, L.; West, A. H.; Richter-Addo, G. B. *Chem. Rev.* **2002**, *102*, 1019-1065.

(8) Mansuy, D.; Battioni, P.; Chottard, J.-C.; Riche, C.; Chiaroni, A. *J. Am. Chem. Soc.* **1983**, *105*, 455-463.

(9) Wang, L.-S.; Chen, L.; Khan, M. A.; Richter-Addo, G. B. *Chem. Commun.* **1996**, 323-324.

(10) Godbout, N.; Sanders, L. K.; Salzmann, R.; Havlin, R. H.; Wojdelski, M.; Oldfield, E. *J. Am. Chem. Soc.* **1999**, *121*, 3829-3844.

(11) Fox, S. J.; Chen, L.; Khan, M. A.; Richter-Addo, G. B. *Inorg. Chem.* **1997**, *36*, 6465-6467.

(12) Chen, L.; Fox, J. B., Jr.; Yi, G.-B.; Khan, M. A.; Richter-Addo, G. B. *J. Porph. Phthalocyanines* **2001**, *5*, 702-707.

(13) Chen, L.; Khan, M. A.; Richter-Addo, G. B.; Young, V. G., Jr.; Powell, D. R. *Inorg. Chem.* **1998**, *37*, 4689-4696.

(14) Rillema, D. P.; Nagle, J. K.; Barringer, L. F., Jr.; Meyer, T. J. *J. Am. Chem. Soc.* **1981**, *103*, 56-62.

(15) Bosch, E.; Kochi, J. K. *J. Org. Chem.* **1994**, *59*, 5573-5586.

(16) Connelly, N. G.; Draggett, P. T.; Green, M.; Kuc, T. A. *J. Chem. Soc., Dalton Trans.* **1977**, 70-73.

(17) Crotti, C.; Sishta, C.; Pacheco, A.; James, B. R. *Inorg. Chim. Acta* **1988**, *141*, 13-15.

(18) Data for (OEP)Os(PhNO)(1–MeIm). ^{1}H NMR ($CDCl_3$): δ 9.18 (s, 4H, *meso*–H of OEP), 6.17 (br tt,1H, *p*–H of PhNO), 5.74 (m, 2H, *m*–H of PhNO), 4.61 (dd (apparent t), J = 1.2/1.2, 1H of 1–MeIm), 3.75 (m, 16H, CH_2CH_3 of OEP), 2.99 (m, 2H, *o*–H of PhNO), 2.08 (s, 3H, CH_3 of 1–MeIm), 1.75 (t, J = 8, 24H, CH_2CH_3 of OEP), 1.33 (br, 1H of 1–MeIm), 1.05 (dd (apparent t), J = 1.2/1.2, 1H of 1–MeIm).

(19) Richter-Addo, G. B.; Legzdins, P. *Metal Nitrosyls*; Oxford University Press: New York, 1992. p64-65, and references therein.

(20) Buchler, J. W.; Kokisch, W.; Smith, P. D. *Struct. Bonding* **1978**, *34*, 79-134.

(21) Eaton, S. S.; Eaton, G. R. *J. Am. Chem. Soc.* **1977**, *99*, 6594-6599.

(22) Eaton, S. S.; Eaton, G. R. *J. Am. Chem. Soc.* **1975**, *97*, 3660-3666.

(23) Yi, G.-B.; Khan, M. A.; Richter-Addo, G. B. *Inorg. Chem.* **1996**, *35*, 3453-3454.

(24) Miranda, K. M.; Bu, X.; Lorkovic, I.; Ford, P. C. *Inorg. Chem.* **1997**, *36*, 4838-4848.

(25) Bohle, D. S.; Hung, C.-H.; Powell, A. K.; Smith, B. D.; Wocadlo, S. *Inorg. Chem.* **1997**, *36*, 1992-1993.

(26) Hodge, S. J.; Wang, L.-S.; Khan, M. A.; Young, V. G., Jr.; Richter-Addo, G. B. *Chem. Commun.* **1996**, 2283-2284.

(27) Yi, G.-B.; Khan, M. A.; Powell, D. R.; Richter-Addo, G. B. *Inorg. Chem.* **1998**, *37*, 208-214.

(28) Yi, G.-B.; Khan, M. A.; Richter-Addo, G. B. *Chem. Commun.* **1996**, 2045-2046.

(29) Yi, G.-B.; Chen, L.; Khan, M. A.; Richter-Addo, G. B. *Inorg. Chem.* **1997**, *36*, 3876-3885.

(30) Bonnet, J. J.; Eaton, S. S.; Eaton, G. R.; Holm, R. H.; Ibers, J. A. *J. Am. Chem. Soc.* **1973**, *95*, 2141-2149.

(31) Kadish, K. M.; Hu, Y.; Mu, X. H. *J. Heterocycl. Chem.* **1991**, *28*, 1821-1824.

(32) Little, R. G.; Ibers, J. A. *J. Am. Chem. Soc.* **1973**, *95*, 8583-8590.

(33) Groves, J. T.; Han, Y.; Van_engen, D. *J. Chem. Soc., Chem. Commun.* **1990**, 436-437.

(34) Birnbaum, E. R.; Schaefer, W. P.; Labinger, J. A.; Bercaw, J. E.; Gray, H. B. *Inorg. Chem.* **1995**, *34*, 1751-1755.

(35) Le Maux, P.; Bahri, H.; Simonneaux, G.; Toupet, L. *Inorg. Chem.* **1995**, *34*, 4691-4697.

(36) Morice, C.; Le Maux, P.; Simonneaux, G.; Toupet, L. *J. Chem. Soc., Dalton Trans.* **1998**, 4165-4171.

(37) Slebodnick, C.; Seok, W. K.; Kim, K.; Ibers, J. A. *Inorg. Chim. Acta* **1996**, *243*, 57-65.

(38) Salzmann, R.; Ziegler, C. J.; Godbout, N.; McMahon, M. T.; Suslick, K. S.; Oldfield, E. *J. Am. Chem. Soc.* **1998**, *120*, 11323-11334.

(39) Camenzind, M. J.; James, B. R.; Dolphin, D.; Sparapany, J. W.; Ibers, J. A. *Inorg. Chem.* **1988**, *27*, 3054-3057.

(40) Galardon, E.; Le Maux, P.; Toupet, L.; Simonneaux, G. *Organometallics* **1998**, *17*, 565-569.

(41) Bailey, A. J.; James, B. R. *Chem. Commun.* **1996**, 2343-2344 and p2505 (1997, Erratum).

(42) Hopf, F. R.; O'Brein, T. P.; Scheidt, W. R.; Whitten, D. G. *J. Am. Chem. Soc.* **1975**, *97*, 277-281.

(43) Ariel, S.; Dolphin, D.; Domazetis, G.; James, B. R.; Leung, T. W.; Rettig, S. J.; Trotter, J.; Williams, G. M. *Can. J. Chem.* **1984**, *62*, 755-762.

(44) Ball, R. G.; Domazetis, G.; Dolphin, D.; James, B. R.; Trotter, J. *Inorg. Chem.* **1981**, *20*, 1556-1562.

(45) Lee, F.-W.; Choi, M.-Y.; Cheung, K.-K.; Che, C.-M. *J. Organomet. Chem.* **2000**, *595*, 114-125.

(46) James, B. R.; Pacheco, A.; Rettig, S. J.; Ibers, J. A. *Inorg. Chem.* **1988**, *27*, 2414-2421.

(47) Richter-Addo, G. B.; Wheeler, R. A.; Hixon, C. A.; Chen, L.; Khan, M. A.; Ellison, M. K.; Schulz, C. E.; Scheidt, W. R. *J. Am. Chem. Soc.* **2001**, *123*, 6314-6326.

(48) Fomitchev, D. V.; Coppens, P.; Li, T.; Bagley, K. A.; Chen, L.; Richter-Addo, G. B. *Chem. Commun.* **1999**, 2013-2014.

(49) Salzmann, R.; McMahon, M. T.; Godbout, N.; Sanders, L. K.; Wojdelski, M.; Oldfield, E. *J. Am. Chem. Soc.* **1999**, *121*, 3818-3828.

(50) Nasri, H.; Ellison, M. K.; Chen, S.; Huynh, B. H.; Scheidt, W. R. *J. Am. Chem. Soc.* **1997**, *119*, 6274-6283.

(51) Nasri, H.; Wang, Y.; Huynh, B. H.; Walker, F. A.; Scheidt, W. R. *Inorg. Chem.* **1991**, *30*, 1483-1489.

Chapter 6. Epilogue

The general research goal described in this dissertation was to investigate the reactions of organic *S*–nitroso and *C*–nitroso compounds with group 8 metalloporphyrins. Importantly, some reports have suggested that organic *S*–nitroso and *C*–nitroso compounds are capable of interacting directly with the metal center in heme–containing biomolecules such as hemoglobin,[1] myoglobin,[2] cytochrome P450,[3] and guanylyl cyclase.[4] For example, it has been suggested that RSNO may be able to bind directly to the heme site of guanylyl cyclase (GC). In addition, various amine–containing drugs can be metabolized by cytochrome P450 to result in the formation of *C*–nitroso compounds that subsequently bind to the heme.

Due to this possibility of direct interactions of *S*–nitroso and *C*–nitroso compounds with heme, our research group has investigated the interactions of these nitroso compounds with metalloporphyrins. We have shown that RSNO compounds can be activated by metalloporphyrins,[5-12] whereas ArNO compounds can directly bind to metalloporphyrins.[12-17] These results have also led us to investigate which factors are really involved in the activation or binding of nitroso compounds by metalloporphyrins.

My Ph.D. work with RSNO compounds has shown that additions of RSNO to (OEP)Os(CO) are not significantly affected by nature of R group (i.e., 1°, 2°, and 3° alkyl).[10] This suggests that the activation of RSNO by metalloporphyrins does not depend on the alkyl substituent in RSNO compounds. Interestingly, it has been known that RSNO compounds are decomposed by some trace metals such as Cu^{+}, Fe^{2+}, Hg^{2+}, and Ag^{+} in solution, whereas Zn^{2+}, Ca^{2+}, Mg^{2+}, and Fe^{3+} do not catalyze the decomposition of RSNO compounds.[18-20] Hence, our future work could be focused on determining whether the oxidation state of metal (and the kind of metal) in metalloporphyrins affect the activation of RSNO. This study might also provide some insight on the possible successful synthesis of the adducts of RSNO with

metalloporphyrins.

Together with our group's previous work with nitrosoarene compounds (some of which have a dipolar resonance contribution),[13-16] my Ph.D. work also suggests that the nature of binding (N–bound vs O–bound) of the ArNO compounds to metalloporphyrins depends on the formal oxidation state of metal (i.e., electron–density around metal center) rather than the ArNO dipolar resonance contribution. This poses additional questions that need to be addressed. For example, *(i)* how will nitrosoarenes bind to d^6 metalloporphyrins containing very electron–withdrawing porphyrins such as 5,10,15,20–tetrakis(heptafluoropropyl)porphyrin (THFP), *(ii)* can spectroelectrochemistry detect transient species during electron–transfer reactions involving ArNO. In addition, determining whether the bound ArNO ligands can be activated in the metalloporphyrin–dependent chemistry also needs to be pursued. Indeed, the several examples of the C–N bond cleavage and resultant metal–NO formation have been known for some transition metal complexes containing *C*–nitroso ligands.[21,22]

Importantly, my Ph.D. work has laid the "inorganic" foundation for our research group's biochemistry projects (in collaboration with Dr. Ann West's laboratory) with the heme biomolecules such as myoglobin, cytochrome P450, and their interactions with *S*–nitroso and *C*–nitroso compounds.

References

(1) Gibson, Q. H. *Biochem. J.* **1960**, *77*, 519-526.

(2) Mansuy, D.; Chottard, J. C.; Chottard, G. *Eur. J. Biochem.* **1977**, *76*, 617-623.

(3) Fukuto, J. M.; Brady, J. F.; Burstyn, J. N.; VanAtta, R. B.; Valentine, J. S.; Cho, A. K. *Biochemistry* **1986**, *25*, 2714-2719.

(4) Stone, J. R.; Marletta, M. A. *Biochemistry* **1995**, *34*, 16397-16403.

(5) Yi, G.-B.; Khan, M. A.; Richter-Addo, G. B. *Chem. Commun.* **1996**, 2045-2046.

(6) Yi, G.-B.; Chen, L.; Khan, M. A.; Richter-Addo, G. B. *Inorg. Chem.* **1997**, *36*, 3876-3885.

(7) Chen, L.; Khan, M. A.; Richter-Addo, G. B. *Inorg. Chem.* **1998**, *37*, 533-540.

(8) Yi, G.-B.; Khan, M. A.; Powell, D. R.; Richter-Addo, G. B. *Inorg. Chem.* **1998**, *37*, 208-214.

(9) Lee, J.; Yi, G.-B.; Khan, M. A.; Richter-Addo, G. B. *Inorg. Chem.* **1999**, *38*, 4578-4584.

(10) Lee, J.; Yi, G.-B.; Powell, D. R.; Khan, M. A.; Richter-Addo, G. B. *Can. J. Chem.* **2001**, *79*, 830-840.

(11) Andreasen, L. V.; Lorkovic, I. M.; Richter-Addo, G. B.; Ford, P. C. *Nitric Oxide: Biol. Chem.* **2002**, *6*, 228-235.

(12) Richter-Addo, G. B. *Acc. Chem. Res.* **1999**, *32*, 529-536.

(13) Wang, L.-S.; Chen, L.; Khan, M. A.; Richter-Addo, G. B. *Chem. Commun.* **1996**, 323-324.

(14) Fox, S. J.; Chen, L.; Khan, M. A.; Richter-Addo, G. B. *Inorg. Chem.* **1997**, *36*, 6465-6467.

(15) Chen, L.; Khan, M. A.; Richter-Addo, G. B.; Young, V. G., Jr.; Powell, D. R. *Inorg. Chem.* **1998**, *37*, 4689-4696.

(16) Chen, L.; Fox, J. B., Jr.; Yi, G.-B.; Khan, M. A.; Richter-Addo, G. B. *J. Porph. Phthalocyanines* **2001**, *5*, 702-707.

(17) Lee, J.; Twamley, B.; Richter-Addo, G. B. *Can. J. Chem.* **2001**, In press.

(18) Williams, D. L. H. *Acc. Chem. Res.* **1999**, *32*, 869-876.

(19) McAninly, J.; Williams, D. L. H.; Askew, S. C.; Butler, A. R.; Russell, C. *J. Chem. Soc., Chem. Commun.* **1993**, 1758-1759.

(20) Askew, S. C.; Barnett, D. J.; McAninly, J.; Williams, D. L. H. *J. Chem. Soc., Perkin Trans. 2* **1995**, 741-745.

(21) Goldhaber, A.; Vollhardt, K. P. C.; Walborsky, E. C.; Wolfgruber, M. *J. Am. Chem. Soc.* **1986**, *108*, 516-518.

(22) Becker, P. N.; Bergman, R. G. *J. Am. Chem. Soc.* **1983**, *105*, 2985-2995.

Appendix. Tables 5.1–5.22 of Chapter 5

Table 5.1. Selected Bond lengths (Å) for (TPP)Ru(PhNO)$_2$

Ru(1)-N(5)	1.953(2)	C(5)-C(6)	1.443(4)
Ru(1)-N(1)	2.047(2)	C(6)-C(7)	1.403(4)
Ru(1)-N(6)	2.049(2)	C(7)-C(8)	1.399(4)
Ru(1)-N(4)	2.050(2)	C(8)-C(9)	1.441(4)
Ru(1)-N(2)	2.053(2)	C(9)-C(10)	1.350(4)
Ru(1)-N(3)	2.060(2)	C(10)-C(11)	1.449(3)
N(1)-C(1)	1.373(3)	C(11)-C(12)	1.407(3)
N(1)-C(18)	1.384(3)	C(12)-C(13)	1.406(4)
N(2)-C(3)	1.377(3)	C(13)-C(14)	1.451(3)
N(2)-C(6)	1.378(3)	C(14)-C(15)	1.340(4)
N(3)-C(8)	1.379(3)	C(15)-C(16)	1.447(4)
N(3)-C(11)	1.382(3)	C(16)-C(17)	1.402(4)
N(4)-C(13)	1.376(3)	C(17)-C(18)	1.388(4)
N(4)-C(16)	1.383(3)	C(18)-C(19)	1.443(4)
N(5)-O(1)	1.243(3)	C(19)-C(20)	1.354(4)
N(5)-C(45)	1.468(3)	C(45)-C(46)	1.363(4)
N(6)-O(2)	1.248(3)	C(45)-C(50)	1.367(4)
N(6)-C(51)	1.452(3)	C(46)-C(47)	1.396(5)
C(1)-C(2)	1.404(4)	C(47)-C(48)	1.354(6)
C(1)-C(20)	1.443(4)	C(48)-C(49)	1.357(6)
C(2)-C(3)	1.402(4)	C(49)-C(50)	1.398(5)
C(3)-C(4)	1.445(4)	C(51)-C(52)	1.375(4)
C(4)-C(5)	1.346(4)	C(51)-C(56)	1.400(4)

C(52)-C(53)	1.388(4)	C(54)-C(55)	1.385(5)
C(53)-C(54)	1.374(5)	C(55)-C(56)	1.381(4)

Table 5.2. Selected Bond angles (°) for (TPP)Ru(PhNO)$_2$

N(5)-Ru(1)-N(1)	88.69(9)		
N(5)-Ru(1)-N(6)	171.67(9)	C(3)-N(2)-Ru(1)	126.35(17)
N(1)-Ru(1)-N(6)	83.00(9)	C(6)-N(2)-Ru(1)	126.85(18)
N(5)-Ru(1)-N(4)	87.24(8)	C(8)-N(3)-C(11)	107.1(2)
N(1)-Ru(1)-N(4)	90.46(8)	C(8)-N(3)-Ru(1)	126.22(18)
N(6)-Ru(1)-N(4)	92.28(9)	C(11)-N(3)-Ru(1)	126.06(16)
N(5)-Ru(1)-N(2)	93.00(9)	C(13)-N(4)-C(16)	107.2(2)
N(1)-Ru(1)-N(2)	89.99(8)	C(13)-N(4)-Ru(1)	126.75(17)
N(6)-Ru(1)-N(2)	87.54(8)	C(16)-N(4)-Ru(1)	125.85(17)
N(4)-Ru(1)-N(2)	179.50(9)	O(1)-N(5)-C(45)	112.3(2)
N(5)-Ru(1)-N(3)	90.65(9)	O(1)-N(5)-Ru(1)	123.46(17)
N(1)-Ru(1)-N(3)	179.29(9)	C(45)-N(5)-Ru(1)	124.22(18)
N(6)-Ru(1)-N(3)	97.66(9)	O(2)-N(6)-C(51)	113.1(2)
N(4)-Ru(1)-N(3)	89.79(8)	O(2)-N(6)-Ru(1)	117.40(17)
N(2)-Ru(1)-N(3)	89.77(8)	C(51)-N(6)-Ru(1)	128.09(19)
C(1)-N(1)-C(18)	107.4(2)	N(1)-C(1)-C(2)	126.1(2)
C(1)-N(1)-Ru(1)	126.45(17)	N(1)-C(1)-C(20)	109.1(2)
C(18)-N(1)-Ru(1)	125.99(18)	C(2)-C(1)-C(20)	124.8(2)
C(3)-N(2)-C(6)	106.7(2)	C(3)-C(2)-C(1)	125.1(2)

N(2)-C(3)-C(2)	125.9(2)	N(4)-C(16)-C(15)	108.5(2)
N(2)-C(3)-C(4)	109.2(2)	C(17)-C(16)-C(15)	125.6(2)
C(2)-C(3)-C(4)	125.0(2)	C(18)-C(17)-C(16)	125.8(2)
C(5)-C(4)-C(3)	107.4(2)	N(1)-C(18)-C(17)	126.0(2)
C(4)-C(5)-C(6)	107.5(2)	N(1)-C(18)-C(19)	108.4(2)
N(2)-C(6)-C(7)	125.4(2)	C(17)-C(18)-C(19)	125.5(2)
N(2)-C(6)-C(5)	109.2(2)	C(20)-C(19)-C(18)	107.8(2)
C(7)-C(6)-C(5)	125.3(2)	C(19)-C(20)-C(1)	107.3(2)
C(8)-C(7)-C(6)	125.6(2)	C(46)-C(45)-C(50)	120.9(3)
N(3)-C(8)-C(7)	125.9(2)	C(46)-C(45)-N(5)	119.2(3)
N(3)-C(8)-C(9)	109.3(2)	C(50)-C(45)-N(5)	119.8(3)
C(7)-C(8)-C(9)	124.8(2)	C(45)-C(46)-C(47)	118.8(4)
C(10)-C(9)-C(8)	107.3(2)	C(48)-C(47)-C(46)	120.8(4)
C(9)-C(10)-C(11)	107.8(2)	C(47)-C(48)-C(49)	120.1(4)
N(3)-C(11)-C(12)	126.2(2)	C(48)-C(49)-C(50)	120.1(4)
N(3)-C(11)-C(10)	108.5(2)	C(45)-C(50)-C(49)	119.3(3)
C(12)-C(11)-C(10)	125.3(2)	C(52)-C(51)-C(56)	120.9(3)
C(13)-C(12)-C(11)	124.8(2)	C(52)-C(51)-N(6)	120.1(2)
N(4)-C(13)-C(12)	126.1(2)	C(56)-C(51)-N(6)	119.0(3)
N(4)-C(13)-C(14)	108.8(2)	C(51)-C(52)-C(53)	119.2(3)
C(12)-C(13)-C(14)	125.1(2)	C(54)-C(53)-C(52)	120.6(3)
C(15)-C(14)-C(13)	107.4(2)	C(53)-C(54)-C(55)	119.9(3)
C(14)-C(15)-C(16)	108.0(2)	C(56)-C(55)-C(54)	120.5(3)
N(4)-C(16)-C(17)	125.9(2)	C(55)-C(56)-C(51)	118.9(3)

Table 5.3. Selected Bond lengths (Å) for (TTP)Ru(*o*–tolNO)$_2$

Ru(1)-N(5)	1.967(3)	C(6)-C(7)	1.396(5)
Ru(1)-N(6)	2.029(3)	C(7)-C(8)	1.389(5)
Ru(1)-N(4)	2.041(3)	C(8)-C(9)	1.442(5)
Ru(1)-N(3)	2.042(3)	C(9)-C(10)	1.352(5)
Ru(1)-N(2)	2.044(3)	C(10)-C(11)	1.440(5)
Ru(1)-N(1)	2.055(3)	C(11)-C(12)	1.400(5)
N(1)-C(1)	1.375(4)	C(12)-C(13)	1.402(5)
N(1)-C(18)	1.380(4)	C(13)-C(14)	1.445(5)
N(2)-C(3)	1.382(4)	C(14)-C(15)	1.352(5)
N(2)-C(6)	1.383(4)	C(15)-C(16)	1.434(5)
N(3)-C(11)	1.375(4)	C(16)-C(17)	1.402(5)
N(3)-C(8)	1.380(4)	C(17)-C(18)	1.407(5)
N(4)-C(16)	1.377(4)	C(18)-C(19)	1.438(5)
N(4)-C(13)	1.382(4)	C(19)-C(20)	1.355(5)
N(5)-O(1)	1.251(4)	C(49)-C(50)	1.386(5)
N(5)-C(49)	1.469(5)	C(49)-C(54)	1.391(5)
N(6)-O(2)	1.247(4)	C(50)-C(51)	1.374(6)
N(6)-C(56)	1.455(5)	C(51)-C(52)	1.385(6)
C(1)-C(2)	1.412(5)	C(52)-C(53)	1.370(6)
C(1)-C(20)	1.435(5)	C(53)-C(54)	1.393(6)
C(2)-C(3)	1.397(5)	C(54)-C(55)	1.507(5)
C(3)-C(4)	1.451(5)	C(56)-C(57)	1.386(5)
C(4)-C(5)	1.347(5)	C(56)-C(61)	1.399(5)
C(5)-C(6)	1.438(5)	C(57)-C(58)	1.395(6)

C(58)-C(59)	1.366(7)	C(60)-C(61)	1.390(6)
C(59)-C(60)	1.361(7)	C(61)-C(62)	1.514(6)

Table 5.4. Selected Bond angles (°) for (TTP)Ru(*o*–tolNO)$_2$

N(5)-Ru(1)-N(6)	171.31(12)	C(3)-N(2)-Ru(1)	126.9(2)
N(5)-Ru(1)-N(4)	88.66(12)	C(6)-N(2)-Ru(1)	126.2(2)
N(6)-Ru(1)-N(4)	91.37(12)	C(11)-N(3)-C(8)	107.1(3)
N(5)-Ru(1)-N(3)	87.83(12)	C(11)-N(3)-Ru(1)	127.0(2)
N(6)-Ru(1)-N(3)	83.47(11)	C(8)-N(3)-Ru(1)	125.8(2)
N(4)-Ru(1)-N(3)	89.78(11)	C(16)-N(4)-C(13)	107.0(3)
N(5)-Ru(1)-N(2)	91.94(12)	C(16)-N(4)-Ru(1)	126.5(2)
N(6)-Ru(1)-N(2)	88.04(12)	C(13)-N(4)-Ru(1)	126.5(2)
N(4)-Ru(1)-N(2)	179.40(12)	O(1)-N(5)-C(49)	112.5(3)
N(3)-Ru(1)-N(2)	90.31(11)	O(1)-N(5)-Ru(1)	123.0(2)
N(5)-Ru(1)-N(1)	92.62(12)	C(49)-N(5)-Ru(1)	124.3(2)
N(6)-Ru(1)-N(1)	96.07(11)	O(2)-N(6)-C(56)	112.6(3)
N(4)-Ru(1)-N(1)	90.17(11)	O(2)-N(6)-Ru(1)	120.9(2)
N(3)-Ru(1)-N(1)	179.54(12)	C(56)-N(6)-Ru(1)	124.4(2)
N(2)-Ru(1)-N(1)	89.74(11)	N(1)-C(1)-C(2)	125.9(3)
C(1)-N(1)-C(18)	106.9(3)	N(1)-C(1)-C(20)	109.5(3)
C(1)-N(1)-Ru(1)	126.6(2)	C(2)-C(1)-C(20)	124.6(3)
C(18)-N(1)-Ru(1)	126.0(2)	C(3)-C(2)-C(1)	124.8(3)
C(3)-N(2)-C(6)	106.8(3)	N(2)-C(3)-C(2)	126.0(3)

N(2)-C(3)-C(4)	108.8(3)	N(1)-C(18)-C(17)	125.6(3)
C(2)-C(3)-C(4)	125.2(3)	N(1)-C(18)-C(19)	108.9(3)
C(5)-C(4)-C(3)	107.4(3)	C(17)-C(18)-C(19)	125.5(3)
C(4)-C(5)-C(6)	107.8(3)	C(20)-C(19)-C(18)	107.6(3)
N(2)-C(6)-C(7)	125.5(3)	C(19)-C(20)-C(1)	107.1(3)
N(2)-C(6)-C(5)	109.2(3)	C(50)-C(49)-C(54)	121.7(4)
C(7)-C(6)-C(5)	125.3(3)	C(50)-C(49)-N(5)	118.2(3)
C(8)-C(7)-C(6)	125.6(3)	C(54)-C(49)-N(5)	120.1(3)
N(3)-C(8)-C(7)	126.3(3)	C(51)-C(50)-C(49)	119.6(4)
N(3)-C(8)-C(9)	108.6(3)	C(50)-C(51)-C(52)	119.5(4)
C(7)-C(8)-C(9)	125.0(3)	C(53)-C(52)-C(51)	120.6(4)
C(10)-C(9)-C(8)	107.8(3)	C(52)-C(53)-C(54)	121.2(4)
C(9)-C(10)-C(11)	107.1(3)	C(49)-C(54)-C(53)	117.3(4)
N(3)-C(11)-C(12)	125.7(3)	C(49)-C(54)-C(55)	122.2(4)
N(3)-C(11)-C(10)	109.3(3)	C(53)-C(54)-C(55)	120.5(4)
C(12)-C(11)-C(10)	124.9(3)	C(57)-C(56)-C(61)	122.2(4)
C(11)-C(12)-C(13)	124.8(3)	C(57)-C(56)-N(6)	117.3(4)
N(4)-C(13)-C(12)	125.9(3)	C(61)-C(56)-N(6)	120.4(3)
N(4)-C(13)-C(14)	109.0(3)	C(56)-C(57)-C(58)	118.6(4)
C(12)-C(13)-C(14)	125.1(3)	C(59)-C(58)-C(57)	119.5(4)
C(15)-C(14)-C(13)	106.8(3)	C(60)-C(59)-C(58)	121.4(5)
C(14)-C(15)-C(16)	108.2(3)	C(59)-C(60)-C(61)	121.6(5)
N(4)-C(16)-C(17)	125.9(3)	C(60)-C(61)-C(56)	116.6(4)
N(4)-C(16)-C(15)	108.9(3)	C(60)-C(61)-C(62)	119.4(4)
C(17)-C(16)-C(15)	125.2(3)	C(56)-C(61)-C(62)	123.9(4)
C(16)-C(17)-C(18)	125.2(3)		

Table 5.5. Selected Bond lengths (Å) for (TTP)Ru(N(O)$C_6H_2(Me)_2OMe$–*p*)$_2$

Ru(1)-N(5)	1.990(2)	C(2)-C(3)	1.399(3)
Ru(1)-N(6)	2.024(2)	C(3)-C(4)	1.445(4)
Ru(1)-N(1)	2.0437(19)	C(4)-C(5)	1.345(4)
Ru(1)-N(2)	2.048(2)	C(5)-C(6)	1.445(4)
Ru(1)-N(4)	2.049(2)	C(6)-C(7)	1.401(4)
Ru(1)-N(3)	2.060(2)	C(7)-C(8)	1.396(4)
N(1)-C(18)	1.376(3)	C(8)-C(9)	1.443(4)
N(1)-C(1)	1.377(3)	C(9)-C(10)	1.347(4)
N(2)-C(3)	1.377(3)	C(10)-C(11)	1.434(3)
N(2)-C(6)	1.378(3)	C(11)-C(12)	1.400(3)
N(3)-C(11)	1.376(3)	C(12)-C(13)	1.404(3)
N(3)-C(8)	1.384(3)	C(13)-C(14)	1.440(3)
N(4)-C(16)	1.379(3)	C(14)-C(15)	1.351(4)
N(4)-C(13)	1.380(3)	C(15)-C(16)	1.436(4)
N(5)-O(1)	1.252(3)	C(16)-C(17)	1.400(4)
N(5)-C(49)	1.450(3)	C(17)-C(18)	1.392(3)
N(6)-O(2)	1.252(2)	C(18)-C(19)	1.451(3)
N(6)-C(58)	1.442(3)	C(19)-C(20)	1.343(4)
O(3)-C(53)	1.390(3)	C(49)-C(57)	1.383(4)
O(3)-C(54)	1.433(4)	C(49)-C(50)	1.395(4)
O(4)-C(62)	1.384(3)	C(50)-C(51)	1.381(4)
O(4)-C(63)	1.436(4)	C(51)-C(53)	1.401(4)
C(1)-C(2)	1.399(3)	C(51)-C(52)	1.518(4)
C(1)-C(20)	1.442(3)	C(53)-C(55)	1.384(4)

C(55)-C(57)	1.396(4)	C(60)-C(62)	1.398(4)
C(55)-C(56)	1.506(4)	C(60)-C(61)	1.517(4)
C(58)-C(66)	1.382(4)	C(62)-C(64)	1.399(4)
C(58)-C(59)	1.393(4)	C(64)-C(66)	1.391(4)
C(59)-C(60)	1.381(4)	C(64)-C(65)	1.511(4)

Table 5.6. Selected Bond angles (°) for (TTP)Ru(N(O)$C_6H_2(Me)_2$OMe–*p*)$_2$

N(5)-Ru(1)-N(6)	167.34(8)	C(18)-N(1)-C(1)	107.70(19)
N(5)-Ru(1)-N(1)	84.32(8)	C(18)-N(1)-Ru(1)	126.03(16)
N(6)-Ru(1)-N(1)	83.03(8)	C(1)-N(1)-Ru(1)	126.27(16)
N(5)-Ru(1)-N(2)	87.07(8)	C(3)-N(2)-C(6)	107.1(2)
N(6)-Ru(1)-N(2)	93.55(8)	C(3)-N(2)-Ru(1)	125.84(16)
N(1)-Ru(1)-N(2)	90.40(8)	C(6)-N(2)-Ru(1)	126.70(17)
N(5)-Ru(1)-N(4)	92.69(8)	C(11)-N(3)-C(8)	107.3(2)
N(6)-Ru(1)-N(4)	86.84(8)	C(11)-N(3)-Ru(1)	126.54(16)
N(1)-Ru(1)-N(4)	90.33(8)	C(8)-N(3)-Ru(1)	125.81(17)
N(2)-Ru(1)-N(4)	179.21(8)	C(16)-N(4)-C(13)	106.8(2)
N(5)-Ru(1)-N(3)	95.90(8)	C(16)-N(4)-Ru(1)	126.07(17)
N(6)-Ru(1)-N(3)	96.74(8)	C(13)-N(4)-Ru(1)	126.85(16)
N(1)-Ru(1)-N(3)	179.77(9)	O(1)-N(5)-C(49)	112.1(2)
N(2)-Ru(1)-N(3)	89.61(8)	O(1)-N(5)-Ru(1)	119.08(16)
N(4)-Ru(1)-N(3)	89.66(8)	C(49)-N(5)-Ru(1)	127.87(17)

O(2)-N(6)-C(58)	112.6(2)	C(12)-C(11)-C(10)	124.9(2)
O(2)-N(6)-Ru(1)	117.33(16)	C(11)-C(12)-C(13)	125.5(2)
C(58)-N(6)-Ru(1)	128.23(16)	N(4)-C(13)-C(12)	125.5(2)
C(53)-O(3)-C(54)	113.4(3)	N(4)-C(13)-C(14)	109.1(2)
C(62)-O(4)-C(63)	110.6(2)	C(12)-C(13)-C(14)	125.4(2)
N(1)-C(1)-C(2)	125.9(2)	C(15)-C(14)-C(13)	107.4(2)
N(1)-C(1)-C(20)	108.8(2)	C(14)-C(15)-C(16)	107.6(2)
C(2)-C(1)-C(20)	125.4(2)	N(4)-C(16)-C(17)	125.7(2)
C(1)-C(2)-C(3)	125.3(2)	N(4)-C(16)-C(15)	109.2(2)
N(2)-C(3)-C(2)	126.2(2)	C(17)-C(16)-C(15)	125.1(2)
N(2)-C(3)-C(4)	108.7(2)	C(18)-C(17)-C(16)	125.5(2)
C(2)-C(3)-C(4)	124.9(2)	N(1)-C(18)-C(17)	126.3(2)
C(5)-C(4)-C(3)	107.8(2)	N(1)-C(18)-C(19)	108.1(2)
C(4)-C(5)-C(6)	107.3(2)	C(17)-C(18)-C(19)	125.6(2)
N(2)-C(6)-C(7)	125.8(2)	C(20)-C(19)-C(18)	107.9(2)
N(2)-C(6)-C(5)	109.0(2)	C(19)-C(20)-C(1)	107.5(2)
C(7)-C(6)-C(5)	125.1(2)	C(57)-C(49)-C(50)	121.1(2)
C(8)-C(7)-C(6)	125.2(2)	C(57)-C(49)-N(5)	119.7(2)
N(3)-C(8)-C(7)	126.1(2)	C(50)-C(49)-N(5)	119.1(2)
N(3)-C(8)-C(9)	108.4(2)	C(51)-C(50)-C(49)	120.2(3)
C(7)-C(8)-C(9)	125.5(2)	C(50)-C(51)-C(53)	117.8(3)
C(10)-C(9)-C(8)	107.6(2)	C(50)-C(51)-C(52)	121.0(3)
C(9)-C(10)-C(11)	107.8(2)	C(53)-C(51)-C(52)	121.1(3)
N(3)-C(11)-C(12)	125.8(2)	C(55)-C(53)-O(3)	118.9(3)
N(3)-C(11)-C(10)	109.0(2)	C(55)-C(53)-C(51)	122.6(3)

O(3)-C(53)-C(51)	118.3(3)	C(59)-C(60)-C(61)	121.3(3)
C(53)-C(55)-C(57)	118.4(3)	C(62)-C(60)-C(61)	121.1(3)
C(53)-C(55)-C(56)	121.5(3)	O(4)-C(62)-C(60)	118.4(3)
C(57)-C(55)-C(56)	120.0(3)	O(4)-C(62)-C(64)	119.0(3)
C(49)-C(57)-C(55)	119.6(3)	C(60)-C(62)-C(64)	122.6(3)
C(66)-C(58)-C(59)	121.0(3)	C(66)-C(64)-C(62)	118.2(3)
C(66)-C(58)-N(6)	120.0(2)	C(66)-C(64)-C(65)	121.3(3)
C(59)-C(58)-N(6)	119.0(2)	C(62)-C(64)-C(65)	120.5(3)
C(60)-C(59)-C(58)	120.7(3)	C(58)-C(66)-C(64)	119.9(3)
C(59)-C(60)-C(62)	117.6(3)		

Table 5.7. Selected Bond lengths (Å) for (TPP)Ru(*o*–tolNO)$_2$

Ru(1)-N(3)	1.994(4)	C(9)-C(10)	1.400(3)
Ru(1)-N(3)#1	1.994(4)	C(10)-C(1)#1	1.399(3)
Ru(1)-N(3A)#1	2.040(3)	N(3)-O(1)	1.221(5)
Ru(1)-N(3A)	2.040(3)	N(3)-C(23)	1.467(5)
Ru(1)-N(2)	2.042(2)	C(23)-C(28)	1.327(6)
Ru(1)-N(2)#1	2.042(2)	C(23)-C(24)	1.411(5)
Ru(1)-N(1)#1	2.042(2)	C(24)-C(25)	1.386(6)
Ru(1)-N(1)	2.042(2)	C(24)-C(29)	1.542(7)
N(1)-C(1)	1.357(4)	C(25)-C(26)	1.383(7)
N(1)-C(4)	1.379(3)	C(26)-C(27)	1.383(7)
N(2)-C(9)	1.367(3)	C(27)-C(28)	1.365(6)
N(2)-C(6)	1.381(3)	N(3A)-O(1A)	1.285(5)
C(1)-C(10)#1	1.399(3)	N(3A)-C(23A)	1.460(4)
C(1)-C(2)	1.441(3)	C(23A)-C(28A)	1.348(7)
C(2)-C(3)	1.339(4)	C(23A)-C(24A)	1.395(6)
C(3)-C(4)	1.438(4)	C(24A)-C(25A)	1.368(7)
C(4)-C(5)	1.390(4)	C(24A)-C(29A)	1.501(8)
C(5)-C(6)	1.378(4)	C(25A)-C(26A)	1.366(9)
C(6)-C(7)	1.428(4)	C(26A)-C(27A)	1.388(8)
C(7)-C(8)	1.341(4)	C(27A)-C(28A)	1.355(7)
C(8)-C(9)	1.439(3)		

Symmetry transformations used to generate equivalent atoms:

#1 -x+1,-y+1,-z+1

Table 5.8. Selected Bond angles (°) for (TPP)Ru(*o*–tolNO)$_2$

N(3)-Ru(1)-N(3)#1	180.0(3)	N(3A)-Ru(1)-N(1)	95.79(11)
N(3)-Ru(1)-N(3A)#1	160.28(11)	N(2)-Ru(1)-N(1)	90.01(8)
N(3)#1-Ru(1)-N(3A)#1	19.72(11)	N(2)#1-Ru(1)-N(1)	89.99(8)
N(3)-Ru(1)-N(3A)	19.72(11)	N(1)#1-Ru(1)-N(1)	180.000(1)
N(3)#1-Ru(1)-N(3A)	160.28(11)	C(1)-N(1)-C(4)	107.3(2)
N(3A)#1-Ru(1)N(3A)	180.000(1)	C(1)-N(1)-Ru(1)	126.42(14)
N(3)-Ru(1)-N(2)	97.50(12)	C(4)-N(1)-Ru(1)	126.09(19)
N(3)#1-Ru(1)-N(2)	82.50(12)	C(9)-N(2)-C(6)	107.2(2)
N(3A)#1-Ru(1)-N(2)	100.68(12)	C(9)-N(2)-Ru(1)	126.15(15)
N(3A)-Ru(1)-N(2)	79.32(12)	C(6)-N(2)-Ru(1)	126.30(19)
N(3)-Ru(1)-N(2)#1	82.50(12)	N(1)-C(1)-C(10)#1	126.2(2)
N(3)#1-Ru(1)-N(2)#1	97.50(12)	N(1)-C(1)-C(2)	109.5(2)
N(3A)#1-Ru(1)-N(2)#1	79.32(12)	C(10)#1-C(1)-C(2)	124.3(3)
N(3A)-Ru(1)-N(2)#1	100.68(12)	C(3)-C(2)-C(1)	106.8(2)
N(2)-Ru(1)-N(2)#1	180.000(1)	C(2)-C(3)-C(4)	108.2(2)
N(3)-Ru(1)-N(1)#1	91.75(12)	N(1)-C(4)-C(5)	125.8(2)
N(3)#1-Ru(1)-N(1)#1	88.25(12)	N(1)-C(4)-C(3)	108.1(2)
N(3A)#1-Ru(1)-N(1)#1	95.79(11)	C(5)-C(4)-C(3)	126.0(2)
N(3A)-Ru(1)-N(1)#1	84.21(11)	C(6)-C(5)-C(4)	126.0(2)
N(2)-Ru(1)-N(1)#1	89.99(8)	C(5)-C(6)-N(2)	125.7(3)
N(2)#1-Ru(1)-N(1)#1	90.01(8)	C(5)-C(6)-C(7)	125.6(2)
N(3)-Ru(1)-N(1)	88.25(12)	N(2)-C(6)-C(7)	108.6(2)
N(3)#1-Ru(1)-N(1)	91.75(12)	C(8)-C(7)-C(6)	107.9(2)
N(3A)#1-Ru(1)-N(1)	84.21(11)	C(7)-C(8)-C(9)	107.5(3)

N(2)-C(9)-C(10)	126.1(2)	C(28)-C(27)-C(26)	121.9(5)
N(2)-C(9)-C(8)	108.8(2)	C(23)-C(28)-C(27)	118.9(4)
C(10)-C(9)-C(8)	125.1(3)	O(1A)-N(3A)-C(23A)	111.1(3)
C(1)#1-C(10)-C(9)	124.8(3)	O(1A)-N(3A)-Ru(1)	123.4(2)
O(1)-N(3)-C(23)	115.1(3)	C(23A)-N(3A)-Ru(1)	123.6(3)
O(1)-N(3)-Ru(1)	122.0(2)	C(28A)-C(23A)-C(24A)	123.3(4)
C(23)-N(3)-Ru(1)	122.2(3)	C(28A)-C(23A)-N(3A)	114.9(4)
C(28)-C(23)-C(24)	123.7(3)	C(24A)-C(23A)-N(3A)	121.8(4)
C(28)-C(23)-N(3)	122.0(3)	C(25A)-C(24A)-C(23A)	115.9(5)
C(24)-C(23)-N(3)	114.1(4)	C(25A)-C(24A)-C(29A)	116.9(4)
C(25)-C(24)-C(23)	115.2(4)	C(23A)-C(24A)-C(29A)	127.2(4)
C(25)-C(24)-C(29)	120.2(4)	C(26A)-C(25A)-C(24A)	122.5(5)
C(23)-C(24)-C(29)	124.6(3)	C(25A)-C(26A)-C(27A)	118.6(5)
C(26)-C(25)-C(24)	122.8(5)	C(28A)-C(27A)-C(26A)	120.7(6)
C(25)-C(26)-C(27)	117.4(4)	C(23A)-C(28A)-C(27A)	118.8(5)

Symmetry transformations used to generate equivalent atoms:

#1 -x+1,-y+1,-z+1

Table 5.9. Selected Bond lengths (Å) for (TPP)Ru(PhNO)(py)

Ru(1)-N(5)	1.892(3)	C(6)-C(7)	1.396(5)
Ru(1)-N(3)	2.034(3)	C(7)-C(8)	1.395(5)
Ru(1)-N(2)	2.044(3)	C(8)-C(9)	1.436(5)
Ru(1)-N(4)	2.050(3)	C(9)-C(10)	1.354(5)
Ru(1)-N(1)	2.055(3)	C(10)-C(11)	1.443(5)
Ru(1)-N(6)	2.174(3)	C(11)-C(12)	1.407(5)
O(1)-N(5)	1.259(3)	C(12)-C(13)	1.399(5)
N(1)-C(1)	1.380(4)	C(13)-C(14)	1.443(5)
N(1)-C(18)	1.383(4)	C(14)-C(15)	1.342(5)
N(2)-C(3)	1.380(4)	C(15)-C(16)	1.443(5)
N(2)-C(6)	1.381(4)	C(16)-C(17)	1.405(5)
N(3)-C(11)	1.378(4)	C(17)-C(18)	1.400(5)
N(3)-C(8)	1.379(4)	C(18)-C(19)	1.450(5)
N(4)-C(13)	1.376(4)	C(19)-C(20)	1.340(5)
N(4)-C(16)	1.379(4)	C(45)-C(46)	1.371(5)
N(5)-C(45)	1.475(4)	C(45)-C(50)	1.380(5)
N(6)-C(55)	1.335(5)	C(46)-C(47)	1.388(5)
N(6)-C(51)	1.335(5)	C(47)-C(48)	1.378(6)
C(1)-C(2)	1.407(5)	C(48)-C(49)	1.363(6)
C(1)-C(20)	1.443(5)	C(49)-C(50)	1.387(5)
C(2)-C(3)	1.400(5)	C(51)-C(52)	1.383(5)
C(3)-C(4)	1.438(5)	C(52)-C(53)	1.371(6)
C(4)-C(5)	1.354(5)	C(53)-C(54)	1.378(6)
C(5)-C(6)	1.431(5)	C(54)-C(55)	1.371(6)

Table 5.10. Selected Bond angles (°) for (TPP)Ru(PhNO)(py)

N(5)-Ru(1)-N(3)	88.55(12)	C(13)-N(4)-C(16)	106.9(3)
N(5)-Ru(1)-N(2)	89.50(12)	C(13)-N(4)-Ru(1)	125.5(2)
N(3)-Ru(1)-N(2)	89.79(11)	C(16)-N(4)-Ru(1)	127.4(2)
N(5)-Ru(1)-N(4)	93.34(12)	O(1)-N(5)-C(45)	112.3(3)
N(3)-Ru(1)-N(4)	90.55(11)	O(1)-N(5)-Ru(1)	125.7(2)
N(2)-Ru(1)-N(4)	177.15(12)	C(45)-N(5)-Ru(1)	122.1(2)
N(5)-Ru(1)-N(1)	94.35(11)	C(55)-N(6)-C(51)	116.2(3)
N(3)-Ru(1)-N(1)	177.10(11)	C(55)-N(6)-Ru(1)	120.9(3)
N(2)-Ru(1)-N(1)	90.04(11)	C(51)-N(6)-Ru(1)	122.8(3)
N(4)-Ru(1)-N(1)	89.48(11)	N(1)-C(1)-C(2)	125.1(3)
N(5)-Ru(1)-N(6)	177.07(12)	N(1)-C(1)-C(20)	109.4(3)
N(3)-Ru(1)-N(6)	88.65(11)	C(2)-C(1)-C(20)	125.5(3)
N(2)-Ru(1)-N(6)	89.64(11)	C(3)-C(2)-C(1)	125.4(3)
N(4)-Ru(1)-N(6)	87.54(11)	N(2)-C(3)-C(2)	126.2(3)
N(1)-Ru(1)-N(6)	88.45(11)	N(2)-C(3)-C(4)	108.9(3)
C(1)-N(1)-C(18)	106.7(3)	C(2)-C(3)-C(4)	124.8(3)
C(1)-N(1)-Ru(1)	126.7(2)	C(5)-C(4)-C(3)	107.5(3)
C(18)-N(1)-Ru(1)	126.5(2)	C(4)-C(5)-C(6)	107.6(3)
C(3)-N(2)-C(6)	106.9(3)	N(2)-C(6)-C(7)	125.2(3)
C(3)-N(2)-Ru(1)	126.2(2)	N(2)-C(6)-C(5)	109.1(3)
C(6)-N(2)-Ru(1)	126.8(2)	C(7)-C(6)-C(5)	125.7(3)
C(11)-N(3)-C(8)	106.8(3)	C(8)-C(7)-C(6)	125.6(3)
C(11)-N(3)-Ru(1)	126.1(2)	N(3)-C(8)-C(7)	125.6(3)
C(8)-N(3)-Ru(1)	126.9(2)	N(3)-C(8)-C(9)	109.2(3)

C(7)-C(8)-C(9)	125.2(3)	C(17)-C(16)-C(15)	125.6(3)
C(10)-C(9)-C(8)	107.7(3)	C(18)-C(17)-C(16)	125.2(3)
C(9)-C(10)-C(11)	107.1(3)	N(1)-C(18)-C(17)	126.0(3)
N(3)-C(11)-C(12)	126.1(3)	N(1)-C(18)-C(19)	108.6(3)
N(3)-C(11)-C(10)	109.2(3)	C(17)-C(18)-C(19)	125.4(3)
C(12)-C(11)-C(10)	124.7(3)	C(20)-C(19)-C(18)	107.9(3)
C(13)-C(12)-C(11)	124.7(3)	C(19)-C(20)-C(1)	107.4(3)
N(4)-C(13)-C(12)	126.6(3)	C(46)-C(45)-C(50)	121.3(4)
N(4)-C(13)-C(14)	108.8(3)	C(46)-C(45)-N(5)	118.5(3)
C(12)-C(13)-C(14)	124.5(3)	C(50)-C(45)-N(5)	120.2(3)
C(15)-C(14)-C(13)	107.9(3)	C(45)-C(46)-C(47)	119.0(4)
C(14)-C(15)-C(16)	107.2(3)	C(48)-C(47)-C(46)	120.1(4)
N(4)-C(16)-C(17)	125.2(3)	C(49)-C(48)-C(47)	120.3(4)
N(4)-C(16)-C(15)	109.2(3)	C(48)-C(49)-C(50)	120.4(4)
C(45)-C(50)-C(49)	118.9(4)	C(52)-C(53)-C(54)	118.1(4)
N(6)-C(51)-C(52)	123.5(4)	C(55)-C(54)-C(53)	119.0(4)
C(53)-C(52)-C(51)	119.1(4)	N(6)-C(55)-C(54)	124.0(4)

Table 5.11. Selected Bond lengths (Å) for (TTP)Ru(PhNO)(py)

C(1)-N(1)	1.384(6)	C(17)-C(18)	1.401(8)
C(1)-C(2)	1.397(7)	C(18)-N(1)	1.378(6)
C(1)-C(20)	1.433(7)	C(18)-C(19)	1.446(7)
C(2)-C(3)	1.405(7)	C(19)-C(20)	1.322(7)
C(3)-N(2)	1.383(7)	O(1)-N(5)	1.271(6)
C(3)-C(4)	1.436(7)	C(50)-C(51)	1.355(8)
C(4)-C(5)	1.348(7)	C(50)-C(55)	1.372(8)
C(5)-C(6)	1.447(8)	C(50)-N(5)	1.466(7)
C(6)-N(2)	1.374(7)	C(51)-C(52)	1.389(9)
C(6)-C(7)	1.400(7)	C(52)-C(53)	1.378(9)
C(7)-C(8)	1.393(8)	C(53)-C(54)	1.384(9)
C(8)-N(3)	1.371(6)	C(54)-C(55)	1.380(8)
C(8)-C(9)	1.439(7)	C(56)-N(6)	1.323(7)
C(9)-C(10)	1.347(7)	C(56)-C(57)	1.386(9)
C(10)-C(11)	1.445(7)	C(57)-C(58)	1.367(9)
C(11)-N(3)	1.380(7)	C(58)-C(59)	1.370(9)
C(11)-C(12)	1.392(8)	C(59)-C(60)	1.382(8)
C(12)-C(13)	1.420(7)	C(60)-N(6)	1.341(7)
C(13)-N(4)	1.377(6)	N(1)-Ru(1)	2.042(4)
C(13)-C(14)	1.431(7)	N(2)-Ru(1)	2.047(5)
C(14)-C(15)	1.345(7)	N(3)-Ru(1)	2.049(4)
C(15)-C(16)	1.454(8)	N(4)-Ru(1)	2.052(5)
C(16)-N(4)	1.382(6)	N(5)-Ru(1)	1.905(5)
C(16)-C(17)	1.410(7)	N(6)-Ru(1)	2.158(5)

Table 5.12. Selected Bond angles (°) for (TTP)Ru(PhNO)(py)

N(1)-C(1)-C(2)	124.8(5)	C(12)-C(13)-C(14)	125.4(5)
N(1)-C(1)-C(20)	108.9(5)	C(15)-C(14)-C(13)	107.8(5)
C(2)-C(1)-C(20)	126.2(5)	C(14)-C(15)-C(16)	106.8(5)
C(1)-C(2)-C(3)	126.3(5)	N(4)-C(16)-C(17)	125.3(5)
N(2)-C(3)-C(2)	125.3(5)	N(4)-C(16)-C(15)	109.4(5)
N(2)-C(3)-C(4)	108.9(5)	C(17)-C(16)-C(15)	125.2(5)
C(2)-C(3)-C(4)	125.8(5)	C(18)-C(17)-C(16)	124.5(5)
C(5)-C(4)-C(3)	107.6(5)	N(1)-C(18)-C(17)	126.8(5)
C(4)-C(5)-C(6)	107.5(5)	N(1)-C(18)-C(19)	108.3(5)
N(2)-C(6)-C(7)	125.9(5)	C(17)-C(18)-C(19)	124.9(5)
N(2)-C(6)-C(5)	108.7(5)	C(20)-C(19)-C(18)	108.2(5)
C(7)-C(6)-C(5)	125.4(5)	C(19)-C(20)-C(1)	108.0(5)
C(8)-C(7)-C(6)	125.2(5)	C(51)-C(50)-C(55)	121.6(6)
N(3)-C(8)-C(7)	125.8(5)	C(51)-C(50)-N(5)	119.1(6)
N(3)-C(8)-C(9)	109.2(5)	C(55)-C(50)-N(5)	119.2(6)
C(7)-C(8)-C(9)	125.0(5)	C(50)-C(51)-C(52)	119.8(6)
C(10)-C(9)-C(8)	107.6(5)	C(53)-C(52)-C(51)	119.3(6)
C(9)-C(10)-C(11)	107.4(5)	C(52)-C(53)-C(54)	120.3(7)
N(3)-C(11)-C(12)	126.8(5)	C(55)-C(54)-C(53)	119.7(7)
N(3)-C(11)-C(10)	108.8(5)	C(50)-C(55)-C(54)	119.2(6)
C(12)-C(11)-C(10)	124.4(5)	N(6)-C(56)-C(57)	125.0(6)
C(11)-C(12)-C(13)	125.5(5)	C(58)-C(57)-C(56)	117.7(7)
N(4)-C(13)-C(12)	124.5(5)	C(59)-C(58)-C(57)	119.6(7)
N(4)-C(13)-C(14)	110.1(5)	C(58)-C(59)-C(60)	118.0(7)

N(6)-C(60)-C(59)	124.3(6)	C(56)-N(6)-Ru(1)	122.3(4)
C(18)-N(1)-C(1)	106.6(4)	C(60)-N(6)-Ru(1)	122.3(4)
C(18)-N(1)-Ru(1)	126.4(4)	N(5)-Ru(1)-N(1)	98.3(2)
C(1)-N(1)-Ru(1)	126.9(4)	N(5)-Ru(1)-N(2)	90.2(2)
C(6)-N(2)-C(3)	107.2(5)	N(1)-Ru(1)-N(2)	90.27(17)
C(6)-N(2)-Ru(1)	126.6(4)	N(5)-Ru(1)-N(3)	85.6(2)
C(3)-N(2)-Ru(1)	126.3(4)	N(1)-Ru(1)-N(3)	176.1(2)
C(8)-N(3)-C(11)	107.1(4)	N(2)-Ru(1)-N(3)	89.58(17)
C(8)-N(3)-Ru(1)	126.4(4)	N(5)-Ru(1)-N(4)	91.9(2)
C(11)-N(3)-Ru(1)	125.2(4)	N(1)-Ru(1)-N(4)	89.77(17)
C(13)-N(4)-C(16)	105.9(5)	N(2)-Ru(1)-N(4)	177.9(2)
C(13)-N(4)-Ru(1)	127.0(4)	N(3)-Ru(1)-N(4)	90.24(17)
C(16)-N(4)-Ru(1)	127.1(4)	N(5)-Ru(1)-N(6)	174.7(2)
O(1)-N(5)-C(50)	111.1(5)	N(1)-Ru(1)-N(6)	86.95(19)
O(1)-N(5)-Ru(1)	123.5(4)	N(2)-Ru(1)-N(6)	90.01(18)
C(50)-N(5)-Ru(1)	123.2(4)	N(3)-Ru(1)-N(6)	89.18(19)
C(56)-N(6)-C(60)	115.4(6)	N(4)-Ru(1)-N(6)	87.86(18)

Table 5.13. Selected Bond lengths (Å) for (TPP)Ru(PhNO)(1–MeIm)

Ru(1)-N(5)	1.884(6)	C(2)-C(3)	1.413(8)
Ru(1)-N(2)	2.039(4)	C(3)-C(4)	1.429(8)
Ru(1)-N(3)	2.040(5)	C(4)-C(5)	1.364(9)
Ru(1)-N(1)	2.050(5)	C(5)-C(6)	1.444(8)
Ru(1)-N(4)	2.062(5)	C(6)-C(7)	1.399(8)
Ru(1)-N(6)	2.135(5)	C(7)-C(8)	1.408(8)
O(1)-N(5)	1.267(7)	C(8)-C(9)	1.449(8)
N(1)-C(1)	1.372(7)	C(9)-C(10)	1.364(9)
N(1)-C(18)	1.371(7)	C(10)-C(11)	1.434(8)
N(2)-C(3)	1.372(7)	C(11)-C(12)	1.390(8)
N(2)-C(6)	1.377(7)	C(12)-C(13)	1.388(8)
N(3)-C(8)	1.368(7)	C(13)-C(14)	1.447(8)
N(3)-C(11)	1.387(7)	C(14)-C(15)	1.347(8)
N(4)-C(16)	1.357(7)	C(15)-C(16)	1.444(7)
N(4)-C(13)	1.384(7)	C(16)-C(17)	1.423(8)
N(5)-C(45)	1.462(8)	C(17)-C(18)	1.407(7)
N(6)-C(54)	1.329(7)	C(18)-C(19)	1.437(7)
N(6)-C(51)	1.370(7)	C(19)-C(20)	1.346(8)
N(7)-C(54)	1.332(8)	C(45)-C(46)	1.368(9)
N(7)-C(52)	1.373(8)	C(45)-C(50)	1.388(8)
N(7)-C(53)	1.450(8)	C(46)-C(47)	1.381(9)
C(1)-C(2)	1.413(8)	C(47)-C(48)	1.382(10)
C(1)-C(20)	1.434(8)	C(48)-C(49)	1.371(10)

C(49)-C(50)	1.399(10)	C(51)-C(52)	1.337(9)

Table 5.14. Selected Bond angles (°) for (TPP)Ru(PhNO)(1–MeIm)

N(5)-Ru(1)-N(2)	90.4(2)	C(6)-N(2)-Ru(1)	127.3(4)
N(5)-Ru(1)-N(3)	89.5(2)	C(8)-N(3)-C(11)	107.3(5)
N(2)-Ru(1)-N(3)	89.60(18)	C(8)-N(3)-Ru(1)	126.7(4)
N(5)-Ru(1)-N(1)	94.2(2)	C(11)-N(3)-Ru(1)	125.9(4)
N(2)-Ru(1)-N(1)	90.60(17)	C(16)-N(4)-C(13)	107.6(5)
N(3)-Ru(1)-N(1)	176.3(2)	C(16)-N(4)-Ru(1)	127.4(4)
N(5)-Ru(1)-N(4)	92.0(2)	C(13)-N(4)-Ru(1)	124.9(4)
N(2)-Ru(1)-N(4)	177.6(2)	O(1)-N(5)-C(45)	111.6(5)
N(3)-Ru(1)-N(4)	90.74(18)	O(1)-N(5)-Ru(1)	126.0(5)
N(1)-Ru(1)-N(4)	88.90(17)	C(45)-N(5)-Ru(1)	122.2(4)
N(5)-Ru(1)-N(6)	177.4(2)	C(54)-N(6)-C(51)	105.1(5)
N(2)-Ru(1)-N(6)	89.79(19)	C(54)-N(6)-Ru(1)	128.0(4)
N(3)-Ru(1)-N(6)	87.90(19)	C(51)-N(6)-Ru(1)	126.7(4)
N(1)-Ru(1)-N(6)	88.37(19)	C(54)-N(7)-C(52)	106.2(5)
N(4)-Ru(1)-N(6)	87.82(18)	C(54)-N(7)-C(53)	127.6(6)
C(1)-N(1)-C(18)	106.7(4)	C(52)-N(7)-C(53)	126.2(6)
C(1)-N(1)-Ru(1)	125.8(4)	N(1)-C(1)-C(2)	125.7(5)
C(18)-N(1)-Ru(1)	127.3(3)	N(1)-C(1)-C(20)	109.6(5)
C(3)-N(2)-C(6)	105.7(5)	C(2)-C(1)-C(20)	124.6(5)
C(3)-N(2)-Ru(1)	127.1(4)	C(1)-C(2)-C(3)	125.9(5)

N(2)-C(3)-C(2)	124.7(5)	C(14)-C(15)-C(16)	106.8(5)
N(2)-C(3)-C(4)	111.2(6)	N(4)-C(16)-C(17)	126.2(5)
C(2)-C(3)-C(4)	124.1(5)	N(4)-C(16)-C(15)	109.7(5)
C(5)-C(4)-C(3)	106.2(5)	C(17)-C(16)-C(15)	124.2(5)
C(4)-C(5)-C(6)	107.2(5)	C(18)-C(17)-C(16)	123.7(5)
N(2)-C(6)-C(7)	125.6(5)	N(1)-C(18)-C(17)	126.3(5)
N(2)-C(6)-C(5)	109.7(5)	N(1)-C(18)-C(19)	109.1(4)
C(7)-C(6)-C(5)	124.7(5)	C(17)-C(18)-C(19)	124.5(5)
C(6)-C(7)-C(8)	124.3(5)	C(20)-C(19)-C(18)	107.6(5)
N(3)-C(8)-C(7)	126.5(5)	C(19)-C(20)-C(1)	107.0(5)
N(3)-C(8)-C(9)	109.6(5)	C(46)-C(45)-C(50)	121.5(6)
C(7)-C(8)-C(9)	123.9(6)	C(46)-C(45)-N(5)	120.3(5)
C(10)-C(9)-C(8)	106.3(6)	C(50)-C(45)-N(5)	118.1(6)
C(9)-C(10)-C(11)	108.2(5)	C(45)-C(46)-C(47)	119.7(6)
N(3)-C(11)-C(12)	125.6(5)	C(48)-C(47)-C(46)	119.9(7)
N(3)-C(11)-C(10)	108.5(5)	C(49)-C(48)-C(47)	120.1(7)
C(12)-C(11)-C(10)	125.9(5)	C(48)-C(49)-C(50)	120.7(7)
C(13)-C(12)-C(11)	126.4(5)	C(45)-C(50)-C(49)	117.9(7)
N(4)-C(13)-C(12)	126.2(5)	C(52)-C(51)-N(6)	109.6(6)
N(4)-C(13)-C(14)	107.9(5)	C(51)-C(52)-N(7)	107.3(6)
C(12)-C(13)-C(14)	125.9(5)	N(6)-C(54)-N(7)	111.9(5)
C(15)-C(14)-C(13)	108.1(5)		

Table 5.15. Selected Bond lengths (Å) for (TPP)Ru(*o*–tolNO)(1–MeIm)

Ru(1)-N(7)	1.915(4)	C(2)-C(3)	1.415(7)
Ru(1)-N(4)	2.040(4)	C(3)-C(4)	1.447(6)
Ru(1)-N(1)	2.050(4)	C(4)-C(5)	1.341(7)
Ru(1)-N(3)	2.052(4)	C(5)-C(6)	1.446(7)
Ru(1)-N(2)	2.055(4)	C(6)-C(7)	1.391(7)
Ru(1)-N(5)	2.165(4)	C(7)-C(8)	1.410(7)
N(1)-C(1)	1.365(6)	C(8)-C(9)	1.439(7)
N(1)-C(18)	1.373(6)	C(9)-C(10)	1.347(7)
N(2)-C(3)	1.361(6)	C(10)-C(11)	1.439(7)
N(2)-C(6)	1.388(6)	C(11)-C(12)	1.410(7)
N(3)-C(11)	1.376(6)	C(12)-C(13)	1.402(7)
N(3)-C(8)	1.379(6)	C(13)-C(14)	1.446(7)
N(4)-C(16)	1.375(6)	C(14)-C(15)	1.343(7)
N(4)-C(13)	1.377(6)	C(15)-C(16)	1.441(7)
N(5)-C(55)	1.313(6)	C(16)-C(17)	1.396(7)
N(5)-C(52)	1.356(7)	C(17)-C(18)	1.403(7)
N(6)-C(53)	1.340(7)	C(18)-C(19)	1.428(7)
N(6)-C(55)	1.342(6)	C(19)-C(20)	1.335(7)
N(6)-C(54)	1.468(6)	C(45)-C(46)	1.382(7)
N(7)-O(1)	1.255(5)	C(45)-C(50)	1.398(7)
N(7)-C(45)	1.463(6)	C(46)-C(47)	1.400(8)
C(1)-C(2)	1.388(7)	C(47)-C(48)	1.378(9)
C(1)-C(20)	1.461(7)	C(48)-C(49)	1.367(8)

C(49)-C(50)	1.400(7)	C(52)-C(53)	1.351(7)
C(50)-C(51)	1.492(8)		

Table 5.16. Selected Bond angles (°) for (TPP)Ru(*o*–tolNO)(1–MeIm)

C(46)-C(45)-C(50)	122.5(5)	C(3)-N(2)-C(6)	106.9(4)
N(7)-Ru(1)-N(4)	88.29(15)	C(3)-N(2)-Ru(1)	126.3(3)
N(7)-Ru(1)-N(1)	89.85(15)	C(6)-N(2)-Ru(1)	126.5(3)
N(4)-Ru(1)-N(1)	89.57(15)	C(11)-N(3)-C(8)	106.8(4)
N(7)-Ru(1)-N(3)	93.68(16)	C(11)-N(3)-Ru(1)	126.6(3)
N(4)-Ru(1)-N(3)	90.20(16)	C(8)-N(3)-Ru(1)	126.2(3)
N(1)-Ru(1)-N(3)	176.45(15)	C(16)-N(4)-C(13)	106.9(4)
N(7)-Ru(1)-N(2)	94.01(15)	C(16)-N(4)-Ru(1)	127.0(3)
N(4)-Ru(1)-N(2)	177.68(15)	C(13)-N(4)-Ru(1)	125.7(3)
N(1)-Ru(1)-N(2)	90.18(16)	C(55)-N(5)-C(52)	104.8(4)
N(3)-Ru(1)-N(2)	89.91(15)	C(55)-N(5)-Ru(1)	127.8(3)
N(7)-Ru(1)-N(5)	178.39(16)	C(52)-N(5)-Ru(1)	127.4(4)
N(4)-Ru(1)-N(5)	91.66(15)	C(53)-N(6)-C(55)	107.0(4)
N(1)-Ru(1)-N(5)	88.54(15)	C(53)-N(6)-C(54)	126.1(4)
N(3)-Ru(1)-N(5)	87.92(15)	C(55)-N(6)-C(54)	126.8(5)
N(2)-Ru(1)-N(5)	86.03(15)	O(1)-N(7)-C(45)	112.3(4)
C(1)-N(1)-C(18)	107.5(4)	O(1)-N(7)-Ru(1)	124.4(3)
C(1)-N(1)-Ru(1)	125.6(3)	C(45)-N(7)-Ru(1)	123.2(3)
C(18)-N(1)-Ru(1)	126.9(3)	N(1)-C(1)-C(2)	127.2(5)

N(1)-C(1)-C(20)	108.1(4)	C(15)-C(14)-C(13)	107.6(4)
C(2)-C(1)-C(20)	124.6(4)	C(14)-C(15)-C(16)	107.4(4)
C(1)-C(2)-C(3)	124.9(5)	N(4)-C(16)-C(17)	125.4(4)
N(2)-C(3)-C(2)	125.7(4)	N(4)-C(16)-C(15)	109.2(4)
N(2)-C(3)-C(4)	109.7(4)	C(17)-C(16)-C(15)	125.1(4)
C(2)-C(3)-C(4)	124.6(4)	C(16)-C(17)-C(18)	125.8(5)
C(5)-C(4)-C(3)	107.0(4)	N(1)-C(18)-C(17)	125.1(4)
C(4)-C(5)-C(6)	107.9(5)	N(1)-C(18)-C(19)	109.2(4)
N(2)-C(6)-C(7)	125.8(4)	C(17)-C(18)-C(19)	125.6(4)
N(2)-C(6)-C(5)	108.4(4)	C(20)-C(19)-C(18)	107.8(4)
C(7)-C(6)-C(5)	125.7(4)	C(19)-C(20)-C(1)	107.3(4)
C(6)-C(7)-C(8)	125.3(4)	C(46)-C(45)-N(7)	117.8(4)
N(3)-C(8)-C(7)	126.1(4)	C(50)-C(45)-N(7)	119.6(5)
N(3)-C(8)-C(9)	109.0(4)	C(45)-C(46)-C(47)	118.9(5)
C(7)-C(8)-C(9)	124.9(4)	C(48)-C(47)-C(46)	119.9(6)
C(10)-C(9)-C(8)	107.5(4)	C(49)-C(48)-C(47)	119.8(5)
C(9)-C(10)-C(11)	107.5(4)	C(48)-C(49)-C(50)	122.8(5)
N(3)-C(11)-C(12)	125.4(4)	C(45)-C(50)-C(49)	116.0(5)
N(3)-C(11)-C(10)	109.2(4)	C(45)-C(50)-C(51)	121.9(5)
C(12)-C(11)-C(10)	125.3(4)	C(49)-C(50)-C(51)	122.0(5)
C(13)-C(12)-C(11)	124.9(4)	C(53)-C(52)-N(5)	110.1(5)
N(4)-C(13)-C(12)	126.7(4)	N(6)-C(53)-C(52)	106.4(5)
N(4)-C(13)-C(14)	108.8(4)	N(5)-C(55)-N(6)	111.6(5)
C(12)-C(13)-C(14)	124.5(4)		

Table 5.17. Selected Bond lengths (Å) for (TTP)Ru(N(O)$C_6H_2(Me)_2$OMe-*p*)(1-MeIm)

Ru(1)-N(5)	1.919(5)	C(1)-C(20)	1.460(7)
Ru(1)-N(1)	2.049(4)	C(2)-C(3)	1.408(7)
Ru(1)-N(2)	2.059(4)	C(3)-C(4)	1.449(7)
Ru(1)-N(4)	2.059(4)	C(4)-C(5)	1.354(7)
Ru(1)-N(3)	2.062(5)	C(5)-C(6)	1.441(7)
Ru(1)-N(6)	2.144(5)	C(6)-C(7)	1.423(7)
N(1)-C(1)	1.376(7)	C(7)-C(8)	1.403(7)
N(1)-C(18)	1.398(6)	C(8)-C(9)	1.465(8)
N(2)-C(3)	1.372(6)	C(9)-C(10)	1.354(8)
N(2)-C(6)	1.376(6)	C(10)-C(11)	1.442(8)
N(3)-C(8)	1.383(7)	C(11)-C(12)	1.409(8)
N(3)-C(11)	1.388(7)	C(12)-C(13)	1.401(8)
N(4)-C(13)	1.386(7)	C(13)-C(14)	1.440(8)
N(4)-C(16)	1.391(7)	C(14)-C(15)	1.368(9)
N(5)-O(1)	1.291(6)	C(15)-C(16)	1.453(8)
N(5)-C(49)	1.457(7)	C(16)-C(17)	1.393(8)
N(6)-C(61)	1.339(7)	C(17)-C(18)	1.397(8)
N(6)-C(58)	1.371(8)	C(18)-C(19)	1.449(7)
N(7)-C(61)	1.345(8)	C(19)-C(20)	1.353(7)
N(7)-C(59)	1.347(8)	C(49)-C(57)	1.373(9)
N(7)-C(60)	1.457(8)	C(49)-C(50)	1.408(9)
O(2)-C(53)	1.410(8)	C(50)-C(51)	1.367(10)
O(2)-C(54)	1.447(11)	C(51)-C(53)	1.397(12)
C(1)-C(2)	1.405(7)	C(51)-C(52)	1.576(11)

C(53)-C(55)	1.380(11)	C(55)-C(56)	1.537(11)
C(55)-C(57)	1.383(9)	C(58)-C(59)	1.365(10)

Table 5.18. Bond angles (°) for (TTP)Ru(N(O)$C_6H_2(Me)_2$OMe–*p*)(1–MeIm)

N(5)-Ru(1)-N(1)	83.9(2)	C(3)-N(2)-Ru(1)	126.2(3)
N(5)-Ru(1)-N(2)	90.44(19)	C(6)-N(2)-Ru(1)	126.8(3)
N(1)-Ru(1)-N(2)	89.69(16)	C(8)-N(3)-C(11)	107.1(4)
N(5)-Ru(1)-N(4)	91.00(19)	C(8)-N(3)-Ru(1)	125.2(4)
N(1)-Ru(1)-N(4)	90.79(17)	C(11)-N(3)-Ru(1)	127.3(4)
N(2)-Ru(1)-N(4)	178.52(19)	C(13)-N(4)-C(16)	107.2(4)
N(5)-Ru(1)-N(3)	99.4(2)	C(13)-N(4)-Ru(1)	127.2(4)
N(1)-Ru(1)-N(3)	176.69(19)	C(16)-N(4)-Ru(1)	125.5(4)
N(2)-Ru(1)-N(3)	90.24(17)	O(1)-N(5)-C(49)	111.6(5)
N(4)-Ru(1)-N(3)	89.19(18)	O(1)-N(5)-Ru(1)	121.8(4)
N(5)-Ru(1)-N(6)	170.29(19)	C(49)-N(5)-Ru(1)	125.5(4)
N(1)-Ru(1)-N(6)	86.62(17)	C(61)-N(6)-C(58)	104.7(5)
N(2)-Ru(1)-N(6)	91.82(17)	C(61)-N(6)-Ru(1)	125.3(4)
N(4)-Ru(1)-N(6)	86.82(18)	C(58)-N(6)-Ru(1)	129.7(4)
N(3)-Ru(1)-N(6)	90.07(18)	C(61)-N(7)-C(59)	106.0(5)
C(1)-N(1)-C(18)	107.5(4)	C(61)-N(7)-C(60)	127.5(6)
C(1)-N(1)-Ru(1)	127.0(3)	C(59)-N(7)-C(60)	126.5(6)
C(18)-N(1)-Ru(1)	125.4(4)	C(53)-O(2)-C(54)	113.5(7)
C(3)-N(2)-C(6)	106.9(4)	N(1)-C(1)-C(2)	125.9(5)

N(1)-C(1)-C(20)	109.1(4)	N(4)-C(16)-C(15)	108.6(5)
C(2)-C(1)-C(20)	125.0(5)	C(17)-C(16)-C(15)	125.3(5)
C(1)-C(2)-C(3)	124.5(5)	C(16)-C(17)-C(18)	125.8(5)
N(2)-C(3)-C(2)	126.5(5)	C(17)-C(18)-N(1)	126.2(5)
N(2)-C(3)-C(4)	109.2(4)	C(17)-C(18)-C(19)	125.8(5)
C(2)-C(3)-C(4)	124.3(5)	N(1)-C(18)-C(19)	108.0(5)
C(5)-C(4)-C(3)	107.2(5)	C(20)-C(19)-C(18)	108.5(5)
C(4)-C(5)-C(6)	107.1(5)	C(19)-C(20)-C(1)	106.9(5)
N(2)-C(6)-C(7)	125.6(5)	C(57)-C(49)-C(50)	121.5(6)
N(2)-C(6)-C(5)	109.5(4)	C(57)-C(49)-N(5)	122.6(6)
C(7)-C(6)-C(5)	124.9(5)	C(50)-C(49)-N(5)	115.9(6)
N(3)-C(8)-C(7)	127.5(5)	C(51)-C(50)-C(49)	118.6(7)
N(3)-C(8)-C(9)	108.5(5)	C(50)-C(51)-C(53)	119.4(7)
C(7)-C(8)-C(9)	124.0(5)	C(50)-C(51)-C(52)	120.8(9)
C(10)-C(9)-C(8)	107.4(5)	C(53)-C(51)-C(52)	119.8(8)
C(9)-C(10)-C(11)	107.7(5)	C(55)-C(53)-C(51)	121.9(7)
N(3)-C(11)-C(12)	124.8(5)	C(55)-C(53)-O(2)	118.0(8)
N(3)-C(11)-C(10)	109.3(5)	C(51)-C(53)-O(2)	120.0(8)
C(13)-C(12)-C(11)	125.9(5)	C(53)-C(55)-C(57)	118.5(7)
N(4)-C(13)-C(12)	125.5(5)	C(53)-C(55)-C(56)	122.0(7)
N(4)-C(13)-C(14)	109.3(5)	C(57)-C(55)-C(56)	119.5(7)
C(12)-C(13)-C(14)	125.2(6)	C(49)-C(57)-C(55)	119.9(7)
C(15)-C(14)-C(13)	107.5(6)	C(59)-C(58)-N(6)	108.8(6)
C(14)-C(15)-C(16)	107.4(5)	N(7)-C(59)-C(58)	108.3(6)
N(4)-C(16)-C(17)	126.1(5)	N(6)-C(61)-N(7)	112.3(5)

Table 5.19. Selected Bond lengths (Å) for (TTP)Ru(PhNO)(1–MeIm)

Ru(1)-N(5)	1.884(5)	C(3)-C(4)	1.430(7)
Ru(1)-N(4)	2.030(5)	C(4)-C(5)	1.399(7)
Ru(1)-N(1)	2.041(4)	C(5)-C(6)	1.392(7)
Ru(1)-N(3)	2.049(4)	C(6)-C(7)	1.440(7)
Ru(1)-N(2)	2.051(4)	C(7)-C(8)	1.330(7)
Ru(1)-N(6)	2.149(4)	C(8)-C(9)	1.429(8)
O(1)-N(5)	1.251(6)	C(9)-C(10)	1.402(7)
N(1)-C(1)	1.358(6)	C(10)-C(11)	1.391(8)
N(1)-C(4)	1.382(7)	C(11)-C(12)	1.435(7)
N(2)-C(6)	1.352(7)	C(12)-C(13)	1.334(8)
N(2)-C(9)	1.375(6)	C(13)-C(14)	1.434(7)
N(3)-C(14)	1.365(7)	C(14)-C(15)	1.392(7)
N(3)-C(11)	1.371(6)	C(15)-C(16)	1.408(7)
N(4)-C(16)	1.369(7)	C(16)-C(17)	1.425(8)
N(4)-C(19)	1.379(7)	C(17)-C(18)	1.333(8)
N(5)-C(49)	1.427(8)	C(18)-C(19)	1.428(8)
N(6)-C(57)	1.317(7)	C(19)-C(20)	1.395(7)
N(6)-C(55)	1.363(7)	C(49)-C(50)	1.363(10)
N(7)-C(57)	1.347(8)	C(49)-C(54)	1.389(10)
N(7)-C(56)	1.362(8)	C(50)-C(51)	1.403(11)
N(7)-C(58)	1.456(8)	C(51)-C(52)	1.346(14)
C(1)-C(20)	1.393(8)	C(52)-C(53)	1.403(13)
C(1)-C(2)	1.425(7)	C(53)-C(54)	1.388(10)
C(2)-C(3)	1.345(7)	C(55)-C(56)	1.331(9)

Table 5.20. Selected Bond angles (°) for (TTP)Ru(PhNO)(1–MeIm)

N(5)-Ru(1)-N(4)	90.7(2)	C(16)-N(4)-C(19)	105.9(4)
N(5)-Ru(1)-N(1)	90.03(19)	C(16)-N(4)-Ru(1)	126.4(4)
N(4)-Ru(1)-N(1)	89.31(17)	C(19)-N(4)-Ru(1)	127.5(4)
N(5)-Ru(1)-N(3)	93.56(18)	O(1)-N(5)-C(49)	113.5(5)
N(4)-Ru(1)-N(3)	90.72(17)	O(1)-N(5)-Ru(1)	125.7(4)
N(1)-Ru(1)-N(3)	176.41(18)	C(49)-N(5)-Ru(1)	120.7(4)
N(5)-Ru(1)-N(2)	92.50(19)	C(57)-N(6)-C(55)	104.5(5)
N(4)-Ru(1)-N(2)	176.82(18)	C(57)-N(6)-Ru(1)	126.3(4)
N(1)-Ru(1)-N(2)	90.85(17)	C(55)-N(6)-Ru(1)	129.2(4)
N(3)-Ru(1)-N(2)	88.92(16)	C(57)-N(7)-C(56)	106.7(5)
N(5)-Ru(1)-N(6)	178.76(19)	C(57)-N(7)-C(58)	126.6(5)
N(4)-Ru(1)-N(6)	89.60(17)	C(56)-N(7)-C(58)	126.7(6)
N(1)-Ru(1)-N(6)	88.76(17)	N(1)-C(1)-C(20)	125.2(4)
N(3)-Ru(1)-N(6)	87.65(17)	N(1)-C(1)-C(2)	109.1(5)
N(2)-Ru(1)-N(6)	87.23(17)	C(20)-C(1)-C(2)	125.7(5)
C(1)-N(1)-C(4)	107.5(4)	C(3)-C(2)-C(1)	107.7(5)
C(1)-N(1)-Ru(1)	127.4(4)	C(2)-C(3)-C(4)	107.6(5)
C(4)-N(1)-Ru(1)	125.2(3)	N(1)-C(4)-C(5)	125.8(5)
C(6)-N(2)-C(9)	106.7(4)	N(1)-C(4)-C(3)	108.1(4)
C(6)-N(2)-Ru(1)	126.0(3)	C(5)-C(4)-C(3)	126.0(5)
C(9)-N(2)-Ru(1)	127.2(3)	C(6)-C(5)-C(4)	126.1(5)
C(14)-N(3)-C(11)	107.1(4)	N(2)-C(6)-C(5)	126.1(5)
C(14)-N(3)-Ru(1)	125.4(3)	N(2)-C(6)-C(7)	109.2(4)
C(11)-N(3)-Ru(1)	127.3(3)	C(5)-C(6)-C(7)	124.7(5)

C(8)-C(7)-C(6)	107.5(5)	C(18)-C(17)-C(16)	106.9(5)
C(7)-C(8)-C(9)	107.3(5)	C(17)-C(18)-C(19)	108.2(5)
N(2)-C(9)-C(10)	125.3(5)	N(4)-C(19)-C(20)	124.4(5)
N(2)-C(9)-C(8)	109.2(4)	N(4)-C(19)-C(18)	108.9(5)
C(10)-C(9)-C(8)	125.4(5)	C(20)-C(19)-C(18)	126.7(5)
C(11)-C(10)-C(9)	125.3(5)	C(1)-C(20)-C(19)	126.2(5)
N(3)-C(11)-C(10)	125.8(4)	C(50)-C(49)-C(54)	122.3(7)
N(3)-C(11)-C(12)	108.6(5)	C(50)-C(49)-N(5)	118.4(7)
C(10)-C(11)-C(12)	125.5(5)	C(54)-C(49)-N(5)	119.2(7)
C(13)-C(12)-C(11)	107.8(5)	C(49)-C(50)-C(51)	118.0(9)
C(12)-C(13)-C(14)	107.4(5)	C(52)-C(51)-C(50)	119.3(10)
N(3)-C(14)-C(15)	125.9(5)	C(51)-C(52)-C(53)	124.1(10)
N(3)-C(14)-C(13)	109.0(5)	C(54)-C(53)-C(52)	115.8(10)
C(15)-C(14)-C(13)	125.1(5)	C(53)-C(54)-C(49)	120.4(9)
C(14)-C(15)-C(16)	126.3(5)	C(56)-C(55)-N(6)	111.1(6)
N(4)-C(16)-C(15)	124.8(5)	C(55)-C(56)-N(7)	106.2(6)
C(15)-C(16)-C(17)	125.0(5)	N(6)-C(57)-N(7)	111.5(5)
N(4)-C(16)-C(17)	110.2(5)		

Table 5.21. Selected Bond lengths (Å) for (TTP)Ru(*o*–tolNO)(1–MeIm)

Ru(1)-N(5)	1.871(7)	C(2)-C(3)	1.407(9)
Ru(1)-N(4)	2.031(6)	C(3)-C(4)	1.433(10)
Ru(1)-N(3)	2.046(6)	C(4)-C(5)	1.351(9)
Ru(1)-N(2)	2.042(6)	C(5)-C(6)	1.450(10)
Ru(1)-N(1)	2.058(5)	C(6)-C(7)	1.411(9)
Ru(1)-N(6)	2.152(7)	C(7)-C(8)	1.381(10)
O(1)-N(5)	1.285(8)	C(8)-C(9)	1.446(9)
N(1)-C(18)	1.368(8)	C(9)-C(10)	1.357(10)
N(1)-C(1)	1.384(8)	C(10)-C(11)	1.456(9)
N(2)-C(6)	1.360(9)	C(11)-C(12)	1.390(10)
N(2)-C(3)	1.386(9)	C(12)-C(13)	1.405(9)
N(3)-C(8)	1.374(9)	C(13)-C(14)	1.437(10)
N(3)-C(11)	1.379(9)	C(14)-C(15)	1.348(10)
N(4)-C(16)	1.383(9)	C(15)-C(16)	1.429(10)
N(4)-C(13)	1.392(8)	C(16)-C(17)	1.417(9)
N(5)-C(53B)	1.455(12)	C(17)-C(18)	1.399(10)
N(5)-C(53A)	1.469(10)	C(18)-C(19)	1.430(9)
N(6)-C(52)	1.330(9)	C(19)-C(20)	1.341(10)
N(6)-C(49)	1.388(10)	C(49)-C(50)	1.352(11)
N(7)-C(52)	1.314(10)	C(53A)-C(54A)	1.3900
N(7)-C(50)	1.365(10)	C(53A)-C(58A)	1.3900
N(7)-C(51)	1.474(10)	C(54A)-C(55A)	1.3900
C(1)-C(2)	1.395(10)	C(55A)-C(56A)	1.3900
C(1)-C(20)	1.430(9)	C(56A)-C(57A)	1.3900

C(57A)-C(58A)	1.3900	C(55B)-C(56B)	1.3900
C(58A)-C(59A)	1.499(2)	C(56B)-C(57B)	1.3900
C(53B)-C(54B)	1.3900	C(57B)-C(58B)	1.3900
C(53B)-C(58B)	1.3900	C(58B)-C(59B)	1.499(2)
C(54B)-C(55B)	1.3900		

Table 5.22. Selected Bond lengths angles (°) for (TTP)Ru(*o*–tolNO)(1–MeIm)

N(5)-Ru(1)-N(4)	92.6(3)	C(18)-N(1)-Ru(1)	127.5(4)
N(5)-Ru(1)-N(3)	89.9(2)	C(1)-N(1)-Ru(1)	125.3(5)
N(4)-Ru(1)-N(3)	90.7(2)	C(6)-N(2)-C(3)	106.5(6)
N(5)-Ru(1)-N(2)	90.9(3)	C(6)-N(2)-Ru(1)	127.8(5)
N(4)-Ru(1)-N(2)	176.5(2)	C(3)-N(2)-Ru(1)	125.6(5)
N(3)-Ru(1)-N(2)	89.0(2)	C(8)-N(3)-C(11)	108.6(6)
N(5)-Ru(1)-N(1)	94.9(3)	C(8)-N(3)-Ru(1)	126.7(5)
N(4)-Ru(1)-N(1)	89.1(2)	C(11)-N(3)-Ru(1)	124.7(5)
N(3)-Ru(1)-N(1)	175.2(2)	C(16)-N(4)-C(13)	104.6(6)
N(2)-Ru(1)-N(1)	90.9(2)	C(16)-N(4)-Ru(1)	127.8(5)
N(5)-Ru(1)-N(6)	178.4(2)	C(13)-N(4)-Ru(1)	127.6(5)
N(4)-Ru(1)-N(6)	87.2(2)	O(1)-N(5)-C(53B)	110.7(9)
N(3)-Ru(1)-N(6)	88.5(2)	O(1)-N(5)-C(53A)	106.5(8)
N(2)-Ru(1)-N(6)	89.3(2)	C(53B)-N(5)-C(53A)	17.8(7)
N(1)-Ru(1)-N(6)	86.6(2)	O(1)-N(5)-Ru(1)	126.4(5)
C(18)-N(1)-C(1)	107.1(5)	C(53B)-N(5)-Ru(1)	122.8(9)

C(53A)-N(5)-Ru(1)	125.2(7)	N(3)-C(11)-C(12)	127.3(6)
C(52)-N(6)-C(49)	103.0(7)	N(3)-C(11)-C(10)	107.7(6)
C(52)-N(6)-Ru(1)	128.3(5)	C(12)-C(11)-C(10)	125.0(7)
C(49)-N(6)-Ru(1)	128.6(5)	C(11)-C(12)-C(13)	126.2(6)
C(52)-N(7)-C(50)	108.0(7)	N(4)-C(13)-C(12)	123.5(7)
C(52)-N(7)-C(51)	126.8(7)	N(4)-C(13)-C(14)	110.6(6)
C(50)-N(7)-C(51)	125.2(7)	C(12)-C(13)-C(14)	125.8(6)
N(1)-C(1)-C(2)	126.3(6)	C(15)-C(14)-C(13)	106.4(6)
N(1)-C(1)-C(20)	108.2(6)	C(14)-C(15)-C(16)	108.0(7)
C(2)-C(1)-C(20)	125.5(7)	N(4)-C(16)-C(17)	124.8(7)
C(1)-C(2)-C(3)	125.6(7)	N(4)-C(16)-C(15)	110.4(6)
N(2)-C(3)-C(2)	125.9(7)	C(17)-C(16)-C(15)	124.7(7)
N(2)-C(3)-C(4)	109.3(6)	C(18)-C(17)-C(16)	125.1(6)
C(2)-C(3)-C(4)	124.8(7)	N(1)-C(18)-C(17)	125.5(6)
C(5)-C(4)-C(3)	107.7(7)	N(1)-C(18)-C(19)	109.2(6)
C(4)-C(5)-C(6)	106.5(7)	C(17)-C(18)-C(19)	125.3(6)
N(2)-C(6)-C(7)	125.2(7)	C(20)-C(19)-C(18)	107.4(6)
N(2)-C(6)-C(5)	110.0(6)	C(19)-C(20)-C(1)	108.2(7)
C(7)-C(6)-C(5)	124.8(7)	C(50)-C(49)-N(6)	110.8(7)
C(8)-C(7)-C(6)	124.8(6)	N(7)-C(50)-C(49)	105.3(7)
N(3)-C(8)-C(7)	126.5(6)	N(6)-C(52)-N(7)	112.9(7)
N(3)-C(8)-C(9)	108.4(6)	C(54A)-C(53A)-C(58A)	120.0
C(7)-C(8)-C(9)	125.1(6)	C(54A)-C(53A)-N(5)	119.7(8)
C(10)-C(9)-C(8)	107.6(7)	C(58A)-C(53A)-N(5)	119.7(8)
C(9)-C(10)-C(11)	107.6(6)	C(53A)-C(54A)-C(55A)	120.0

C(54A)-C(55A)-C(56A)	120.0	C(53B)-C(54B)-C(55B)	120.0
C(57A)-C(56A)-C(55A)	120.0	C(58B)-C(53B)-N(5)	113.9(10)
C(56A)-C(57A)-C(58A)	120.0	C(56B)-C(55B)-C(54B)	120.0
C(57A)-C(58A)-C(53A)	120.0	C(55B)-C(56B)-C(57B)	120.0
C(57A)-C(58A)-C(59A)	114.9(11)	C(58B)-C(57B)-C(56B)	120.0
C(53A)-C(58A)-C(59A)	125.1(11)	C(57B)-C(58B)-C(53B)	120.0
C(54B)-C(53B)-C(58B)	120.0	C(57B)-C(58B)-C(59B)	102.5(14)
C(54B)-C(53B)-N(5)	125.9(10)	C(53B)-C(58B)-C(59B)	131.7(14)